



NEW TRANSFORMATIONS BASED ON ACTIVATION OF INERT CARBON- HALOGEN BONDS WITH AND WITHOUT TRANSITION

Miloserdov Fedor Mikhailovich

Dipòsit Legal: T 825-2015

ADVERTIMENT. L'accés als continguts d'aquesta tesi doctoral i la seva utilització ha de respectar els drets de la persona autora. Pot ser utilitzada per a consulta o estudi personal, així com en activitats o materials d'investigació i docència en els termes establerts a l'art. 32 del Text Refós de la Llei de Propietat Intel·lectual (RDL 1/1996). Per altres utilitzacions es requereix l'autorització prèvia i expressa de la persona autora. En qualsevol cas, en la utilització dels seus continguts caldrà indicar de forma clara el nom i cognoms de la persona autora i el títol de la tesi doctoral. No s'autoritza la seva reproducció o altres formes d'explotació efectuades amb finalitats de lucre ni la seva comunicació pública des d'un lloc aliè al servei TDX. Tampoc s'autoritza la presentació del seu contingut en una finestra o marc aliè a TDX (framing). Aquesta reserva de drets afecta tant als continguts de la tesi com als seus resums i índexs.

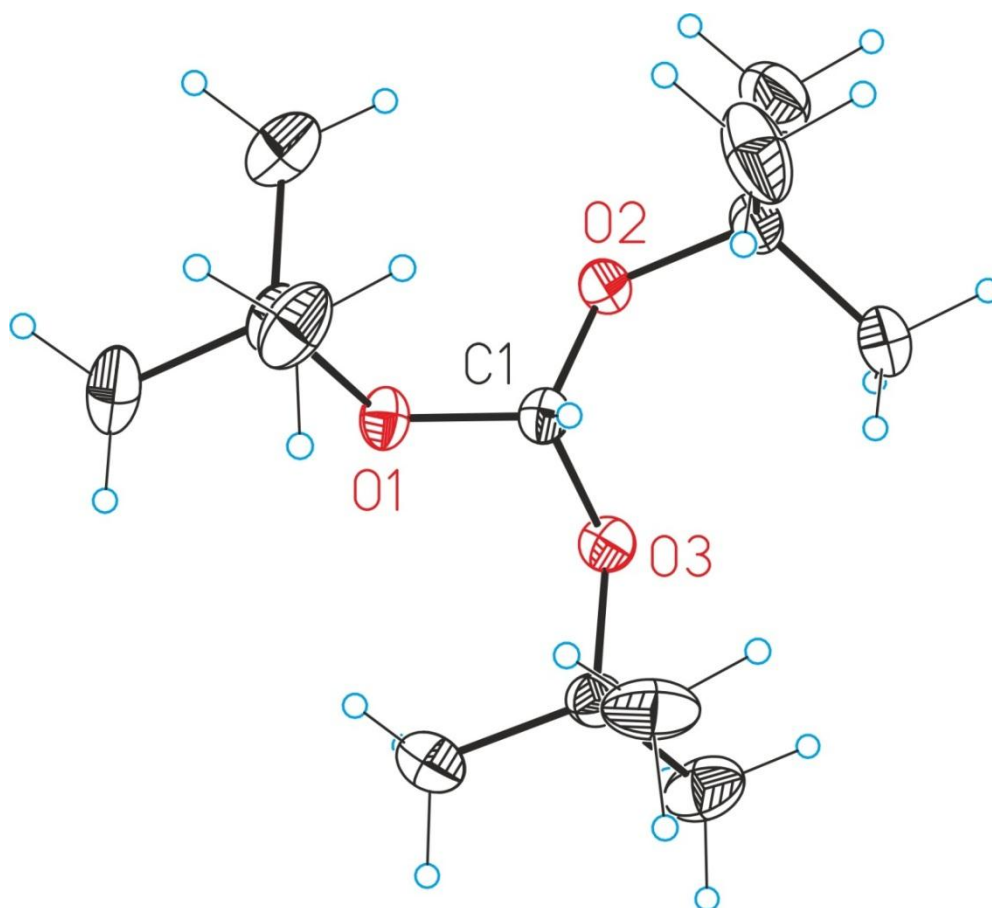
ADVERTENCIA. El acceso a los contenidos de esta tesis doctoral y su utilización debe respetar los derechos de la persona autora. Puede ser utilizada para consulta o estudio personal, así como en actividades o materiales de investigación y docencia en los términos establecidos en el art. 32 del Texto Refundido de la Ley de Propiedad Intelectual (RDL 1/1996). Para otros usos se requiere la autorización previa y expresa de la persona autora. En cualquier caso, en la utilización de sus contenidos se deberá indicar de forma clara el nombre y apellidos de la persona autora y el título de la tesis doctoral. No se autoriza su reproducción u otras formas de explotación efectuadas con fines lucrativos ni su comunicación pública desde un sitio ajeno al servicio TDR. Tampoco se autoriza la presentación de su contenido en una ventana o marco ajeno a TDR (framing). Esta reserva de derechos afecta tanto al contenido de la tesis como a sus resúmenes e índices.

WARNING. Access to the contents of this doctoral thesis and its use must respect the rights of the author. It can be used for reference or private study, as well as research and learning activities or materials in the terms established by the 32nd article of the Spanish Consolidated Copyright Act (RDL 1/1996). Express and previous authorization of the author is required for any other uses. In any case, when using its content, full name of the author and title of the thesis must be clearly indicated. Reproduction or other forms of for profit use or public communication from outside TDX service is not allowed. Presentation of its content in a window or frame external to TDX (framing) is not authorized either. These rights affect both the content of the thesis and its abstracts and indexes.

DOCTORAL THESIS

New Transformations Based on Activation of Inert Carbon-Halogen Bonds with and without Transition Metals

Fedor M. Miloserdov



Rovira i Virgili University

Institute of Chemical Research of Catalonia

UNIVERSITAT ROVIRA I VIRGILI
NEW TRANSFORMATIONS BASED ON ACTIVATION OF INERT CARBON-HALOGEN BONDS WITH AND WITHOUT TRANSITION
Miloserdov Fedor Mikhailovich
Dipòsit Legal: T 825-2015

UNIVERSITAT ROVIRA I VIRGILI
NEW TRANSFORMATIONS BASED ON ACTIVATION OF INERT CARBON-HALOGEN BONDS WITH AND WITHOUT TRANSITION
Miloserdov Fedor Mikhailovich
Dipòsit Legal: T 825-2015

UNIVERSITAT ROVIRA I VIRGILI
NEW TRANSFORMATIONS BASED ON ACTIVATION OF INERT CARBON-HALOGEN BONDS WITH AND WITHOUT TRANSITION
Miloserdov Fedor Mikhailovich
Dipòsit Legal: T 825-2015

Fedor M. Miloserdov

New Transformations Based on Activation of
Inert Carbon-Halogen Bonds with and without
Transition Metals

DOCTORAL THESIS

Supervised by Dr. Vladimir V. Grushin

Institut Català d'Investigació Química (ICIQ)



UNIVERSITAT ROVIRA I VIRGILI

Tarragona

2015

UNIVERSITAT ROVIRA I VIRGILI
NEW TRANSFORMATIONS BASED ON ACTIVATION OF INERT CARBON-HALOGEN BONDS WITH AND WITHOUT TRANSITION
Miloserdov Fedor Mikhailovich
Dipòsit Legal: T 825-2015



UNIVERSITAT
ROVIRA I VIRGILI
DEPARTAMENT DE
QUÍMICA ANALÍTICA
I QUÍMICA ORGÀNICA

C/ Marcel·li Domingo s/n
Campus Sescelades
43007 Tarragona
Tel. 34 977 55 97 69
Fax 34 977 55 84 46
e-mail: secqaqo@urv.net

INSTITUT CATALÀ
D'INVESTIGACIÓ
QUÍMICA (ICIQ)



Av Països Catalans 16
43007 Tarragona
Tel. 34 977 92 08 24
Fax 34 977 92 08 25
e-mail: iciq@iciq.es.

I STATE that the present study, entitled “New Transformations Based on Activation of Inert Carbon-Halogen Bonds with and without Transition Metals”, presented by Fedor M. Miloserdov for the award of the degree of Doctor, has been carried out under my supervision at the Institute of Chemical Research of Catalonia (ICIQ).

Tarragona, 9 January 2015

Doctoral Thesis Supervisor

Vladimir V. Grushin, PhD

UNIVERSITAT ROVIRA I VIRGILI
NEW TRANSFORMATIONS BASED ON ACTIVATION OF INERT CARBON-HALOGEN BONDS WITH AND WITHOUT TRANSITION
Miloserdov Fedor Mikhailovich
Dipòsit Legal: T 825-2015

*Dedicated to my Grandfather Fedor E. Miloserdov
and Great-Grandmother Alexandra I. Kalinina*

UNIVERSITAT ROVIRA I VIRGILI
NEW TRANSFORMATIONS BASED ON ACTIVATION OF INERT CARBON-HALOGEN BONDS WITH AND WITHOUT TRANSITION
Miloserdov Fedor Mikhailovich
Dipòsit Legal: T 825-2015

First and foremost, I would like to express my deepest gratitude to my thesis supervisor Prof. Vladimir Grushin for the opportunity to perform my M.Sc. and Ph.D. studies in his research group. Through Prof. Grushin I gained the priceless chemical knowledge and experience to succeed in my studies, but more importantly the inspiration he gave me by showing how interesting and exciting scientific research can be. His unique guidance with strong leadership but also understanding and mutual respect encouraged me to do better. Finally I would like to personally thank Prof. Grushin for many valued chemistry and life lessons learned from him during my studies.

I want to thank my former teachers and supervisors, especially Galina V. Farina, Olga V. Plugatarenko, Maria B. Postnikova, Sergey E. Semenov, Dmitrii M. Roitershtein, Alexander S. Dorofeev, and Ilya Yu. Titov.

I am grateful to the ICIQ research and administrative staff for all their help and cooperation during my research work. My special thanks go to Noemí Panadès Muñoz for her tremendous help with administrative issues and to Drs. Jordi Benet-Buchholz, Eddy Martin, Marta Martínez Belmonte and Eduardo C. Escudero-Adán for numerous crystallographic studies. I also thank Germán Gómez and Israel Macho for their assistance with NMR experiments.

I would like to express my appreciation to all former and current members of the Grushin research group, especially Andrey Konovalov, Liubov Panferova, Drs. Anton Lishchynskiy, Hamidreza Samouei, Noel Nebra, Alexander Ushkov, Olesya Tomashenko, Alessandro Zanardi, Prof. Shin Takemoto, Juan del Pozo, and Maksim Novikov for their assistance in the laboratory and interesting discussions. I am thankful to all of my lab mates and friends Masha Kirillova, Tameem Bader, Dina Fakhrnasova, Sanaz Mazloomi, Jhenia Gorbacheva and Andrew Romine for making my stay in Tarragona such an enjoyable experience.

I thank Dr. Claire L. McMullin, Dr. David McKay, and Prof. Stuart A. Macgregor of Heriot-Watt University for computational studies and for fruitful collaboration. It is a pleasure to acknowledge Drs. Hamidreza Samouei and Bianca K. Muñoz for their preliminary work that was essential for my studies described in Chapter 2 of this Thesis. I thank Prof. Vladimir I. Bakhmutov for many helpful discussions.

The ICIQ foundation and the Spanish Ministry of Economy and Competitiveness (MINECO) are gratefully acknowledged for their financial support and for the FPI Ph.D. fellowship (BES-2012-054922).

Last but not least, I thank my family, especially my father, mother, and brother for all their love, encouragement, and support (even at a distance).



At the printing of this manuscript, the results presented herein have been published in:

- Palladium-Catalyzed Aromatic Azidocarbonylation
F. M. Miloserdov, V. V. Grushin, *Angew. Chem. Int. Ed.* **2012**, *51*, 3668.
- The Challenge of Palladium-Catalyzed Aromatic Azidocarbonylation: From Mechanistic and Catalyst Deactivation Studies to a Highly Efficient Process
F. M. Miloserdov, C. L. McMullin, M. Martínez Belmonte, J. Benet-Buchholz, V. I. Bakhmutov, S. A. Macgregor, V. V. Grushin, *Organometallics* **2014**, *33*, 736.
- Alcoholysis of fluoroform
F. M. Miloserdov, V. V. Grushin, *J. Fluorine Chem.* **2014**, *167*, 105.
- Exceedingly Facile Ph-X Activation (X = F, Cl, Br, I) with Ru(II): Arresting Kinetics, Autocatalysis, and Mechanisms
F. M. Miloserdov, D. McKay, B. K. Muñoz, H. Samouei, S. A. Macgregor, V. V. Grushin, submitted for publication.

Other publications (during the graduate studies) not directly related to the topics covered in this manuscript:

- Well-Defined CuC_2F_5 Complexes and Pentafluoroethylation of Acid Chlorides.
L. I. Panferova, F. M. Miloserdov, A. Lishchynskiy, M. Martínez Belmonte, J. Benet-Buchholz, V. V. Grushin, *Angew. Chem. Int. Ed.* **2015**,
DOI: 10.1002/anie.201500341.
- Solid-State Structure and Solution Reactivity of $[(\text{Ph}_3\text{P})_4\text{Ru}(\text{H})_2]$ and Related Ru(II) Complexes Used in Catalysis: A Reinvestigation
H. Samouei, F. M. Miloserdov, E. C. Escudero-Adán, V. V. Grushin, *Organometallics* **2014**, *33*, 7279.
- On the Feasibility of Nickel-Catalyzed Trifluoromethylation of Aryl Halides
J. Jover, F. M. Miloserdov, J. Benet-Buchholz, V. V. Grushin, F. Maseras, *Organometallics* **2014**, *33*, 6531.
- CF_3 -Ph Reductive Elimination from $[(\text{Xantphos})\text{Pd}(\text{CF}_3)(\text{Ph})]$
V. I. Bakhmutov, F. Bozoglian, K. Gómez, G. González, V. V. Grushin, S. A. Macgregor, E. Martin, F. M. Miloserdov, M. A. Novikov, J. A. Panetier, L. V. Romashov, *Organometallics* **2012**, *31*, 1315.

UNIVERSITAT ROVIRA I VIRGILI
NEW TRANSFORMATIONS BASED ON ACTIVATION OF INERT CARBON-HALOGEN BONDS WITH AND WITHOUT TRANSITION
Miloserdov Fedor Mikhailovich
Dipòsit Legal: T 825-2015

Table of Contents

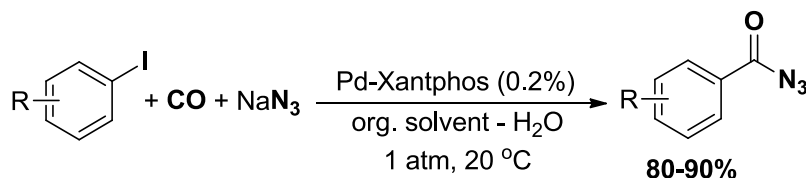
1. Synopsis	7
2. General Introduction: Activation of Inert Carbon-Halogen Bonds	23
3. Chapter 1. Palladium-Catalyzed Azidocarbonylation of Aromatic Iodides	45
- Introduction	46
- Objectives	51
- Results	53
- Conclusions	92
- Experimental Section	95
4. Chapter 2. Mechanistic Study of Aryl Halide Activation with Ruthenium (II) Hydrido Complexes	131
- Introduction	132
- Objectives	137
- Results	138
- Conclusions	172
- Experimental Section	174
5. Chapter 3. Alcoholysis of Fluoroform	187
- Introduction	188
- Objectives	191
- Results	192
- Conclusions	199
- Experimental Section	200

Synopsis

Results of the current doctoral work are presented and discussed in detail in three Chapters. All three research projects deal with activation and cleavage of inert carbon-halogen bonds. Chapter 1 describes a new chemical transformation, the Pd-catalyzed synthesis of aroyl azides from iodoarenes, CO, and sodium azide. In Chapter 2, we report a mechanistic study of the novel Ph-X (X = I, Br, Cl) activation with Ru(II) complexes. Chapter 3 deals with C-F activation of highly inert fluoroform (CHF₃) using alkali metal hydroxides and alkoxides. A summary of the work performed on each of these three projects is presented below.

I. Palladium-Catalyzed Azidocarbonylation of Aromatic Iodides

Aroyl azides (ArCON₃) are useful building blocks and intermediates in the preparation of various valuable chemicals.¹ We have developed a methodologically unprecedented catalytic route to aroyl azides from iodoarenes, CO, and NaN₃ (Scheme S1).^{2,3}



Scheme S1. Pd-catalyzed azidocarbonylation of iodoarenes.

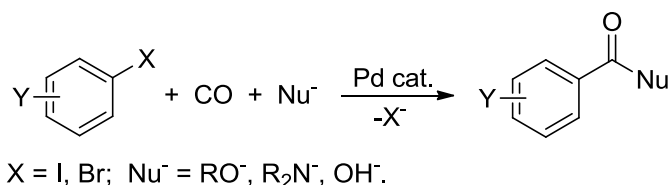
While looking similar to the long-known⁴ Heck alkoxy-, hydroxy-, and aminocarbonylation reactions (Scheme S2), the azidocarbonylation is a vastly more challenging transformation in at least three respects.

¹ Bräse, S.; Banert, K. *Organic Azides: Syntheses and Applications*, John Wiley & Sons: Chichester, 2010.

² Miloserdov, F. M.; Grushin, V. V. *Angew. Chem. Int. Ed.* 2012, *51*, 3668.

³ Miloserdov, F. M.; McMullin, C. L.; Belmonte, M. M.; Benet-Buchholz, J.; Bakhmutov, V. I.; Macgregor, S. A.; Grushin, V. V. *Organometallics* 2014, *33*, 736.

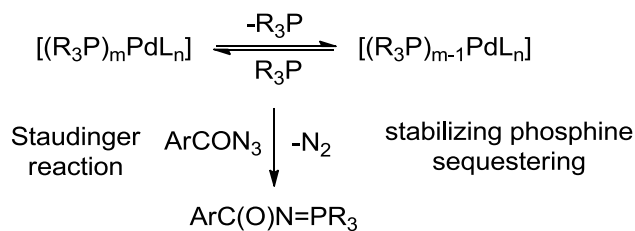
⁴ (a) Schoenberg, A.; Bartoletti, I.; Heck, R. F. *J. Org. Chem.* 1974, *39*, 3318. (b) Schoenberg, A.; Heck, R. F. *J. Org. Chem.* 1974, *39*, 3327. (c) Schoenberg, A.; Heck, R. F. *J. Am. Chem. Soc.* 1974, *96*, 7761. (d) Garrou, P. E.; Heck, R. F. *J. Am. Chem. Soc.* 1976, *98*, 4115.



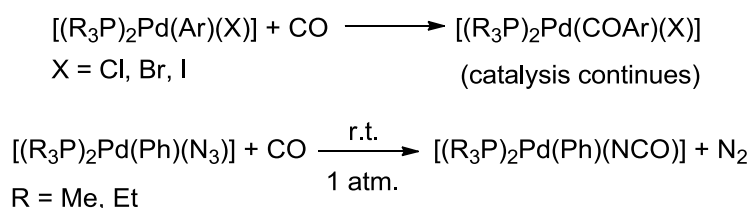
Scheme S2. The Heck carbonylation of aryl halides.

- (1) Heck-type carbonylation reactions usually occur at 80 °C or above. At such temperatures, aryl azides are unstable, undergoing the Curtius rearrangement to isocyanates.
- (2) The desired aryl azide product is highly reactive toward tertiary phosphines (the Staudinger reaction), and therefore can quickly and irreversibly deactivate the catalyst by sequestering the PR₃ ligands stabilizing the Pd center (Scheme S3).
- (3) A key step in the catalytic loop governing the carbonylation reaction is migratory insertion of CO into the Pd-C bond of [(R₃P)₂Pd(Ar)(X)], the intermediate that is produced in the preceding step of Ar-X substrate oxidative addition to R₃P-stabilized Pd(0). For X = I, Br, and Cl, this reaction usually occurs easily and cleanly at room temperature and atmospheric pressure.^{4d} In sharp contrast, complexes of the type [(R₃P)₂Pd(Ph)N₃] (R = Me, Et) do not undergo CO insertion into the Pd-Ph bond but are rather converted to [(R₃P)₂Pd(Ph)NCO] with concomitant release of N₂ under similar conditions (r.t., 1 atm CO),⁵ as shown in Scheme S4.

⁵ Kim, Y.-J.; Kwak, Y.-S.; Lee, S.-W. *J. Organomet. Chem.* 2000, 603, 152.



Scheme S3. Staudinger reaction leading to Pd catalyst deactivation.

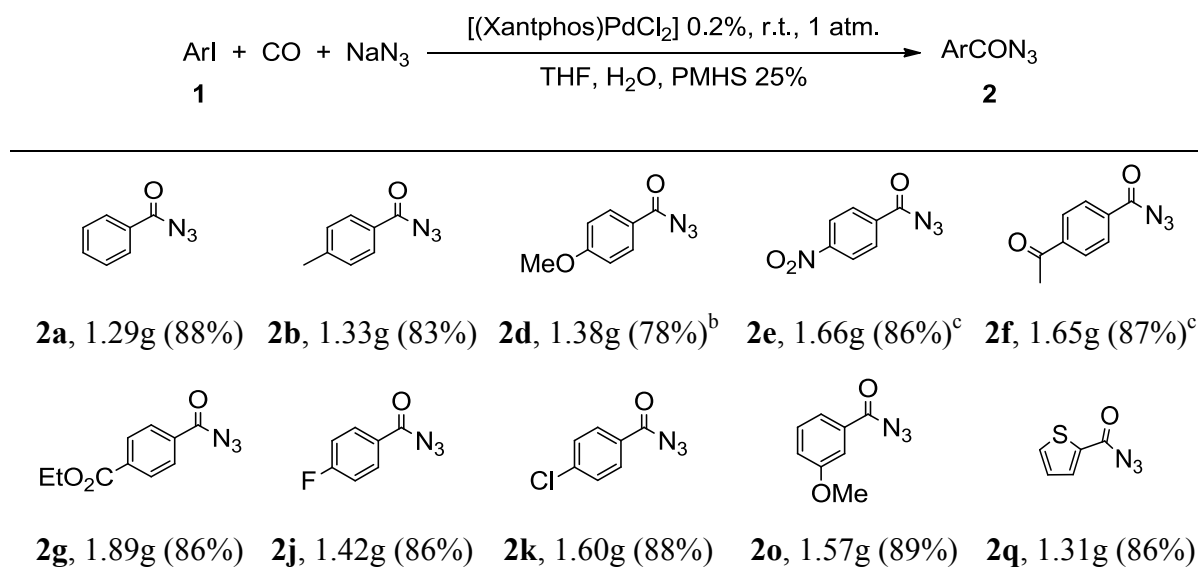


Scheme S4. Different reactivity of σ -aryl palladium halides and azides toward CO.

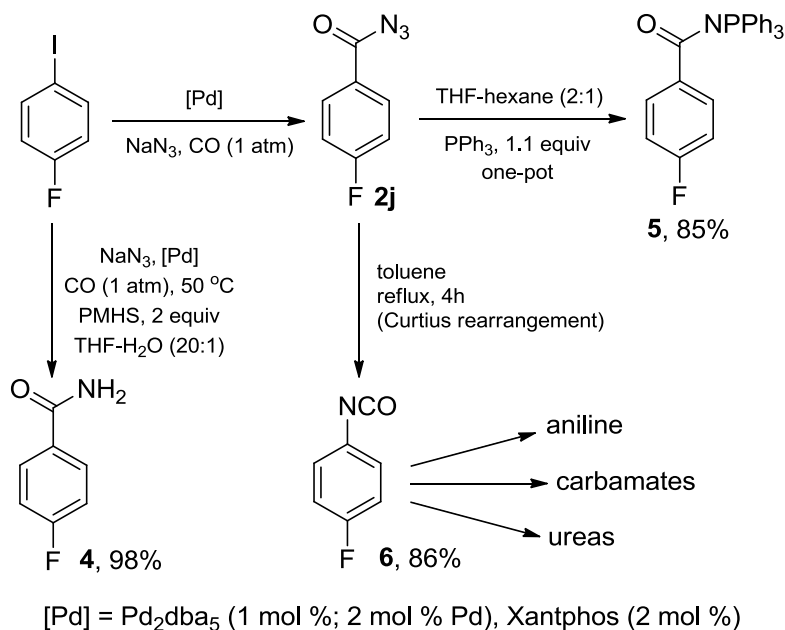
The key to success in the development of the aromatic azidocarbonylation (Scheme S1) was the finding of the highly efficient Xantphos-based system that catalyzes this reaction under exceedingly mild conditions (20-50 °C, 1 atm of CO).⁶ After initial optimization² the catalytic synthesis of aroyl azides was demonstrated for a broad variety of substrates with 2 mol % Pd. However, subsequent catalyst deactivation studies yielded a reliable process occurring efficiently in the presence of only 0.2 mol % of air-stable [(Xantphos)PdCl₂] as added catalyst. The reaction has been demonstrated on a gram scale for a number of substrates bearing various functional groups on the aromatic ring (Table S1).³ The desired products can be isolated pure or used without isolation, i.e. *in situ*, for further transformations to primary benzamides, isocyanates, ureas, etc. (Scheme S5).

⁶ The Xantphos-based catalytic system is unique. In the presence of other ligands (PPh₃, *o*-Tol₃P, Cy₃P, *t*-Bu₃P, dppe, dppp, dppb, dppf, *rac*-BINAP, *i*-Pr-Xantphos, *t*-Bu-Xantphos, and DPEphos), PhCON₃ was produced from PhI in only 0-6% yield under a variety of conditions.

Table S1. Pd-catalyzed azidocarbonylation of iodoarenes (10 mmol) in the presence of [(Xantphos)PdCl₂]-CH₂Cl₂ (0.2 mol %) and PMHS.^a All yields are isolated yields of pure products.



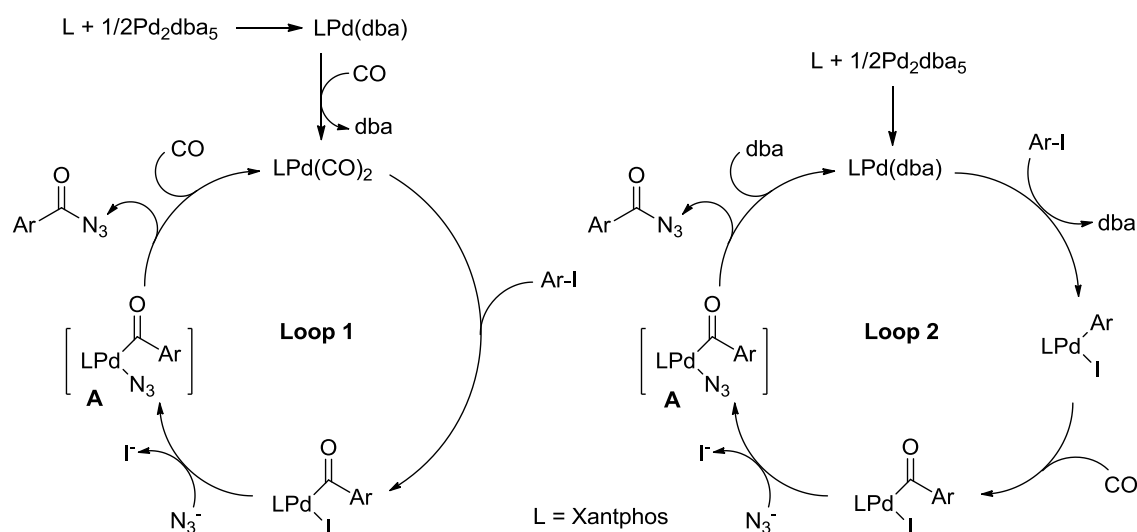
^a Reaction conditions: ArI (10 mmol), NaN₃ (12 mmol), [(Xantphos)PdCl₂]-CH₂Cl₂ (0.02 mmol; 0.2 mol % Pd), K₂CO₃ (0.2 mmol; 2 mol %), in THF (0.5 mL) and water (2 mL) at 23 °C. ^b 2 mL THF. ^c 3 mL THF.



Scheme S5. Examples of transformations of an aroyl azide produced by the azidocarbonylation reaction and used without isolation.

Considering the explosive properties and shock-sensitivity of certain (but not all) organic azides, a detailed safety study of the Pd-catalyzed azidocarbonylation reaction has been carried out. As a result of this evaluation, the reaction and its products have been found safe to perform and use on the laboratory scale. In accord with this conclusion, we have not had a single accident working on the azidocarbonylation project. It is worth to emphasize, however, that all azido derivatives should always be handled with care.

Experimental and computational⁷ studies have identified two main reaction pathways for the process (Scheme S6), both involving Ar-I oxidative addition to Pd(0) as the rate-determining step.



Scheme S6. Established mechanisms of Pd-catalyzed azidocarbonylation of aryl iodides in the presence of CO in excess (Loop 1) and under CO-deficient conditions (Loop 2).

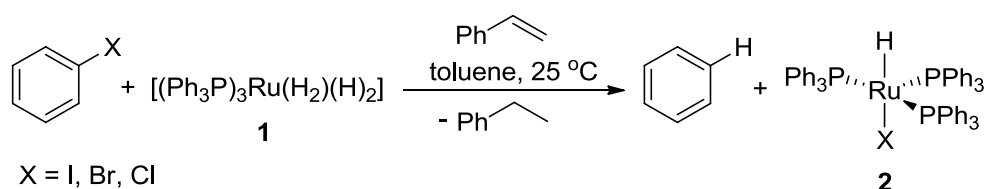
In the presence of CO in excess, ArI is activated by the less electron-rich Pd(0) bearing both Xantphos and CO (Scheme S6, Loop 1). Under CO-deficient conditions, a lower-energy pathway is followed (Scheme S6, Loop 2), involving Ar-I oxidative

⁷ The DFT computational studies were performed by Dr. C. L. McMullin and Prof. S. A. Macgregor (Heriot-Watt University, U.K.).

addition to more reactive, carbonyl-free (Xantphos)Pd(0). Mass transfer in the triphasic liquid-liquid-gas system employed for the reaction plays an important role in the competition between these two reaction channels, uniformly leading to a common aryl azido intermediate **A** that undergoes exceedingly facile ArCO-N₃ reductive elimination. Both catalytic loops have been modeled stoichiometrically by the synthesis and full characterization, including by X-ray diffraction, of the intermediates involved: [(Xantphos)Pd(dba)], [(Xantphos)Pd(CO)₂], [(Xantphos)Pd(COPh)I], and [(Xantphos)Pd(Ph)(N₃)].

II. Mechanistic Study of Aryl Halide Activation with Ruthenium (II) Hydrido Complexes

In 2011, an interesting Ph-X (X = Cl, Br, I) bond cleavage reaction with [(Ph₃P)₃Ru(H₂)(H)₂] (**1**) in the presence of styrene (Scheme S7) was found in our laboratories.⁸



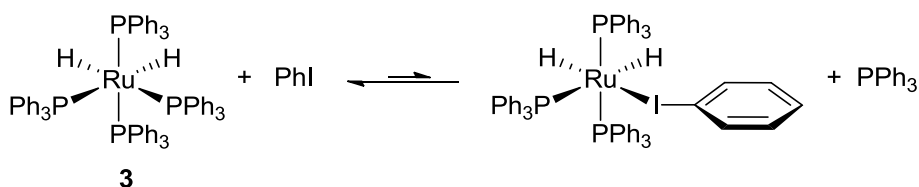
Scheme S7. Ph-X activation with [(Ph₃P)₃Ru(H₂)(H)₂]-styrene.

Such facile Ph-X activation with ruthenium at room temperature is unprecedented. It is particularly intriguing that **1** is devoid of highly basic, bulky phosphine ligands that are critical for efficient Ar-X activation, especially for X = Cl.⁹ Preliminary mechanistic

⁸ (a) Muñoz, B. K., 2011, unpublished results. (b) Miloserdov, F. M.; McKay, D.; Muñoz, B. K.; Samouei, H.; Macgregor, S. A.; Grushin, V. V., submitted for publication.

⁹ (a) Grushin, V. V.; Alper, H. *Chem. Rev.* 1994, **94**, 1047. (b) Grushin, V. V.; Alper, H. *Top. Organomet. Chem.* 1999, **3**, 193. (c) Littke, A. F.; Fu, G. C. *Angew. Chem., Int. Ed.* 2002, **41**, 4176. (d) Bedford, R. B.; Cazin, C. S. J.; Holder, D. *Coord. Chem. Rev.* 2004, **248**, 2283.

studies have shown that the reaction of halobenzenes with **1**-styrene is a nonradical process and suggested that the reactive species might be 5-coordinate $[(\text{Ph}_3\text{P})_3\text{Ru}(\text{H})_2]$ that is generated by hydrogenation of styrene with **1**.^{8,10} This 16-e complex can also be produced upon dissociation of Ph_3P and N_2 from $[(\text{Ph}_3\text{P})_4\text{Ru}(\text{H})_2]$ (**3**) and $[(\text{Ph}_3\text{P})_3\text{Ru}(\text{H})_2(\text{N}_2)]$ (**4**), respectively.^{10b} Therefore, both **3** and **4** have also been tested in the reaction and found⁸ to activate phenyl halides. Two more interesting observations have been made.^{8b,11} One is that in the presence of PhI in large excess (ca. 300 equiv), **3** rapidly equilibrates with *mer*- $[(\text{Ph}_3\text{P})_3\text{Ru}(\text{H})_2(\text{PhI})]$ (Scheme S8).



Scheme S8. Equilibrium between $[(\text{Ph}_3\text{P})_4\text{Ru}(\text{H})_2]$ (**3**) and $[(\text{Ph}_3\text{P})_3\text{Ru}(\text{H})_2(\text{PhI})]$.

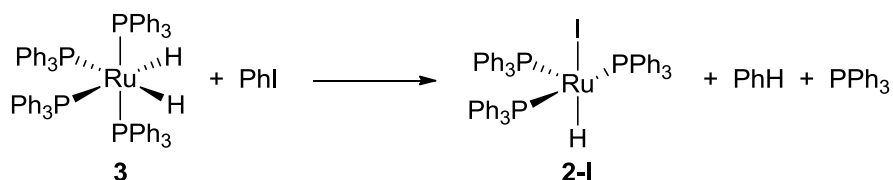
The most striking finding, however, has been the *linear* decay of **3** and formation of **2-I** in the reaction with PhI in excess (Scheme S9) until nearly full conversion of **3** (90-95%). In other words, the rates of disappearance of **3** and of the formation of **2-I** were concentration independent, i.e. *zeroth* order. Such arresting kinetic behavior has not been reported for inert bond activation with transition metal complexes and cannot be rationalized by conventional kinetic schemes.¹² Therefore, we have carried out a detailed experimental and computational study of the reactions of $[(\text{Ph}_3\text{P})_4\text{Ru}(\text{H})_2]$ (**3**) with iodo-, bromo-, and chlorobenzene in order to establish their mechanism.^{8b,13}

¹⁰ (a) $[(\text{Ph}_3\text{P})_3\text{Ru}(\text{H})_2]$ is an elusive species that has been convincingly proposed as a highly reactive intermediate but never unambiguously characterized in the solid state or in solution.^{10b} (b) Samouei, H.; Miloserdov, F. M.; Escudero-Adán, E. C.; Grushin, V. V. *Organometallics* 2014, **33**, 7279 and references cited therein.

¹¹ Samouei, H., 2013, unpublished results.

¹² Espenson, J. H. *Chemical Kinetics and Reaction Mechanisms, 2nd Ed.*; McGraw-Hill: New York, 1995.

¹³ The DFT computational studies were performed by Dr. D. McKay and Prof. S. A. Macgregor (Heriot-Watt University, U.K.).



Scheme S9. Reaction of $[(\text{Ph}_3\text{P})_4\text{Ru}(\text{H}_2)]$ (**3**) with PhI.

The rate law (Eq S1) for the activation of PhI with **3** (Scheme S9), as determined by the method of initial rates, shows that the reaction is first order in both **3** and PhI and negative first order in PPh_3 . This is consistent with a mechanism involving pre-equilibrium between **3** and *mer*- $[(\text{Ph}_3\text{P})_3\text{Ru}(\text{H})_2(\text{PhI})]$ (Scheme S8). However, Eq S1 could not account for the observed zeroth order behavior. We therefore proposed that this discrepancy might be due to autocatalysis,¹⁴ and studied the reaction of **3** with PhI after full conversion to **2-I** in more detail. Monitoring the reaction of **3** with PhI by ^1H and $^{31}\text{P}\{^1\text{H}\}$ NMR revealed a startling kinetic profile showing that after the nearly quantitative formation of **2-I**, it decayed exponentially (Figure S1).

$$d[\mathbf{2-I}]/dt = k_1[\mathbf{3}][\text{PhI}][\text{PPh}_3]^{-1} \quad (\text{Eq S1})$$

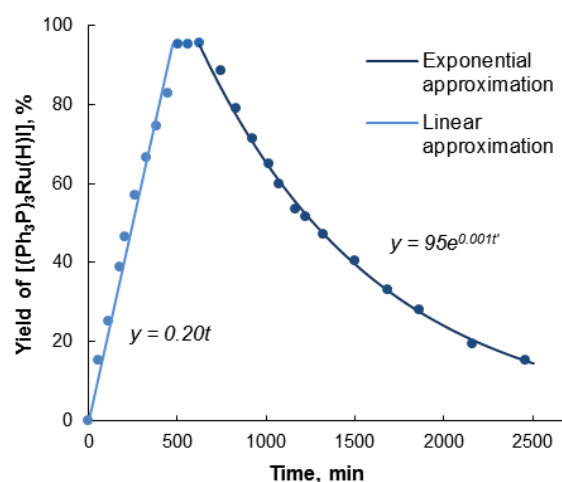


Figure S1. Kinetic profile from the reaction of **3** (0.0051 M) with PhI (1.49 M) at 25 °C.

¹⁴ (a) Singh, K. J.; Hoepker, A. C.; Collum, D. B. *J. Am. Chem. Soc.* 2008, *130*, 18008. (b) Hoepker, A. C.; Gupta, L.; Ma, Y.; Faggini, M. F.; Collum, D. B. *J. Am. Chem. Soc.* 2011, *133*, 7135.

The final product of the reaction appeared to be $[(\text{Ph}_3\text{P})_4\text{Ru}_2\text{I}_2(\mu\text{-I})_2]$ (**5**; Figure S2), indicating that **2-I** produced in the first step reacts with PhI (excess) to give **5** along with PhH and one equiv of PPh_3 (Scheme S10). An independent kinetic study of the reaction of **2-I** with PhI leading to **5** has produced the kinetic law presented in Eq S2. Like the first step, i.e. the formation of **2-I** from **3** (Scheme S9), the reaction of **2-I** with PhI is positive first order in both the Ru complex (**2-I**) and PhI and negative first order in PPh_3 .

$$-d[\mathbf{2-I}]/dt = k_2[\mathbf{2-I}][\text{PhI}][\text{PPh}_3]^{-1} \quad (\text{Eq S2})$$

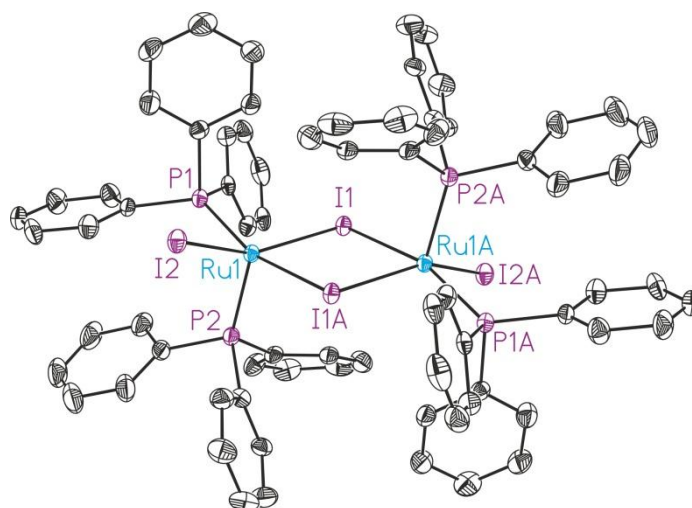
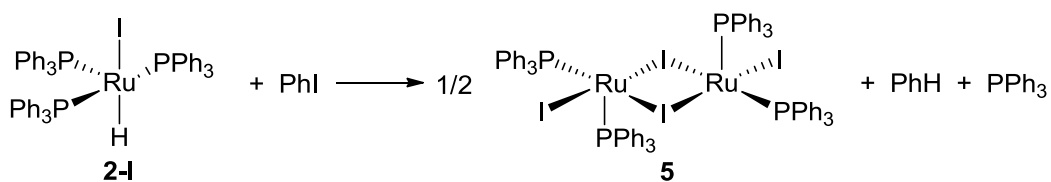
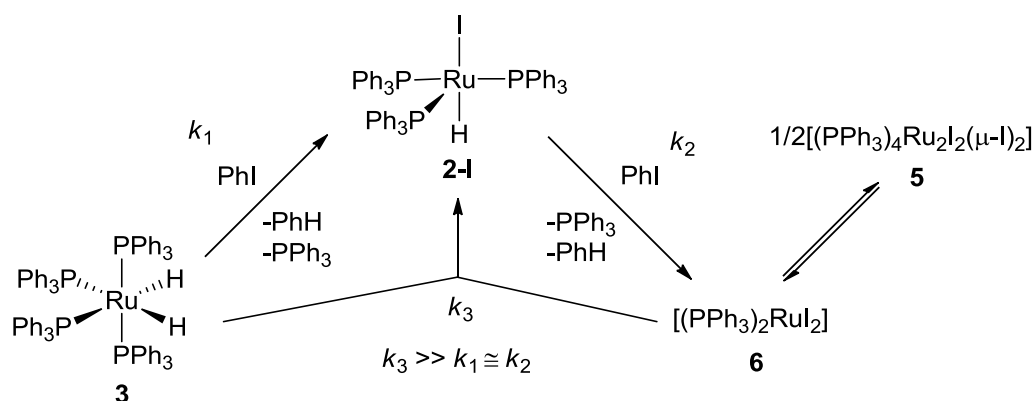


Figure S2. ORTEP drawing of $[(\text{Ph}_3\text{P})_4\text{Ru}_2\text{I}_2(\mu\text{-I})_2]$ (**5**) with all H atoms omitted for clarity and thermal ellipsoids drawn to the 50% probability level.



Scheme S10. Reaction of $[(\text{Ph}_3\text{P})_3\text{Ru}(\text{H})\text{I}]$ (**2-I**) with PhI.

Once formed in the first step, **2-I** reacts with PhI after PPh₃ dissociation (Eq S2) to give [(Ph₃P)₂RuI₂] (**6**) that may dimerize to produce **5** (see above). It has been shown in an independent experiment, however, that **6** comproportionates with the as yet unreacted starting dihydride **3** to revive **2-I** in a reaction that is considerably faster than both that between PhI and **3** and the dimerization leading to **5** (Scheme S11). In this way, the condition for the autocatalysis ($k_3 \gg k_2$) is met.



Scheme S11. Mechanistic scheme for autocatalysis in the reaction of **3** with PhI.

The coincidental similarity of $k_1 = 1.24 \times 10^{-5} \text{ min}^{-1}$ (1st step, Eq S1) and $k_2 = 6.8 \times 10^{-6} \text{ min}^{-1}$ (2nd step, Eq S2) at 25 °C results in the zeroth order behavior observed for the decay of **3** and the formation of **2-I**. This rare kinetic case is methodologically similar to the autocatalysis in the lithium diisopropylamide-mediated ortho-lithiation reactions studied by Collum.¹⁴ The model presented in Scheme S11 provides an excellent fit to the kinetic data, as shown in Figure S3. Similar studies have been conducted for the reactions of **3** with PhBr (50 °C) and PhCl (neat, 55 °C).

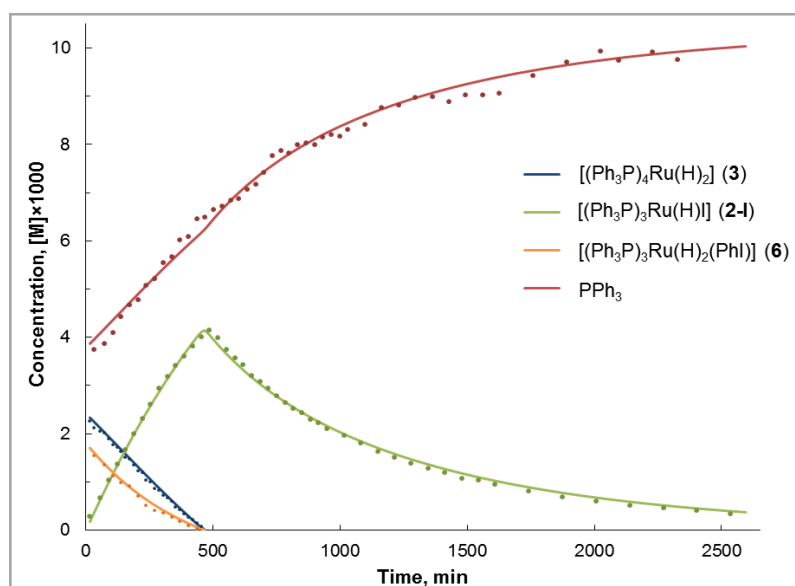


Figure S3. Plot of concentrations vs time for the reaction of $[(\text{Ph}_3\text{P})_4\text{Ru}(\text{H})_2]$ (0.0042 M initial concentration) with PhI (1.49 M) at 25 °C, as monitored by $^1\text{H}\{^31\text{P}\}$ and $^31\text{P}\{^1\text{H}\}$ NMR spectroscopy. Data points are from the experimental measurements. The curves are from the kinetic model.

The performed DFT study¹³ accords with the experimental data showing that both the initial and onward reactions involve phosphine pre-dissociation from Ru as the first step. Halobenzene coordination to Ru through the halogen atom and subsequent rearrangement to a π -bound η^2 -PhX complex leads to the efficient Ph-X bond breaking, followed by Ph-H reductive elimination. The calculations suggest that the rate-determining step in all of the reactions of PhX (X = I, Br, Cl) but one is the cleavage of the C-X bond. The only exception, likely for steric reasons, is the reaction of **3** with PhI, where the highest barrier was calculated for the formation of the π -bound η^2 -PhX adduct. The computed ΔG^\ddagger values are in excellent agreement with those derived from the experimentally determined rate constants k_1 and k_2 using the Eyring equation (Table S2).

Table S2. Computed and experimentally determined ΔG^\ddagger values (kcal/mol) for Ph-X activation with **3** (1st step) and **2** (2nd step).

	1 st Ph-X Activation		2 nd Ph-X Activation	
	DFT	Experiment	DFT	Experiment
I	+27.8	+26.6	+27.4	+26.9
Br	+30.4	+29.5	+31.3	+29.7
Cl	+34.0	-	+33.7	+32.4

III. Alcoholysis of Fluoroform

In recent years, fluoroform (CHF_3 , HFC-23) has become a center of attention as a potent greenhouse gas with the second highest global warming potential of 11,700 (100 years) and a long, 264-year atmospheric lifetime. The continuous release of HFC-23 waste streams into the atmosphere should be stopped as otherwise it will likely lead to an ecological disaster.¹⁵ Therefore, the large quantities of the side-generated fluoroform should be destroyed or utilized.¹⁶ As fluoroform currently lacks industrial applications on a scale comparable with that of its production, the destruction of HFC-23 is the only viable solution to the problem.¹⁷ The available methods to eliminate large quantities of fluoroform, a flame retardant, are thermal oxidation, catalytic hydrolysis, and plasma destruction. All of these processes are costly and none of them is free from considerable drawbacks. Therefore, it is highly desirable to develop alternative utilization processes.

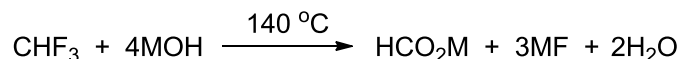
We have studied reactions of fluoroform with simple bases, NaOH and KOH, as well as with alkali metal alkoxides in the corresponding alcohols under mild conditions. Surprisingly little has been previously reported on such reactions.

¹⁵ Bomgardner, M. M. *Chem. Eng. News* 2013, 91, 6.

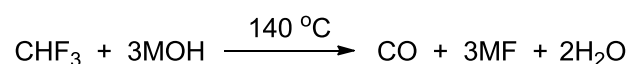
¹⁶ Grushin, V. V. *Chim. Oggi* 2014, 32, 81.

¹⁷ Han, W.; Li, Y; Tang, H; Liu, H *J. Fluorine Chem.* 2012, 140, 7.

We have found¹⁸ that CHF₃ readily reacts with NaOH or KOH under solvent-free conditions at 140 °C and initial pressure of 50 psi. The reaction produces the corresponding formate salt (55-65%) and fluoride as the main products along with small quantities (ca. 10%) of CO (Scheme S12).



M = Na, K



M = Na, K

Scheme S12. Reactions of fluoroform with alkali metal hydroxides.

The reactions of fluoroform with NaOH in various alcohols ROH occur in the temperature range of 80-120 °C to give NaF, HCO₂Na, and the corresponding orthoformate HC(OR)₃. There have been no publications reporting the formation of orthoformates from fluoroform, although the reaction of chloroform with alkali metal alkoxides is widely used to prepare the corresponding orthoformate esters.¹⁹ The conversion of the base did not exceed 45-60%, with the yield of the orthoformate decreasing in the order R = Et (20%) > Me (15%) > *i*-Pr (10%) > *t*-Bu (<0.5%). The formation of small quantities of the corresponding ROCHF₂ (ca. 0.5%) was observed in all of these reactions.

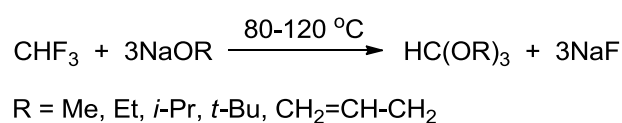
Against previously reported observations,²⁰ fluoroform is sufficiently reactive toward MOR (M = Na, K) in ROH (R = Me, Et, *i*-Pr, *t*-Bu, and Allyl) to give the corresponding orthoformate esters in 55-90% yield, provided the reactions are carried out at 80-120 °C

¹⁸ Miloserdov, F. M.; Grushin, V. V. *J. Fluorine Chem.* 2014, 167, 105.

¹⁹ DeWolfe, R. H. *Carboxylic Ortho Acid Derivatives; Preparation and Synthetic Applications* (Organic Chemistry, a Series of Monographs, Vol. 14); Academic Press: New York, 1970.

²⁰ Hine, J.; Dowell, A. M. Jr.; Singley, J. E. Jr. *J. Am. Chem. Soc.* 1956, 78, 479.

(Scheme S13). Particularly notable is the formation of $\text{HC}(\text{OBu-}t)_3$ (75-80% yield), an exotic organic compound that has been previously synthesized only once and only in 3% yield.²¹ The reaction of CHF_3 with $t\text{-BuONa}$ in $t\text{-BuOH}$ has been successfully scaled up (0.1 mol) to furnish pure $\text{HC}(\text{OBu-}t)_3$ in 62% isolated yield (4.8 g). The structure of this compound has been confirmed by single-crystal X-ray diffraction (Figure S4).



Scheme S13. Reactions of fluoroform with alkali metal alkoxides.

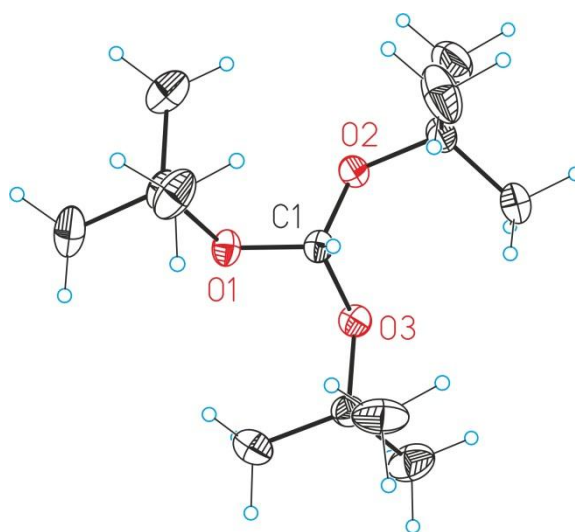


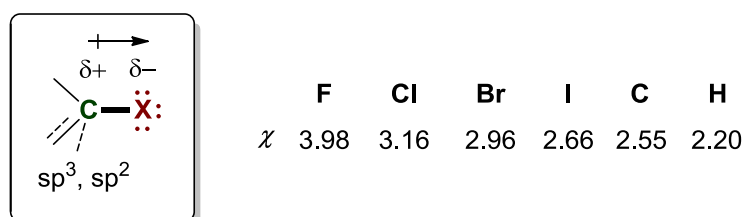
Figure S4. ORTEP drawing of $\text{HC}(\text{OBu-}t)_3$ with thermal ellipsoids drawn at the 50% probability level.

²¹ Hine, J.; Dalsin, P. D.; Schreck, J. O. *J. Org. Chem.* 1969, *34*, 3609.

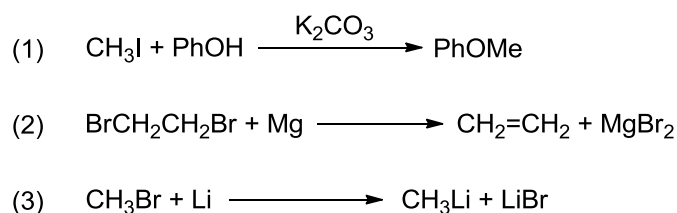
UNIVERSITAT ROVIRA I VIRGILI
NEW TRANSFORMATIONS BASED ON ACTIVATION OF INERT CARBON-HALOGEN BONDS WITH AND WITHOUT TRANSITION
Miloserdov Fedor Mikhailovich
Dipòsit Legal: T 825-2015

*General Introduction:
Activation of Inert Carbon-Halogen Bonds*

Organic halides (halocarbons) are chemical compounds that contain a covalent carbon-halogen bond C-X, where X = F, Cl, Br or I. Chemical properties of halocarbons are largely attributed to the higher electronegativity^{1,2} of the halogens relative to carbon, which results in polarization of the C-X bond and induction of a partial positive charge on the carbon atom (Scheme 1).³ As a result, in chemical transformations organic halides usually participate as electrophiles or oxidants or both (Scheme 2). The reactivity of the carbon-halogen bond varies significantly depending on the nature of both X and the organic group R in the organic halide RX.⁴ To define what is implied by activation of inert carbon-halogen bonds, we will provide an overview of the main types of chemical transformations of organic halides and their mechanisms.



Scheme 1. Pauling electronegativity¹ values for C, H, and halogens (X).²



Scheme 2. Examples of chemical transformations where a halocarbon reacts as an electrophile (1), an oxidant (2), and both an electrophile and an oxidant (3).

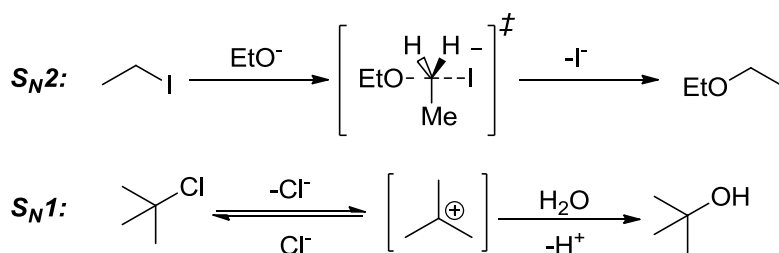
¹ Pauling, L. *J. Am. Chem. Soc.* 1932, 54, 3570.

² Allred, A. L. *J. Inorg. Nucl. Chem.* 1961, 17, 215.

³ Vollhardt, K. P. C.; Schore, N. E. *Organic Chemistry: Structure and Function 6th Ed.*; W. H. Freeman and Company: New York, 2011.

⁴ Patai S., Ed. *The Chemistry of Carbon-Halogen Bond*; John Wiley & Sons: Bristol, 1973.

Substitution reactions at the C(sp³)-X bond. Nucleophilic substitution reactions of alkyl halides typically proceed via S_N2 or S_N1 mechanisms (Scheme 3).^{3,5} The backside attack of a nucleophile in S_N2 reactions can occur with substrates that are not too sterically hindered, and, as a result, this mechanism can operate only for primary and some secondary alkyl halides. For secondary alkyl halides, S_N2 reactions occur stereospecifically, with inversion of configuration (Walden inversion),⁶ which makes these reactions a useful synthetic tool to achieve the desired stereochemistry in organic synthesis. The reactivity of alkyl halides RX in S_N2 reactions is in the order X = I > Br > Cl > F,⁷ correlating with both the strength of the R-X bond and the ability of the heavier halides to be a better leaving group.⁴



Scheme 3. Examples of S_N2 (top) and S_N1 (bottom) reactions.

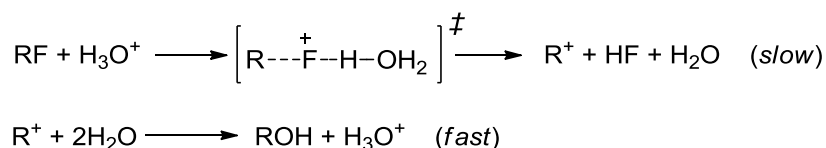
Nucleophilic substitution reactions of tertiary alkyl halides are conventionally governed by S_N1 mechanism. Initial ionization of the C-X bond results in the formation of a stable tertiary carbocation, which then quickly reacts with the nucleophile to give the product (Scheme 3, bottom). As carbocations usually cannot be obtained under basic conditions, S_N1 mechanism is typically proposed only for reactions in acidic or neutral

⁵ (a) March, J. *Advanced organic chemistry: reactions, mechanisms and structure*, 4th Ed.; John Wiley & Sons: New York, 1992. (b) Clayden, J.; Greeves, N.; Warren, S.; Wothers, P. *Organic Chemistry*, Oxford University Press: New York, 2008.

⁶ Walden, P. *Ber. Dtsch. Chem. Ges.* 1896, 29, 133.

⁷ (a) For instance, primary alkyl fluorides are ca. 10⁴ times less reactive toward basic alcoholysis than their bromide counterparts.^{7b} (b) Chapman, N. B.; Levy, J. L. *J. Chem. Soc.* 1952, 1673.

media.⁸ In certain cases, S_N1 substitution can also occur at secondary and, even more rarely, primary carbon atoms. Such reactions are observed for alkyl halide substrates bearing a strong carbocation-stabilizing group such as OR or NR₂. In contrast with S_N2 reactions, S_N1 displacement is not stereospecific, leading to racemization because the carbocation intermediate is planar and therefore can be attacked by nucleophiles from both sides of the plane. Ionization of the C-X bond is the rate limiting step of S_N1 substitution.⁹ As a result, the reaction is significantly accelerated in polar solvents and occurs more readily when a more stable carbocation and a better leaving group are involved. The same order of reactivity X = I > Br > Cl > F is usually observed for S_N1 nucleophilic displacement.^{4,10} It is worth to note that S_N1 hydrolysis can be promoted by Lewis acids (often Ag⁺) and, for some alkyl fluorides, by Brønsted acids. For instance, hydrolysis of alkyl fluorides produces HF, which autocatalyzes the transformation (Scheme 4).^{10b} Nucleophilic displacement reactions of allyl-substituted haloalkanes (S_N1' or S_N2') can be accompanied with migration of the double bond.



Scheme 4. Acid-autocatalyzed hydrolysis of alkyl fluorides.

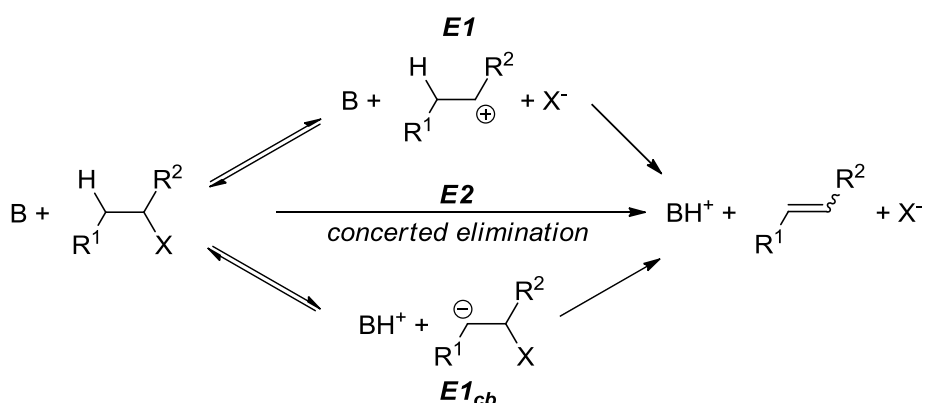
β-Elimination reactions of alkyl halides. Elimination of HX from alkyl halides to give alkenes is another classical organic transformation. Three possible mechanisms for

⁸ Grossman, R.B. *The Art of Writing Reasonable Organic Reaction Mechanisms, 2nd Ed.*; Springer-Verlag: New York, 2003.

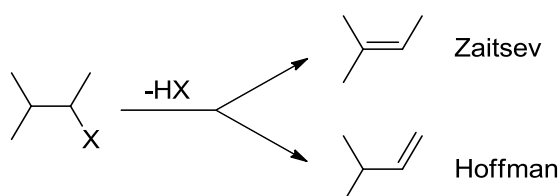
⁹ Bateman, L. C.; Church, M. G.; Hughes, E. D.; Ingold, C. K.; Taher, N. A. *J. Chem. Soc.* 1940, 979.

¹⁰ (a) In general, alkyl fluorides are more stable and much less reactive toward nucleophiles than their heavier halogen analogues. For instance, hydrolysis of secondary and tertiary fluoroalkanes occurs only at 120-160 °C.^{10b} There are, however, some exceptions, such as the Friedel-Crafts alkylation with RX where the reverse order of reactivity is observed: X = F > Cl > Br > I, with alkyl fluorides being most reactive.^{10c} (b) Chapman, N. B.; Levy, J. L. *J. Chem. Soc.* 1952, 1677. (c) Calloway, N. O. *J. Am. Chem. Soc.* 1937, 59, 1474.

HX elimination, E1, E2, and E1_{cb} are shown in Scheme 5.⁴ The E1 mechanism is similar to that of S_N1, involving halide dissociation leading to the corresponding carbocationic species. The latter strongly favors a Zaitsev-type transition state for the subsequent deprotonation and, as a result, more substituted alkenes are usually produced (Scheme 6).⁴ E1 reactions proceed under conditions that are similar to those for S_N1 reactions and are also favored by good leaving groups and occur more readily for the heavier halides.



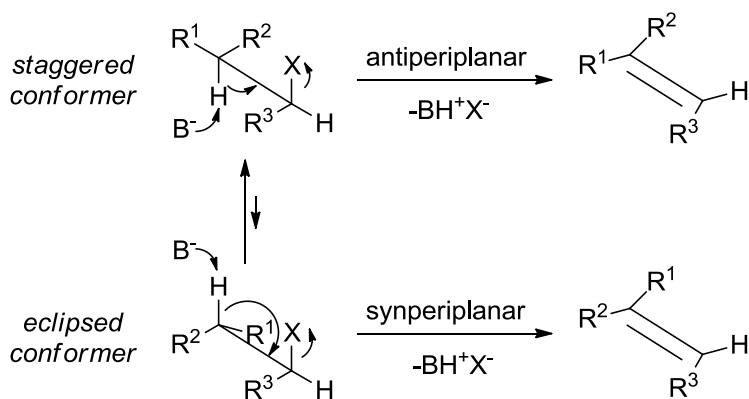
Scheme 5. E1, E2 and E1_{cb} mechanism for β-Elimination reaction.



Scheme 6. The Zaitsev and Hoffman outcomes of HX elimination reactions.

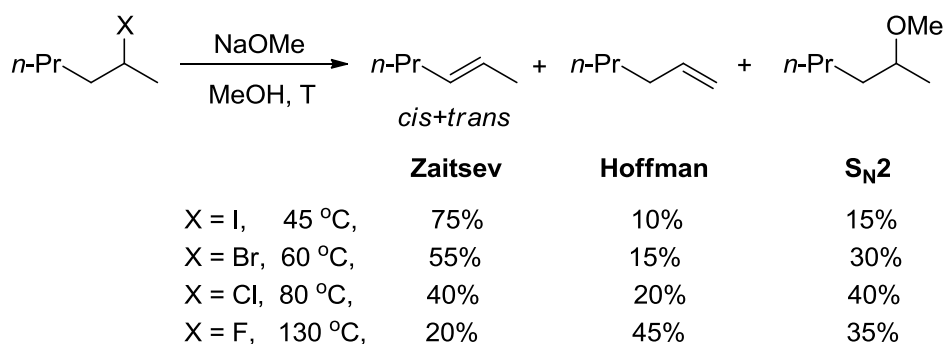
Under basic conditions, E1_{cb} and E2 elimination pathways are more common. For substrates with significantly acidic β-hydrogen atoms, deprotonation precedes the C-X bond cleavage (E1_{cb}). In the vast majority of cases, however, the E2 mechanism

operates, i.e. HX eliminates in a concerted manner. Such transformation require the formation of a periplanar intermediate where the orbitals of the reacting C-H and C-X bonds are parallel (Scheme 7). Two conformations are generally possible for C(sp³)-X substrates: synperiplanar (eclipsed) and antiperiplanar (staggered).⁸ As the latter is usually more stable, the antiperiplanar transition state lies lower in energy. The order of reactivity with respect to the nature of the halogen for E2 and E1 reactions is the same (I > Br > Cl > F). The Hoffman to Zaitsev olefin product ratio in E2 reactions strongly depends on the nature of the halogen. As can be seen from Scheme 8, the quantity of the Hoffman elimination product increases in the order F > Cl > Br > I.¹¹ This is rationalized in terms of the E2 transition state being of considerable E1-character for weaker C-X bonds and better leaving groups X⁻, yet more like E1_{cb} for strongly bound, more electronegative halides (Scheme 9). Stronger stabilization of the thus induced partial positive charge in the branched transition state and the partial negative charge in the terminal transition state accounts for the isomer ratio observed.¹¹

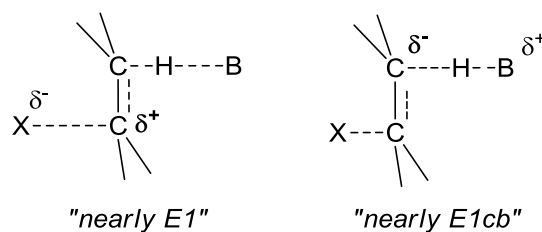


Scheme 7. Antiperiplanar and synperiplanar pathways for E2 elimination.

¹¹ Bartsch, R. A.; Bunnett, J. F. *J. Am. Chem. Soc.* 1968, *90*, 408.



Scheme 8. The Zaitsev, Hoffman, and S_N2 products of basic methanolysis of 2-halohexanes.



Scheme 9. E2 transition states approaching E1 (left) and E1_{cb} (right) intermediates.

α -Elimination reactions. Haloalkanes can react via HX elimination from the same carbon atom to produce carbenes. The simplest example of α -elimination of HX is the generation of dihalocarbenes from the corresponding haloforms and a base (Scheme 10). In many instances, biphasic conditions facilitate this process.¹² The reaction proceeds via a mechanism similar to that of E1_{cb}, the initial step being deprotonation to give the trihaloalkyl anion, which then eliminates the halide to give the carbene.¹³ The latter can be used for numerous transformations, including the formation of cyclopropanes,¹² ring expansion,¹⁴ the Reimer-Tiemann formylation,¹⁵ the synthesis of

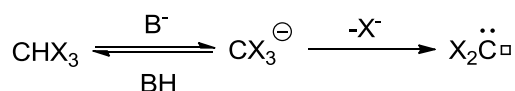
¹² Fedoryński, M. *Chem. Rev.* 2003, 103, 1099.

¹³ Hine, J.; Dowell, A. M., Jr.; Singley, J. E., Jr. *J. Am. Chem. Soc.* 1956, 78, 479.

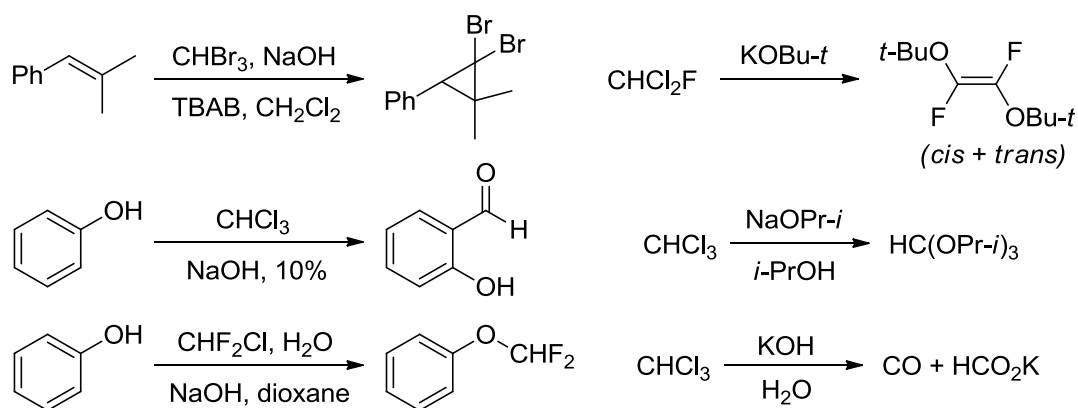
¹⁴ (a) Alexander, E. R.; Herrick, A. B.; Roder, T. M. *J. Am. Chem. Soc.* 1950, 72, 2760. (b) Rees, C. W.; Smithen, C. E. *J. Chem. Soc.* 1964, 938.

¹⁵ Wynberg, H. *Chem. Rev.* 1960, 60, 169.

orthoformates,¹⁶ and symmetric alkenes,¹⁷ or, in certain cases, undergoes hydrolysis to CO and the formate anion (Scheme 11). For basic hydrolysis, the following order of reactivity has been observed: $\text{CHBrClF} \gg \text{CHBrCl}_2 > \text{CHBr}_2\text{Cl} \approx \text{CHCl}_2\text{I} > \text{CHBr}_3 > \text{CHCl}_3 \gg \text{CHF}_3$.¹³ Because of the poor reactivity of fluoroform, CHClF_2 is conventionally employed to generate difluorocarbene.¹⁸



Scheme 10. Mechanism of dihalocarbene formation from haloforms.



Scheme 11. Examples of reactions involving dihalocarbene intermediates.

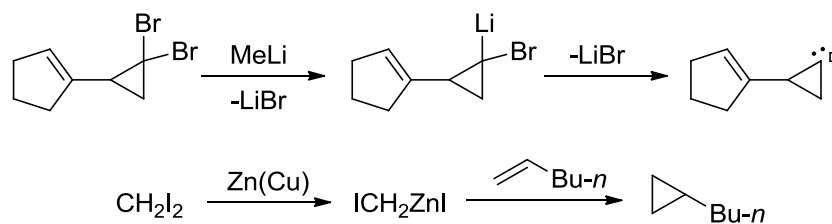
While alcoholysis of haloforms proceeds exclusively through the carbene intermediate, similar reactions of dihalomethanes predominantly occur via $\text{S}_{\text{N}}2$ nucleophilic substitution.¹⁹ *gem*-Dihaloalkanes can be used to generate carbenes or carbenoids via metal-halide exchange or metalation pathways (Scheme 12). For example, the CH_2I_2 -Zn/Cu system gives rise to ICH_2ZnI , a carbenoid that is widely used in organic synthesis for alkene cyclopropanation (the Simmons-Smith reaction).^{3,5,8}

¹⁶ DeWolfe, R. H. *Carboxylic Ortho Acid Derivatives; Preparation and Synthetic Applications* (Organic Chemistry, a Series of Monographs, Vol. 14); Academic Press: New York, 1970.

¹⁷ Hine, J.; Dalsin, P. D.; Schreck, J. O. *J. Org. Chem.* 1969, **34**, 3609.

¹⁸ Miller, T. G.; Thanassi, J. W. *J. Org. Chem.* 1960, **25**, 2009.

¹⁹ Hine, J.; Duke, R. B.; Glod, E. F. *J. Am. Chem. Soc.* 1969, **91**, 2317.



Scheme 12. Carbene and carbenoid generation from gem-dihaloalkanes.

Unreactive organic halides. The problem of aromatic carbon-halogen bond activation. The above-described nucleophilic displacement and elimination reactions of alkyl halides constitute one of the most important, powerful tools of organic synthesis. There are, however, classes of halocarbons that exhibit poor reactivity even under drastic conditions, e.g., many organic fluorides.^{7,10,13,20}

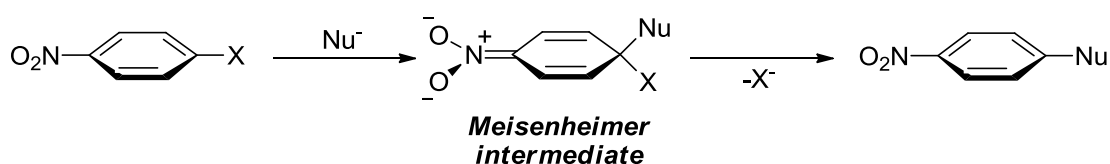
Most haloarenes (ArX) such as simple halobenzenes represent one of the most well-known examples of organic molecules bearing inert carbon-halogen bonds. Nucleophilic substitution at the aromatic carbon atom cannot occur via conventional S_N1 and S_N2 mechanisms for a number of reasons. Ionization of the Ar-X bond would produce the aryl cation Ar⁺ that is highly unstable. As a result, haloarenes cannot undergo nucleophilic displacement reactions via the S_N1 mechanism. Furthermore, S_N2 reactions of haloarenes do not occur because the back-side of the C-X bond is blocked by the aromatic ring for nucleophilic attack.

Aromatic compounds are ubiquitous in chemistry and biology. Modern drugs, crop protection agents, polymers, dyes, materials for electronics, explosives, etc. contain aromatic moieties. Given the exceptional importance of aromatic compounds in our everyday life, it is critical to find ways to activate and functionalize the unreactive Ar-X bonds for use of readily available and easily accessible, inexpensive aryl halides in

²⁰ (a) Richmond, T. G. *Top. Organomet. Chem.* **1999**, 3, 244. (b) Amii, H.; Uneyama, K. *Chem. Rev.* **2009**, 109, 2119. (c) Clot, E.; Eisenstein, O.; Jasim, N.; Macgregor, S. A.; McGrady, J. E.; Perutz, R. N. *Acc. Chem. Res.* **2011**, 44, 333. (d) Whittlesey, M. K.; Peris, E. *ACS Catal.* **2014**, 4, 3152.

synthesis. An overview of general methods for activation of haloarenes is provided below.

Aromatic nucleophilic substitution (S_NAr). One of the oldest ways to enhance the reactivity of the highly inert Ar-X bonds is to introduce strong electron-withdrawing substituents into other positions of the aromatic ring.²¹ Such electron-deficient aryl halides are susceptible to nucleophilic attack on the π -system of the ring, leading to the formation of the so-called Meisenheimer intermediate, which then undergoes halide elimination to give the product (Scheme 13).



Scheme 13. S_NAr reaction.

In S_NAr reactions, the initial nucleophilic attack disrupts aromaticity and gives the tetrahedral Meisenheimer complex that for many ArX substrates lies too high in energy and is therefore inaccessible. However, S_NAr substitution can efficiently proceed for the so-called *activated* haloarenes containing groups that delocalize the electron density and stabilize the Meisenheimer intermediate. For instance, aryl halides bearing strong electron-withdrawing substituents on the ring (NO_2 , CN, COR, etc.), polyhalogenated arenes (C_6F_6 , C_6Cl_6 , etc.), and halogenated nitrogen heterocycles such as pyridine, pyrazine, pyrimidine, etc.²² can react with nucleophiles via the S_NAr pathway. In a

²¹ (a) Miller, J. *Aromatic Nucleophilic Substitution*; Elsevier: London, 1968. (b) Terrier, F. *Nucleophilic Aromatic Displacement: The Influence of the Nitro Group*; VCH: New York, 1991.

²² In some heterocyclic systems also ANRORC mechanism, involving ring opening, is operative. See, for example: Van der Plas, H. C. *Acc. Chem. Res.* 1978, 11, 462.

considerable number of cases, Meisenheimer complexes are stable enough for isolation and characterization, including by single-crystal X-ray diffraction.²³ The reactivity of Meisenheimer-type substrates in S_NAr displacement processes strongly depends on (i) the overall electron-deficiency of the aromatic ring, (ii) the nature of the nucleophile, (iii) the nature of the leaving group, and (iv) reaction medium. In most instances, aromatic fluorides are the best substrates for S_NAr reactions. This is not always the case, however, for reactions conducted in aprotic media where fluoride is a poor nucleofuge.^{5,21} Although S_NAr reactions are broadly used in synthesis, their scope is limited by the need to have strong electron-withdrawing groups present on the aromatic ring of the substrate.

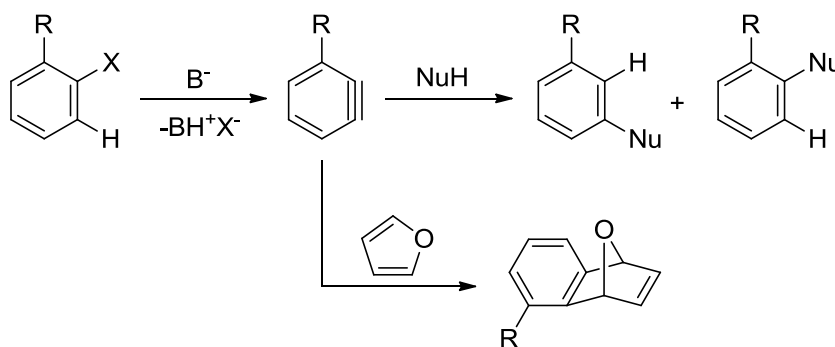
Aromatic nucleophilic substitution via aryne intermediates. As discussed above, β -elimination reactions are common for haloalkanes. A similar transformation is also known for aryl halides. Deprotonation of the C-H bond ortho to the halogen on the ring gives rise to arynes, highly reactive species that easily react with nucleophiles and undergo other transformations such as Diels-Alder cycloaddition²⁴ (Scheme 14). Strong bases such as KNH_2 , n -BuLi, and LDA or harsh conditions are usually needed to deprotonate aryl halides, which limits considerably the substrate scope of this reaction. Another major drawback of this methodology is the poor regioselectivity of nucleophilic attack on unsymmetrically substituted arynes. Both electronic and steric factors influence which of the two sites is predominantly attacked.^{5,25} Very recently, it was shown that the distortion of the aryne geometry can also have an impact on

²³ For original reports of structurally characterized Meisenheimer salts, see: (a) Ueda, H.; Sakabe, N.; Tanaka, J.; Furusaki, A. *Nature* 1967, *215*, 956. (b) Ueda, H.; Sakabe, N.; Tanaka, J.; Furusaki, A. *Bull. Chem. Soc. Jpn.* 1968, *41*, 2866. (c) Destro, R.; Gramaccioli, C. M.; Simonetta, M. *Acta Cryst.* 1968, *B24*, 1369. (d) Messmer, G. G.; Palenik, G. J. *Acta Crystallogr.* 1971, *B27*, 314.

²⁴ Wittig, G.; Pohmer, L. *Angew. Chem.* 1955, *67*, 348.

²⁵ Gilchrist, T.L. *Arynes*, In: *The Chemistry of Functional Groups, Supplement C*, pt. 1, Patai, S.; Rappoport, Z. Eds.; John Wiley & Sons: New York, 1983.

regioselectivity of nucleophilic addition to 3-substituted benzyne.²⁶ An unexpected order of reactivity ($\text{Br} > \text{I} > \text{Cl} \gg \text{F}$)²⁷ for the reaction of halobenzenes with KNH_2 in liquid ammonia has been rationalized in the seminal work of Roberts et al.²⁸ For the C-X bond cleavage step, the “normal” reactivity order ($\text{I} > \text{Br} > \text{Cl} > \text{F}$) is expected. However, for C-H deprotonation, the reverse order is observed ($\text{F} > \text{Cl} > \text{Br} > \text{I}$), paralleling the halogen atom electronegativities. It was therefore concluded,²⁸ that in the reactions of PhX with KNH_2 the rate determining step is deprotonation for $\text{X} = \text{I}$ and Br , but C-X cleavage for $\text{X} = \text{Cl}$ and F .⁵



Scheme 14. Generation and reactions of arynes.

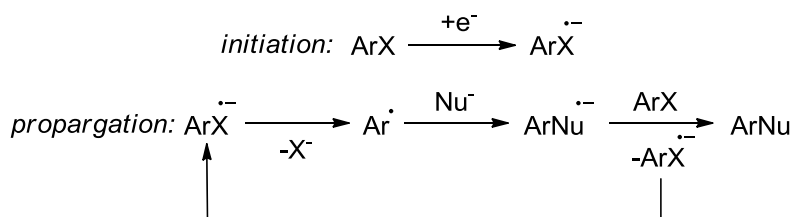
Radical nucleophilic aromatic substitution ($\text{S}_{\text{RN}}1$).²⁹ These reactions occur via a chain radical mechanism, as shown in Scheme 15. Single electron transfer (SET) to the haloarene substrate ArX produces the corresponding radical anion, which eliminates X^- to give the aryl radical. This radical then reacts with the anionic nucleophile to give the radical anion of the product. Finally, SET from the resultant $\text{ArNu}^{\cdot-}$ to ArX furnishes the desired substitution product with the simultaneous regeneration of $\text{ArX}^{\cdot-}$, etc.

²⁶ Medina, J. M.; Mackey, J. L.; Garg, N. K.; Houk, K. N. *J. Am. Chem. Soc.* 2014, *136*, 15798.

²⁷ Bergstrom, F. W.; Wright, R. E.; Chandler, C.; Gilkey, W. A. *J. Org. Chem.* 1936, *1*, 170.

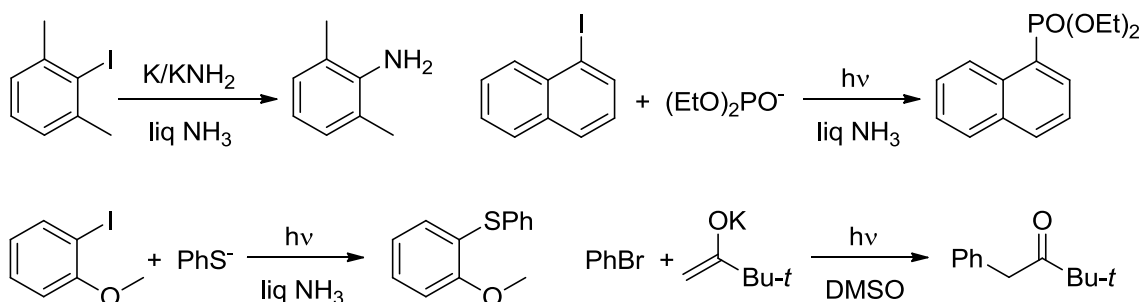
²⁸ Roberts, J.D.; Semenov, D.A.; Simmons, H.E., Jr.; Carlsmith, L.A. *J. Am. Chem. Soc.* 1956, *78*, 601.

²⁹ (a) Bunnett, J. F. *Acc. Chem. Res.* 1978, *11*, 413. (b) Rossi, R. A.; de Rossi, R. H. *Aromatic Substitution by the $\text{S}_{\text{RN}}1$ Mechanism*; American Chemical Society: Washington, DC, 1983.



Scheme 15. $S_{RN}1$ mechanism.

Nucleophilic reagents that can be used in $S_{RN}1$ reactions are usually limited to amides and some C-, S-, and P-nucleophiles. The order of reactivity of ArX (I > Br >> Cl > F) indicates that the radical anion dissociation is the rate-determining step of the entire process. Therefore, aryl bromides and iodides are usually the substrates of choice for $S_{RN}1$ transformations. Selected examples of $S_{RN}1$ reactions are shown in Scheme 16.

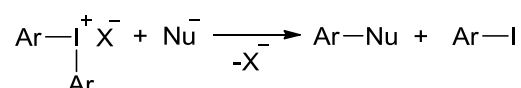


Scheme 16. Examples of aromatic $S_{RN}1$ reactions.

Oxidation of halogen on the aromatic ring. Reactions of diarylhalonium salts. A highly efficient way to enhance the reactivity of the Ar-X bond is to convert the substrate to the corresponding diarylhalonium cation.³⁰ A number of methods exist to synthesize aromatic iodonium salts, some of which are now commercially available.

³⁰ (a) Yusubov, M. S.; Maskaev, A. V.; Zhdankin, V. V. *ARKIVOC* 2011, 370. (b) Merritt, E. A.; Olofsson, B. *Angew. Chem., Int. Ed.* 2009, 48, 9052.

Diaryliodonium cations are highly reactive toward nucleophiles,^{30,31} as shown in Scheme 17. Many of such reactions can occur with excellent chemoselectivity at as low as room temperature. The mechanism of these transformations likely involves attack of a nucleophile on the iodine atom, followed by C-Nu reductive elimination from the resultant tricoordinate I(III) intermediate.



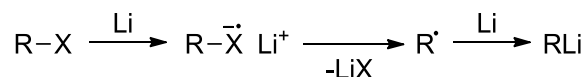
Scheme 17. Nucleophilic displacement reactions of diaryliodonium salts.

While there are many advantages in using diaryliodonium salts to effect aromatic nucleophilic substitution, this methodology also has some serious drawbacks. First, iodonium salts are costly and easily accessible only for a limited number of substituents on the ring. Second, the atom economy of the S_N reactions of iodonium salts is rather low since only one of the two aromatic rings undergoes substitution; the other ring along with the iodine atom is the leaving group (Scheme 17). Third, unsymmetrically substituted diaryliodonium cations [ArIAr']⁺ usually react with nucleophiles to give a mixture of all possible products: ArI, Ar'Nu, Ar'I, and ArNu. Finally, many neutral nucleophiles induce poorly selective radical reactions of iodonium salts. Aromatic bromonium and chloronium salts that have been known since the 1950's are both more reactive and much less accessible than their iodonium congeners.³²

³¹ (a) Grushin, V. V. *Acc. Chem. Res.* 1992, 25, 529. (b) Grushin, V. V. *Chem. Soc. Rev.* 2000, 29, 315.

³² Nesmeyanov, A. N.; Makarova, L. G.; Tolstaya, T. P. *Tetrahedron* 1957, 1, 145.

Reactions with active main group metals and halogen-metal exchange. Organic halides are convenient starting materials for the preparation of organometallic compounds by two major methods: metal insertion and halogen-metal exchange. Reactions of aryl halides with metallic Li, Na,³³ Mg, Ca,³⁴ and Zn³⁵ are initiated by SET from the metal to ArX, followed by halide elimination, e.g., Scheme 18. Similar to S_{RN}1 reactions, the order of reactivity of ArX toward metals is I > Br >> Cl >> F. Reactions of Li, Mg, and Zn with aryl (and alkyl) halides to prepare organometallic compounds are commonly used on both the laboratory and industrial scale.



Scheme 18. SET mechanism of the reaction of Li with organic halides.

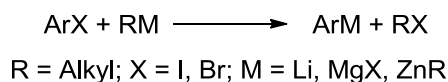
Alternatively, aryl halides might be conveniently converted to the corresponding Li, Mg, or Zn organometallic derivatives upon treatment with some metal alkyls (Scheme 19). The driving force behind this metal-halogen exchange reaction is the formation of a less basic and more stable metal aryl. The mechanism of this exchange has puzzled researchers for many decades and still remains unclear. For instance, evidence has been obtained for three distinct reaction pathways operating in the halogen-lithium exchange, namely (1) S_N2 substitution at the halogen atom; (2) via an “ate-complex”; and (3) involving SET, as shown in Scheme 20.^{8,36} Both aromatic bromides and iodides undergo efficient metal-halogen exchange reactions, whereas aryl chlorides react more sluggishly.

³³ Seyferth, D. *Organometallics* 2006, 25, 2.

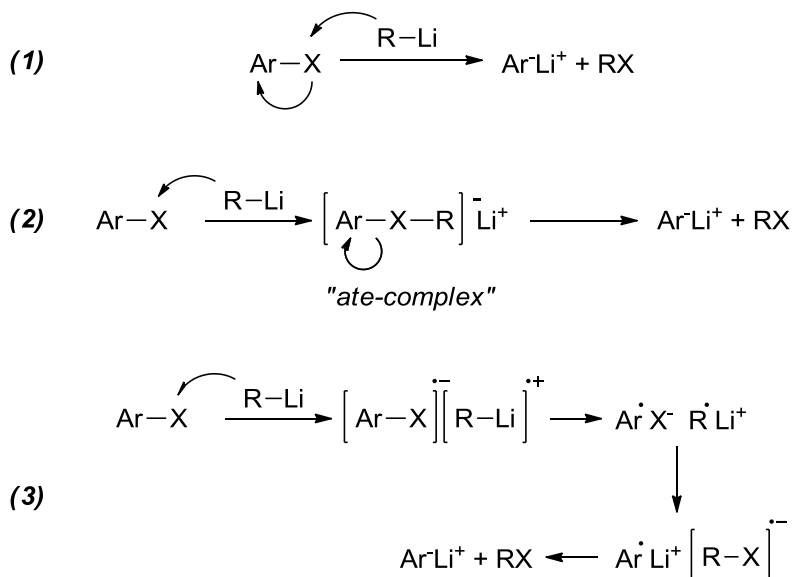
³⁴ Wu, T.-C.; Xiong, H.; Rieke, R. D. *J. Org. Chem.* 1990, 55, 5045.

³⁵ Zn is often considered as a main-block element. See, for example: Jensen, W. B. *J. Chem. Educ.* 2003, 80, 953.

³⁶ Bailey, W. F.; Patricia, J. J. *J. Organomet. Chem.* 1988, 352, 1.



Scheme 19. Metal-halide exchange reaction of aryl halides.



Scheme 20. Three mechanisms of Li-halogen exchange reactions of aryl halides.

The metal insertion reactions usually require room or elevated temperatures to occur. Under such conditions, strongly basic and nucleophilic products are not compatible with many functional groups. Homogeneous metal-halogen exchange can often be performed under much milder conditions. For example, some Li-halogen exchange reactions readily occur at as low as $-78\text{ }^{\circ}\text{C}$.⁸ Such low temperatures are also suitable for the preparation of Grignard reagents via RMgX/ArX exchange.³⁷

³⁷ Knochel, P.; Dohle, W.; Gommermann, N.; Kneisel, F. F.; Kopp, F.; Korn, T.; Sapountzis, I.; Vu, V. A. *Angew. Chem. Int. Ed.* 2003, 42, 4302.

Ar-X activation with transition metals. Stoichiometric and especially catalytic activation of aryl halides with transition metals is arguably the most powerful arylation methodology known to date. Since the original report by Ullmann and Bielecki³⁸ in 1901, copper-catalyzed/promoted reactions of aromatic iodides and bromides have been widely used in synthesis for carbon-heteroatom and carbon-carbon bond formation.³⁹ Over the last 40 years, however, the scene has been largely dominated by reactions catalyzed by palladium complexes which, with proper ligand design, can activate and functionalize not only aryl iodides and bromides, but even most unreactive chloroarenes.⁴⁰ Two critical findings of the late 1960's triggered the birth of Pd-catalyzed reactions of aromatic halides. In 1967-68, Moritani and Fujiwara⁴¹ and independently and simultaneously Heck⁴² reported that σ -phenyl palladium species generated by aromatic palladation or transmetalation can arylate olefins. In 1968, Fitton, Johnson, and McKeon⁴³ of Union Carbide communicated efficient activation of haloarenes via Ar-X oxidative addition to a zerovalent palladium complex $[(\text{Ph}_3\text{P})_4\text{Pd}]$. The highly creative, skillful merge of the two findings quickly followed to lead to the discovery of the catalytic Mizoroki-Heck reaction,^{44,45} the point of growth of what has now become the modern palladium catalytic chemistry of haloarenes.

The general idea of Pd-catalyzed S_N reactions of haloarenes is illustrated by Scheme 21 showing the overall equation and a widely accepted mechanism for the catalysis. In the first step, the Ar-X bond (X = I, Br, Cl) is activated and cleaved via oxidative

³⁸ Ullmann, F.; Bielecki, J. *Ber. Dtsch Chem. Ges.* 1901, *34*, 2174.

³⁹ For selected reviews, see: (a) Ley, S. V.; Thomas, A. W. *Angew. Chem. Int. Ed.* 2003, *42*, 5400. (b) Beletskaya, I. P.; Cheprakov, A. V. *Coord. Chem. Rev.* 2004, *248*, 2337. (c) Monnier, F.; Taillefer, M. *Angew. Chem. Int. Ed.* 2009, *48*, 6954.

⁴⁰ (a) Grushin, V. V.; Alper, H. *Chem. Rev.* 1994, *94*, 1047. (b) Grushin, V. V.; Alper, H. *Top. Organomet. Chem.* 1999, *3*, 193. (c) Littke, A. F.; Fu, G. C. *Angew. Chem. Int. Ed.* 2002, *41*, 4176.

⁴¹ Moritani, I.; Fujiwara, Y. *Tetrahedron Lett.* 1967, 1119.

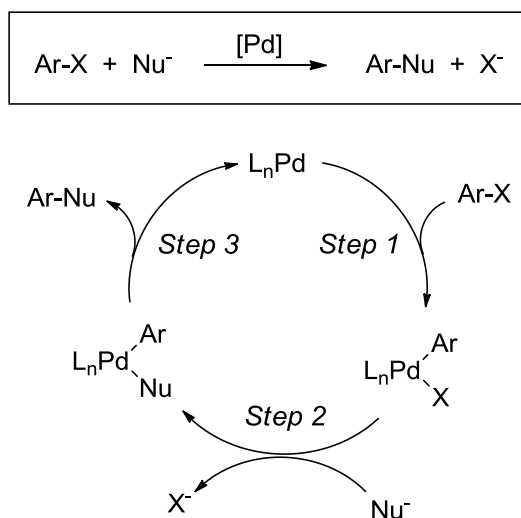
⁴² Heck, R. F. *J. Am. Chem. Soc.* 1968, *90*, 5518.

⁴³ Fitton, P.; Johnson, M. P.; McKeon, J. E. *J. Chem. Soc., Chem. Commun.* 1968, 6.

⁴⁴ Mizoroki, T.; Mori, K.; Ozaki, A. *Bull. Chem. Soc. Jpn.* 1971, *44*, 581.

⁴⁵ Heck, R. F.; Nolley, J. P. Jr. *J. Org. Chem.* 1972, *37*, 2320.

addition to a Pd(0) catalyst to produce a σ -aryl palladium halide complex. The latter then undergoes ligand exchange of the halide ligand with the incoming nucleophile (step 2), followed by reductive elimination of Ar-Nu, the desired product, and concomitant regeneration of catalytically active Pd(0) to commence another catalytic turnover. A broad variety of nucleophiles have been successfully employed in this catalytic process, including carbon nucleophiles, in which case the reaction is conventionally called coupling or cross-coupling.⁴⁶



Scheme 21. Pd-catalyzed aromatic nucleophilic displacement.

Most widely used are coupling reactions with Grignard reagents (Kumada-Corriu),⁴⁷ organotin (Stille)⁴⁸ and organozinc (Negishi)^{46,49} compounds, arylboronic acids (Suzuki-Miyaura),⁵⁰ alkynyl carbanions (Sonogashira),⁵¹ and arylsilanes (Hiyama).⁵² Palladium-catalyzed arylations of various N-, O-, S-, and P-nucleophiles have also been

⁴⁶ de Meijere, A.; Diederich, F., Eds. *Metal-Catalyzed Cross-Coupling Reactions, 2nd Ed.*; Wiley-VCH: Weinheim, 2004.

⁴⁷ Knappe, C. E. I.; Jacobi von Wangelin, A. *Chem. Soc. Rev.* 2011, 40, 4948.

⁴⁸ Espinet, P.; Echavarren, A. M. *Angew. Chem. Int. Ed.* 2004, 43, 4704.

⁴⁹ Casares, J. A.; Espinet, P.; Fuentes, B.; Salas, G. *J. Am. Chem. Soc.* 2007, 129, 3508.

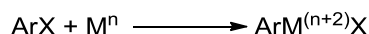
⁵⁰ Miyaura, N.; Suzuki, A. *Chem. Rev.* 1995, 95, 2457.

⁵¹ Chinchilla, R.; Nájera, C. *Chem. Rev.* 2007, 107, 874.

⁵² Denmark, S. E.; Regens, C. S. *Acc. Chem. Res.* 2008, 41, 1486.

successfully developed. These transformations often exhibit high functional group tolerance and are applicable to a broad variety of haloarene substrates. The development of palladium catalysis for the chemistry of haloarenes has been occurring at a tremendous pace, as manifested by tens of thousands of research reports and thousands of review articles, book chapters, and monographs on the subject published over the last 20 years.

Metals other than Pd can be used to effect coupling reactions of aryl halides, including Cu and Ni. A key step of these transformations is oxidative addition of the Ar-X bond to Pd(0), Ni(0), or Cu(I) centers, which increases the oxidation state of the metal by two (Scheme 22). Three main mechanisms of oxidative addition reactions are known.⁵³ One is of S_N2 type with the transition metal center playing the role of a nucleophile. The reaction of Vaska's complex with methyl iodide is a typical example of an S_N2 oxidative addition (Scheme 23).⁵⁴ Like conventional S_N2 reactions (see above), this type of oxidative addition is not applicable to aromatic halides.⁵⁵ Another mechanism that sometimes governs Ar-X oxidative addition involves SET, e.g., the reaction of aryl iodides with [Ni(PEt₃)₄] (Scheme 24).⁵⁶



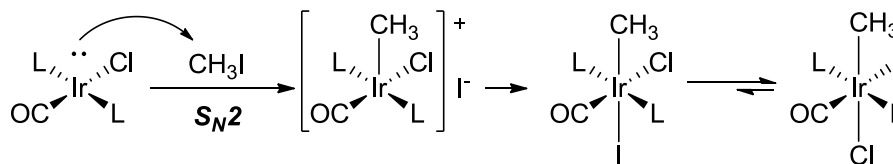
Scheme 22. Ar-X oxidative addition.

⁵³ (a) Hartwig, J. F. *Organotransition Metal Chemistry: From Bonding to Catalysis*; University Science Books: Sausalito, 2010. (b) Komiya, S.; Hirano, M. *Activation of Substrates with Polar Single Bonds*. In: *Fundamentals of Molecular Catalysis (Current Methods in Inorganic Chemistry, Vol. 3)*, Kurosawa, H.; Yamamoto, A. Eds.; Elsevier: Amsterdam, 2003.

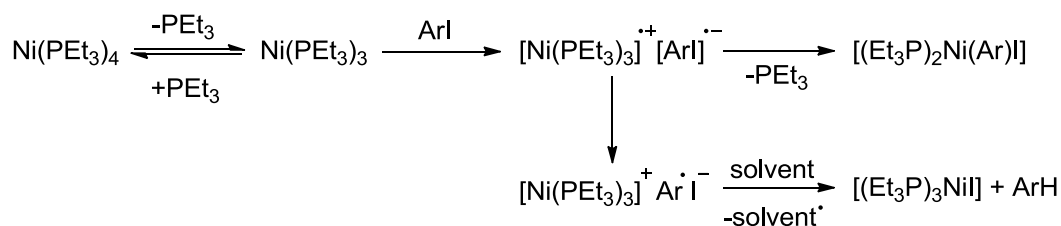
⁵⁴ Chock, P. B.; Halpern, J. *J. Am. Chem. Soc.* 1966, *88*, 3511.

⁵⁵ Evidence has been reported for S_NAr oxidative addition of electron-deficient (activated) ArX to Ni(0). See: Foà, M.; Cassar, L. *J. Chem. Soc., Dalton Trans.* 1975, 2572.

⁵⁶ Tsou, T. T.; Kochi, J. K. *J. Am. Chem. Soc.* 1979, *101*, 6319.

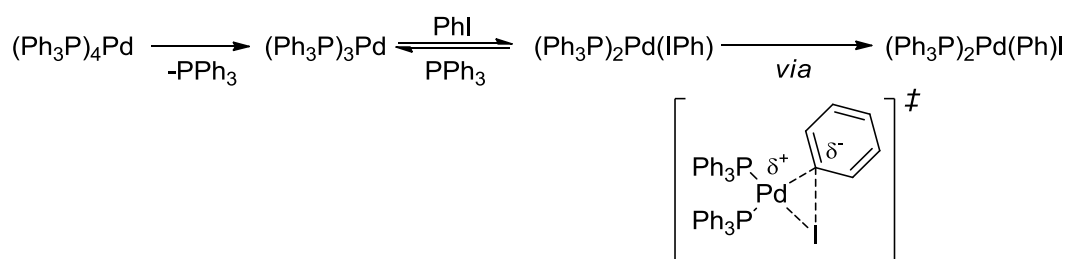


Scheme 23. S_N2 mechanism of oxidative addition.



Scheme 24. SET mechanism of oxidative addition.

The most common mechanism of oxidative addition of aryl halides to complexes of transition metals in low oxidation states is concerted three-center,⁵³ as shown in Scheme 25.⁵⁷ It is this mechanism that is operational in most Pd-catalyzed reactions of haloarenes. Concerted oxidative addition involves ArX precoordination to the metal center, which obviously requires a vacant site in the inner coordination sphere of the complex. The reactivity of aryl halide toward oxidative addition largely depends on the C-X bond strength^{53,58} that increases in the row $X = I < Br < Cl < F$.



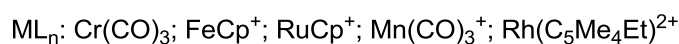
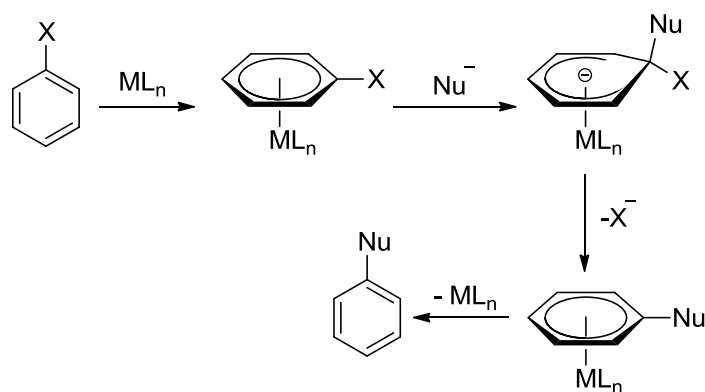
Scheme 25. Oxidative addition of iodobenzene to a Pd(0) complex.

⁵⁷ Amatore, C.; Pflüger, F. *Organometallics* 1990, 9, 2276.

⁵⁸ Kononov, A. I.; Lishchynskiy, A.; Grushin, V. V. *J. Am. Chem. Soc.* 2014, 136, 13410.

In concerted oxidative addition, the metal center acts as a nucleophile and the organic halide as an electrophile. Therefore, the presence of electron-withdrawing groups on the aromatic ring and electron-rich ligands facilitates these transformations. Bulky basic phosphines are often the ligands of choice for activation of most unreactive haloarenes⁵³ because such ligands provide the metal center with both electron density and coordinative unsaturation (see above). As expected, the reactivity toward oxidative addition of metals within the same group varies inversely with their electronegativity, e.g., Ni ($\chi = 1.91$) > Pd ($\chi = 2.20$) > Pt ($\chi = 2.28$).

ArX activation by π -coordination to transition metals. Electrophilicity of aryl halides can be increased dramatically by coordination of Lewis acidic metal centers to the π -system of the aromatic ring. For instance, the effect of π -coordination of some metal ions to ArX with respect to X can be comparable to that of three nitro groups in the ortho and para positions.⁵⁹ Unsurprisingly, therefore, haloarene π -complexes often exhibit high reactivity in S_NAr reactions (Scheme 26).



Scheme 26. S_NAr reactions of π -coordinated haloarenes.

⁵⁹ Goryunov, L. I.; Romanova, N. M.; Zhilovskii, G. S.; Shteingarts, V. D. *Russ. J. Org. Chem.* 2007, 43, 1765.

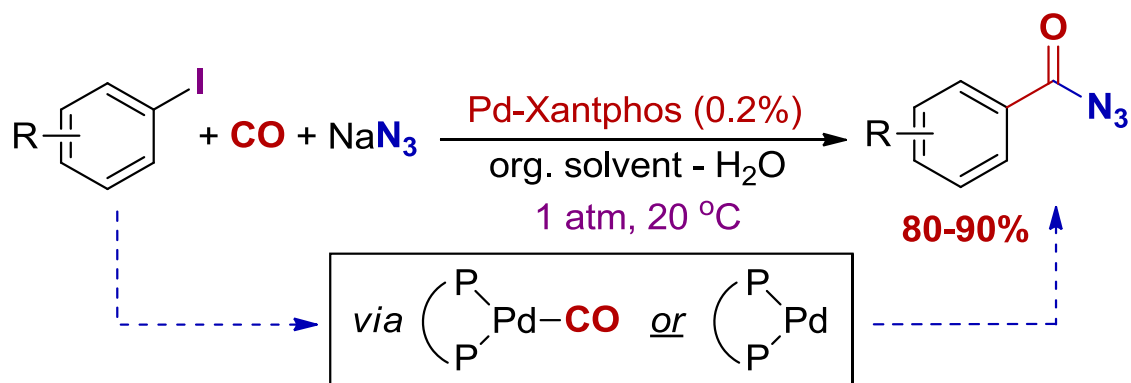
The order of reactivity of π -complexes of ArX toward nucleophiles is characteristic of S_NAr , i.e. $X = F > Cl > Br > I$, chloroarenes being considerably less reactive than their fluoro analogues. Bromo- and iodoarenes are poor substrates for S_NAr -type reactions. The higher the positive charge on the metal, the greater the reactivity of the Ar-X bond in $[L_nM(ArX)]$. For instance, the effect of ML_n is similar to that of one, two, and three nitro groups in the ortho and/or para positions for $Cr(CO)_3$, $Mn(CO)_3^+$, and $Rh(\eta^5-C_5Me_4Et)^{2+}$, respectively.⁶⁰ The nature of the metal within one group can have a significant effect on reactivity of ArX toward nucleophiles ($Fe > Ru > Os$) or virtually no effect ($Cr \approx Mo \approx W$). As follows from Scheme 26, π -coordination-induced S_NAr reactions of haloarenes could, in principle, be performed in a catalytic manner. For that to happen, however, arene/arene ligand exchange between the product $[L_nM(ArNu)]$ and the substrate ArX should occur at rates comparable to those of the nucleophilic displacement step. Although some such reactions have been reported,⁶¹ overall there has been little progress in the area because of the intrinsically high inertness of η^6 -arene complexes involved.

⁶⁰ Semmelhack, M. F.; Chlenov, A. *Top. Organomet. Chem.* 2004, 7, 43.

⁶¹ See, for example: (a) Houghton, R. P.; Voyle, M. *J. Chem. Soc. Perkin Trans. I* 1984, 925. (b) Goryunov, L. I.; Litvak, V. V.; Shteingarts V. D. *Izv. Sib. Otd. Akad. Nauk SSSR, Ser. Khim. Nauk* 1985, 1, 132. (c) Goryunov, L. I.; Litvak, V. V.; Shteingarts V. D. *Zh. Org. Khim.* 1987, 23, 1230. (d) Otsuka, M.; Endo, K.; Shibata, T. *Chem. Commun.* 2010, 46, 336. (e) Otsuka, M.; Yokoyama, H.; Endo, K.; Shibata, T. *Synlett* 2010, 2601.

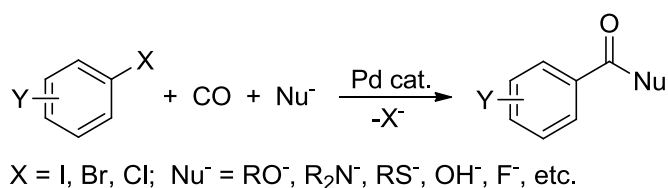
Chapter 1

Palladium-Catalyzed Azidocarbonylation of Aromatic Iodides



Introduction

In 1974, Schoenberg and Heck¹ reported their groundbreaking discovery of Pd-catalyzed carbonylation of haloarenes (Scheme 1.1). Since then, this reaction has become one of the most powerful tools for the synthesis of aromatic carbonyl compounds in both laboratory and industrial settings.²



Scheme 1.1. Heck Pd-catalyzed carbonylation of aryl halides.

While a broad variety of organic nucleophiles have been employed in the Pd-catalyzed carbonylation of haloarenes to furnish a variety of products (Scheme 1.2), the use of inorganic nucleophiles is much less common. With the exception of alkali bases that are frequently utilized in the synthesis of the corresponding benzoates,^{2,3} only three examples of the application of inorganic nucleophiles in the Heck-type carbonylation are known. In the 1980's, Tanaka reported the cyanocarbonylation⁴ and fluorocarbonylation⁵ with KCN and CsF, respectively. Since then, the

¹ (a) Schoenberg, A.; Bartoletti, I.; Heck, R. F. *J. Org. Chem.* 1974, **39**, 3318. (b) Schoenberg, A.; Heck, R. F. *J. Org. Chem.* 1974, **39**, 3327. (c) Schoenberg, A.; Heck, R. F. *J. Am. Chem. Soc.* 1974, **96**, 7761.

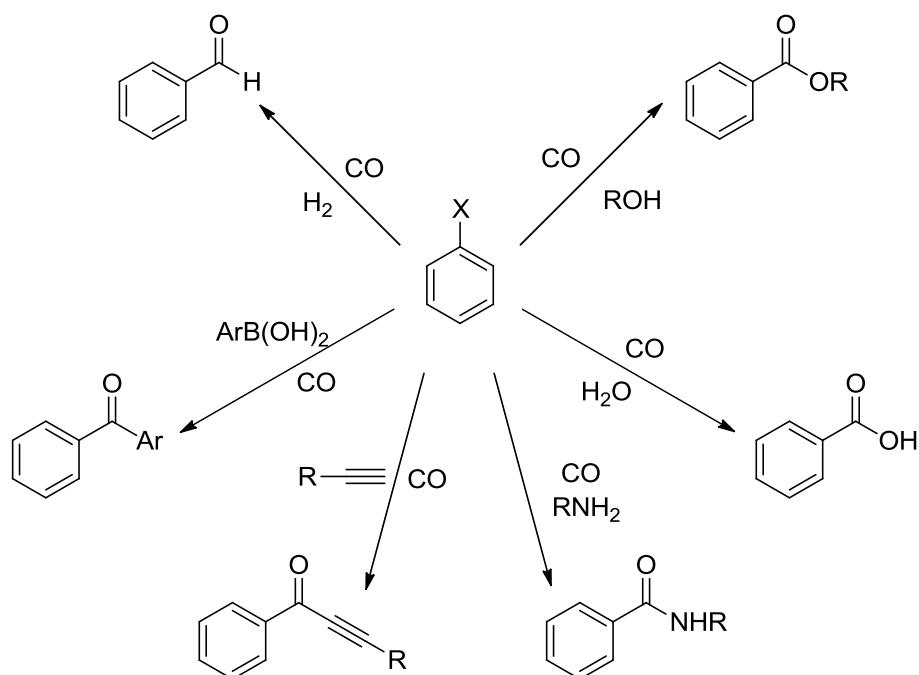
² For recent reviews on Pd-catalyzed carbonylation reactions of aryl halides, see: (a) Fang, W.; Zhu, H.; Deng, Q.; Liu, S.; Liu, X.; Shen, Y.; Tu, T. *Synthesis* 2014, **46**, 1689. (b) Wu, X.-F.; Neumann, H.; Beller, M. *Chem. Rev.* 2013, **113**, 1. (c) Roy, S.; Roy, S.; Gribble, G. W. *Tetrahedron* 2012, **68**, 9867. (d) Wu, X.-F.; Neumann, H.; Beller, M. *Chem. Soc. Rev.* 2011, **40**, 4986. (e) Magano, J.; Dunetz, J. R. *Chem. Rev.* 2011, **111**, 2177. (f) Grigg, R.; Mutton, S. P. *Tetrahedron* 2010, **66**, 5515. (g) Brennfürer, A.; Neumann, H.; Beller, M. *Angew. Chem. Int. Ed.* 2009, **48**, 4114. (h) Barnard, C. F. J. *Organometallics* 2008, **27**, 5402.

³ (a) Cassar, L.; Foà, M. *J. Organomet. Chem.* 1973, **51**, 381. (b) Bumagin, N. A.; Nikitin, K. V.; Beletskaya, I. P. *J. Organomet. Chem.* 1988, **358**, 563. (c) Grushin, V. V.; Alper, H. *Organometallics* 1993, **12**, 3846. (d) Grushin, V. V.; Alper, H. *J. Am. Chem. Soc.* 1995, **117**, 4301.

⁴ Tanaka, M. *Bull. Chem. Soc. Jpn.* 1981, **54**, 637.

⁵ Sakakura, T.; Chaisupakitsin, M.; Hayashi, T.; Tanaka, M. *J. Organomet. Chem.* 1987, 205.

fluorocarbonylation has been demonstrated for aryl bromides.⁶ The third example is most recent: in 2013, Quesnel and Arndtsen reported the chlorocarbonylation of aryl iodides with Ph_3PBnCl or Bu_4NCl as the chloride source in the presence of a $\text{Pd-P}(t\text{-Bu})_3$ catalyst.^{7,8} There have been no reports of Pd-catalyzed carbonylation reactions with other inorganic nucleophiles such as bromide, iodide, sulfide, cyanate, thiocyanate, acetate,⁹ nitrite, azide, etc.



Scheme 1.2. Common types of Pd-catalyzed aromatic carbonylation.²

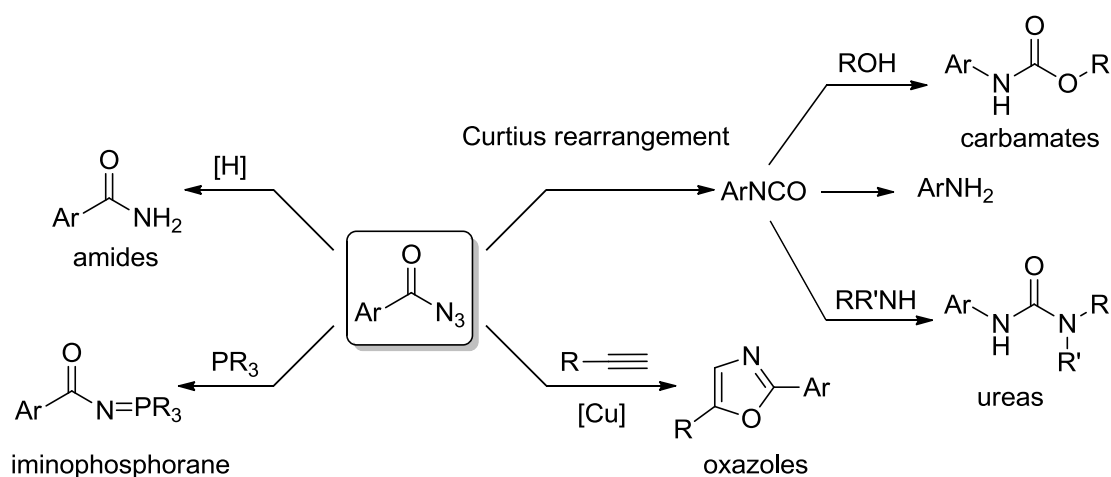
⁶ (a) Okano, T.; Harada, N.; Kiji, J. *Bull. Chem. Soc. Jpn.* 1992, **65**, 1741. (b) Ueda, T.; Konishi, H.; Manabe, K. *Org. Lett.* 2013, **15**, 5370.

⁷ Quesnel, J. S.; Arndtsen, B. A. *J. Am. Chem. Soc.* 2013, **135**, 16841.

⁸ (a) It worth to note, that the first examples of Pd-catalyzed chloro^{8b} and fluorocarbonylation^{8c} reactions under drastic conditions were disclosed in DuPont patents filed in the 1960's before the Heck reports.¹ (b) Mador, I. L.; Scheben, J. A. U.S. Patent 3452090, 1969. (c) Prichard, W. W. U.S. Patent 3632633, 1972.

⁹ (a) The use of benzoates for the synthesis of corresponding anhydrides was reported^{9b} (b) Pri-Bar, I.; Alper, H. *J. Org. Chem.* 1989, **54**, 36.

Aroyl azides are important building blocks in the preparation of various useful compounds.¹⁰ The most widely known and used transformation of aroyl azides is the Curtius rearrangement furnishing aromatic isocyanates, which can be converted to the corresponding anilines, carbamates, or ureas. The reduction of benzoyl azides affords primary amides. Tertiary phosphines are often employed as reducing agents for alkyl and aryl azides (the Staudinger reduction)¹¹ but not for acyl azides because the initially produced N-acyl iminophosphoranes (Scheme 1.3) are more hydrolytically stable than their N-alkyl or N-aryl analogues.¹² A formal [3+2] cycloaddition reaction of benzoyl azides with alkynes to give oxazoles has been recently reported¹³ (Scheme 1.3).



Scheme 1.3. Selected reactions of aroyl azides.

¹⁰ For general reviews, see: (a) Scriven, E. F. V.; Turnbull, K. *Chem. Rev.* 1988, **88**, 297. (b) Bräse, S.; Gil, C.; Knepper, K.; Zimmermann, V. *Angew. Chem. Int. Ed.* 2005, **44**, 5188. (c) Bräse, S.; Banert, K. *Organic Azides: Syntheses and Applications*; John Wiley & Sons: Chichester, 2010.

¹¹ For a recent review of the Staudinger reaction, see: Iula, D. M., In: *Name Reactions for Functional Group Transformations*; Li, J. J.; Corey, E. J., Eds. John Wiley & Sons: Hoboken, N. J., 2007, 129.

¹² Frøyen, P. *Phosphorus, Sulfur Silicon Relat. Elem.* 1993, **78**, 161.

¹³ (a) Cano, I.; Álvarez, E.; Nicasio, M. C.; Pérez, P. J. *J. Am. Chem. Soc.* 2011, **133**, 191. (b) Haldón, E.; Besora, M.; Cano, I.; Cambeiro X. C.; Pericàs M. A.; Maseras, F.; Nicasio, M. C.; Pérez, P. J. *Chem. Eur. J.* 2014, **20**, 3463.

Benzoyl azides were for the first time synthesized by Theodor Curtius in the 19th century. In 1890, Curtius reported the preparation of the new class of organic compounds that he named “benzoylazoimides”, from benzoylhydrazine and nitrous acid¹⁴ (Figure 1.1; Scheme 1.4, i). Back then, chemists identified the azido-group as a triazirine. The linearity of the azido moiety was established only 40 years later by Pauling and Hendricks who determined the structures of sodium azide and potassium azide by single-crystal X-ray diffraction.¹⁵ In 1933, Pauling and Brockway confirmed the linearity of the N₃ group in organic azides in a study of methyl azide by electron diffraction.¹⁶

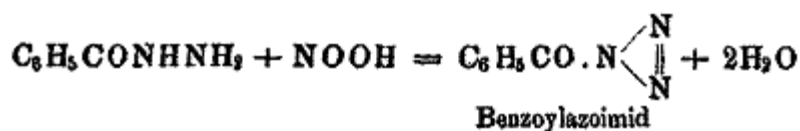


Figure 1.1. The chemical equation of the first benzoyl azide synthesis as it appears in the original Curtius publication.¹⁴

Another traditional approach to acyl azides is based on the reaction of the corresponding acid chlorides with sodium azide (Scheme 1.4, ii). For aromatic derivatives, this method was first used by Powell in 1929.¹⁷ Alternative protocols were later developed for other activated benzoic acid derivatives, including mixed anhydrides¹⁸ and N-acylbenzotriazoles¹⁹ (Scheme 1.4, ii). One-step processes have been

¹⁴ Curtius, Th. *Chem. Ber.* 1890, *23*, 3023.

¹⁵ Hendricks, S. B.; Pauling, L. *J. Am. Chem.* 1925, *47*, 2904.

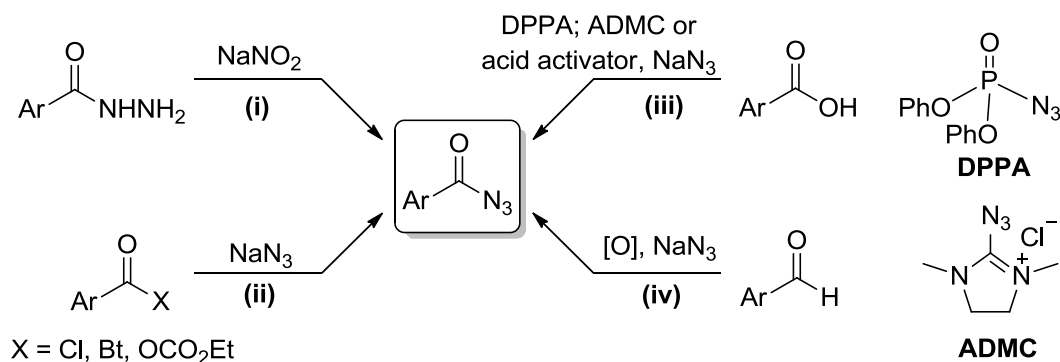
¹⁶ Brockway, L. O.; Pauling, L. *Proc. Nat. Acad. Sci.* 1933, *19*, 860.

¹⁷ Powell, G. *J. Am. Chem. Soc.* 1929, *51*, 2436.

¹⁸ (a) Weinstock, J. *J. Org. Chem.* 1961, *26*, 3511. (b) Song, X.-J.; Tan, X.-H.; Wang, Y.-G. *Phosphorus Sulfur Silicon Relat. Elem.* 2007, *182*, 1907. (c) Bandgar, B. P.; Pandit, S. S. *Tetrahedron Lett.* 2002, *43*, 3413.

¹⁹ Katritzky, A. R.; Widyan, K.; Kirichenko, K. *J. Org. Chem.* 2007, *72*, 5802.

developed for the direct azidation of carboxylic acids involving acid activators,²⁰ or with more reactive azide sources (DPPA²¹ and ADMC,²² Scheme 1.4, iii), and oxidative azidation of aldehydes²³ (Scheme 1.4, iv).



Scheme 1.4. Conventional syntheses of aryl azides.

²⁰ (a) Frøyen, P. *Phosphorus Sulfur Silicon Relat. Elem.* 1994, *89*, 57. (b) Kim, J.-G.; Jang, D. O. *Synlett* 2008, *13*, 2072. (c) Sridhar, R.; Perumal, P. T. *Synth. Commun.* 2003, *33*, 607. (d) Narendra, B. N.; Lamani, R. S.; Sureshbabu, V. V. *Tetrahedron Lett.* 2010, *51*, 3002. (e) Gumaste, V. K.; Bhawal, B. M.; Deshmukh, A. R. A. S. *Tetrahedron Lett.* 2002, *43*, 1345. (f) El-Faham, A.; Abdul-Ghani, M. *Org. Prep. Proced. Int.* 2003, *35*, 369. (g) Tale, R. H.; Patil, K. M. *Tetrahedron Lett.* 2002, *43*, 9715.

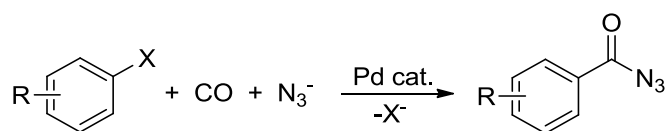
²¹ (a) Shioiri, T.; Ninomiya, K.; Yamada, Sh.-i. *J. Am. Chem. Soc.* 1972, *94*, 6203. (b) Bolshan, Yu.; Tomaszewski, M. J.; Santhakumar, V. *Tetrahedron Lett.* 2007, *48*, 4925. (c) Lago, J. M.; Arrieta, A.; Palomo, C. *Synth. Commun.* 1983, *13*, 289.

²² Kitamura, M.; Tashiro, N.; Takamoto, Yu.; Tatsuo, O. *Chem. Lett.* 2010, *39*, 732.

²³ (a) Lee, J. G.; Kwak, K. H. *Tetrahedron Lett.* 1992, *33*, 3165. (b) Elmorsy, S. S. *Tetrahedron Lett.* 1995, *36*, 1341. (c) Chen, D.-J.; Chen, Z.-C. *Tetrahedron Lett.* 2000, *41*, 7361. (d) Bose, D. S.; Reddy, A. V. N. *Tetrahedron Lett.* 2003, *44*, 3543. (e) Arote, N. D.; Akamanchi, K. G. *Tetrahedron Lett.* 2007, *48*, 5661. (f) Sarkar, S. D.; Studer, A. *Org. Lett.* 2010, *12*, 1992.

Objectives

As can be seen from the above, benzoyl azides are valuable versatile building blocks and intermediates in organic synthesis. However, the available synthetic routes toward these compounds from carbonyl derivatives require use of highly reactive chemicals, which limits functional group compatibility and, as a result, the substrate scope. Novel synthetic methods with high functional group tolerance to prepare aroyl azides are certainly in demand. Considering all of the above, the objective of our work was to develop the first Pd-catalyzed carbonylation of aryl halides with azide as the nucleophile (Scheme 1.5).



Scheme 1.5. General equation for Pd-catalyzed azidocarbonylation.

Furthermore, in case of success, our objective was to study the mechanism of the azidocarbonylation reaction. Since the pioneering work of Fitton and co-workers,²⁴ oxidative addition of haloarenes to tertiary phosphine complexes of zerovalent palladium has been thoroughly investigated. Also, migratory insertion of CO into a variety of complexes of the type $[(\text{R}_3\text{P})\text{M}(\text{Ar})\text{X}]$ ($\text{M} = \text{Pt}, \text{Pd}, \text{Ni}$) has been studied in detail by Garrou and Heck.²⁵ Surprisingly, however, very little mechanistic information has been reported on oxidative addition of aryl halides to tertiary phosphine-stabilized Pd(0) complexes in the presence of CO, i.e. under catalytic conditions of the Heck carbonylation that has been known and widely used for nearly 40 years.¹ Therefore, it

²⁴ (a) Fitton, P.; McKeon, J. E. *Chem. Commun.* 1968, 4. (b) Fitton, P.; Johnson, M. P.; McKeon, J. E. *Chem. Commun.* 1968, 6. (c) Fitton, P.; Rick, E. A. *J. Organomet. Chem.* 1971, 28, 287.

²⁵ Garrou, P. E.; Heck, R. F. *J. Am. Chem. Soc.* 1976, 98, 4115.

was important to investigate the mechanism of Pd-catalyzed azidocarbonylation by experimental and computational means.²⁶

²⁶ The DFT computational studies were performed by Dr. C. L. McMullin and Prof. S. A. Macgregor (Heriot-Watt University, U.K.).

Results

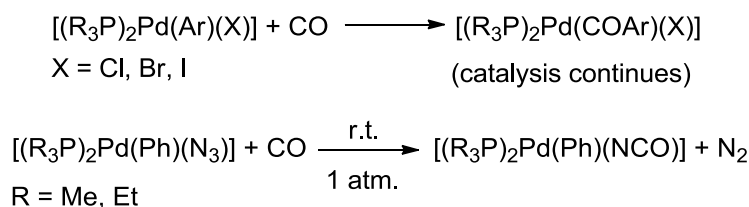
Challenges of Pd-Catalyzed Azidocarbonylation of Aryl Halides. It is shown in the Introduction that since the pioneering reports from Heck¹ in 1974, the Pd-catalyzed reaction of aryl halides ArX with CO and nucleophiles (Scheme 1.1) has been widely used for the synthesis of various carboxylic acid derivatives, such as esters and amides.² It would be most natural to consider this type of carbonylation for the synthesis of ArCON₃ (Scheme 1.5). In spite of the substantial amount of work done in the area,²⁻⁹ however, there have been no reports of azidocarbonylation reactions.

As methodologically new, high functional group tolerance routes to aroyl azides are certainly in demand, the question arises as to why Pd-catalyzed aromatic azidocarbonylation reactions (Scheme 1.5) have not been developed. Upon superficial considerations, there should be no fundamental difference between azide and other nucleophiles that have been successfully used in the carbonylation reactions of haloarenes. However, in-depth analysis of the literature data on aroyl azides and mechanisms of palladium catalysis suggests that the development of Pd-catalyzed aromatic azidocarbonylation could be extremely challenging, if not impossible. In particular:

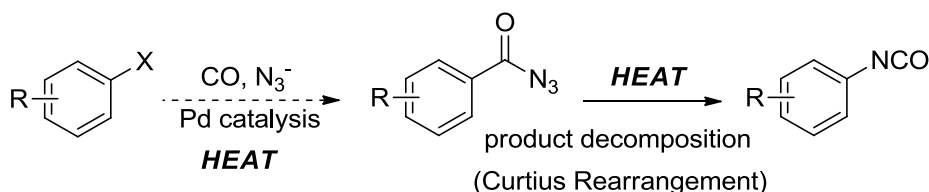
(1) A key step in the catalytic loop governing the carbonylation reaction is migratory insertion of CO into the Pd-C bond of [(R₃P)₂Pd(Ar)(X)], the intermediate that is produced in the preceding step of Ar-X substrate oxidative addition to R₃P-stabilized Pd(0).²⁵ For X = I, Br, and Cl, this reaction usually occurs easily and cleanly at room temperature and atmospheric pressure (Scheme 1.6). In sharp contrast, complexes of the type *trans*-[(R₃P)₂Pd(Ph)N₃] (R = Me, Et) do not undergo CO insertion into the Pd-Ph

bond but are rather converted to *trans*-[(R₃P)₂Pd(Ph)NCO] with concomitant release of N₂ under similar conditions (r.t., 1 atm CO),²⁷ as shown in Scheme 1.6.

(2) Being thermally stable, carboxylic acid derivatives (salts, esters, amides, etc.) formed in the carbonylation reactions (Scheme 1.1) easily survive the elevated temperatures that are needed for the process to occur. In sharp contrast, aryl azides are thermally unstable, undergoing the Curtius rearrangement (Scheme 1.7) at such temperatures (80 °C and above).



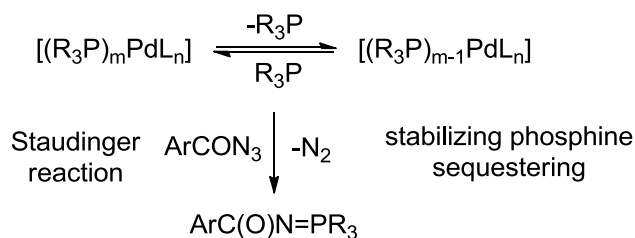
Scheme 1.6. Different reactivity of σ -aryl palladium halides and azides toward CO.



Scheme 1.7. The Curtius rearrangement of benzoyl azides.

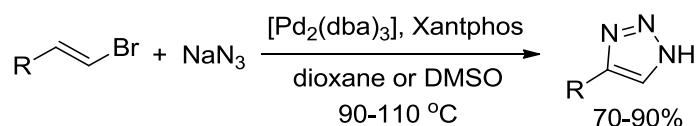
(3) The desired product, ArCON₃, is not only thermally unstable but also highly reactive toward tertiary phosphines that are used as stabilizing ligands for Pd catalysts employed in carbonylation and other coupling reactions. The facile Staudinger reaction¹¹ of the ArCON₃ produced with the reversibly dissociated PR₃ ligand would lead to immediate catalyst deactivation from the quick and irreversible formation of the corresponding iminophosphorane ArC(O)N=PR₃ (Scheme 1.8).

²⁷ Kim, Y.-J.; Kwak, Y.-S.; Lee, S.-W. *J. Organomet. Chem.* 2000, 603, 152.



Scheme 1.8. Staudinger reaction leading to Pd catalyst deactivation.

Initial Studies. Our initial goal was to develop the Pd-catalyzed synthesis of aryl azides from the corresponding haloarenes and an inorganic azide source such as NaN_3 (Table 1.1). All our attempts to perform this transformation were unsuccessful, although Pd-catalyzed azidation of vinylic bromides to give 1*H*-1,2,3-triazoles has been reported (Scheme 1.9).²⁸ As both oxidative addition of ArX to $\text{Pd}(0)$ and halide/azide metathesis reactions of $\text{Pd}(\text{II})$ complexes^{27,29} are well-known, we reasoned that it is the Ar-N_3 reductive elimination from $\text{Pd}(\text{II})$ that is most likely the problematic step of the process (Scheme 1.10).



Scheme 1.9. Pd-catalyzed reaction of vinylic halides with N_3^- .

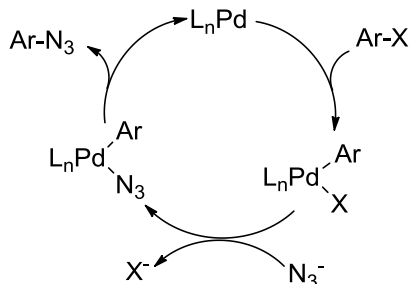
²⁸ For Pd-catalyzed azidation of alkenyl bromides to 1*H*-1,2,3-triazoles, see: Barluenga, J.; Valdés, C.; Beltrán, G.; Escribano, M.; Aznar, F. *Angew. Chem. Int. Ed.* 2006, 45, 6893.

²⁹ For selected examples of the facile formation of various organopalladium azido complexes from the corresponding $\text{Pd}(\text{II})$ halides and NaN_3 , see: (a) Kim, Y.-J.; Choi, J.-C.; Park, K.-H. *Bull. Korean Chem. Soc.* 1994, 15, 690. (b) Kim, Y.-J.; Kim, D.-H.; Song, S.-W.; Son, T.-i. *Bull. Korean Chem. Soc.* 1998, 19, 125. (c) Kim, Y.-J.; Chang, X.; Han, J.-T.; Lim, M. S.; Lee, S. W. *Dalton Trans.* 2004, 3699. (d) Lee, K.-E.; Jeon, H.-T.; Han, S.-Y.; Ham, J.; Kim, Y.-J.; Lee, S. W. *Dalton Trans.* 2009, 6578.

Table 1.1. Conditions screening for Pd-catalyzed azidation of PhBr.

$$\text{PhBr} + \text{NaN}_3 \xrightarrow{\text{Pd catalyst}} \text{PhN}_3$$

Catalyst (5 mol %) ³⁰	Solvent, Temperature	Result
P(<i>t</i> -Bu) ₃ , Pd ₂ (dba) ₅ (1:1)	THF, 50 °C	<<1% PhN ₃
P(<i>t</i> -Bu) ₃ , Pd ₂ (dba) ₅ (1:1)	THF/CH ₃ CN (1:4) 50 °C	<<1% PhN ₃
P(<i>t</i> -Bu) ₃ , Pd ₂ (dba) ₅ (1:1)	C ₆ H ₆ /H ₂ O (1:1), 80 °C	—
P(<i>t</i> -Bu) ₃ , Pd ₂ (dba) ₅ (2:1)	Xylene, 130 °C	<<1% PhN ₃
P(<i>t</i> -Bu) ₃ , Pd ₂ (dba) ₅ (1:1)	<i>t</i> -BuOH, 70 °C	<<1% PhN ₃
IPrPd(allyl)Cl, NaO <i>t</i> -Bu (1:1)	THF, 50° C	—
IPrPd(allyl)Cl, NaO <i>t</i> -Bu (1:1)	DMF, 80° C	—
Xantphos, Pd ₂ (dba) ₅	THF, 50° C	—



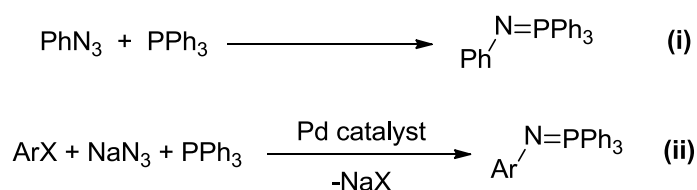
Scheme 1.10. Proposed mechanism for Pd-catalyzed azidation of aryl halides.

To study Ar-N₃ reductive elimination from Pd(II), the product-forming step in the proposed catalytic loop, we prepared [(Ph₃P)₂Pd(Ph)(N₃)] from [(Ph₃P)₂Pd(Ph)(Br)] and NaN₃. This complex was found to be exclusively trans both in solution (¹H and ³¹P{¹H} NMR) and in the solid state (X-ray diffraction). Interestingly, [(Ph₃P)₂Pd(Ph)(N₃)] was

³⁰ (a) The empirical composition Pd₂(dba)₅ was derived from the elemental analysis data.^{30b} (b) Ushkov, A. V.; Grushin, V. V. *J. Am. Chem. Soc.* 2011, *133*, 10999.

found to crystallize in two polymorphic forms displaying either a staggered or an eclipsed conformation along the P-Pd-P axis (Figures 1.2 and 1.3).

The new azido complex *trans*-[(Ph₃P)₂Pd(Ph)(N₃)] appeared to be unexpectedly thermally stable, exhibiting no sign of decomposition at 80-100 °C in benzene or toluene for 15-24 h. At 135 °C in xylenes, however, [(Ph₃P)₂Pd(Ph)(N₃)] decomposed to give mostly Ph₂ and PhN=PPh₃ (GC-MS). The iminophosphorane was evidently produced by the Staudinger reaction¹¹ of the transient PhN₃ with the PPh₃ ligand (Scheme 1.11, i). Attempts to perform this reaction catalytically, i.e. in the presence of excess PPh₃ (Scheme 1.11, ii), were unsuccessful.



Scheme 1.11. (i) Staudinger reaction between phenyl azide and triphenylphosphine and (ii) Pd-catalyzed formation of iminophosphoranes from aryl halides.

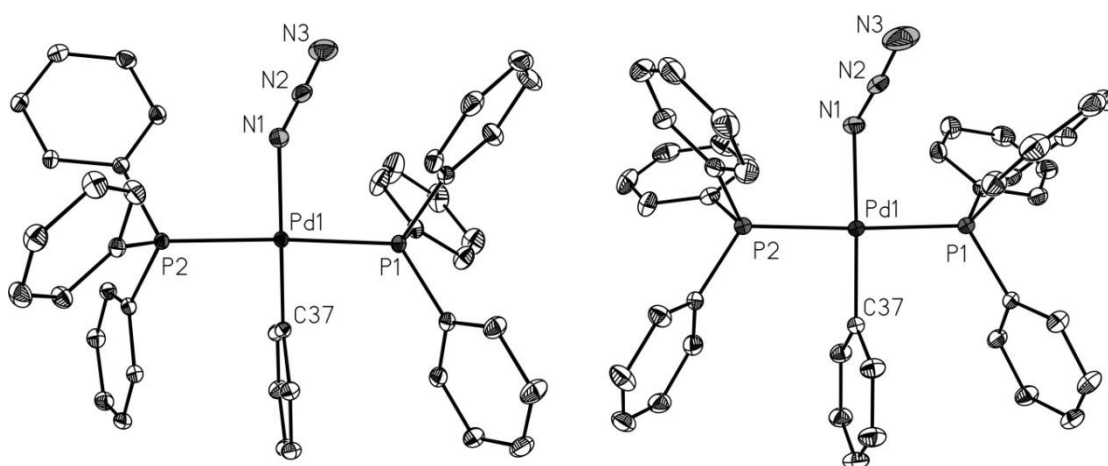


Figure 1.2. ORTEP drawings of the two conformers of *trans*-[(Ph₃P)₂Pd(Ph)(N₃)] (left: staggered; right: eclipsed) with all H atoms omitted and thermal ellipsoids drawn to the 50% probability level.

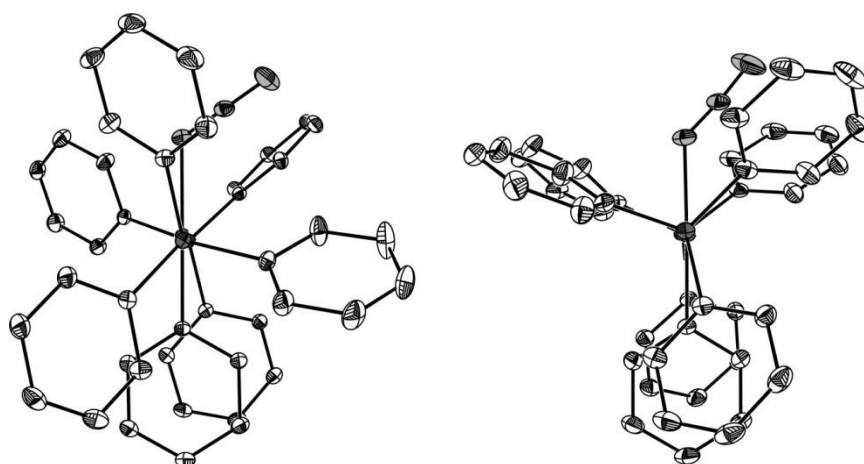
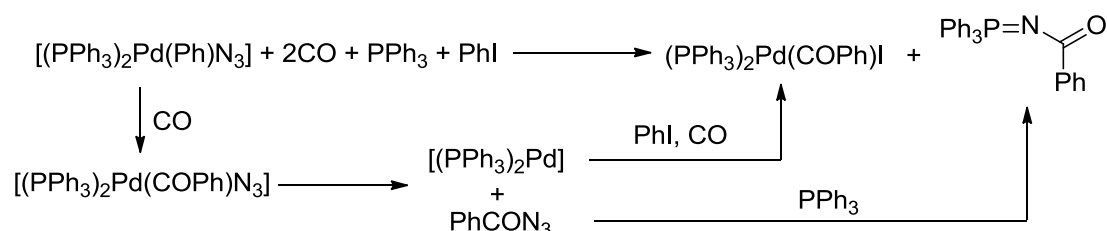


Figure 1.3. ORTEP views of the staggered (left) and eclipsed (right) conformers of *trans*- $[(\text{Ph}_3\text{P})_2\text{Pd}(\text{Ph})(\text{N}_3)]$ along the P-Pd-P axis with all H atoms omitted and thermal ellipsoids drawn to the 50% probability level.

Importantly, during these studies we found that bubbling CO through a solution of $[(\text{Ph}_3\text{P})_2\text{Pd}(\text{Ph})(\text{N}_3)]$ containing PhI and PPh_3 in benzene at 50 °C triggered a transformation to $[(\text{Ph}_3\text{P})_2\text{Pd}(\text{COPh})\text{I}]^{25}$ and $\text{PhC}(\text{O})\text{N}=\text{PPh}_3^{31}$ in high yield (> 90%, $^{31}\text{P}\{^1\text{H}\}$ NMR, Scheme 1.12, Figure 1.4). The formation of the latter indicated that PhCON_3 was formed as an intermediate that was sequestered by PPh_3 in the Staudinger reaction. These observations prompted our search for a Pd catalyst for the synthesis of aroyl azides directly from ArI , CO, and N_3^- .



Scheme 1.12. Proposed mechanism for the formation of $[(\text{Ph}_3\text{P})_2\text{Pd}(\text{COPh})\text{I}]$ and $\text{PhC}(\text{O})\text{N}=\text{PPh}_3$ from $[(\text{Ph}_3\text{P})_2\text{Pd}(\text{Ph})(\text{N}_3)]$, CO, PhI and PPh_3 .

³¹ Albright, T. A.; Freeman, W. J.; Schweizer, E. E. *J. Org. Chem.* 1976, 41, 2716.

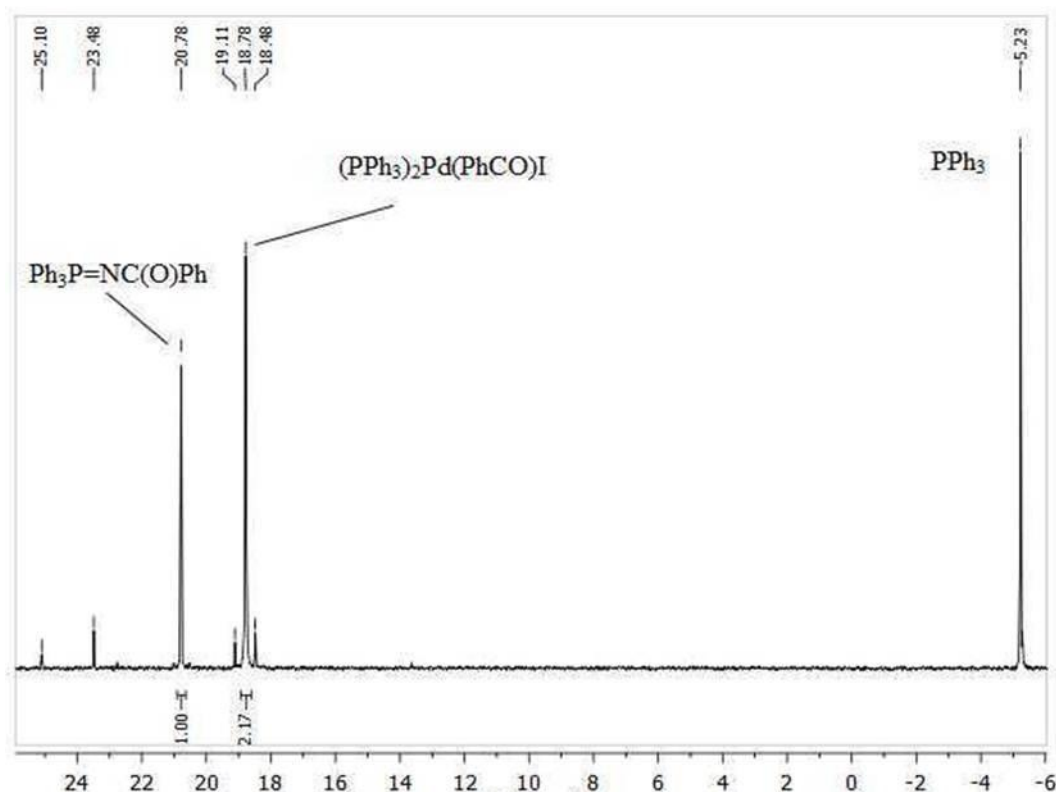


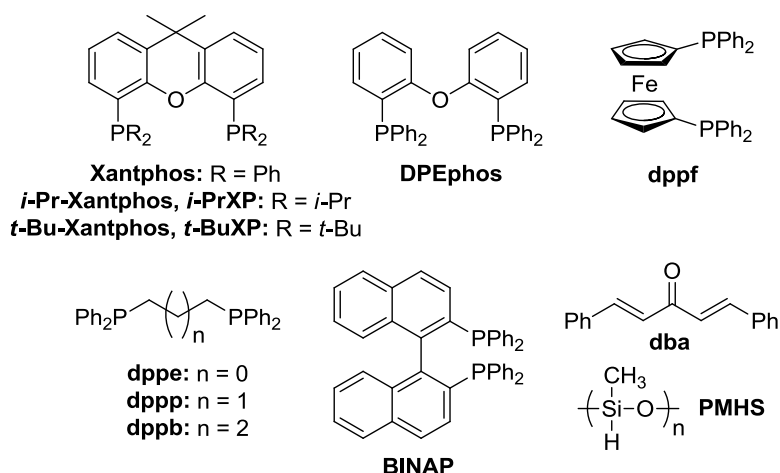
Figure 1.4. $^{31}\text{P}\{^1\text{H}\}$ NMR spectrum of the reaction solution obtained upon treatment of a mixture of $[(\text{PPh}_3)_2\text{Pd}(\text{Ph})(\text{N}_3)]$, PhI , and PPh_3 in C_6D_6 with CO .

Development of the Aromatic Azidocarbonylation. As was mentioned above, the azidocarbonylation differs principally, in a number of respects, from the known Pd-catalyzed aromatic carbonylation reactions. The three reactivity patterns considered above (Schemes 1.6-1.8) cast serious doubts on the very possibility of Pd-catalyzed aromatic azidocarbonylation. Therefore, a thorough scouting and optimization of the catalytic system was required to find conditions to avoid the Curtius rearrangement (Scheme 1.7) and the Staudinger reaction (Scheme 1.8) that are detrimental to the catalysis.

Initial series of experiments allowed us to identify Xantphos as by far the best ligand for the reaction (Table 1.2). Numerous runs in the presence of other ligands (PPh_3 , *o*- ToI_3P , Cy_3P , *t*- Bu_3P , *dppe*, *dppp*, *dppb*, *dppf*, *rac*-BINAP, *i*-Pr-Xantphos, *t*-Bu-Xantphos, and DPEphos, Scheme 1.13) under various conditions produced

PhCON₃ in only 0-6% yield. The highest catalytic activity was observed for a 1:1 Pd(0) to Xantphos molar ratio, in accord with the literature data.³² It is noteworthy that Xantphos³³ has been found³⁴ to be a superior ligand for many Pd-catalyzed carbonylation reactions.

It was also noticed in the preliminary studies that better conversions and yields could be achieved in the presence of reducing agents such as Zn dust or PMHS. It was proposed that like in Pd-catalyzed cyanation of haloarenes,³⁵ the reductant somehow recuperates the deactivated catalyst. Indeed, it was found in one experiment (Table 1.2, entry 10) that after the reaction had stalled at 64% conversion, the addition of Zn dust revitalized the process and 90% conversion was quickly reached.³⁶



Scheme 1.13. Selected ligands and other materials used.

³² Klingensmith, L. M.; Strieter, E. R.; Barder, T. E.; Buchwald, S. L. *Organometallics* 2006, 25, 82.

³³ For selected reviews on Xantphos and related ligands, see: (a) Kamer, P. C. J.; Van Leeuwen, P. W. N. M.; Reek, J. N. H. *Acc. Chem. Res.* 2001, 34, 895. (b) Freixa, Z.; Van Leeuwen, P. W. N. M. *Dalton Trans.* 2003, 1890. (c) Freixa, Z.; Van Leeuwen, P. W. N. M. *Coord. Chem. Rev.* 2008, 252, 1755. (d) Van Leeuwen, P. W. N. M.; Freixa, Z. In: *Modern Carbonylation Methods*; Kollar, L., Ed.; Wiley-VCH: Weinheim, 2008, 1.

³⁴ For efficient catalysis of other carbonylation reactions with Xantphos/Pd, see: (a) Lou, R.; VanAlstine, M.; Sun, X.; Wentland, M. P. *Tetrahedron Lett.* 2003, 44, 2477. (b) Martinelli, J. R.; Watson, D. A.; Freckmann, D. M. M.; Barder, T. E.; Buchwald, S. L. *J. Org. Chem.* 2008, 73, 7102. (c) Ueda, T.; Konishi, H.; Manabe, K. *Org. Lett.* 2013, 15, 5370. (d) Korsagen, S.; Nielsen, D. U.; Taaning, R. H.; Skrydstrup, T. *Angew. Chem. Int. Ed.* 2013, 52, 9763. (e) Schranck, J.; Burhardt, M.; Bornschein, C.; Neumann, H.; Skrydstrup, T.; Beller, M. *Chem. - Eur. J.* 2014, 20, 9534. (f) Neumann, K. T.; Laursen, S. R.; Lindhardt, A. T.; Bang-Andersen, B.; Skrydstrup, T. *Org. Lett.* 2014, 16, 2216. (g) Masuda, Y.; Ishida, N.; Murakami, M. *Chem. - Asian J.* 2015, 10, 321.

³⁵ Erhardt, S.; Grushin, V. V.; Kilpatrick, A. H.; Macgregor, S. A.; Marshall, W. J.; Roe, D. C. *J. Am. Chem. Soc.* 2008, 130, 4828.

³⁶ The promoting effect of reducing agents was later rationalized and successfully used in the design of the more efficient catalytic system (see below).

Table 1.2. Ligand optimization for Pd-catalyzed azidocarbonylation of PhI.^a

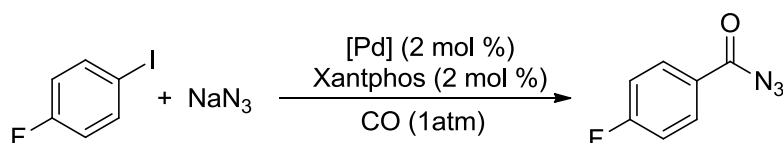
		x mol % [Pd] m mol % ligand n mol % additive					GC-MS			
PhI + NaN ₃		CO (1 atm), THF					PhCON ₃	→		PhNCO
entry	x	[Pd] ³⁰	m	ligand	n	additive	temp, °C	time, h	conv, % ^b	yield, % ^b
1	5	Pd ₂ dba ₅	-	-	-	-	50	22	0	0
2	5			Pd(PPh ₃) ₄	-	-	50	22	< 1	< 1
3	5	Pd ₂ dba ₅	5	P(<i>t</i> -Bu) ₃	-	-	50	22	7	6
4	5	Pd ₂ dba ₅	5	PCy ₃	-	-	50	22	7	2
5	5	Pd ₂ dba ₅	10	Dppf	-	-	50	22	2	1
6	5	Pd ₂ dba ₅	5	Xantphos	-	-	23	68	47	47
7	5	Pd ₂ dba ₅	10	P(<i>o</i> -tol) ₃	-	-	23	20	2	1
8	2	Pd(OAc) ₂	4	Xantphos	-	-	50	5	67	65
9	2			XantphosPdPhBr	-	-	50	4	22	22
10 ^c	2			XantphosPdPhBr	-	-	23	24	55	52
					50	Zn	50	4	96	87
11	2	Pd(OAc)₂	2	Xantphos	50	Zn	50	4	90	87
12	2	Pd(OAc) ₂	2	Xantphos	50	PMHS	50	4	98	81
13	2	Pd(OAc) ₂	2	Dppf	50	Zn	50	22	1	1
14	2	Pd(OAc) ₂	2	Dppe	50	Zn	50	22	< 1	< 1
15	2	Pd(OAc) ₂	2	Dppp	50	Zn	50	22	< 1	< 1
16	2	Pd(OAc) ₂	2	Dppb	50	Zn	50	22	< 1	< 1
17	2	Pd(OAc) ₂	2	(±)-BINAP	50	Zn	50	24	< 1	< 1
18	2	Pd(OAc) ₂	2	<i>i</i> -PrXP	50	Zn	50	24	1	1
19	2	Pd(OAc) ₂	2	<i>t</i> -BuXP	50	Zn	50	24	0	0
20	2	Pd(OAc) ₂	2	DPEphos	50	Zn	50	7	12	5

^a Reaction conditions: iodobenzene (1 mmol), NaN₃ (2 mmol), [Pd] (1 mol %), ligand (m mol %) and additive (n mol %) in THF (5 mL). ^b Determined by GC-MS. ^c After 24 h at r.t. Zn additive added and temperature increased to 50 °C.

During this ligand scouting study, the reaction mixtures were analyzed by GC-MS. However, PhCON₃ could not be detected directly under such conditions because of its facile Curtius rearrangement to PhNCO in the GC injector. The conversions and yields

were, therefore, derived from the quantities of PhNCO observed by GC-MS (Table 1.2). Having identified Xantphos as the best ligand for the reaction, we further optimized the process, using 4-FC₆H₄I as a substrate (Table 1.3) in order to monitor the reaction by “noninvasive” ¹⁹F NMR spectroscopy.

Table 1.3. Reaction optimization with Xantphos.^a



entry	solvent (mL)	additive (equiv)	time, h	conversion, % ^b	yield, % ^{b,c}
1 ^{d,e}	THF (5)	Zn (0.5)	7	94	76
2	THF (2)	-	2	26	26
3	THF (2)	NaI (1)	2	14	14
4 ^e	THF (2)	H ₂ O (5.6)	2	92	87
5 ^{d,e}	THF (5)	Zn (0.5) H ₂ O (5.6)	0.67	99	71
6	THF (2)	H ₂ O (5.6)	2	92	74
7	THF (2)	H ₂ O (5.6) NaI (1)	2	70	58
8	THF (2) H ₂ O (2)	-	2	> 99	89
9	toluene (2) H ₂ O (2)	-	2	> 99	97
10	THF (2) hexane (1) H ₂ O (3)	-	2	99	95
11 ^f	toluene (1) H ₂ O (1)	-	7	88	87

^a Reaction conditions: 4-fluoroiodobenzene (1 mmol), NaN₃ (1.2 mmol), Pd₂dba₅³⁰ (2 mol %), and Xantphos (2 mol %) at 23 °C. ^b Determined by ¹⁹F NMR. ^c Main side-product: 4-fluorobenzamide. ^d Pd(OAc)₂ (2 mol %) was used in place of Pd₂dba₅. ^e At 50 °C. ^f 1 mol % Pd and 1 mol % Xantphos.

It is worth to emphasize at this point that in the preliminary isolation attempts we found that, in most instances, the product (ArCON_3) and the starting material (ArI) exhibited nearly identical R_f parameters and could not be separated by column chromatography. Therefore, in order to isolate the product in pure form, the reaction should be driven to full conversion. As was previously noted, under anhydrous conditions, higher conversions and yields were achieved in the presence of a reducing agent, e.g., Zn dust or polymethylhydrosiloxane (PMHS). However, Zn and PMHS were apparently reducing, at least partially, the aroyl azide product to ArCONH_2 (Table 1.3, entry 1).

In search for a solution to the abovementioned problems, we noticed that after 80-90% conversion was reached, the azidocarbonylation became sluggish, indicating that the iodide released from the ArI substrate might deactivate the catalyst by competing for coordination sites on Pd.³⁷ Indeed, NaI deliberately added to the reaction mixture slowed down the reaction considerably (Table 1.3, entries 2 and 3).³⁸ It was therefore proposed that the deactivating effect of iodide could be minimized or eliminated altogether by performing the reaction in an H_2O -organic solvent biphasic system because no excess of inorganic salts would be accumulated in the water-immiscible organic phase. The very first runs performed with additional water surpassed our expectations, producing ArCON_3 in 87% yield at 92% conversion. Moreover, the use of additional water eliminated the need for a reductant additive to easily reach high yields and conversions. Even better results were achieved in biphasic systems H_2O -benzene or H_2O -toluene (Table 1.3, entry 9). However, benzene is toxic and toluene's b.p. of 110 °C would prevent isolation of the volatile and thermally unstable ArCON_3 product. After a series of tests it was found that the aromatic organic phase can be successfully

³⁷ (a) Shen, Q.; Ogata, T.; Hartwig, J. F. *J. Am. Chem. Soc.* 2008, *130*, 6586. (b) Fors, B. P.; Davis, N. R.; Buchwald, S. L. *J. Am. Chem. Soc.* 2009, *131*, 5766.

³⁸ It was established in a separate experiment that NaN_3 in excess does not deactivate the catalyst.

substituted with nontoxic, low-boiling THF-hexane (2:1 v/v; Table 1.3, entry 10). We also attempted the reaction with less than 2% Pd. Although high conversions (up to 88%) and yields (up to 87%) could be obtained with 1% Pd (Table 1.3, entry 11), we settled on 2 mol % of the catalyst in order to reach full conversion that is critical for isolation of the product in pure form (see above).

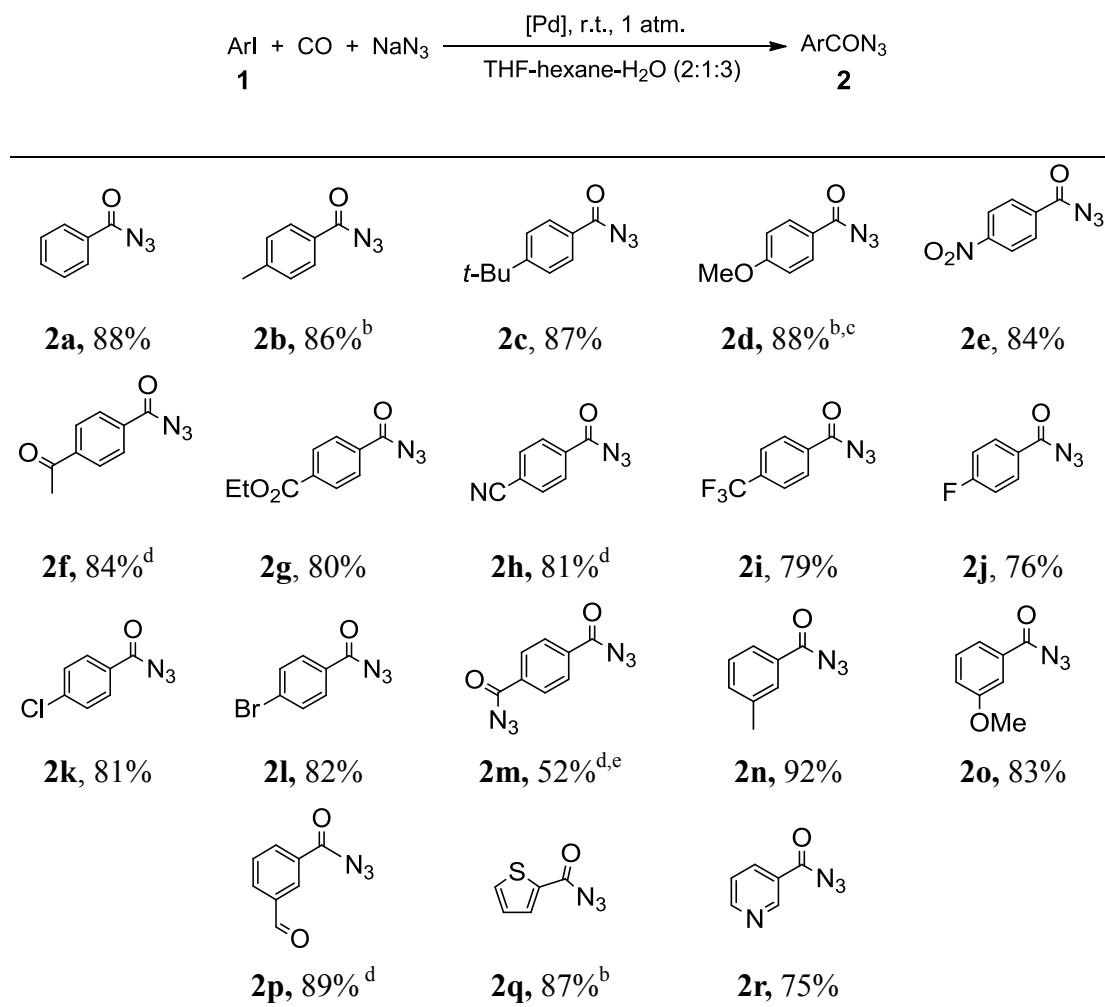
With optimized conditions in hand, a series of aryl iodides (**1**) were successfully converted to the corresponding aryl azides (**2**), as summarized in Table 1.4. All conversions were quantitative, allowing us to isolate the pure products in good to excellent yield. The reaction exhibited high functional group tolerance and smoothly and cleanly occurred with both electron-withdrawing (**2e-l**, **2p**) and electron-donating (**2b-d**, **2n**) substituents on the aromatic ring. The isolated yields were usually in a 80-90% range with only a few exceptions, such as the lower yield of the doubly azidocarbonylated product (**2m**, 52%) obtained from p-diiodobenzene and the higher, 92% yield of m-toluoyl azide **2n**.

Both 2-iodothiophene and 3-iodopyridine were cleanly converted to the corresponding azidocarbonyl derivatives (**2q** and **2r**) in 87% and 75% isolated yield, respectively. In contrast, 2-iodopyridine produced a mixture of products under similar conditions, including 2-PyNCO, 2-PyCONH₂, and 2-PyNH₂. This outcome is likely due to the lower thermal stability of 2-PyCON₃³⁹ and, possibly, to the well-known⁴⁰ dimerization of 2-pyridyl Pd derivatives via the N atoms of the Py ring (Scheme 1.14).

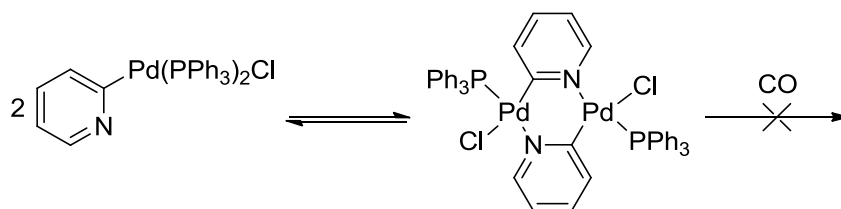
³⁹ Saikachi, H.; Kitagawa, T.; Nasu, A.; Sasaki, H. *Chem. Pharm. Bull.* 1981, 29, 237.

⁴⁰ (a) Bertani, R.; Berton, A.; Di Bianca, F.; Crociani, B. *J. Organomet. Chem.* 1986, 303, 283. (b) Isobe, K.; Nanjo, K.; Nakamura, Y.; Kawaguchi, S. *Bull. Chem. Soc. Jpn.* 1986, 59, 2141.

Table 1.4. Pd-catalyzed azidocarbonylation of iodoarenes.^a

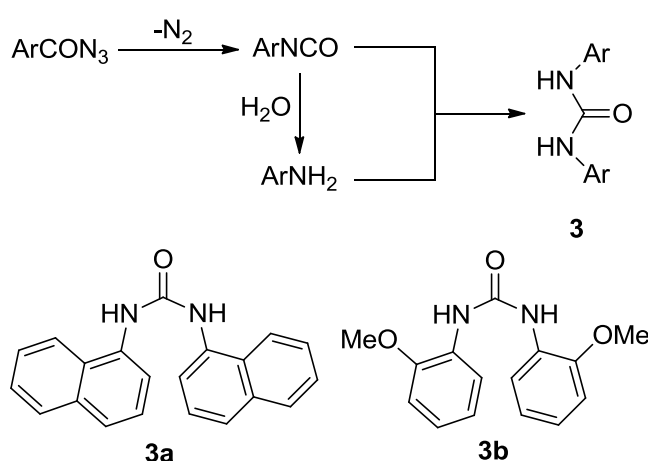


^a Reaction conditions: ArI (1 mmol), NaN₃ (1.2 mmol), Pd₂(dba)₃³⁰ (0.01 mmol; 2 mol % Pd), Xantphos (2 mol %) in THF (2 mL), hexane (1 mL), and water (3 mL). ^b 50 °C (oil bath). ^c Isolated product contained ca. 2% of PhCON₃ as a result of P-Ar/Pd-Ar' exchange. ^d Isolated product contained dba. ^e With 1 mmol of 1,4-diiodobenzene (1m) and double amounts of all reagents and solvents.



Scheme 1.14. Dimerization of 2-pyridyl Pd derivatives via the N atoms of the Py ring.

With ortho-substituted aryl iodide substrates, the reaction did not produce aryl azides but rather gave amides, amines, and diarylureas. A mixture of all three was formed in the reaction of 2-iodotoluene. 2-Iodoanisole and 1-iodonaphthalene reacted more selectively to give predominantly ureas. In this way, N,N'-bis(1-naphthyl)urea (**3a**; 76% yield) and N,N'-bis(2-methoxyphenyl)urea (**3b**; 74% yield, ca. 80% purity by ^1H NMR) were isolated from the reactions of 1-iodonaphthalene and 2-iodoanisole, respectively. Considering the fact that ortho-substituted ArCON_3 are 50-200 times less stable toward the Curtius rearrangement than their meta- and para-isomers,^{39,41} the different reaction outcome for iodoarenes bearing an ortho substituent is hardly surprising. The steric bulk of a group in the ortho position weakens the conjugation between the aromatic ring and the $-\text{CON}_3$ function, thereby destabilizing the latter and lowering the barrier to the Curtius rearrangement. As a result, ortho-substituted aryl azides formed in the reaction quickly rearrange to the corresponding isocyanates. Conversion of the latter to an aniline under the reaction conditions, followed by its addition to the as yet unreacted isocyanate, gives the urea (Scheme 1.15).



Scheme 1.15. *In situ* formation of ureas from originally produced ortho-substituted ArCON_3 .

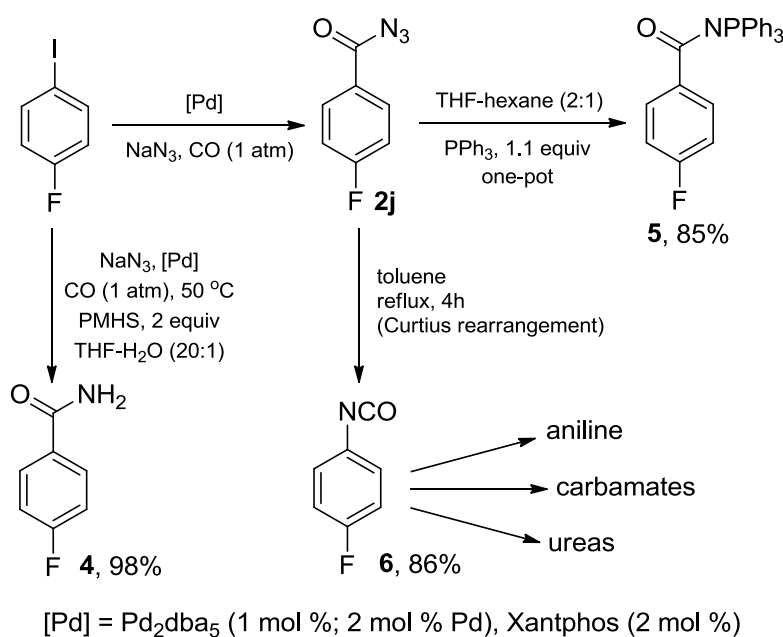
⁴¹ Yukawa, Y.; Tsuno, Y. *J. Am. Chem. Soc.* 1958, *80*, 6346.

As mentioned above, aryl azides are reactive compounds that can be used in a variety of useful transformations. We were able to demonstrate that some of these transformations could be conveniently carried out in situ, without isolation of the aryl azide product formed in the catalytic process (Scheme 1.16). The substrate of choice was 4-fluoroiodobenzene (**1j**) so that the transformations could be conveniently monitored by ¹⁹F NMR. Conducting the azidocarbonylation of **1j** in the presence of PMHS (2 equiv) at 50 °C gave rise to 4-fluorobenzamide (**4**) in nearly quantitative yield. It is worth noting that catalytic carbonylation of aryl halides to primary benzamides represents a considerable challenge.² In another experiment, the entire reaction mixture containing freshly produced **2j** was treated with PPh₃ (1.1 equiv) to prompt the Staudinger reaction that furnished iminophosphorane **5** in 85% overall yield. Furthermore, performing the azidocarbonylation in toluene-water provided a convenient means to carry out the Curtius rearrangement by simply separating and heating the toluene phase containing the ArCON₃ product. In this way, 4-fluorophenylisocyanate (**6**) was obtained in 86% yield (Scheme 1.16), as calculated on the amount of **1j** used. Aryl isocyanates⁴² are widely used in the production of a broad variety of polymers, materials, and valuable chemicals, including carbamates, anilines, and ureas. Examples of the synthesis of aromatic isocyanates from the corresponding aryl halides are extremely rare. Tkatchenko et al.⁴³ have patented Ni-catalyzed reaction of haloarenes with NaOCN to produce aryl isocyanates and their derivatives in up to 50% yield. Most recently, Buchwald's group⁴⁴ demonstrated direct Pd-catalyzed transformation of aryl chlorides and triflates to aryl isocyanates that were converted in situ to unsymmetrical ureas^{44a} and carbamates.^{44b}

⁴² Ulrich, H. *Chemistry and Technology of Isocyanates*; John Wiley & Sons: Chichester, 1997.

⁴³ Tkatchenko, I.; Jaouhari, R.; Bonnet, M.; Dawkins, G.; Lecolier, S. U.S. Patent 4749806, 1987

⁴⁴ (a) Vinogradova, E.V.; Fors, B. P.; Buchwald, S. L. *J. Am. Chem. Soc.* 2012, *134*, 11132. (b) Vinogradova, E. V.; Park, N. H.; Fors, B. P.; Buchwald, S. L. *Org. Lett.* 2013, *15*, 1394



Scheme 1.16. Reaction scope experiments (¹⁹F NMR yields).

Catalyst Deactivation Studies Leading to Major Improvements. As mentioned above, attempts to lower the catalyst loading from 2% to 1% resulted in incomplete conversion. Identification and in-depth understanding of side transformations resulting in catalyst deactivation can be a powerful tool for the design and development of efficient catalytic processes.^{30,35} Therefore, in order to come up with an even more efficient protocol for the azidocarbonylation we studied the loss of catalytic activity in the reaction.

To gain insight into the loss of catalytic activity, we first set up a reaction with a larger quantity of iodobenzene (10 mmol PhI in 0.5 mL of THF) and a lower amount of the Xantphos-Pd₂(dba)₅ catalyst (0.2 mol % Pd). After 2 h under such conditions, the organic phase turned deep purple in color and the catalytic process stopped at ca. 65% conversion. The ³¹P{¹H} NMR spectrum of the organic phase displayed a broad resonance at 6.4 ppm that could not be assigned to any of the identified intermediates

involved in the catalytic loop (see below). The dark purple color suggested that the signal at 6.4 ppm might be from [(Xantphos)PdI₂] (**7**). This assumption was probed by an independent synthesis of **7** from [(Xantphos)PdCl₂] (**8**) and NaI. Both the color and ³¹P{¹H} NMR parameters displayed by the thus prepared **7** (97% yield) appeared identical with those displayed by the catalyst deactivation product. Furthermore, spiking the reaction mixture containing the deactivated catalyst with an authentic sample of **7** resulted in growth in intensity of the ³¹P{¹H} NMR signal at 6.4 ppm. We therefore concluded that the loss of catalytic activity should be attributed to gradual conversion of Pd species in the system to **7**. As was established in an independent experiment, **7** was indeed poorly catalytically active in the azidocarbonylation reaction.⁴⁵ As a new compound, **7** was fully characterized and found to exist as a mixture of cis and trans isomers both in solution and in the solid state (Figure 1.5). In solution, the cis to trans ratio was solvent and temperature dependent. While only *trans*-**7** could be observed in benzene at room temperature, both the cis and trans isomers of **7** were detected in CH₂Cl₂ (³¹P{¹H} NMR). This trend is similar to the reported^{46,47} behavior of [(Xantphos)Pd(Ph)(CF₃)]. Furthermore, the cis to trans ratio for **7** in CH₂Cl₂, as determined by ³¹P{¹H} IGD NMR, was 1:3.5 and 1:1.2 at 25 °C and -30 °C, respectively. Such solvent and temperature dependence of the cis to trans ratio for square-planar *d*⁸ complexes is well-known.⁴⁸

While it is not entirely clear how **7** is formed during the catalytic process, the revealed catalyst deactivation pattern differs considerably from that previously established for the related Pd-catalyzed aromatic cyanation.³⁵ Importantly, unlike

⁴⁵ Under identical conditions (10 mmol PhI in 0.5 mL of THF) with **7** (0.2 mol %) as added catalyst at room temperature, the reaction stopped after 2 h at ca. 20% conversion.

⁴⁶ Grushin, V. V.; Marshall, W. J. *J. Am. Chem. Soc.* 2006, *128*, 12644.

⁴⁷ Bakmutov, V. I.; Bozogljan, F.; Gómez, K.; González, G.; Grushin, V. V.; Macgregor, S. A.; Martin, E.; Miloserdov, F. M.; Novikov, M. A.; Panetier, J. A.; Romashov, L. V. *Organometallics* 2012, *31*, 1315.

⁴⁸ See, for example: (a) Redfield, D. A.; Nelson, J. H. *Inorg. Chem.* 1973, *12*, 15. (b) Anderson, G. K.; Cross, R. J. *Chem. Soc. Rev.* 1980, *9*, 185.

cyanide, azide is not capable of displacing the phosphine ligand on Pd(II) complexes involved in the transformation. Possible reaction pathways from the catalytically active Pd species discussed below to **7** might involve single electron transfer (SET) or redox processes. Although occurring to a minor extent, these side-reactions eventually lead to the formation of inactive **7** as the major Pd species in the reaction medium. Luckily however, this catalyst deactivation does not involve structural changes to the phosphine ligand. Evidently, during the catalysis the P centers of Xantphos remain inaccessible to engage in the Staudinger reaction (Scheme 1.8) and are not oxidized in the Pd(II)/P(III) to Pd(0)/P(V) process.⁴⁹ We therefore reasoned that the catalytic activity could be regained by reducing the poisoned catalyst in the form of [(Xantphos)PdI₂] (**7**) to Xantphos-stabilized Pd(0). This proposal would also explain the above-mentioned beneficial effect of certain reducing agents on the azidocarbonylation process.³⁶

To probe the proposed deactivation pathway, we attempted the reduction of **7**. Both Zn dust and PMHS were found to reduce **7** to Pd(0), the low-cost, stable, and environmentally friendly PMHS being not only more attractive but also showing

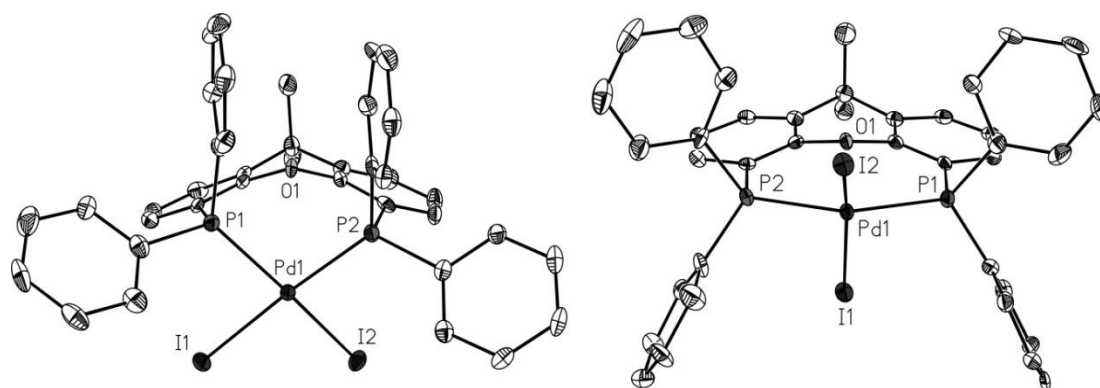
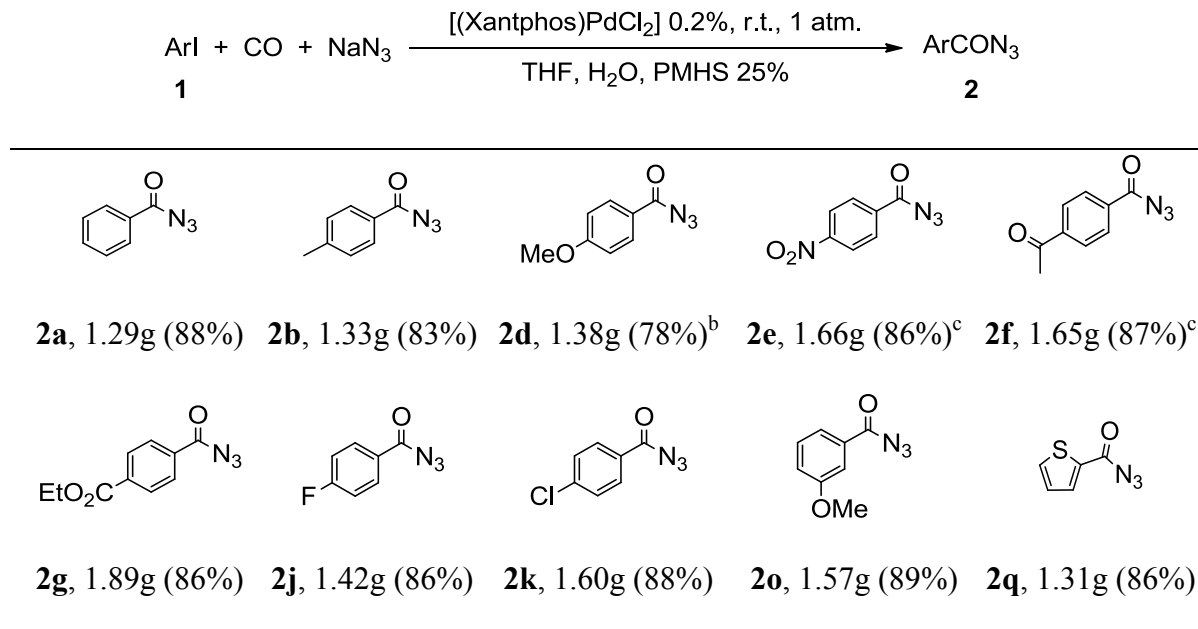


Figure 1.5. ORTEP drawing of *cis*-[(Xantphos)PdI₂]·CH₂Cl₂ (*cis*-**7**·CH₂Cl₂, left) and *trans*-[(Xantphos)PdI₂] (*trans*-**7**, right) with the CH₂Cl₂ molecule and all H atoms omitted and thermal ellipsoids drawn to the 50% probability level.

⁴⁹ Grushin, V. V. *Chem. Rev.* 2004, 104, 1629.

superior performance. After a series of catalytic runs, it was established that in the presence of 0.25 mol equiv of PMHS, iodobenzene can be azidocarbonylated at >99% conversion in 4-6 h with only 0.2% Pd.⁵⁰ Performing the reaction in the presence of PMHS also allowed to use air-stable and easily accessible [(Xantphos)PdCl₂] (**8**) as added catalyst in place of the oxygen-sensitive Xantphos-Pd₂(dba)₃ system. In this way, **8** is reduced in situ with PMHS to give catalytically active Xantphos-ligated Pd(0). Another advantage of using **8** is the avoidance of the presence in the reaction of dba that might contaminate the aroyl azide product. We also took into consideration that the reduction of [(Xantphos)PdCl₂] with PMHS in the presence of water produces HCl, which lowers the pH of the medium, thereby increasing the concentration of hazardous

Table 1.5. Pd-catalyzed azidocarbonylation of iodoarenes (10 mmol) in the presence of **8** (0.2 mol %) and PMHS.^a All yields are isolated yields of pure products.



^a Reaction conditions: ArI (10 mmol), NaN₃ (12 mmol), [(Xantphos)PdCl₂]-CH₂Cl₂ (**8**; 0.02 mmol; 0.2 mol % Pd), K₂CO₃ (0.2 mmol; 2 mol %), in THF (0.5 mL) and water (2 mL) at 23 °C. ^b 2 mL THF. ^c 3 mL THF.

⁵⁰ In the presence of larger quantities of PMHS (2 equiv) at 50 °C, the aroyl azide product undergoes reduction to the corresponding benzamide (see above).

hydrazoic acid. Although HCl is generated in only minute quantities, 0.4% (2 equiv per **8** that is used in the amount of 0.2 mol %), we performed the catalytic reaction in the presence of K₂CO₃ (2%) to neutralize the HCl and thus prevent the formation of HN₃. Under the optimized new conditions, a series of aryl iodides were successfully converted to the corresponding aryl azides with only 0.2 mol % of **8** (Table 1.5). These reactions were performed on a 10 mmol scale and furnished the corresponding pure products in 78-89% isolated yield.

Attempted Azidocarbonylation of Aryl Bromides. Numerous attempts to efficiently azidocarbonylate considerably less reactive bromoarenes were unsuccessful. Although ligands, solvents, and temperature were varied in a broad range, the conversion never exceeded 5% even for more electrophilic, electron-deficient aryl bromides. At elevated temperatures required for Ar-Br oxidative addition to Xantphos-stabilized Pd(0) to occur, the catalyst is quickly deactivated by the Staudinger reaction of the ArCON₃ product with the phosphine ligand. In the presence of CO, activation of bromoarenes with tertiary phosphine complexes of zerovalent palladium is even more sluggish and therefore even higher temperatures are needed (see below). Indeed, evidence has been reported^{51,52} for diminished reactivity of phosphine-ligated Pd(0) under CO pressure. This is in full accord with the fact that higher CO concentrations result in more efficient displacement of the phosphine ligands on the metal with π -acidic carbonyls, thereby diminishing reactivity of the Pd(0) center toward electrophiles.

⁵¹ Ozawa, F.; Soyama, H.; Yanagihara, H.; Aoyama, I.; Takino, H.; Izawa, K.; Yamamoto, T.; Yamamoto, A. *J. Am. Chem. Soc.* 1985, *107*, 3235.

⁵² (a) Mägerlein, W.; Beller, M.; Indolese, A. F. *J. Mol. Catal. A: Chem.* 2000, *156*, 213. (b) Gaviño, R.; Pellegrini, S.; Castanet, Y.; Mortreux, A.; Mentré, O. *Appl. Catal., A* 2001, *217*, 91.

Safety. The reactions summarized in Table 1.5 produced gram quantities of aryl azides that were isolated and purified. As many azido derivatives are explosive, comments are due on safety aspects of the developed catalytic azidocarbonylation method. The so-called “azidophobia” often originates from the extreme shock sensitivity of certain metal azides.⁵³ While care must be exercised when handling organic azides, some of them are less explosive than others and have been safely used on a large scale.⁵⁴ We have not experienced safety problems running the azidocarbonylation reactions and manipulating organic azide derivatives reported herein.

In the current work, we dealt not only with organic azides but also with azido complexes of palladium. The simplest palladium azide, $[\text{Pd}(\text{N}_3)_2]$, is highly shock sensitive and explosive.⁵⁵ Tetraazidopalladates such as $[\text{Pd}(\text{NH}_3)_4]^{2+}[\text{Pd}(\text{N}_3)_4]^{2-}$ are detonated by friction or shock.^{55b} On the other hand, non-homoleptic Pd(II) azide derivatives bearing other ligands can be stable and nonexplosive, e.g., $[\text{Py}_2\text{Pd}(\text{N}_3)_2]$.^{55b} All of the phosphine-ligated mono-azido organopalladium complexes prepared in this work are stable compounds that did not exhibit any signs of explosiveness. It was conceivable, however, that small quantities of diazido Pd(II) species could emerge in the catalytic process from metathesis reactions of the NaN_3 reagent with $[(\text{Xantphos})\text{PdI}_2]$ (**7**, catalyst deactivation product) or $[(\text{Xantphos})\text{PdCl}_2]$ (**8**, added catalyst). To assess safety of such diazido species, we prepared $[(\text{Xantphos})\text{Pd}(\text{N}_3)_2]$ (**9**) by reacting **8** with sodium azide in $\text{CHCl}_3 - \text{H}_2\text{O}$ (94% yield). Complex **9** was fully characterized, including by single-crystal X-ray diffraction (Figure 1.6) and found to be stable. This diazide was not shock-sensitive (striking with a hammer) and did not show any signs of

⁵³ See footnote 77 in: Kolb, H. C.; Finn, M. G.; Sharpless, K. B. *Angew. Chem. Int. Ed.* 2001, 40, 2004.

⁵⁴ González-Bobes, F.; Kopp, N.; Li, L.; Deerberg, J.; Sharma, P.; Leung, S.; Davies, M.; Bush, J.; Hamm, J.; Hrytsak, M. *Org. Process Res. Dev.* 2012, 16, 2051 and references cited therein.

⁵⁵ (a) Beck, W.; Fehlhammer, W. P.; Pöllmann, P.; Schuierer, E.; Feldl, K. *Chem. Ber.* 1967, 100, 2335. (b) Beck, W.; Klapötke, T. M.; Knizek, J.; Nöth, H.; Schütt, T. *Eur. J. Inorg. Chem.* 1999, 523.

decomposition in DMF at 100 °C after 4 hours. We conclude that Xantphos-stabilized azido palladium species involved in the catalytic process are safe to work with. One must bear in mind, however, that (i) in the presence of NaN₃ and in the absence of stabilizing tertiary phosphine or other ligands, a Pd(II) source may be converted to highly explosive species such as [Pd(N₃)₂]⁵⁵ and (ii) azido derivatives should always be handled with care.

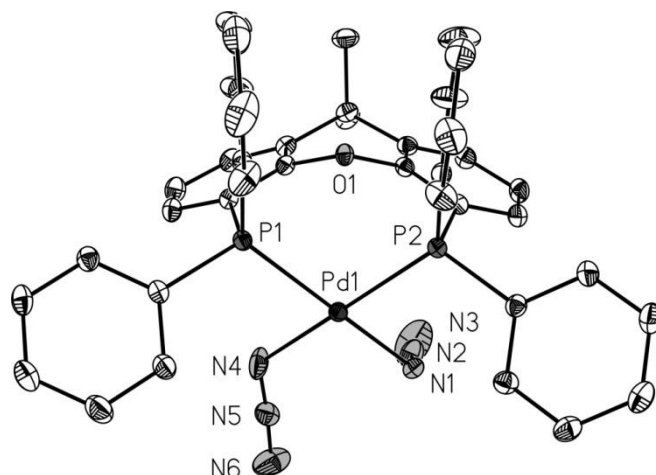


Figure 1.6. ORTEP drawing of *cis*-[(Xantphos)Pd(N₃)₂]*·*CHCl₃ (*cis*-9·CHCl₃) with the CHCl₃ molecule and all H atoms omitted and thermal ellipsoids drawn to the 50% probability level.

Experimental Mechanistic Studies. In parallel with the development of an efficient catalytic azidocarbonylation process we studied the mechanism of this reaction. Like all Pd-catalyzed cross-coupling reactions of aryl halides, the azidocarbonylation involves oxidative addition of the haloarene substrate to Pd(0) as the first key step. Oxidative addition of PhI to Pd₂(dba)₃/Xantphos at room temperature to give [(Xantphos)Pd(Ph)I] (**10**) has been reported previously.⁴⁶ We reasoned, however, that in the presence of CO, Ar-I activation with Xantphos-stabilized Pd(0) might involve mixed phosphino-carbonyl species and lead to a different outcome. Surprisingly little is known about

oxidative addition to Pd(0) complexes bearing both tertiary phosphine and CO ligands.^{51,56}

Mixing Xantphos with Pd₂(dba)₅ in a 1:1 ligand to Pd ratio in benzene-*d*₆ produced two ³¹P{¹H} NMR-observable species, [(Xantphos)Pd(dba)] (**11**; two doublets at 11.3 and 13.5 ppm; *J*_{P-P} = 10.6 Hz) and [(Xantphos)₂Pd] (two broad multiplets at 3.5 and 6.0 ppm)⁴⁶ in a 4:1 ratio. This pattern is similar to the one previously reported³² for the 4,7-di-*tert*-butylXantphos-Pd₂(dba)₃ system. The structure of **11** (Figure 1.7) was established by an X-ray diffraction study of **11**·3THF obtained from a repeat of the reaction of Xantphos with Pd₂(dba)₅ in THF.

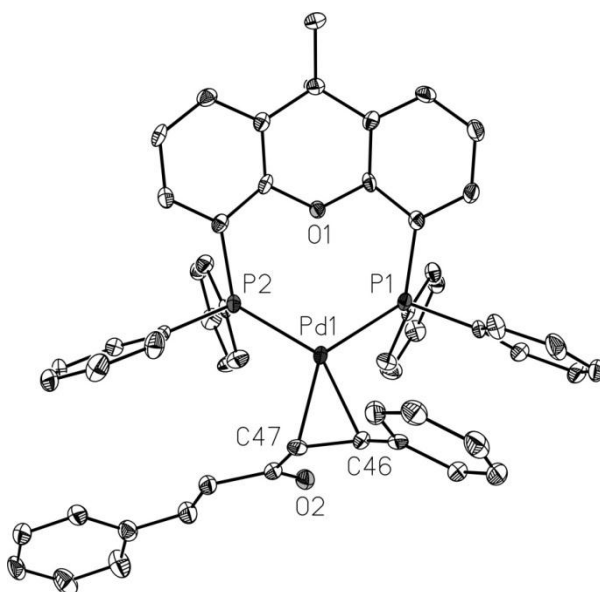


Figure 1.7. ORTEP drawing of [(Xantphos)Pd(dba)]·3THF (**11**·3THF) with the THF molecules and all H atoms omitted for clarity and thermal ellipsoids drawn to the 50% probability level.

⁵⁶ Reported mechanistic information on oxidative addition of organic halides to mixed phosphino carbonyl Pd(0) species is extremely limited. For selected examples, see: (a) Kudo, K.; Sato, M.; Hidai, M.; Uchida, Y. *Bull. Chem. Soc. Jpn.* 1973, *46*, 2820. (b) Stille, J. K.; Lau, K. S. Y. *J. Am. Chem. Soc.* 1976, *98*, 5841. (c) Lau, K. S. Y.; Wong, P. K.; Stille, J. K. *J. Am. Chem. Soc.* 1976, *98*, 5832.

Adding CO (1 atm) to the solution of [(Xantphos)Pd(dba)] and [(Xantphos)₂Pd] generated from Xantphos and Pd₂(dba)₅ in benzene-*d*₆ or THF resulted in instantaneous full conversion of both complexes and the appearance of only one singlet resonance at 10.5 ppm (C₆D₆) in the ³¹P{¹H} NMR spectrum. Two strong bands at 1974 and 2014 cm⁻¹ in the FT-IR spectrum of the reaction solution in THF suggested⁵⁷ that the species resonating at 10.5 ppm in the ³¹P{¹H} NMR spectrum is a dicarbonyl complex, likely [(Xantphos)Pd(CO)₂] (**12**). This structure was indeed established by single crystal X-ray diffraction of **12**·hexane (Figure 1.8) obtained from an independent experiment (see below).

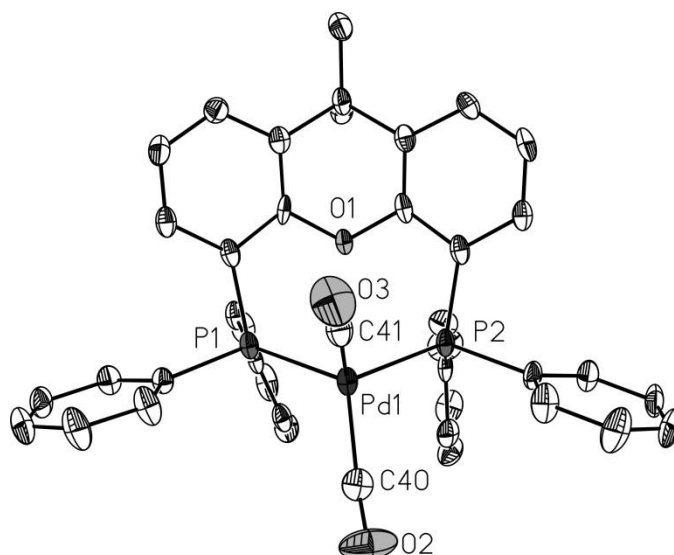
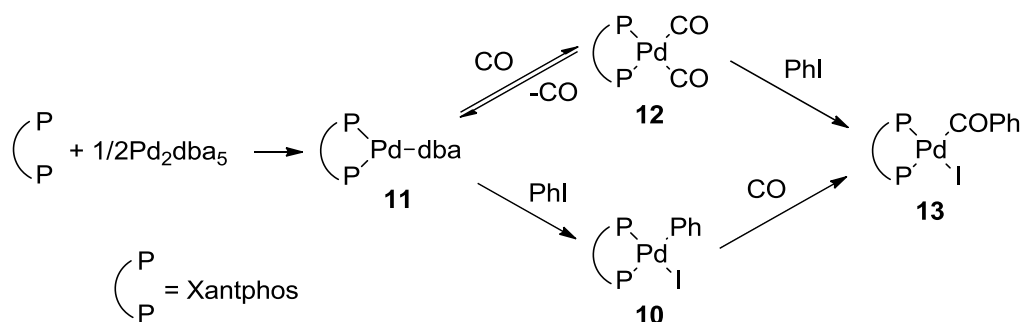


Figure 1.8. ORTEP drawing of [(Xantphos)Pd(CO)₂]·*n*-C₆H₁₄ (**12**·hexane) with cocrystallized hexane and all H atoms omitted and thermal ellipsoids drawn to the 50% probability level.

⁵⁷ Braterman, P. S. *Metal Carbonyl Spectra*; Academic Press: London, 1975.

We then found that bubbling argon through a solution of **12** (generated from **11** and CO) quantitatively produced **11** within one minute. These observations clearly indicated that although CO binds more tightly to (Xantphos)Pd(0) than dba, the formation of **12** from **11** is reversible and that the equilibrium between the two can be easily shifted to **11** under CO-deficient conditions. Both **11** and **12** were found to react with PhI. The reaction of **11** with PhI has been previously shown to produce [(Xantphos)Pd(Ph)I] (**10**; see above). In the current work, we found that **10** readily reacted with CO (1 atm) to give selectively the product of CO insertion into the Pd-Ph bond [(Xantphos)Pd(COPh)I] (**13**) that was also formed upon addition of PhI to **12** under CO (Scheme 1.17). Complex **13** was isolated and fully characterized, including by single-crystal X-ray diffraction (Figure 1.9). Like its bromo congener [(Xantphos)Pd(COPh)Br],^{34b} **13** was found to be cis in the crystal, yet displayed only one ³¹P{¹H} NMR singlet in THF, benzene, and CD₂Cl₂. Although this behavior could be attributed to **13** being exclusively trans in solution, it is likely that the complex undergoes facile cis-trans isomerization that may not be frozen out on the NMR time scale. A very low barrier of only 6.1 kcal/mol was later computed for this isomerization (see below).²⁶



Scheme 1.17. Two oxidative addition pathways leading to **13**.

As follows from Scheme 1.17, there are two possible oxidative addition pathways leading to the key intermediate **13**. If Ar-I oxidative addition is the rate-limiting step, the catalytic process should be slower at higher concentrations of CO favoring the formation of **12**. The latter is less electron-enriched than **11** because of the stronger π -acidity of two CO ligands as compared with dba. Slower reaction rates under higher CO pressures have been reported⁵² for Pd-catalyzed alkoxy carbonylation reactions. The literature data⁵⁸ on solubility of CO in benzene allowed us to estimate the CO to Pd ratio in our standard catalytic azidocarbonylation runs (1 atm, 25 °C) at ca. 1:1. Under such conditions, 4-fluoroiodobenzene was azidocarbonylated at 99% conversion in 2 h. In a repeat of this run under 7 atm of CO (CO: Pd = ca. 8), only 25% conversion was reached after the same period of time, indicating that [CO] does influence the rate-limiting oxidative addition step, as shown in Scheme 1.17. This conclusion was then confirmed by computational studies (see below).²⁶

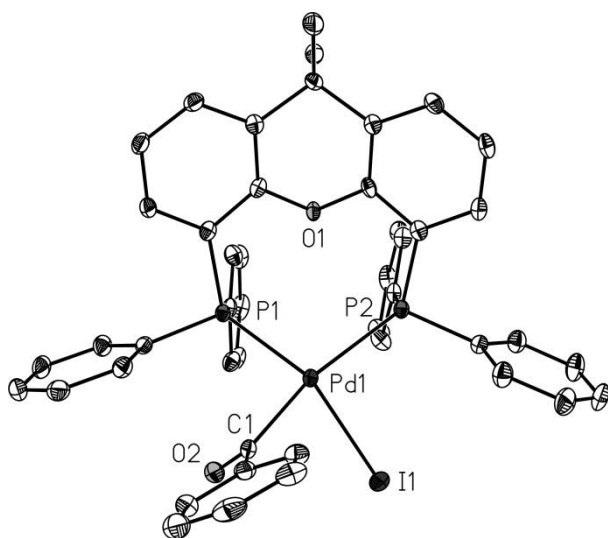
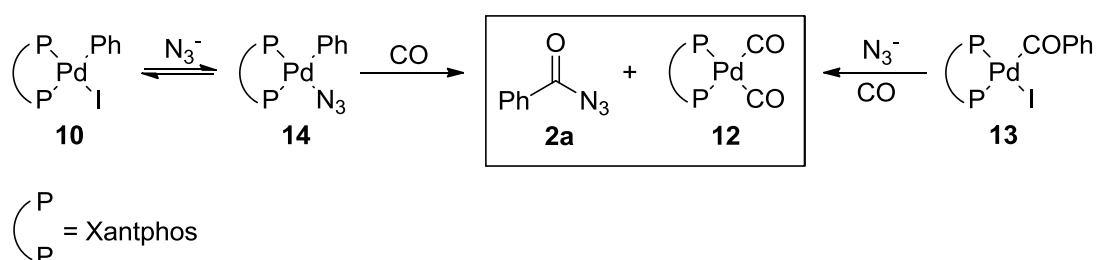


Figure 1.9. ORTEP drawing of *cis*-[(Xantphos)Pd(COPh)I]·0.5THF (*cis*-**13**·0.5THF) with the THF molecule and all H atoms omitted and thermal ellipsoids drawn to the 50% probability level.

⁵⁸ Gjaldbæk, J. Chr. *Acta Chem. Scand.* 1952, 6, 623.

Both products of the oxidative addition, **10** and **13**, were found to readily react with azide, as shown in Scheme 1.18. Treatment of **13** with $[\text{Bu}_4\text{N}]^+\text{N}_3^-$ in benzene⁵⁹ under CO resulted in the instantaneous clean formation of PhCON_3 along with $[(\text{Xantphos})\text{Pd}(\text{CO})_2]$ (**12**). In this way, the modeled catalytic cycle was closed because PhCON_3 is the final product of the process and **12** can commence another turnover by Ar-I activation via the oxidative addition (Scheme 1.17).



Scheme 1.18. Reactions of **10** and **13** with CO and N_3^- .

Intermediate **10** that would be produced under CO-deficient conditions (Scheme 1.17) was also reactive toward azide (Scheme 1.18). The reaction of **10** with 1.1 equiv of $[\text{Bu}_4\text{N}]^+\text{N}_3^-$ in benzene produced $[(\text{Xantphos})\text{Pd}(\text{Ph})(\text{N}_3)]$ (**14**) quantitatively. This anionic ligand exchange also readily occurred with NaN_3 under biphasic conditions in the absence of a phase-transfer agent. In benzene – aqueous NaN_3 , thermodynamic equilibrium between **10** and **14** was reached within 5 minutes at vigorous stirring. However, only ca. 60% conversion to **14** was observed at equilibrium even in the presence of 10 equiv of NaN_3 . To isolate **14**, the bromo analogue⁶⁰ of **10** was used because in the presence of water the equilibrium between the Pd-X and Pd- N_3 (**14**)

⁵⁹ X-ray quality crystals of tetrabutylammonium azide formed from its benzene solution on standing. One of them was used for crystal structure determination of $[\text{Bu}_4\text{N}]^+\text{N}_3^-$ (See the Experimental Section for details).

⁶⁰ Fujita, K.; Yamashita, M.; Puschmann, F.; Alvarez-Falcon, M. M.; Incarvito, C. D.; Hartwig, J. F. *J. Am. Chem. Soc.* 2006, *128*, 9044.

complexes is shifted more toward the latter for X = Br than I⁶¹ since bromide is more strongly hydrated than iodide. The anion exchange extraction⁶² of the Br⁻ from [(Xantphos)Pd(Ph)Br] in CH₂Cl₂ with aqueous NaN₃ gave **14** that was isolated pure and fully characterized in solution by ¹H and ³¹P{¹H} NMR data and in the solid state by single-crystal X-ray diffraction (Figure 1.10).

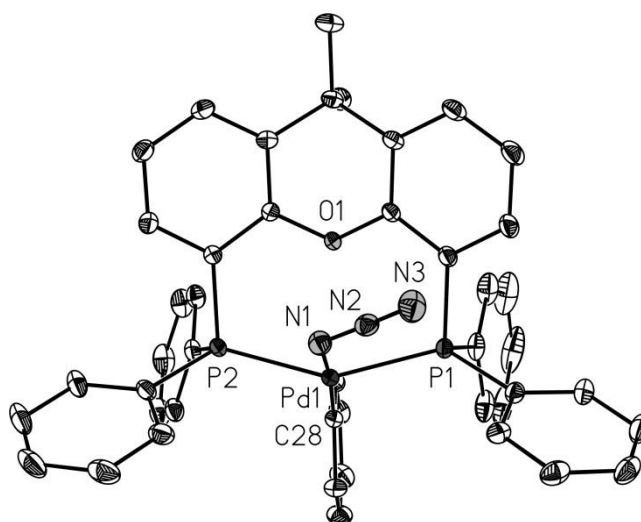


Figure 1.10. ORTEP drawing of *trans*-[(Xantphos)Pd(Ph)(N₃)] (**trans-14**) with all H atoms omitted and thermal ellipsoids drawn to the 50% probability level.

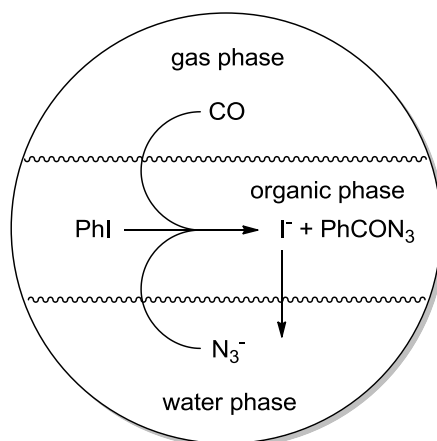
Bubbling CO through a solution of **14** in benzene-*d*₆ resulted in the instantaneous formation of PhCON₃ and [(Xantphos)Pd(CO)₂] (**12**; Scheme 1.18). Repeating this reaction in toluene with subsequent addition of hexanes produced X-ray quality crystals for the structure determination of **12** (Figure 1.8).

The above-described results pointed clearly to two reaction pathways to PhCON₃ with simultaneous regeneration of Pd(0), via **13** and via **14** (Schemes 1.17 and 1.18). Both routes likely lead to [(Xantphos)Pd(COPh)(N₃)] (**15**) as a common intermediate that undergoes PhCO-N₃ reductive elimination. The competition between these two

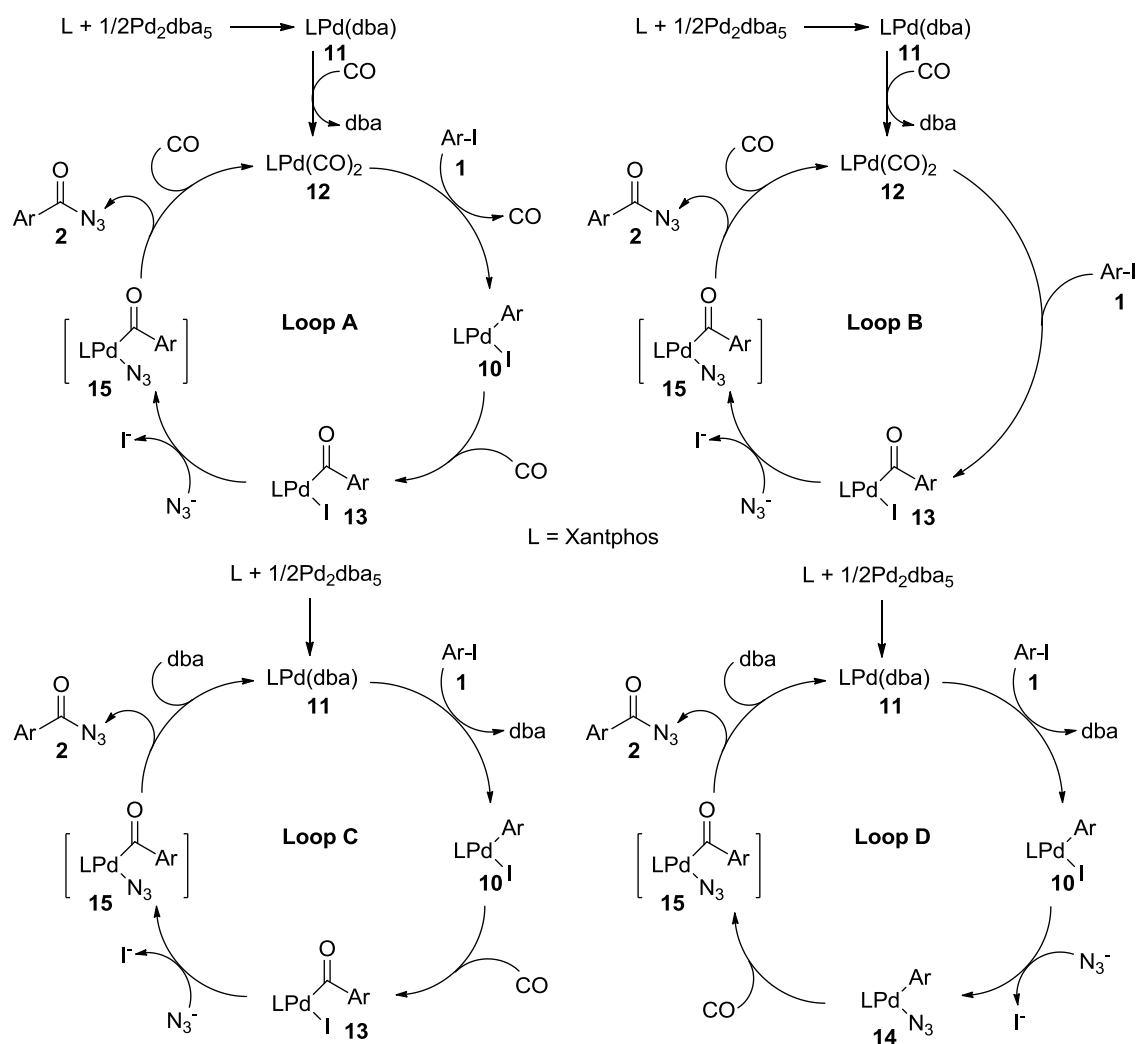
⁶¹ (a) Grushin, V. V. *Angew. Chem. Int. Ed.* 1998, *37*, 994. (b) Flemming, J. P.; Pilon, M. C.; Borbulevitch, O. Ya.; Antipin, M. Yu.; Grushin, V. V. *Inorg. Chim. Acta* 1998, *280*, 87.

⁶² Coyle, R. J.; Slovokhotov, Yu. L.; Antipin, M. Yu.; Grushin, V. V. *Polyhedron* 1998, *17*, 3059.

reaction channels is expected to be strongly dependent on concentrations of CO and N_3^- , the nature of the medium, and other factors that control anionic ligand exchange and migratory insertion processes as well as mass transfer in the triphasic liquid-liquid-gas system (Scheme 1.19). Two extreme cases could be considered. If the catalytic reaction is performed in the presence of CO in excess ($[Pd] < [CO]$), the pathway involving **13** is expected to dominate because the facile migratory insertion of CO into the Pd-C bond of **10** is a homogeneous process rapidly occurring in the organic phase, whereas the alternative route, via **14**, requires slower anionic ligand exchange at the liquid-liquid interface of the biphasic system. The prevailing catalytic cycle would then involve the sequence **12** \rightarrow **10** \rightarrow **13** \rightarrow **15** \rightarrow **12** (loop A in Scheme 1.20). It remains unknown if the oxidative addition of ArI to **12** occurs via pre-dissociation of both carbonyl ligands from the Pd center. If it does, then **10** is likely involved in the cycle, albeit as a short-living intermediate that is quickly transformed to **13** via facile CO insertion. However, if at least one CO ligand remains on Pd during the Ar-I oxidative addition, the formation of **10** might be skipped, with **12** going directly to **13**, i.e. **12** \rightarrow **13** \rightarrow **15** \rightarrow **12** (Scheme 1.20, loop B). Under CO-deficient conditions ($[Pd] > [CO]$), two other catalytic pathways are possible, **11** \rightarrow **10** \rightarrow **13** \rightarrow **15** \rightarrow **11** (loop C) and **11** \rightarrow **10** \rightarrow **14** \rightarrow **15** \rightarrow **11** (loop D). The competition between C and D would obviously depend on relative rates of the transformation of **10** to **13** (CO insertion) and to **14** (I^-/N_3^- exchange), as well as of carbonylation of **14** to **15**. As described above, the possibility for all four pathways, A, B, C, and D (Scheme 1.20) has been demonstrated by stoichiometric experiments. Regardless of which of the reaction channels wins the competition, the process invariably leads to the desired aroyl azide product. Importantly, unlike $[(R_3P)_2Pd(Ph)(N_3)]^{27}$ ($R = Me, Et$; see above), **14** does *not* form a Pd-NCO species via N_2 loss upon treatment with CO.



Scheme 1.19. Pd-catalyzed azidocarbonylation of PhI under triphasic conditions.



Scheme 1.20. Four possible catalytic loops for Pd-catalyzed azidocarbonylation of ArI.

In our experimental mechanistic studies, we have succeeded in isolation and full characterization of all intermediates involved in the azidocarbonylation process (Schemes 1.17, 1.18, and 1.20; Ar = Ph), except for [(Xantphos)Pd(COPh)(N₃)] (**15**). As **15** is too unstable for isolation and/or detection, quickly undergoing reductive elimination of PhCON₃, various routes to **15** and the product forming C-N coupling step were studied by computational means.²⁶

Computational Studies.²⁶ The density functional theory (DFT) calculations have been employed to assess the different mechanistic possibilities outlined in Scheme 1.20.⁶³

We initially considered the different species that may be involved in the initial Ph-I oxidative addition step under conditions of excess CO (i.e. loop A vs. loop B; Scheme 1.20). The most stable Pd(0) precursor under these circumstances is [(Xantphos)Pd(CO)₂] (**12**; $G = 0.0$ kcal/mol), and successive CO dissociations from this species lead to trigonal-planar [(Xantphos)Pd(CO)] ($G = +12.2$ kcal/mol) and [(Xantphos)Pd] ($G = +38.1$ kcal/mol; see Figure 1.11). PhI can add to the latter to give an η^2 -adduct bound through the C_{ipso}-C_{ortho} bond (**11**; $G = +26.7$ kcal/mol) which is the direct precursor to C-I cleavage. This proceeds with a small additional barrier of 4.7 kcal/mol through a pseudo-tetrahedral transition state (TS_{0A1}; see Figure 1.12) which leads initially to **13** ($G = +11.2$ kcal/mol), an isomer of **10** featuring a square-pyramidal geometry with a weakly bound axial iodide and a κ^3 -P,O,P Xantphos ligand.⁶⁴ Elongation of the Pd-O bond leads to *trans*-**10** ($G = +4.2$ kcal/mol) with a

⁶³ For additional computational details, see the original publication: Miloserdov, F. M.; McMullin, C. L.; Martínez Belmonte, M.; Benet Buchholz, J.; Bakhmutov, V. I.; Macgregor, S. A.; Grushin, V. V. *Organometallics*, 2014, 33, 736.

⁶⁴ For previous computational studies of Ph-X activation (X = Cl, Br) at [Pd(Xantphos)], see: Hicks, J. D.; Hyde, A. M.; Cuezva, A. M.; Buchwald, S. L. *J. Am. Chem. Soc.* 2009, 131, 16720. Structure 2a reported

minimal barrier of 1.7 kcal/mol. Alternatively, Ph-I cleavage may occur at [(Xantphos)Pd(CO)]. In this case no η^2 -adduct could be located, possibly due to increased steric encumbrance around the Pd center; instead the most stable precursor located is a non-covalently bound adduct in which PhI lies above the metal coordination plane with the iodine directed toward the Pd centre (I2; Pd...I = 3.06 Å; $G = +8.8$ kcal/mol). From here Ph-I bond cleavage occurs via TS_{0A2} ($G = +23.5$ kcal/mol) which displays a distorted trigonal-bipyramidal geometry with CO and I in the axial sites (see Figure 1.12). TS_{0A2} also features significant elongation of the Pd-P2 distance (by *ca.* 0.14 Å *cf.* I2) and IRC calculations show this bond breaks completely in forming intermediate I4(I) (Pd...P2 = 3.66 Å; $G = +6.5$ kcal/mol). I4(I) displays square-planar coordination geometry around Pd with CO again trans to I, this being favored (as in TS_{0A2}) due to the trans arrangement of π -acceptor and π -donor ligands. Figure 1.11 shows that Ph-I bond activation is most accessible via [(Xantphos)Pd(CO)] and proceeds with an overall barrier of 23.5 kcal/mol to form [(Xantphos)Pd(CO)(I)(Ph)] directly, i.e. suggesting that loop B will be in operation (Scheme 1.20).

We have also considered Ph-I activation under low CO concentrations. In these conditions the likely Pd(0) precursor is [(Xantphos)Pd(dba)] (**11**), which is computed to lie 10.0 kcal/mol above [(Xantphos)Pd(CO)₂]. The estimated barrier (via TS_{0A1}) would therefore be 21.4 kcal/mol, assuming facile displacement of dba by PhI, and this is consistent with more facile aryl halide activation in the absence of CO noted above.

in that work is related to I3 located here, although in that case no Pd-O interaction was apparent and a different orientation of the Ph ligand was seen.

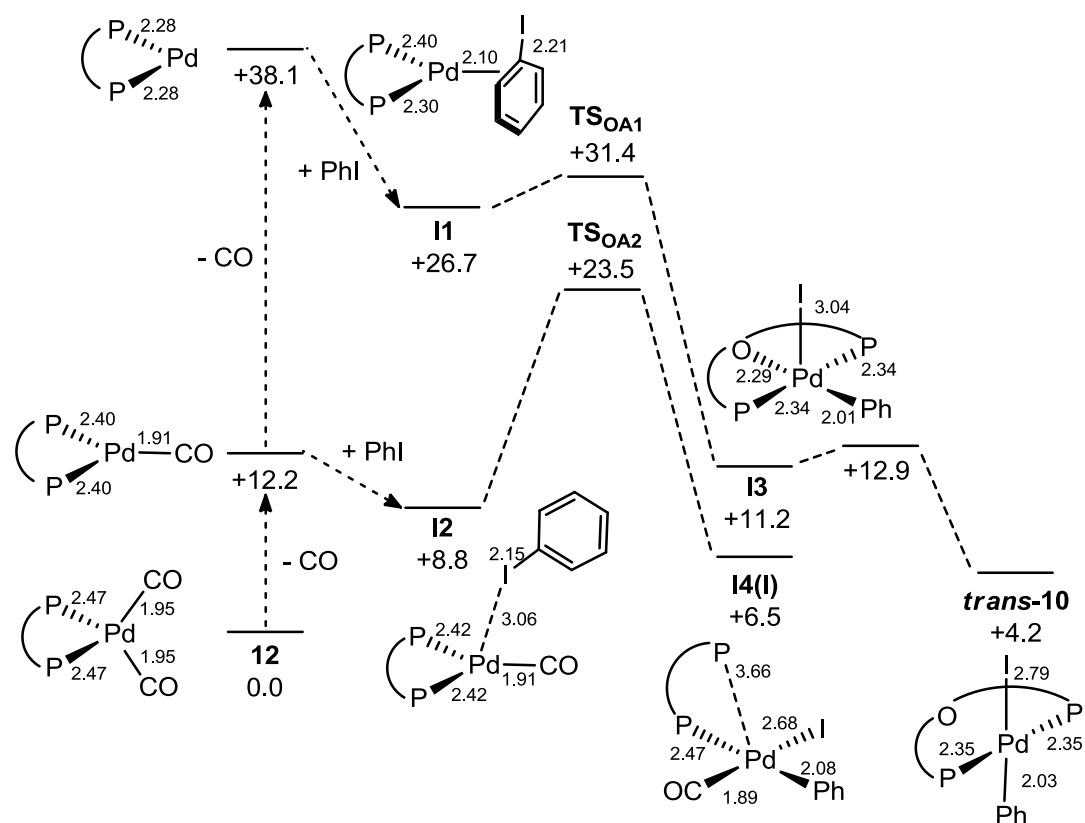


Figure 1.11. Alternative computed reaction profiles for PhI activation at $[(Xantphos)Pd(CO)_2]$ (12). Relative free energies in water are given in kcal/mol.

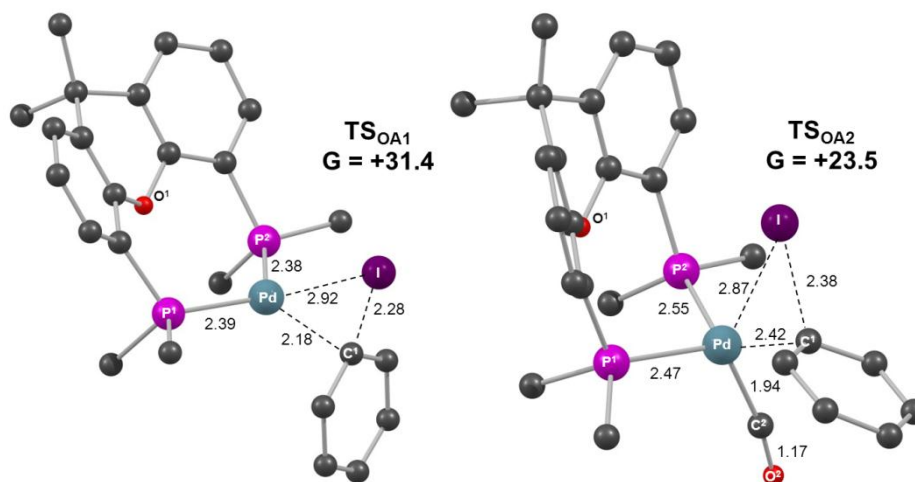


Figure 1.12. Computed geometries for TS_{OA1} (left), and TS_{OA2} (right). Xantphos Ph groups are truncated at the ipso carbon and H atoms are omitted for clarity.

The computed reaction profile for the remainder of the catalytic cycle along loop **B** is shown in Figure 1.13. CO migratory insertion in **I4(I)** proceeds via **TS_{MI(I)}** (Figure 1.14) with a barrier of 4.4 kcal/mol and forms *trans*-**13** at -7.8 kcal/mol⁶⁵ which is computed to be 0.4 kcal/mol less stable than *cis*-**13** in solution. Formation of *cis*-**15** may proceed via *trans-cis* isomerization in **13** and I/N₃⁻ exchange, or via I/N₃⁻ exchange in *trans*-**13** followed by *trans-cis* in **15**. Both possibilities appear to be readily accessible, for example *trans-cis* isomerization in **13** has a barrier of only 6.1 kcal/mol, while both I/N₃⁻ exchange processes are computed to lie close to equilibrium.⁶⁶ Once *cis*-**15** is formed C-N bond formation proceeds via **TS_{RC}** (Figure 1.14) with a barrier of 11.9 kcal/mol, readily accessible at room temperature and so consistent with the non-observation of **15** experimentally.⁶⁷ This gives **I5** the most stable form of which has PhCON₃ bound as an η²-arene fashion through a C_{ipso}-C_{ortho} bond (*G* = -6.4 kcal/mol). The PhCON₃ product can then be displaced from **I5** by CO to regenerate [(Xantphos)Pd(CO)]. Each of these steps is readily accessible and the calculations suggest that after rate-limiting oxidative addition the formation of products and regeneration of the catalyst **12** will be rapid and strongly exergonic ($\Delta G = -30.4$ kcal/mol).

Further calculations probed the effect of I/N₃⁻ exchange on the migratory insertion process. I/N₃⁻ substitution in **I4(I)** gives **I4(N₃)** (*G* = +6.0 kcal/mol) in which azide is now trans to CO. Thus I/N₃⁻ exchange is again close to equilibrium ($\Delta G = -0.5$

⁶⁵ Alternative isomers of **I4(I)** are possible, e.g. with CO trans to phosphine and Ph trans to I. However, migratory insertion has been shown to be facilitated when the transferring group (here Ph) is trans to a highest trans influence co-ligand, i.e. as in **I4(I)**, in which Ph is trans to phosphine. For a related example, see: Macgregor, S. A.; Neave, G. W. *Organometallics*, 2004, 23, 891.

⁶⁶ We²⁶ have not attempted to locate transition states for I/N₃⁻ exchange, but have assumed this readily occurs under the reaction conditions, as was shown to be the case experimentally for the conversion of **10** to **14**.

⁶⁷ We²⁶ also attempted to locate a pathway for C-N bond formation via the direct nucleophilic attack of free azide at the benzoyl ligand in **15**. Several linear transits were run to probe this possibility, with optimizations being run with the water solvent being included in the SCF procedure in order to treat the free anionic nucleophile. However, in all cases the approach of azide led to facile formation of a Pd-N₃ bond (with displacement of iodide or one arm of the Xantphos ligand) prior to C-N bond formation.

kcal/mol), although the subsequent migratory insertion transition state is now less accessible than for the iodide analogue ($TS_{MI}(N_3)$: $G = +15.4$ kcal/mol *cf.* $TS_{MI}(I)$ at $+10.9$ kcal/mol). Both processes are more accessible than the preceding (overall rate-limiting) Ph-I oxidative addition and so a proportion of the catalysis could therefore proceed through $I4(N_3)$ leading to the direct formation of *trans*-15.

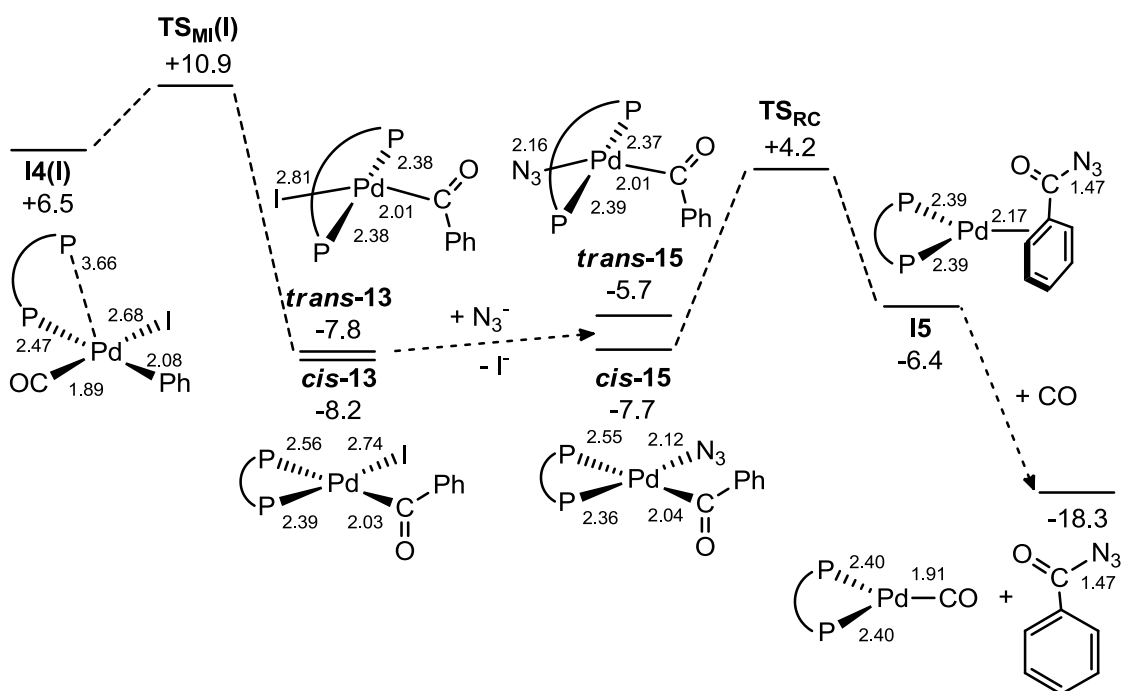


Figure 1.13. Computed reaction profile for the formation of $[(Xantphos)Pd(CO)]$ and $PhCON_3$ from $I4(I) + N_3^-$. Relative free energies in water are given in kcal/mol.

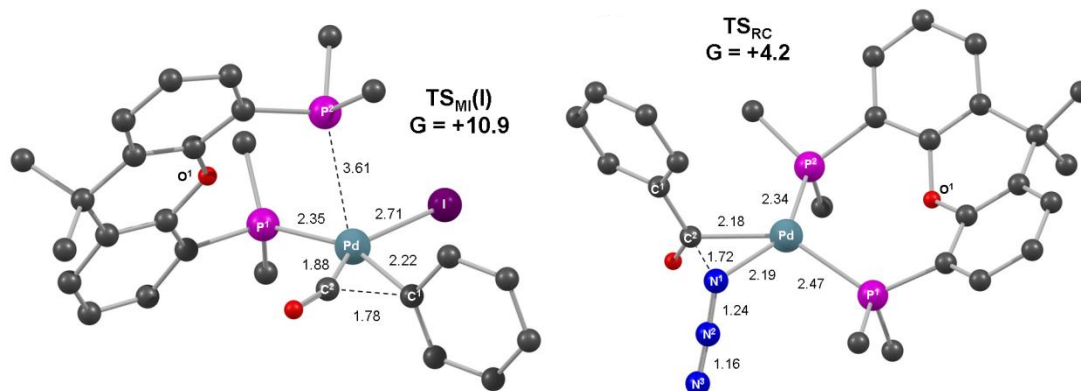


Figure 1.14. Computed geometries for $TS_{MI}(I)$ (left), and TS_{RC} (right). Xantphos Ph groups are truncated at the ipso carbon and hydrogen atoms are omitted for clarity.

Azidocarbonylation Mechanism. As follows from the above, the biggest drawback of the Pd-catalyzed azidocarbonylation is its inapplicability to aryl bromides. Being less reactive than aryl iodides, bromoarenes can be activated via oxidative addition to Xantphos-stabilized Pd(0) only at elevated temperatures that aryl azides do not survive. Furthermore, diminished stability constants of various Pd(Xantphos) units involved in the catalysis at higher temperatures facilitate the Staudinger reaction leading to catalyst deactivation, as described above. It is particularly important that Ar-X activation with phosphine-stabilized Pd(0) takes place with a higher activation barrier in the presence than in the absence of CO. Our studies shed new light on this poorly studied and understood key mechanistic feature (see below).

The azidocarbonylation reaction occurs under triphasic liquid-liquid-gas conditions (Scheme 1.19). Aside from mass-transfer that clearly depends on such parameters as agitation rate and pressure, the rate-determining step of the catalytic process is Ar-I activation with Pd(0). The experimental and computational results obtained in the current work allow us to analyze two extreme cases: (1) the catalytic reaction is carried out with CO in excess ($[Pd] < [CO]$; loops **A** and **B** in Scheme 1.20) and (2) the process occurs under CO-deficient conditions ($[Pd] > [CO]$; loops **C** and **D** in Scheme 1.20). The experimentally observed slower reaction rate at higher concentrations of CO (see above) accords with the computational results. The prohibitively high barrier (38.1 kcal/mol) to the loss of both carbonyl ligands from the (Xantphos)Pd(0) moiety (Figure 1.11) rules out Ar-I oxidative addition to the carbonyl-free Pd(0) in the presence of CO in excess. Dissociation of only one CO from [(Xantphos)Pd(CO)₂], however, occurs with a much lower free energy cost of only 12.2 kcal/mol suggesting that [(Xantphos)Pd(CO)] is accessible. (In the presence of larger quantities of CO, the equilibrium between the two is obviously shifted to the unreactive dicarbonyl complex.)

Furthermore, it has been demonstrated by the calculations that the monocarbonyl [(Xantphos)Pd(CO)] can activate the Ph-I bond with the overall barrier of 23.5 kcal/mol. This is consistent with the estimated value $\Delta G^\ddagger \approx 21.5 \pm 0.5$ kcal/mol at 296 K from the experimental data for oxidative addition of 4-FC₆H₄I to [(Xantphos)Pd(CO)₂] (see the Experimental Section). However, [(Xantphos)Pd(Ar)(I)] is not on the reaction coordinate in this case and the process is mediated by [(Xantphos)Pd(CO)(Ar)(I)] leading to [(Xantphos)Pd(COAr)I], as shown in Figure 1.13 for Ar = Ph. Therefore, in the presence of CO in excess, the reaction is governed by loop **B**, not **A** (Scheme 1.20).

We define CO-deficient conditions as [Pd] \approx or $>$ [CO] and CO diffusion rate is slower than that of the catalytic reaction. Under such conditions, loops **C** and **D** (Scheme 1.20) are expected to be operational since the Pd(0) produced in the product-forming step would undergo fast Ar-I oxidative addition before the CO consumed in the catalytic cycle is replenished from the gas phase. With [(Xantphos)Pd(dba)] (**11**) as the resting state of the Pd(0) form of the active catalyst, the computed barrier is 21.4 kcal/mol (see above). The resultant stable and isolable intermediate [(Xantphos)Pd(Ph)(I)]⁴⁶ (**10**) can then either undergo carbonylation to [(Xantphos)Pd(COPh)I] (**13**) when CO becomes available (loop **C**) or react with azide to form [(Xantphos)Pd(Ph)(N₃)], (**14**; loop **D**). Mass transfer is involved in both processes since the Pd catalyst is located in the organic phase, the azide source (NaN₃) is in the immiscible aqueous layer, and CO is in the headspace. Although under anhydrous conditions the experimentally observed equilibrium between **10** and **14** is shifted entirely to the latter,⁶⁸ in benzene – aqueous NaN₃ both are present in comparable quantities (see above). However, **10** and **14** exhibit different reactivities toward CO. The computed data (in water) suggest that migratory insertion of CO into

⁶⁸ As described above, upon addition of 1 equiv of [Bu₄N]N₃ to [(Xantphos)Pd(Ph)(I)] (**10**) in benzene [(Xantphos)Pd(Ph)(N₃)] (**14**) is formed quantitatively (³¹P NMR). This translates into 14:10 $>$ 100, considering the sensitivity of the method (ca. 1%).

the Pd-C bond of **10** is $>10^3$ times faster than that of **14**. This indicates that if CO diffusion into the organic phase is slower than the iodide/azide ligand exchange, of the two loops **C** and **D** it is the former that will be by far the largest contributor to the overall catalytic transformation. The influence of the anionic ligand X on both kinetics and thermodynamics of the reactions of $[(R_3P)_2Pd(Ar)X]$ with CO has long been recognized.²⁵ For instance, $[(Ph_3P)_2Pd(Ar)X]$ species undergo full conversion to the corresponding $[(Ph_3P)_2Pd(COAr)X]$ more rapidly when X = I than for X = Br for a given Ar ligand. However, CO insertion into the Pd-Ph bond of $[(R_3P)_2Pd(Ph)Cl]$ is reversible for both R = Ph²⁵ and Cy.⁶⁹

As seen from the above, three different catalytic cycles (loops **B**, **C**, and **D** in Scheme 1.19) can govern the azidocarbonylation reaction. With CO in excess in the organic phase, loop **B** is operational. Under CO-deficient conditions, loops **C** and (to a much smaller extent) **D** operate in the process. It is quite possible that under the conditions conventionally used in the current work, i.e. $[Pd] \approx [CO]$ in the organic phase at 1 atm (see above), the reaction occurs largely via the **C** channel at the beginning when the concentration of the iodoarene substrate is high and the rate-limiting oxidative addition is faster than CO mass transfer. The formation of less reactive Pd(0) carbonyls is skipped in this way and, as a result, it is the more reactive CO-free Pd(0) that effects the Ar-I oxidative addition. As $[ArI]$ drops during the reaction, the rate of its oxidative addition first becomes comparable with, and eventually slower than, the CO diffusion rate which is constant. In other words, the mechanism that operates at the beginning of the reaction (loop **C**) is gradually replaced with the other, higher barrier channel (loop **B**). Poorly efficient azide/iodide ligand exchange in the organic solvent – water biphasic system (e.g., slow agitation) would result in accumulation of stable

⁶⁹ Huser, M.; Youinou, M.-T.; Osborn, J. A. *Angew. Chem., Int. Ed. Engl.* 1989, 28, 1386.

[(Xantphos)Pd(COPh)I] (**13**) and consequently higher concentrations of CO, thus favoring the more energy demanding channel (loop **B**). The diminished reactivity of aryl bromides prohibits the intrinsically faster catalytic cycles **C** and **D** from operation because Ar-Br oxidative addition to Pd(0) is considerably slower than CO mass transfer under the standard reaction conditions. The only mechanistic option left for aryl bromides is loop **B** involving the less reactive form of Pd(0), [(Xantphos)Pd(CO)₂] (**12**).

Why Xantphos? Of numerous tertiary phosphines screened in the current work, Xantphos is the only efficient ligand for the Pd-catalyzed azidocarbonylation reaction. The well-established remarkable catalytic activity of Xantphos-stabilized transition metal complexes^{33,34} is often attributed to its wide bite angle. It has been recently demonstrated,⁴⁷ however, that factors other than that may be involved. To understand the origin of the uniquely excellent performance of the Xantphos-Pd catalyst in the azidocarbonylation reaction, a separate mechanistic study is needed, similar to the one performed in the current work but with analogous Pd complexes bearing ligands other than Xantphos.

Conclusions

The objectives of this study have been fully met. We have discovered the first aromatic azidocarbonylation reaction, the formation of aroyl azides from aryl iodides, CO, and NaN₃ in the presence of a Pd catalyst. This transformation is vastly more challenging than other Heck-type Pd-catalyzed carbonylation reactions because (i) the product, ArCON₃, is thermally unstable (Curtius rearrangement) under conventional ArX carbonylation conditions; (ii) the Pd catalyst may be easily and irreversibly deactivated by the exceedingly facile Staudinger reaction of the aroyl azide product with the stabilizing tertiary phosphine ligand; and (iii) the azido ligand on Pd may react with CO to give isocyanate with concomitant loss of N₂.²⁷ Remarkably, all these problems are obviated by the use of the unique Pd-Xantphos catalytic system that effects the transformation in organic solvent – H₂O biphasic media at room temperature and 1 atm of CO. Efficiently catalyzed by the Pd-Xantphos system, the azidocarbonylation reaction has a broad scope and can be used with a wide variety of meta- and para-substituted aryl iodides. Functional groups such as alkyl, alkoxy, acyl, alkoxy carbonyl, nitro, cyano, and even formyl are easily tolerated.

The catalyst deactivation study identified [(Xantphos)PdI₂] (**7**) as the main product of catalyst poisoning. As luckily no structural changes to the Xantphos ligand are involved in the deactivation process, the non-organometallic Pd(II) complex **7** can be reduced in situ to catalytically Pd(0), thereby regaining the catalytic activity. The identification of readily available and cheap PMHS as the particularly efficient reducing agent for this purpose has led to the development of the markedly efficient process employing only 0.2 mol % of readily available and easily accessible, air-stable [(Xantphos)PdCl₂] (**8**) as added catalyst. Cross-coupling reactions of haloarenes employing such a low Pd catalyst loading are rare. Considering the above-explained vulnerability of the reaction,

it is truly remarkable that nearly quantitative conversions can be achieved with such small quantities of the catalyst. Furthermore, the reaction exhibits >85% selectivity if run under optimized conditions. The low catalyst loading in combination with the high conversion and selectivity allow the straightforward and safe preparation of pure aryl azides in ca. 80-90% isolated yield on a 1-2 g scale. Nonetheless, if an aryl azide is desired for further transformations such as to the corresponding isocyanate, benzamide, iminophosphorane, etc., those reactions may be performed in situ, without isolation of the originally produced ArCON₃ (Scheme 1.16).

Like any other catalytic process, the azidocarbonylation reaction has limitations. First, it is inapplicable to aryl bromides that are activated by Pd(0) at temperatures that prompt the rearrangement of the aryl azide product and its reaction with the stabilizing phosphine ligand, which leads to catalyst deactivation. Second, ortho-substituted iodoarenes, when azidocarbonylated, give rise to the corresponding ArCON₃ that are innately less stable toward the Curtius rearrangement. In certain cases, the reaction of ortho-substituted substrates can produce the corresponding symmetric ureas in good yield (Scheme 1.15).

A detailed mechanistic study of the azidocarbonylation reaction by experimental and computational²⁶ means has shown that two main reaction pathways can operate in the process. Oxidative addition of the Ar-I bond to Pd(0) is the rate-determining step of both routes. In the presence of CO in excess, the Ar-I bond is activated by the less electron-rich Pd center of a mixed carbonyl phosphine complex. Under CO-deficient conditions, a lower energy barrier pathway is followed, involving Ar-I oxidative addition to a more reactive carbonyl-free Xantphos-stabilized Pd(0) species. Mass transfer in the triphasic liquid-liquid-gas system used in the current work plays an important role in the competition between these two mechanistic routes, uniformly

leading to a common aroyl azido intermediate that undergoes ArCO-N₃ reductive elimination.

It is hoped that the novel azidocarbonylation reaction will find applications in the synthesis of some otherwise poorly accessible aroyl azides such as **2p** that bears a formyl group on the ring. We also believe that the previously unavailable mechanistic information obtained in our work will be of help in the design and optimization of other Pd-catalyzed carbonylation reactions of aromatic electrophiles. It is also worth to note that the developed azidocarbonylation reaction is potentially suitable for such applications as CO sensing⁷⁰ and ¹¹C radiolabeling. The ¹¹C positron emission tomography (PET) is a powerful diagnostic tool that currently employs ¹¹CO₂, ¹¹CH₃I, and ¹¹CO precursors for the preparation of radiotracers.⁷¹ The short lifetime of the ¹¹C isotope ($\tau_{1/2} = 20.4$ min) dictates the need for highly efficient and selective organic transformations that produce the desired ¹¹C-containing product within ca. 10 min. Pd-catalyzed carbonylation reactions have been used to produce ¹¹C-labeled aldehydes, ketones, carboxylic acids, and their derivatives.^{71,72} It is believed that the azidocarbonylation reaction may find applications in ¹¹C PET, considering (i) the appropriate time scale (see the Experimental Section), (ii) the fact that aroyl azides are highly reactive and versatile reagents in synthesis (Scheme 1.3),¹⁰ and (iii) the demonstrated possibility to use the ArCON₃ product for further transformations without isolation (Scheme 1.16).

⁷⁰ Yan, T.; Chen, J.; Wu, S.; Mao, Z.; Liu, Z. *Org. Lett.* 2014, *16*, 3296.

⁷¹ For a general review of ¹¹C-labeling, see: Antoni, G.; Kihlberg, T.; Långström, B. In: *Handbook of Nuclear Chemistry, 2nd Ed., Vol. 4*; Vértes, A.; Nagy, S.; Klencsár, Z.; Lovas, R. G.; Rösch, F., Eds.; Springer: Dordrecht, 2011, p. 1977.

⁷² For recent examples of Pd-catalyzed carbonylation reactions with ¹¹CO, see: (a) Kealey, S.; Plisson, C.; Collier, T. L.; Long, N. J.; Husbands, S. M.; Martarello, L.; Gee, A. D. *Org. Biomol. Chem.* 2011, *9*, 3313. (b) Eriksson, J.; van den Hoek, J.; Windhorst, A. D. *J. Labelled Compd. Radiopharm.* 2012, *55*, 223. (c) Takashima-Hirano, M.; Ishii, H.; Suzuki, M. *ACS Med. Chem. Lett.* 2012, *3*, 804. (d) Dahl, K.; Schou, M.; Amini, N.; Halldin, C. *Eur. J. Org. Chem.* 2013, 1228.

Experimental Section

Caution: care should be exercised when handling azide derivatives that may be potentially explosive. Exposing phosphine-free palladium compounds to a source of azide must be avoided in order to eliminate the risk of generating highly explosive, shock-sensitive materials.⁵⁵ Aryl azides, pure or in solution, should not be exposed to temperatures exceeding 60 °C to avoid decomposition via the Curtius rearrangement.

General consideration. All chemicals were purchased from Aldrich, Alfa Aesar, TCI, Deutero, and Pressure Chemical companies. Benzene, toluene, THF, dichloromethane, hexanes, pentane, and other solvents were used as received, unless otherwise noted. Anhydrous, oxygen-free benzene, benzene-*d*₆, toluene, THF, and hexanes for mechanistic studies were obtained by distillation from Na/OCPh₂. CD₂Cl₂ and CDCl₃ were vacuum-transferred from CaH₂. All solvents for experiments in an inert atmosphere were stored over freshly activated 4 Å molecular sieves in a glovebox. Column chromatography was performed on 60A silica gel (40-63 μm). *i*-Pr-Xantphos,⁷³ Pd₂(dba)₃,^{30b} [(Ph₃P)₂Pd(Ph)Br],⁷⁴ [(Xantphos)Pd(Ph)I] (**10**),⁴⁶ [(Xantphos)Pd(Ph)Br],⁶⁰ [(Xantphos)PdCl₂]·CH₂Cl₂ (**8**),⁷⁵ were prepared by the literature procedures. ¹H, ¹⁹F, ³¹P, and ¹³C NMR spectra were recorded on Bruker Avance 400 Ultrashield and Bruker Avance 500 Ultrashield NMR spectrometers. Single crystal X-ray diffraction studies were performed on a Bruker-Nonius diffractometer and a Bruker Apex DUO Kappa 4-axis goniometers equipped with APPEX 2 4K CCD area detectors. An Agilent Technologies 7890A-5975C instrument was used for GC-MS analysis. FT-IR measurements in solution were performed with a Thermo Nicolet FT-IR 5700 Nexus

⁷³ Asensio, G.; Cuenca, A. B.; Esteruelas, M. A.; Medio-Simón, M.; Oliván, M.; Valencia, M. *Inorg. Chem.* 2010, *49*, 8665.

⁷⁴ Grushin, V. V. *Organometallics* 2000, *19*, 1888.

⁷⁵ Johns, A. M.; Utsunomiya, M.; Incarvito, C. D.; Hartwig, J. F. *J. Am. Chem. Soc.* 2006, *128*, 1828.

spectrometer equipped with a DLaTGS detector and a KBr beamsplitter at 4 cm^{-1} resolution. A Bruker Optics FTIR Alpha spectrometer with a DTGS detector and a KBr beamsplitter at 4 cm^{-1} resolution was used for FT-IR measurements of solid samples. Elemental analyses were performed by the Microanalysis Center at the Complutense University of Madrid.

Experimental Procedures for Table 1.2. A 25-mL flask equipped with a Teflon-coated magnetic stir bar was charged, in air, with NaN_3 (130 mg; 2 mmol), and all air-stable components and additives such as Pd_2dba_5 , $\text{Pd}(\text{OAc})_2$, dppf, dppe, dppp, dppb, Xantphos, DPEphos, (\pm)-BINAP, and Zn. The flask was then brought to a glovebox where all air-sensitive components were added along with iodobenzene (204 mg; 1 mmol) and rigorously anhydrous THF (5 mL). The flask was sealed with a rubber septum, brought out of the glovebox, quickly evacuated through a needle and immediately backfilled with CO from a balloon (see Table 1.2 for specifics). The reactions were monitored by GS-MS analysis of the samples prepared by diluting 0.05 mL of the reaction mixture with 1.5 mL of CHCl_3 . As can be seen from Table 1.2, by far the best results were obtained using Xantphos as the stabilizing ligand.

Experimental Procedures for Table 1.3. A 25-mL flask equipped with a Teflon-coated stir bar was charged, in air, with NaN_3 , a Pd catalyst precursor, Xantphos, an additive (optionally), and brought to a glovebox where 4-fluoroiodobenzene and all solvents (except water) were added. The flask was sealed with a rubber septum, brought out, quickly evacuated through a needle and backfilled with CO from a balloon. With the CO balloon still attached, the flask was connected to a 25-mL graduated glass syringe with silicone oil-lubricated plunger. After the syringe was purged with CO from

the balloon (3×20 mL) and filled up with CO, the balloon was disconnected from the flask. Degassed water was added via syringe (optionally, see Table 1.3). The reaction was performed at vigorous stirring and monitored by ^{19}F NMR. For ^{19}F NMR analysis, 0.1 mL of the reaction mixture was diluted with 0.5 mL of THF. The yield and conversion were calculated as percentage of the integral intensity of the peaks from the product (δ : -104.5 ppm) and from the starting material (δ : -115.4 ppm), respectively, in the overall sum of integrals for all peaks in the spectrum.

Azidocarbonylation of ArI with 2 mol % of Xantphos-Pd₂(dba)₅ catalyst.

Preparation of the catalyst. A mixture of Pd₂(dba)₅ (69 mg; 0.1 mmol Pd), Xantphos (58 mg; 0.1 mmol), and anhydrous, oxygen-free THF (5 mL) was stirred under argon for 30 min. The resultant catalyst solution was used for the reactions as described below.

Experimental Procedures for Table 1.4. General procedure. In air, a 25-mL flask containing a magnetic stir bar was charged with NaN₃ (78 mg; 1.2 mmol), an iodoarene (1 mmol), THF (1 mL), hexane (1 mL), and deionized water (3 mL). The flask was sealed with a rubber septum, degassed by the freeze-pump-thaw method, and backfilled with CO to 1 atm. After a CO-filled 25-mL graduated glass syringe with a silicone-oil-lubricated plunger was connected to the flask, the catalyst solution (1 mL; 0.02 mmol of Pd, 0.02 mmol of Xantphos) was syringed in at vigorous stirring. The mixture was agitated at room temperature until CO consumption ceased and sufficient conversion was achieved (GC-MS). Ether (10 mL) was added, the organic phase was separated and the aqueous layer was extracted with ether (2×10 mL). The combined ethereal solutions were dried over MgSO₄, filtered, and evaporated under reduced pressure at

room temperature. The pure product was isolated by chromatography of the residue with hexane-ether or pentane-ether for more volatile aryl azides.

Benzoyl azide (2a).¹⁹ In air, a 25-mL flask containing a magnetic stir bar was charged with NaN₃ (78 mg; 1.2 mmol), iodobenzene (204 mg; 1 mmol), THF (1 mL), hexane (1 mL), and deionized water (3 mL). The flask was sealed with a rubber septum, degassed by the freeze-pump-thaw method, and backfilled with CO to 1 atm. A CO-filled 25-mL graduated glass syringe with a silicone-oil-lubricated plunger was connected to the flask. The catalyst solution (1 mL; 0.02 mmol of Pd, 0.02 mmol of Xantphos) was syringed in at vigorous stirring. Carbon monoxide consumption began immediately. After 2 h, 98% conversion of PhI was observed (GC-MS). The mixture was agitated for one more hour. Ether (10 mL) was added, the organic phase was separated, and the aqueous layer was extracted with ether (2 × 10 mL). The combined ether solutions were dried over MgSO₄, filtered, and evaporated under reduced pressure at room temperature. Column chromatography of the residue with pentane-ether (9:1) produced benzoyl azide **2a** as a colorless oil that crystallized on standing in a refrigerator at +8 °C. The yield was 130 mg (88%), m.p. 25-26 °C (lit.¹⁹ 32-34 °C). ¹H NMR (500 MHz, CDCl₃), δ: 7.43 (m, 2H), 7.60 (m, 1H), 7.97 (m, 2H). ¹³C NMR (126 MHz, CDCl₃), δ: 128.8, 129.6, 130.9, 134.5, 172.7.

4-Methylbenzoyl azide (2b).¹⁹ In air, a 25-mL flask containing a magnetic stir bar was charged with NaN₃ (78 mg; 1.2 mmol), 4-iodotoluene (218 mg; 1 mmol), THF (1 mL), hexane (1 mL), and deionized water (3 mL). The flask was sealed with a rubber septum, degassed by the freeze-pump-thaw method, backfilled with CO to 1 atm., and placed in a preheated oil bath at 50 °C. A CO-filled 25-mL graduated glass syringe with

a silicone-oil-lubricated plunger was connected to the flask, and the catalyst solution (1 mL; 0.02 mmol of Pd, 0.02 mmol of Xantphos) was syringed in at vigorous stirring. Carbon monoxide consumption began immediately. After 30 min > 99% conversion of 4-iodotoluene was observed (GC-MS). The mixture was stirred at 50 °C for 30 more minutes. Ether (10 mL) was added, the organic phase was separated, and the aqueous layer was extracted with ether (2 × 10 mL). The combined ether solutions were dried over MgSO₄, filtered, and evaporated under reduced pressure at room temperature. Column chromatography of the residue with hexane–ether (9:1) produced 4-methylbenzoyl azide **2b** as a colorless oil that crystallized on standing in a refrigerator at +8 °C. The yield was 138 mg (86%), m.p. 35-36 °C (lit.¹⁹ 32-34 °C). ¹H NMR (500 MHz, CDCl₃), δ: 2.40 (s, 3H, Me), 7.24 (m, 2H), 7.90 (m, 2H). ¹³C NMR (126 MHz, CDCl₃), δ: 22.0, 128.3, 129.6, 129.8, 145.6, 172.6.

4-(tert-Butyl)benzoyl azide (2c).⁷⁶ In air, a 25-mL flask containing a magnetic stir bar was charged with NaN₃ (78 mg; 1.2 mmol), 1-(tert-butyl)-4-iodobenzene (260 mg; 1 mmol), THF (1 mL), hexane (1 mL) and deionized water (3 mL). The flask was sealed with a rubber septum, degassed by the freeze-pump-thaw method, and backfilled with CO to 1 atm. A CO-filled 25-mL graduated glass syringe with a silicone-oil-lubricated plunger was connected to the flask. The catalyst solution (1 mL; 0.02 mmol of Pd, 0.02 mmol of Xantphos) was syringed in at vigorous stirring. Carbon monoxide consumption began immediately. After 2 h, > 99% conversion of 1-(tert-butyl)-4-iodobenzene was observed (GC-MS). The mixture was agitated for one more hour. Ether (10 mL) was added, the organic phase was separated, and the aqueous layer was extracted with ether (2 × 10 mL). The combined ether solutions were dried over MgSO₄, filtered, and

⁷⁶ Yasuhide, Y.; Yuho, T. *J. Am. Chem. Soc.* 1957, *79*, 5530.

evaporated under reduced pressure at room temperature. Column chromatography of the residue with hexane–ether (9:1) produced 4-(*tert*-butyl)benzoyl azide **2c** as white crystalline solid. The yield was 176 mg (87%), m.p. 66–67 °C (lit.⁷⁶ 63–65 °C). ¹H NMR (500 MHz, CDCl₃), δ: 1.32 (s, 9H, *t*-Bu), 7.45 (m, 2H), 7.94 (m, 2H). ¹³C NMR (126 MHz, CDCl₃), δ: 31.3, 35.5, 125.9, 128.2, 129.6, 158.6, 172.6.

4-Methoxybenzoyl azide (2d).⁷⁷ In air, a 25-mL flask containing a magnetic stir bar was charged with NaN₃ (78 mg; 1.2 mmol), 4-iodoanisole (234 mg; 1 mmol), THF (1 mL), hexane (1 mL) and deionized water (3 mL). The flask was sealed with a rubber septum, degassed by the freeze-pump-thaw method, backfilled with CO to 1 atm., and placed in a preheated oil bath at 50 °C. A CO-filled 25-mL graduated glass syringe with a silicone-oil-lubricated plunger was connected to the flask and the catalyst solution (1 mL; 0.02 mmol of Pd, 0.02 mmol of Xantphos) was syringed in at vigorous stirring. Carbon monoxide consumption began immediately. After 1 h, 99% conversion of 4-iodoanisole was observed (GC-MS). The mixture was stirred at 50 °C for 30 more minutes. Ether (10 mL) was added, the organic phase was separated, and the aqueous layer was extracted with ether (2 × 10 mL). The combined ether solutions were dried over MgSO₄, filtered, and evaporated under reduced pressure at room temperature. Column chromatography of the residue with hexane–ether (9:1) produced 4-methoxybenzoyl azide **2d** as pale yellow microcrystalline solid. The yield was 159 mg (contained 2% of PhCON₃; calculated at 156 mg of pure **2d** (88%) by ¹H NMR), m.p. 69–70 °C (lit.⁷⁷ 70–71 °C). ¹H NMR (500 MHz, CDCl₃), δ: 3.86 (s, 3H, OMe), 6.91 (m, 2H), 7.97 (m, 2H). ¹³C NMR (101 MHz, CDCl₃), δ: 55.8, 114.2, 123.5, 132.0, 164.8, 171.9.

⁷⁷ Prakash, G. K. S.; Iyer, P. S.; Arvanaghi, M.; Olah, G. A. *J. Org. Chem.* 1983, *48*, 3358.

4-Nitrobenzoyl azide (2e).⁷⁷ In air, a 25-mL flask containing a magnetic stir bar was charged with NaN₃ (78 mg; 1.2 mmol), 4-nitroiodobenzene (249 mg; 1 mmol), THF (1 mL), hexane (1 mL) and deionized water (3 mL). The flask was sealed with a rubber septum, degassed by the freeze-pump-thaw method, and backfilled with CO to 1 atm. A CO-filled 25-mL graduated glass syringe with a silicone-oil-lubricated plunger was connected to the flask. The catalyst solution (1 mL; 0.02 mmol of Pd, 0.02 mmol of Xantphos) was syringed in at vigorous stirring. After 20 min, > 99% conversion of 4-nitroiodobenzene was observed (GC-MS). The mixture was agitated for 40 more minutes. Ether (10 mL) was added, the organic phase was separated and the aqueous layer was extracted with ether (2 × 10 mL). The combined ether solutions were dried over MgSO₄, filtered, and evaporated under reduced pressure at room temperature. Column chromatography of the residue with hexane–ether (9:1) produced 4-nitrobenzoyl azide **2e** as white crystalline solid. The yield was 161 mg (84%), m.p. 73-74 °C (lit.⁷⁷ 64-66 °C). ¹H NMR (500 MHz, CDCl₃), δ: 8.19 (m, 2H), 8.29 (m, 2H). ¹³C NMR (101 MHz, CDCl₃), δ: 124.0, 130.8, 135.9, 151.4, 171.1.

4-Acetylbenzoyl azide (2f).⁷⁸ In air, a 25-mL flask containing a magnetic stir bar was charged with NaN₃ (78 mg; 1.2 mmol), 4-iodoacetophenone (246 mg; 1 mmol), THF (1 mL), hexane (1 mL) and deionized water (3 mL). The flask was sealed with a rubber septum, degassed by the freeze-pump-thaw method, and backfilled with CO to 1 atm. A CO-filled 25-mL graduated glass syringe with a silicone-oil-lubricated plunger was connected to the flask. The catalyst solution (1 mL; 0.02 mmol of Pd, 0.02 mmol of Xantphos) was syringed in at vigorous stirring. Carbon monoxide consumption began immediately. After 15 min, > 99% conversion of 4-iodoacetophenone was observed

⁷⁸ Sigman, M. E.; Autrey, T.; Schuster, G. B. *J. Am. Chem. Soc.* 1988, *110*, 4297.

(GC-MS). The mixture was agitated for 30 more minutes. Ether (10 mL) was added, the organic phase was separated and the aqueous layer was extracted with ether (2 × 10 mL). The combined ether solutions were dried over MgSO₄, filtered, and evaporated under reduced pressure at room temperature. Column chromatography of the residue with hexane–ether (2:1) produced 171 mg of a yellow solid that contained dibenzylideneacetone (¹H NMR; 0.05 mmol or ca. 12 mg). The 84% yield was therefore calculated for 159 mg of the product. To remove the dba, the solid was washed with hexane (3 × 2 mL). After drying, 140 mg (74%) of pure 4-acetylbenzoyl azide **2f** were obtained as a pale yellow solid with m.p. 66-67 °C (lit.⁷⁸ 64-65 °C). ¹H NMR (400 MHz, CDCl₃), δ: 2.63 (s, 3H, Me), 8.00 (m, 2H), 8.10 (m, 2H). ¹³C NMR (101 MHz, CDCl₃), δ: 27.1, 123.6, 129.9, 134.4, 141.4, 172.0, 197.5.

Ethyl 4-(azidocarbonyl)benzoate (2g). In air, a 25-mL flask containing a magnetic stir bar was charged with NaN₃ (78 mg; 1.2 mmol), ethyl 4-iodobenzoate (276 mg; 1 mmol), THF (1 mL), hexane (1 mL) and deionized water (3 mL). The flask was sealed with a rubber septum, degassed by the freeze-pump-thaw method, and backfilled with CO to 1 atm. A CO-filled 25-mL graduated glass syringe with a silicone-oil-lubricated plunger was connected to the flask. The catalyst solution (1 mL; 0.02 mmol of Pd, 0.02 mmol of Xantphos) was syringed in at vigorous stirring. After 1 h, > 99% conversion of ethyl 4-iodobenzoate was observed (GC-MS). The mixture was agitated for 30 more minutes. Ether (10 mL) was added. The organic phase was separated and the aqueous layer was extracted with ether (2 × 10 mL). The combined ether solutions were dried over MgSO₄, filtered, and evaporated under reduced pressure at room temperature. Column chromatography of the residue with hexane–ether (9:1) produced ethyl 4-(azidocarbonyl)benzoate **2g** as a white solid. The yield was 175 mg (80%),

m.p. 38-40 °C. Anal. Calcd. for C₁₀H₉N₃O₃, (%): C, 54.8; H, 4.1; N, 19.2. Found: C, 55.2; H, 4.2; N, 18.5. ¹H NMR (CDCl₃, 400 MHz), δ: 1.39 (t, *J* = 7.1 Hz, 3H, CH₃), 4.39 (q, *J* = 7.1 Hz, 2H, CH₂), 8.02-8.13 (m, 4H). ¹³C NMR (101 MHz, CDCl₃), δ: 14.5, 61.8, 129.6, 130.0, 134.3, 135.7, 165.7, 172.1. IR (neat, cm⁻¹): 2183, 2135, 1713, 1684, 1576, 1454, 1410, 1368, 1234, 1176, 1106, 990, 869, 847, 787, 709, 562, 434.

4-Cyanobenzoyl azide (2h).⁷⁹ In air, a 25-mL flask containing a magnetic stir bar was charged with NaN₃ (78 mg; 1.2 mmol), 4-iodobenzonitrile (229 mg; 1 mmol), THF (1 mL), hexane (1 mL) and deionized water (3 mL). The flask was sealed with a rubber septum, degassed by the freeze-pump-thaw method, and backfilled with CO to 1 atm. A CO-filled 25-mL graduated glass syringe with a silicone-oil-lubricated plunger was connected to the flask. The catalyst solution (1 mL; 0.02 mmol of Pd, 0.02 mmol of Xantphos) was syringed in at vigorous stirring. After 30 min, 97% conversion of 4-iodobenzonitrile was observed (GC-MS). The mixture was agitated for 1.5 more hours. Ether (10 mL) was added, the organic phase was separated and the aqueous layer was extracted with ether (2 × 10 mL). The combined ether solutions were dried over MgSO₄, filtered, and evaporated under reduced pressure at room temperature. Column chromatography of the residue with hexane–ether (2:1) produced 151 mg of **2h** contaminated with dibenzylideneacetone (¹H NMR; 0.05 mmol, ca. 12 mg). Therefore, the 81% yield was calculated for 139 mg of the product. To remove the dba impurity the solid was washed with hexane (3 × 3 mL). After drying, pure 4-cyanobenzoyl azide **2h** was obtained as a white solid in the amount of 92 mg (52%), m.p. 87-88 °C (lit.⁷⁹ 83 °C). ¹H NMR (500 MHz, CDCl₃), δ: 7.74 (m, 2H), 8.11 (m, 2H). ¹³C NMR (125 MHz, CDCl₃), δ: 117.9, 117.9, 130.8, 132.7, 134.4, 171.3.

⁷⁹ Shingaki, T. *Nippon Kagaku Zasshi* 1959, 80, 55.

4-(Trifluoromethyl)benzoyl azide (2i). In air, a 25-mL flask containing a magnetic stir bar was charged with NaN_3 (78 mg; 1.2 mmol), 1-iodo-4-(trifluoromethyl)benzene (272 mg; 1 mmol), THF (1 mL), hexane (1 mL) and deionized water (3 mL). The flask was sealed with a rubber septum, degassed by the freeze-pump-thaw method, and backfilled with CO to 1 atm. A CO-filled 25-mL graduated glass syringe with a silicone-oil-lubricated plunger was connected to the flask. The catalyst solution (1 mL; 0.02 mmol of Pd, 0.02 mmol of Xantphos) was syringed in at vigorous stirring. After 1 h, 97% conversion of 1-iodo-4-(trifluoromethyl)benzene was observed (GC-MS). The mixture was agitated for one more hour. Ether (10 mL) was added. The organic phase was separated and the aqueous layer was extracted with ether (2×10 mL). The combined ether solutions were dried over MgSO_4 , filtered, and evaporated under reduced pressure at room temperature. Column chromatography of the residue with pentane–ether (9:1) produced 4-(trifluoromethyl)benzoyl azide **2i** as a colorless liquid. The yield was 169 mg (79%). Anal. Calcd. for $\text{C}_8\text{H}_4\text{F}_3\text{N}_3\text{O}$ (%): C, 44.7; H, 1.9; N, 19.5. Found: C, 44.0; H, 2.2; N, 16.2. (The sample likely underwent partial decomposition prior to the combustion analysis). ^1H NMR (500 MHz, CDCl_3), δ : 7.71 (d, $J = 8.5$ Hz, 2H), 8.13 (d, $J = 8.3$ Hz, 2H). ^{13}C NMR (101 MHz, CDCl_3), δ : 123.7 (q, $J = 273$ Hz, chemical shifts for 4 peaks: 119.6, 122.3, 125.0, 127.7), 125.9 (q, $J = 4$ Hz), 130.0, 133.9, 135.8 (q, $J = 33$ Hz, chemical shifts for 4 peaks: 135.3, 135.7, 136.0, 136.3), 171.7. ^{19}F NMR (377 MHz, CDCl_3), δ : -63.0. IR (neat, cm^{-1}): 2176, 2135, 1697, 1513, 1412, 1322, 1237, 1167, 1127, 1109, 1065, 1021, 993, 857, 763, 689, 433.

4-Fluorobenzoyl azide (2j).⁷⁷ In air, a 25-mL flask containing a magnetic stir bar was charged with NaN_3 (78 mg; 1.2 mmol), 1-fluoro-4-iodobenzene (222 mg; 1 mmol), THF (1 mL), hexane (1 mL) and deionized water (3 mL). The flask was sealed with a rubber septum, degassed by the freeze-pump-thaw method, and backfilled with CO to 1 atm. A CO-filled 25-mL graduated glass syringe with a silicone-oil-lubricated plunger was connected to the flask. The catalyst solution (1 mL; 0.02 mmol of Pd, 0.02 mmol of Xantphos) was syringed in at vigorous stirring. After 1 h, 98% conversion of 1-fluoro-4-iodobenzene was observed (GC-MS). The mixture was agitated for one more hour. Ether (10 mL) was added and the organic phase was separated and the aqueous layer was extracted with ether (2×10 mL). The combined ether solutions were dried over MgSO_4 , filtered, and evaporated under reduced pressure at room temperature. Column chromatography of the residue with pentane-ether (9:1) produced 4-fluorobenzoyl azide **2j** as colorless oil. The yield was 126 mg (76%). ^1H NMR (500 MHz, CDCl_3), δ : 7.11 (m, 2H), 8.03 (m, 2H). ^{13}C NMR (101 MHz, CDCl_3), δ : 116.2 (d, $J = 22$ Hz, chemical shifts for 2 peaks: 116.0, 116.3), 127.2 (d, $J = 3$ Hz), 132.4 (d, $J = 10$ Hz, chemical shifts for 2 peaks: 132.3, 132.4), 167.3 (d, $J = 257$ Hz, chemical shifts for 2 peaks: 166.6, 168.1), 171.6. ^{19}F NMR (377 MHz, CDCl_3), δ : -102.7.

4-Chlorobenzoyl azide (2k).⁷⁷ In air, a 25-mL flask containing a magnetic stir bar was charged with NaN_3 (78 mg; 1.2 mmol), 1-chloro-4-iodobenzene (238.5 mg; 1 mmol), THF (1 mL), hexane (1 mL) and deionized water (3 mL). The flask was sealed with a rubber septum, degassed by the freeze-pump-thaw method, and backfilled with CO to 1 atm. A CO-filled 25-mL graduated glass syringe with a silicone-oil-lubricated plunger was connected to the flask. The catalyst solution (1 mL; 0.02 mmol of Pd, 0.02 mmol of Xantphos) was syringed in at vigorous stirring. After 20 min, 99% conversion

of 1-chloro-4-iodobenzene was observed (GC-MS). The mixture was agitated for one more hour. Ether (10 mL) was added, the organic phase was separated and the aqueous layer was extracted with ether (2×10 mL). The combined ether solutions were dried over MgSO_4 , filtered, and evaporated under reduced pressure at room temperature. Column chromatography of the residue with hexane–ether (9:1) produced 4-chlorobenzoyl azide **2k** as a white crystalline solid. The yield was 147 mg (81%), m.p. 44-45 °C (lit.⁷⁷ 39-42 °C). ^1H NMR (500 MHz, CDCl_3), δ : 7.41 (m, 2H), 7.94 (m, 2H). ^{13}C NMR (126 MHz, CDCl_3), δ : 129.28, 129.32, 131.0, 141.2, 171.8.

4-Bromobenzoyl azide (2l).⁷⁷ In air, a 25-mL flask containing a magnetic stir bar was charged with NaN_3 (78 mg; 1.2 mmol), 1-bromo-4-iodobenzene (283 mg; 1 mmol), THF (1 mL), hexane (1 mL) and deionized water (3 mL). The flask was sealed with a rubber septum, degassed by the freeze-pump-thaw method, and backfilled with CO to 1 atm. A CO-filled 25-mL graduated glass syringe with a silicone-oil-lubricated plunger was connected to the flask. The catalyst solution (1 mL; 0.02 mmol of Pd, 0.02 mmol of Xantphos) was syringed in at vigorous stirring. After 20 min, > 99% conversion of 1-bromo-4-iodobenzene was observed (GC-MS). The mixture was agitated for 20 more minutes. Ether (10 mL) was added, the organic phase was separated and the aqueous layer was extracted with ether (2×10 mL). The combined ether solutions were dried over MgSO_4 , filtered, and evaporated under reduced pressure at room temperature. Column chromatography of the residue with hexane–ether (9:1) produced 4-bromobenzoyl azide **2l** as a white solid. The yield was 186 mg (82%), m.p. 49-50 °C (lit.⁷⁷ 48 °C). ^1H NMR (500 MHz, CDCl_3), δ : 7.58 (m, 2H), 7.86 (m, 2H). ^{13}C NMR (126 MHz, CDCl_3), δ : 129.8, 130.0, 131.1, 132.3, 172.0.

Terephthaloyl azide (2m).⁸⁰ In air, a 50-mL flask containing a magnetic stir bar was charged with NaN₃ (156 mg; 2.4 mmol), 1,4-diiodobenzene (330 mg; 1 mmol), THF (2 mL), hexane (2 mL) and deionized water (6 mL). The flask was sealed with a rubber septum, degassed by the freeze-pump-thaw method, and backfilled with CO to 1 atm. A CO-filled 25-mL graduated glass syringe with a silicone-oil-lubricated plunger was connected to the flask. The catalyst solution (2 mL; 0.04 mmol of Pd, 0.04 mmol of Xantphos) was syringed in at vigorous stirring. The syringe was refilled with CO after 25 mL of CO had been consumed. After 30 min, > 99% conversion of 1,4-diiodobenzene was observed (GC-MS). The mixture was agitated for 30 more minutes. Ether (20 mL) was added, the organic phase was separated and the aqueous layer was extracted with ether (2 × 20 mL). The combined ether solutions were dried over MgSO₄, filtered, and evaporated under reduced pressure at room temperature. Column chromatography of the residue with hexane–ether (2:1) produced 135 mg of a yellow solid that contained dibenzylideneacetone (¹H NMR; 0.1 mmol, 23 mg). The 52% yield was therefore calculated for 112 mg of the product. Washing of the solid with hexane (3 × 5 mL) followed by drying produced pure terephthaloyl azide **2m** as white solid (82 mg; 38%), m.p. 116 °C (lit.⁸⁰ 105-106 °C). ¹H NMR (500 MHz, CDCl₃), δ: 8.08 (s, 4H). ¹³C NMR (126 MHz, CDCl₃), δ: 129.8, 135.5, 171.9.

3-Methylbenzoyl azide (2n).⁷⁷ In air, a 25-mL flask containing a magnetic stir bar was charged with NaN₃ (78 mg; 1.2 mmol), 3-iodotoluene (218 mg; 1 mmol), THF (1 mL), hexane (1 mL) and deionized water (3 mL). The flask was sealed with a rubber septum, degassed by the freeze-pump-thaw method, and backfilled with CO to 1 atm. A CO-filled 25-mL graduated glass syringe with a silicone-oil-lubricated plunger was

⁸⁰ Katritzky, A. R.; Rogers, J. W.; Witek, R. M.; Vakulenko, A. V.; Mohapatra, P. P.; Steel, P. J.; Damavarapu, R. *J. Energ. Mater.* 2007, 25, 79.

connected to the flask. The catalyst solution (1 mL; 0.02 mmol of Pd, 0.02 mmol of Xantphos) was syringed in at vigorous stirring. After 2 h, >99% conversion of 3-iodotoluene was observed (GC-MS). The mixture was agitated for 30 more minutes. Ether (10 mL) was added, the organic phase was separated and the aqueous layer was extracted with ether (2 × 10 mL). The combined ether solutions were dried over MgSO₄, filtered, and evaporated under reduced pressure at room temperature. Column chromatography of the residue with hexane–ether (9:1) produced 3-methylbenzoyl azide **2n** as a colorless oil. The yield was 148 mg (92%). ¹H NMR (500 MHz, CDCl₃), δ: 2.39 (s, 3H, Me), 7.32 (m, 1H), 7.40 (m, 1H), 7.73-7.88 (m, 2H). ¹³C NMR (126 MHz, CDCl₃), δ: 21.4, 126.9, 128.8, 130.2, 130.8, 135.4, 138.8, 172.9.

3-Methoxybenzoyl azide (2o).⁸¹ In air, a 25-mL flask containing a magnetic stir bar was charged with NaN₃ (78 mg; 1.2 mmol), 3-iodoanisole (234 mg; 1 mmol), THF (1 mL), hexane (1 mL) and deionized water (3 mL). The flask was sealed with a rubber septum, degassed by the freeze-pump-thaw method, and backfilled with CO to 1 atm. A CO-filled 25-mL graduated glass syringe with a silicone-oil-lubricated plunger was connected to the flask. The catalyst solution (1 mL; 0.02 mmol of Pd, 0.02 mmol of Xantphos) was syringed in at vigorous stirring. After 2 h 99% conversion of 3-iodoanisole was observed (GC-MS). The mixture was agitated for 30 more minutes. Ether (10 mL) was added, the organic phase was separated and the aqueous layer was extracted with ether (2 × 10 mL). The combined ether solutions were dried over MgSO₄, filtered, and evaporated under reduced pressure at room temperature. Column chromatography of the residue with hexane–ether (9:1) produced 3-methoxybenzoyl azide **2o** as a yellow oil. The yield was 147 mg (83%). ¹H NMR (500 MHz, CDCl₃),

⁸¹ De Sarkar, S.; Studer, A. *Org. Lett.* 2010, 12, 1992.

δ : 3.84 (s, 3H, OMe), 7.14 (m, 1H), 7.34 (m, 1H), 7.52 (m, 1H), 7.60 (m, 1H). ^{13}C NMR (126 MHz, CDCl_3), δ : 55.7, 113.7, 121.2, 122.1, 129.9, 132.1, 160.0, 172.6.

3-Formylbenzoyl azide (2p). In air, a 25-mL flask containing a magnetic stir bar was charged with NaN_3 (78 mg; 1.2 mmol), 3-iodobenzaldehyde (232 mg; 1 mmol), THF (1 mL), hexane (1 mL) and deionized water (3 mL). The flask was sealed with a rubber septum, degassed by the freeze-pump-thaw method, and backfilled with CO to 1 atm. A CO-filled 25-mL graduated glass syringe with a silicone-oil-lubricated plunger was connected to the flask. The catalyst solution (1 mL; 0.02 mmol of Pd, 0.02 mmol of Xantphos) was syringed in at vigorous stirring. After 15 min, > 99% conversion of 3-iodobenzaldehyde was observed (GC-MS). The mixture was agitated for 15 more minutes. Ether (10 mL) was added, the organic phase was separated and the aqueous layer was extracted with ether (2×10 mL). The combined ether solutions were dried over MgSO_4 , filtered, and evaporated under reduced pressure at room temperature. Column chromatography of the residue with hexane–ether (2:1) produced 167 mg of **2p** as a yellow solid containing dibenzylideneacetone (^1H NMR; 0.05 mmol, 12 mg). The 89% yield was therefore calculated for 155 mg of the product. The solid was washed with hexane (3×2 mL) and dried to give pure, dba-free 3-formylbenzoyl azide **2p** as a pale yellow solid (116 mg; 66%), m.p. 52-53 °C. Anal. Calcd. for $\text{C}_8\text{H}_5\text{N}_3\text{O}_2$ (%): C, 54.9; H, 2.9; N, 24.0. Found: C, 55.6; H, 3.0; N, 23.1 (N content outside the range of the method). ^1H NMR (400 MHz, CDCl_3), δ : 7.63 (m, 1H), 8.11 (m, 1H), 8.26 (m, 1H), 8.48 (m, 1H), 10.05 (s, 1H, COH). ^{13}C NMR (126 MHz, CDCl_3), δ : 129.8, 131.2, 131.9, 134.5, 135.0, 137.0, 171.7, 191.2. IR (neat, cm^{-1}): 2838, 2207, 2152, 1692, 1591, 1442, 1382, 1290, 1250, 1185, 1149, 1009, 924, 904, 818, 724, 674, 649, 563, 482, 454, 426.

Thiophene-2-carbonyl azide (2q).¹⁹ In air, a 25-mL flask containing a magnetic stir bar was charged with NaN₃ (78 mg; 1.2 mmol), 2-iodothiophene (210 mg; 1 mmol), THF (1 mL), hexane (1 mL) and deionized water (3 mL). The flask was sealed with a rubber septum, degassed by the freeze-pump-thaw method, backfilled with CO to 1 atm., and placed in a preheated oil bath at 50 °C. A CO-filled 25-mL graduated glass syringe with a silicone-oil-lubricated plunger was connected to the flask, and the catalyst solution (1 mL; 0.02 mmol of Pd, 0.02 mmol of Xantphos) was syringed in at vigorous stirring. After 30 min, > 99% conversion of 2-iodothiophene was observed (GC-MS). The mixture was stirred at 50 °C for 15 more minutes. Ether (10 mL) was added, the organic phase was separated and the aqueous layer was extracted with ether (2 × 10 mL). The combined ether solutions were dried over MgSO₄, filtered, and evaporated under reduced pressure at room temperature. Column chromatography of the residue with hexane–ether (9:1) produced thiophene-2-carbonyl azide **2q** as off-white crystalline solid. The yield was 133 mg (87%), m.p. 37-38 °C (lit.¹⁹ 35-36 °C). ¹H NMR (400 MHz, CDCl₃), δ: 7.11 (m, 1H), 7.64 (m, 1H), 7.82 (m, 1H). ¹³C NMR (101 MHz, CDCl₃), δ: 128.6, 134.7, 134.9, 135.1, 166.8.

Nicotinoyl azide (2r).¹⁹ In air, a 25-mL flask containing a magnetic stir bar was charged with NaN₃ (78 mg; 1.2 mmol), 3-iodopyridine (205 mg; 1 mmol), THF (1 mL), hexane (1 mL) and deionized water (3 mL). The flask was sealed with a rubber septum, degassed by the freeze-pump-thaw method, and backfilled with CO to 1 atm. A CO-filled 25-mL graduated glass syringe with a silicone-oil-lubricated plunger was connected to the flask. The catalyst solution (1 mL; 0.02 mmol of Pd, 0.02 mmol of Xantphos) was syringed in at vigorous stirring. After 15 min, 99% conversion of 3-iodopyridine was observed (GC-MS). The mixture was agitated for 15 more minutes.

Ether (10 mL) was added, the organic phase was separated and the aqueous layer was extracted with ether (2×10 mL). The combined ether solutions were dried over MgSO_4 , filtered, and evaporated under reduced pressure at room temperature. Column chromatography of the residue with hexane–ether (2:1) produced a reddish solid (124 mg; contaminated with Pd). The solid was redissolved in 10 mL of hexane-ether (2:1) and the solution filtered through a pad of Celite. Evaporation of the solvents gave **2r** as an orange solid (111 mg, 75% yield), m.p. 46-49 °C (lit.¹⁹ 48-50 °C). ^1H NMR (500 MHz, CDCl_3), δ : 7.39 (m, 1H), 8.25 (m, 1H), 8.80 (m, 1H), 9.18 (m, 1H); ^{13}C NMR (126 MHz, CDCl_3), δ : 123.7, 126.8, 137.0, 150.9, 154.8, 171.5.

Experimental Procedures for Scheme 1.15. 1,3-Di(naphthalen-1-yl)urea (3a).⁸² In air, a 25-mL flask containing a magnetic stir bar was charged with NaN_3 (78 mg; 1.2 mmol), 1-iodonaphthalene (254 mg; 1 mmol), THF (1 mL), hexane (1 mL) and deionized water (3 mL). The flask was sealed with a rubber septum, degassed by the freeze-pump-thaw method, backfilled with CO to 1 atm., and placed in a preheated oil bath at 50 °C. A CO-filled 25-mL graduated glass syringe with a silicone-oil-lubricated plunger was connected to the flask, and the catalyst solution (1 mL; 0.02 mmol of Pd, 0.02 mmol of Xantphos) was syringed in at vigorous stirring. After 4 h the reaction mixture was allowed to cooled to room temperature and filtered. The solid on the filter was washed with dichloromethane (2×10 mL), water (2×10 mL), and ethanol (2×10 mL) and dried to produce **3a** as an off-white microcrystalline solid. The yield was 118 mg (76%), m.p. 294 °C (dec; lit.⁸² 299 °C). ^1H NMR (400 MHz, $\text{DMSO}-d_6$), δ : 7.45-7.75 (m, 8H), 7.96 (d, $J = 8.0$ Hz, 2H), 8.07 (d, $J = 7.5$ Hz, 2H), 8.24 (d, $J = 8.4$ Hz, 2H), 9.17 (s, 2H, 2NH). ^{13}C NMR (101 MHz, $\text{DMSO}-d_6$), δ : 117.5, 121.4, 123.0, 125.8, 125.96, 125.98, 126.00, 128.5, 133.8, 134.4, 153.4.

⁸² Kurth, T. L.; Lewis, F. D. *J. Am. Chem. Soc.* 2003, *125*, 13760.

1,3-Bis(2-methoxyphenyl)urea (3b).⁸³ In air, a 25-mL flask containing a magnetic stir bar was charged with NaN₃ (78 mg; 1.2 mmol), 2-iodoanisole (234 mg; 1 mmol), THF (1 mL), hexane (1 mL) and deionized water (3 mL). The flask was sealed with a rubber septum, degassed by the freeze-pump-thaw method, backfilled with CO to 1 atm., and placed in a preheated oil bath at 50 °C. A CO-filled 25-mL graduated glass syringe with a silicone-oil-lubricated plunger was connected to the flask, and the catalyst solution (1 mL; 0.02 mmol of Pd, 0.02 mmol of Xantphos) was syringed in at vigorous stirring. The mixture was stirred at 50 °C for 7 hours, and cooled to room temperature. Ether (10 mL) was added, the organic phase was separated and the aqueous layer was extracted with ether (2 × 10 mL). The combined ether solutions were dried over MgSO₄, filtered, and evaporated under reduced pressure. Column chromatography of the residue with hexane–ether (3:2) produced 125 mg of 1,3-bis(2-methoxyphenyl)urea **3b** as a pinkish solid of ca. 80 % purity (¹H NMR) with m.p. 165-169 °C (lit.⁸³ 185 °C). ¹H NMR (400 MHz, CDCl₃), δ: 3.86 (s, 6H, 2OMe), 6.86 (m, 2H), 6.92-7.03 (m, 2H), 7.11 (br. s, 2H, NH), 8.10 (m, 2H). ¹³C NMR (101 MHz, CDCl₃), δ: 55.9, 110.4, 119.9, 121.5, 123.1, 128.4, 148.4, 152.6.

Experimental Procedures for Scheme 1.16. 4-Fluorobenzamide (4).⁸⁴ In air, a 25-mL flask containing a magnetic stir bar was charged with NaN₃ (78 mg; 1.2 mmol), 1-fluoro-4-iodobenzene (222 mg; 1 mmol), PMHS (120 mg, 2 equiv), benzotrifluoride (47 mg, 0.322 mmol; internal standard for ¹⁹F NMR), THF (2 mL), and deionized water (100 μL). The flask was sealed with a rubber septum, degassed by the freeze-pump-thaw method, backfilled with CO to 1 atm., and placed in a preheated oil bath at 50 °C. A CO-filled 25-mL graduated glass syringe with a silicone-oil-lubricated plunger was

⁸³ Li, Z.; Wang, Z.; Zhu, W.; Xing, Y. *Synth. Comm.* 2005, *35*, 2325.

⁸⁴ Ramon, S.; Bosson, J.; Diez-Gonzalez, S.; Marion, N.; Nolan, S. P. *J. Org. Chem.* 2010, *75*, 1197.

connected to the flask, and the catalyst solution (1 mL; 0.02 mmol of Pd, 0.02 mmol of Xantphos) was syringed in at vigorous stirring. The mixture was stirred at 50 °C for 4 hours, and cooled to room temperature. Quantitative ^{19}F NMR analysis of the reaction mixture indicated the formation of 4-fluorobenzamide **4** in 98% yield: ^{19}F NMR (377 MHz, THF), δ : -110.8 (lit.⁸⁴ -110.1, DMSO- d_6). The formation of **4** was also confirmed by GC-MS.

4-Fluoro-N-(triphenylphosphoranylidene)benzamide (5).⁸⁵ In air, a 25-mL flask containing a magnetic stir bar was charged with NaN_3 (78 mg; 1.2 mmol), 1-fluoro-4-iodobenzene (222 mg; 1 mmol), benzotrifluoride (48 mg, 0.329 mmol; internal standard for ^{19}F NMR), THF (1 mL), hexane (1 mL), and deionized water (3 mL). The flask was sealed with a rubber septum, degassed by the freeze-pump-thaw method, and backfilled with CO to 1 atm. A CO-filled 25-mL graduated glass syringe with a silicone-oil-lubricated plunger was connected to the flask, and the catalyst solution (1 mL; 0.02 mmol of Pd, 0.02 mmol of Xantphos) was syringed in at vigorous stirring. The mixture was agitated for 1 hour. The flask was unsealed and PPh_3 (288 mg; 1.1 mmol) was added to the generated solution of 4-fluorobenzoyl azide. This mixture was stirred for 2 h and analyzed by NMR. Quantitative ^{19}F NMR analysis of the reaction mixture indicated the formation of **5** in 85% yield: ^{19}F NMR (377 MHz, THF), δ : -112.2. $^{31}\text{P}\{^1\text{H}\}$ NMR (162 MHz, THF), δ : 20.4 (lit.⁸⁵ 21.3). In an independent experiment, isolated 4-fluorobenzoyl azide was treated with PPh_3 in THF to give **5** that displayed identical ^{19}F and ^{31}P NMR parameters.

⁸⁵ Chou, W. N.; Pomerantz, M.; Witzcak, M. K. *J. Org. Chem.* 1990, *55*, 716.

1-Fluoro-4-isocyanobenzene (6).⁸⁶ In air, a 25-mL flask containing a magnetic stir bar was charged with NaN₃ (78 mg; 1.2 mmol), 1-fluoro-4-iodobenzene (222 mg; 1 mmol), benzotrifluoride (46 mg, 0.315 mmol; internal standard for ¹⁹F NMR), toluene (2 mL), and deionized water (3 mL). The flask was sealed with a rubber septum, degassed by the freeze-pump-thaw method, and backfilled with CO to 1 atm. A CO-filled 25-mL graduated glass syringe with a silicone-oil-lubricated plunger was connected to the flask, and the catalyst solution in toluene (1 mL; 0.02 mmol of Pd, 0.02 mmol of Xantphos) was syringed in at vigorous stirring. The catalyst solution was prepared as described on page 97, except toluene (5 mL) was used as the solvent. The mixture was agitated for 2 h, the organic phase was separated, and the aqueous phase was washed with toluene (2 × 5 mL). The combined toluene solutions were filtered through a pad of anhydrous MgSO₄. After the filtrate was kept under reflux for 4 hours in air, ¹⁹F NMR analysis indicated the formation of 4-fluorophenylisocyanate **6** in 86% yield: ¹⁹F NMR (377 MHz, toluene), δ: -116.3 (lit.⁸⁶ -116.6 in CH₃CN). The formation of **6** was also confirmed by GC-MS.

Azidocarbonylation of aryl iodides in the presence of PMHS (0.2 mol % Pd, Table 1.5). General procedure. A 25-mL round-bottom flask equipped with a gas inlet and a Teflon-coated magnetic stir bar was charged, in air, with an iodoarene (10.0 mmol), NaN₃ (0.78 g; 12 mmol), [(Xantphos)PdCl₂]·CH₂Cl₂ (**8**; 17 mg; 0.2 mol %), K₂CO₃ (28 mg; 2 mol %), and water (2 mL). After two freeze-pump-thaw cycles, the flask was backfilled with CO and connected to a CO balloon via a 1.2-mm diameter stainless steel syringe needle. At vigorous stirring, a solution of PMHS (150 mg; 25 mol %) in oxygen-free THF was syringed in and the mixture was agitated

⁸⁶ Weigert, F. J.; Sheppard, W. A. *J. Org. Chem.* 1976, *41*, 4006.

at room temperature. After GC-MS analysis of the organic phase indicated 95-100% conversion of the iodoarene, the product was isolated and purified in air. The reaction mixture was diluted with ether (10 mL) and transferred to a separatory funnel. The reaction flask was rinsed with ether (2×10 mL) and water (10 mL), and the washings were added to the separatory funnel. After shaking, the organic phase was separated and the aqueous phase was washed with Et₂O (2×20 mL). The combined extract and the washings were dried over MgSO₄, filtered, and rotary-evaporated at room temperature. Silica gel column chromatography of the residue gave the pure product (¹H NMR, GC-MS).

Benzoyl azide (2a). Azidocarbonylation of iodobenzene (2.04 g) by the general procedure using a solution of PMHS in THF (0.5 mL) gave >99% conversion after 20 h. Pentane-ether (9:1 v/v) was used for isolation by column chromatography. After solvent removal and drying on a rotary evaporator (100 mbar for 1 h, then 80 mbar for 0.5 h), **2a** was obtained as a colorless oil that crystallized on standing at +8 °C. The yield was 1.29 g (88%).

4-Methylbenzoyl azide (2b). Azidocarbonylation of 4-iodotoluene (2.18 g) by the general procedure using a solution of PMHS in THF (0.5 mL) gave >99% conversion after 16 h. Hexane-ether (9:1 v/v) was used for isolation by column chromatography. After solvent removal and drying on a rotary evaporator, **2b** was obtained as a colorless oil that crystallized on standing at +8 °C. The yield was 1.33 g (83%).

4-Methoxybenzoyl azide (2d). Azidocarbonylation of 4-iodoanisole (2.34 g) by the general procedure using a solution of PMHS in THF (2.0 mL) gave 95% conversion after 44 h. Hexane-ether (9:1 v/v) was used for isolation by column chromatography. After solvent removal and drying on a rotary evaporator, **2d** was obtained as a white crystalline solid. The yield was 1.38 g (78%).

4-Nitrobenzoyl azide (2e). Azidocarbonylation of 4-nitroiodobenzene (2.49 g) by the general procedure using a solution of PMHS in THF (3.0 mL) gave >99% conversion after 19 h. Hexane-ether (2:1 v/v) was used for isolation by column chromatography. After solvent removal and drying on a rotary evaporator, **2e** was obtained as a yellowish crystals. The yield was 1.66 g (86%).

4-Acetylbenzoyl azide (2f). Azidocarbonylation of 4-iodoacetophenone (2.46 g) by the general procedure using a solution of PMHS in THF (3.0 mL) gave >99% conversion after 16 h. Hexane-ether (2:1 v/v) was used for isolation by column chromatography. After solvent removal and drying on a rotary evaporator, **2f** was obtained as white crystals. The yield was 1.65 g (87%).

Ethyl 4-(azidocarbonyl)benzoate (2g). Azidocarbonylation of ethyl 4-iodobenzoate (2.76 g) by the general procedure using a solution of PMHS in THF (0.5 mL) gave 99% conversion after 16 h. Hexane-ether (9:1 v/v) was used for isolation by column chromatography. After solvent removal and drying on a rotary evaporator, **2g** was obtained as white crystals. The yield was 1.89 g (86%).

4-Fluorobenzoyl azide (2j). Azidocarbonylation of 1-fluoro-4-iodobenzene (2.22 g) by the general procedure using a solution of PMHS in THF (0.5 mL) gave >99% conversion after 20 h. Pentane-ether (9:1 v/v) was used for isolation by column chromatography. After solvent removal and drying (100 mbar for 1 h) on a rotary evaporator, **2j** was obtained as a colorless oil. The yield was 1.42 g (86%).

4-Chlorobenzoyl azide (2k). Azidocarbonylation of 1-chloro-4-iodobenzene (2.39 g) by the general procedure using a solution of PMHS in THF (0.5 mL) gave >99% conversion after 20 h. Hexane-ether (9:1 v/v) was used for isolation by column chromatography. After solvent removal and drying on a rotary evaporator, **2k** was obtained as a white crystalline solid. The yield was 1.60 g (88%).

3-Methoxybenzoyl azide (2o). Azidocarbonylation of 3-iodoanisole (2.34 g) by the general procedure using a solution of PMHS in THF (0.5 mL) gave >99% conversion after 19 h. Hexane-ether (9:1 v/v) was used for isolation by column chromatography. After solvent removal and drying on a rotary evaporator, **2o** was obtained as a colorless oil. The yield was 1.57 g (89%).

2-Thiophenecarbonyl azide (2q). Azidocarbonylation of 2-iodothiophene (2.10 g) by the general procedure using a solution of PMHS in THF (0.5 mL) gave >99% conversion after 17 h. Pentane-ether (9:1 v/v) was used for isolation by column chromatography. After solvent removal and drying (100 mbar for 1 h) on a rotary evaporator, **2q** was obtained as a white solid. The yield was 1.31 g (86%).

Catalytic azidocarbonylation with 1 equiv of CO. Inside a glovebox, a 5-mL flask containing a magnetic stir bar was charged with NaN_3 (325 mg; 5.0 mmol), 4-fluoriodobenzene (222 mg; 1.00 mmol), THF (1 mL), and hexane (1 mL). Outside the glovebox, argon-saturated H_2O (3 mL) was added. The flask was quickly evacuated and connected to a 30-mL glass syringe with a silicone oil-lubricated plunger containing CO (25 mL, 1.02 mmol at 299K). The above-described catalyst solution in THF (1 mL; 0.02 mmol Pd; 0.02 mmol Xantphos) was syringed in at vigorous stirring. The CO from the 30-mL syringe was absorbed in 5 min. ^{19}F NMR analysis of a 0.2 mL aliquot of the organic phase in 1 mL of THF indicated 67% conversion to 4-fluorobenzoyl azide (δ : -104.5 ppm).

Azidocarbonylation under CO pressure (100 psi). Inside a glovebox, a 100-mL Fisher-Porter tube was charged with 4-fluoriodobenzene (222 mg; 1.00 mmol), THF (1 mL), hexane (1 mL) and 1 mL of the catalyst solution in THF (see above; 0.02 mmol Pd; 0.02 mmol Xantphos). The tube was sealed and brought out of the glovebox. An argon-saturated solution of NaN_3 (78 mg; 1.2 mmol) in water (3 mL) was added under argon. The mixture was degassed by the freeze-pump-thaw method and pressurized with CO (100 psi). After agitation at room temperature for 2 h, ^{19}F NMR analysis of the organic phase indicated 25% conversion of 4-fluoriodobenzene (δ : -115.4 ppm) to 4-fluorobenzoyl azide (δ : -104.5 ppm) in ca. 20% yield.

Synthesis, Characterization, and Reactions of Pd Complexes.

[(PPh₃)₂Pd(Ph)N₃]. [(PPh₃)₂Pd(Ph)Br] (153 mg; 0.194 mmol) was added to a suspension of NaN_3 (252 mg; 3.9 mmol; 20 equiv) in MeOH (4 mL), and the mixture was sonicated for 1 h. Methanol (15 mL) was added and the liquid phase decanted off.

Preparation of [(Xantphos)PdI₂] (7). A mixture of [(Xantphos)PdCl₂]·CH₂Cl₂ (**8**; 126 mg; 0.15 mmol), NaI (225 mg; 1.50 mmol), deionized water (2 mL), and CH₂Cl₂ (2 mL) was stirred in air for 30 min. The deep purple mixture was diluted with deionized water (5 mL) and CH₂Cl₂ (5 mL). The organic phase was separated and the aqueous phase was washed with CH₂Cl₂ (2 × 5 mL). The combined dichloromethane phase and the washings were dried over Na₂SO₄ and filtered through Celite. The filtrate was evaporated to ca. 5 mL, treated with Et₂O (25 mL), and kept at -32 °C overnight. The dark precipitate was separated, washed with Et₂O (2 × 5 mL) and dried under vacuum. The yield of **7** was 137 mg (97%). This complex is air-stable in the solid state and in solution. Anal. Calcd. for C₃₉H₃₂I₂OP₂Pd (%): C, 49.9; H, 3.4. Found: C, 49.7; H, 3.7. ¹H NMR (CD₂Cl₂, 400 MHz, 298K), δ: 1.78 (br s, 6H, 2CH₃), 6.80-8.01 (br m, 26H). ³¹P{¹H} NMR (CD₂Cl₂, 203 MHz, 298K), δ: 7.1 (s, *trans-7*), 19.5 (s, *cis-7*) in a 3.5:1 ratio. ¹H NMR (CD₂Cl₂, 500 MHz, 273K), δ: 1.76 (s, *trans-7*, 2CH₃), 1.82 (br s, *cis-7*, 2CH₃), 7.02 (br m), 7.17 (br m), 7.21 (t, *J* = 7.6 Hz), 7.27-7.50 (m), 7.58 (t, *J* = 7.4 Hz), 7.60-7.72 (m) with *trans-7* to *cis-7* ratio ca. 2:1. ³¹P{¹H} NMR (CD₂Cl₂, 203 MHz, 273K), δ: 7.4 (*trans-7*), 19.7 (*cis-7*) in a ca. 2:1 ratio. ¹H NMR (CD₂Cl₂, 500 MHz, 243K), δ: 1.74 (s, *trans-7*, 2CH₃), 1.79 (br s, *cis-7*, 2CH₃), 7.13 (br s), 7.21 (t, *J* = 7.7 Hz), 7.31 (dt, *J* = 7.7 and 1.8 Hz), 7.35-7.49 (m), 7.56 (t, *J* = 7.6 Hz), 7.60-7.71 (m). ³¹P{¹H} NMR (CD₂Cl₂, 203 MHz, 243K), δ: 7.8 (*trans-7*), 19.8 (*cis-7*) in a 1.2:1 ratio. ¹H NMR (CD₂Cl₂, 500 MHz, 183K), δ: 1.56 (s, CH₃, *cis-7*), 1.71 (s, 2CH₃, *trans-7*), 1.96 (s, CH₃, *cis-7*), 6.52 (m), 6.59 (t, *J* = 6.9 Hz), 6.69 (t, *J* = 7.5 Hz), 6.81 (t, *J* = 8.8 Hz), 6.90 (t, *J* = 7.4 Hz), 7.03-7.17 (brm), 7.20 (t, *J* = 7.7 Hz), 7.29 (t, *J* = 7.7 Hz), 7.33-7.48 (m), 7.51 (t, *J* = 7.6 Hz), 7.58 (m), 7.66 (t, *J* = 8.5 Hz), 8.66 (br s). ³¹P{¹H} NMR (CD₂Cl₂, 203 MHz, 183K), δ: 8.7 (*trans-7*), 19.8 (*cis-7*) in a ca. 0.8:1 ratio. X-ray quality single crystals of *cis-7*·CH₂Cl₂ were obtained by layering its

Preparation of [(Xantphos)Pd(COPh)I] (13). In a glovebox, a mixture of Pd₂dba₅ (346 mg; 0.5 mmol) and Xantphos (289 mg; 0.5 mmol) in THF (25 mL) was stirred for 1 h. The solution was filtered through Celite to remove small quantities of Pd black. Iodobenzene (0.5 mL) was added to the filtrate, the flask was sealed with a septum, brought out, quickly evacuated through a syringe needle and backfilled with CO. Stirring the solution at room temperature overnight produced a yellow precipitate. Hexane (40 mL) was added in air. The solid was separated by filtration, washed with ether, and dried under vacuum to give 414 mg (84%) of **13** as a THF mono-solvate (¹H NMR). Anal. Calcd. for C₅₀H₄₅IO₃P₂Pd (%): C, 60.7; H, 4.6. Found: C, 60.1; H, 4.3. ¹H NMR (CD₂Cl₂, 500 MHz), δ: 1.67 (s, 6H, 2CH₃), 1.82 (m, 2H, THF), 3.69 (m, 2H, THF), 6.75-6.81 (m, 2H), 7.05-7.13 (m, 4H), 7.14-7.20 (m, 8H), 7.23-7.27 (m, 1H), 7.27-7.32 (m, 4H), 7.34-7.40 (m, 8H), 7.60 (dd, *J*₁ = 7.7 Hz, *J*₂ = 1.4 Hz, 2H), 7.68 (m, 2H). ³¹P{¹H} NMR (CD₂Cl₂, 203 MHz), δ: 3.8. IR (neat, cm⁻¹): 2976, 1705, 1658, 1435, 1410, 1243, 1145, 1095, 1067, 999, 839, 765, 691, 661, 609, 510, 461. Complex **13** is air-stable in the solid state but decomposes in solution. All manipulations with solutions of **13** were therefore performed under argon using dry, oxygen-free solvents. X-ray quality crystals of **13** were obtained by layering a concentrated THF solution of the complex with hexane in a 5-mm NMR tube inside a glovebox. The X-ray structure of **13**·0.5THF is shown in Figure 1.9.

Preparation of [(Xantphos)Pd(Ph)N₃] (14). A mixture of [(Xantphos)Pd(Ph)Br] (126 mg; 0.15 mmol), dichloromethane (2 mL), NaN₃ (200 mg; 3.08 mmol), and deionized water (3 mL) was vigorously stirred for 1 h. The aqueous layer was removed by a pipette, a solution of NaN₃ (200 mg; 3.08 mmol) in water (3 mL) was added to the organic phase, and the mixture was stirred for 1 h. After this procedure was repeated

one more time the organic phase was separated, washed with water (2×5 mL), dried over Na_2SO_4 , evaporated to ca. 1 mL, and treated with ether (15 mL). The precipitated **14** was separated, washed with ether (2×5 mL), and dried under vacuum. The yield of **14** was 82 mg (68%). Anal. Calcd. for $\text{C}_{45}\text{H}_{37}\text{N}_3\text{OP}_2\text{Pd}$ (%): C, 67.2; H, 4.6; N, 5.2. Found: C, 67.1; H, 4.6; N, 5.2. ^1H NMR (CD_2Cl_2 , 400 MHz), δ : 1.80 (s, 6H, CH_3), 6.23 (br. s, 2H, $\text{C}_6\text{H}_5\text{-Pd}$), 6.30-6.42 (m, 1H, $\text{C}_6\text{H}_5\text{-Pd}$), 6.64 (br. s, 2H, $\text{C}_6\text{H}_5\text{-Pd}$), 6.95-7.50 (m, 24H), 7.70 (dd, $J_1 = 7.7$ Hz, $J_2 = 1.4$ Hz, 2H). $^{31}\text{P}\{^1\text{H}\}$ NMR (CD_2Cl_2 , 162 MHz), δ : 11.5. Complex **14** crystallizes in two isomorphous forms, yellow cubes and white needles. Both forms were analyzed by single crystal X-ray diffraction. Only one structure is presented (Figure 1.10) because of the poor quality of the other one.

Reaction of $\text{Pd}_2(\text{dba})_5$ with Xantphos. Inside a glovebox, a 5-mm NMR tube was charged with $\text{Pd}_2(\text{dba})_5$ (7 mg; 0.01 mmol of Pd), Xantphos (6 mg; 0.01 mmol), benzene- d_6 (0.6 mL) and sealed with a rubber septum. $^{31}\text{P}\{^1\text{H}\}$ NMR analysis of the sample showed complete conversion of Xantphos and the formation of two new species, $[(\text{Xantphos})\text{Pd}(\text{dba})]$ (**11**; two doublets at 11.3 and 13.5 ppm $J_{\text{P-P}} = 10.6$ Hz) and $[(\text{Xantphos})_2\text{Pd}]$ (two broad multiplets at 3.5 and 6.0 ppm) in a 4:1 ratio. A similar $^{31}\text{P}\{^1\text{H}\}$ NMR pattern was observed for the reaction mixture obtained similarly using $\text{Pd}_2(\text{dba})_5$ (28 mg; 0.04 mmol of Pd) and Xantphos (23 mg; 0.04 mmol) in THF (2 mL). After one week at room temperature, the THF solution produced X-ray quality crystals of $[(\text{Xantphos})\text{Pd}(\text{dba})] \cdot 3\text{THF}$ (**11**·3THF), see Figure 1.7.

Reaction of $\text{Pd}_2(\text{dba})_5$ with Xantphos and CO. Inside a glovebox, a 5-mm NMR tube was charged with $\text{Pd}_2(\text{dba})_5$ (7 mg; 0.01 mmol of Pd), Xantphos (6 mg; 0.01 mmol), benzene- d_6 (0.6 mL) and sealed with a rubber septum. After the argon

headspace was flushed with CO via a syringe needle, full conversion of the originally produced mixture of [(Xantphos)Pd(dba)] (**11**) and [(Xantphos)₂Pd] to [(Xantphos)Pd(CO)₂], (**12**; s, 10.5 ppm) was observed within 10 min (³¹P{¹H} NMR). Identical results were obtained when THF (0.6 mL) was used in place of benzene-*d*₆. Two strong bands at 1974 and 2014 cm⁻¹ were observed in the FT-IR spectrum of the solution (background subtraction).

Reaction of [(Xantphos)Pd(Ph)I] (10**) with CO.** Inside a glovebox, a 5-mm NMR tube was charged with [(Xantphos)Pd(Ph)I] (**10**; 7 mg; 0.008 mmol) and benzene-*d*₆ (0.5 mL) and sealed with a rubber septum. After the headspace was flushed with CO (syringe needle) for ca. 0.5 min, full conversion of **10** (s, 13.2 ppm) to [(Xantphos)Pd(COPh)I] (**13**; s, 3.2 ppm) was observed by ³¹P{¹H} NMR.

Reaction of [(Xantphos)Pd(CO)₂] (12**) with PhI.** Inside a glovebox, a 5-mm NMR tube was charged with Pd₂(dba)₅ (7 mg; 0.01 mmol of Pd), Xantphos (6 mg; 0.01 mmol), and benzene-*d*₆ (0.6 mL) and sealed with a rubber septum. After the headspace was flushed with CO (syringe needle) for ca. 0.5 min, full conversion to [(Xantphos)Pd(CO)₂], (**12**; s, 10.5 ppm) was observed within 10 min (³¹P{¹H} NMR). Addition of iodobenzene (20 μL) to the thus generated **12** resulted in selective formation of [(Xantphos)Pd(COPh)I] (**13**; ³¹P{¹H} NMR: s, 3.2 ppm) at full conversion.

Reaction of [(Xantphos)Pd(COPh)I] (13**) with [Bu₄N]N₃.** Inside a glovebox, a 5-mm NMR tube was charged with [(Xantphos)Pd(Ph)I] (**10**; 7 mg; 0.008 mmol) and benzene-*d*₆ (0.5 mL) and sealed with a rubber septum. Replacing the argon headspace with CO (syringe needle) resulted in instantaneous reaction leading to full conversion

($^{31}\text{P}\{^1\text{H}\}$ NMR) of **10** (s, 13.2 ppm⁴⁶) to [(Xantphos)Pd(COPh)I] (**13**; s, 3.2 ppm). A solution of $[\text{Bu}_4\text{N}]\text{N}_3$ (10 mg; 0.035 mmol) in benzene- d_6 (0.2 mL) was added via syringe. The $^{31}\text{P}\{^1\text{H}\}$ NMR spectrum recorded within 10 minutes indicated full conversion of **13** to [(Xantphos)Pd(CO) $_2$] (**12**; s, 10.5 ppm). As the resultant solution of **12** and PhCON_3 was highly air-sensitive, the formation of the latter by IR was confirmed in a similar experiment performed in the presence of PhI (see below).

Reaction of [(Xantphos)Pd(COPh)I] (13**) with $[\text{Bu}_4\text{N}]\text{N}_3$ in the presence of PhI.**

Inside a glovebox, a 5-mm NMR tube was charged with Xantphos (6 mg; 0.01 mmol), Pd_2dba_5 (7 mg; 0.01 mmol of Pd) and benzene- d_6 (0.5 mL) and sealed with a rubber septum. The headspace was flushed with CO (syringe needle) for ca. 0.5 min. The addition of iodobenzene (20 μL) to the thus generated [(Xantphos)Pd(CO) $_2$] (**12**; see above) resulted in the selective formation of [(Xantphos)Pd(COPh)I] (**13**; $^{31}\text{P}\{^1\text{H}\}$ NMR: s, 3.2 ppm) at full conversion. To this sample was added via syringe 0.2 mL (1.2 equiv) of a solution of $[\text{Bu}_4\text{N}]\text{N}_3$ (34 mg) in C_6H_6 (2 mL). The FT-IR spectrum registered 10 minutes after the addition of azide indicated the formation of PhCON_3 (**2a**; neat, cm^{-1}): 2133 (N_3); 1695 (C=O) and no presence of PhNCO (2247 cm^{-1}). FT-IR for an authentic sample of **2a**: 2130 (N_3); 1691(C=O).

Reaction of [(Xantphos)Pd(Ph)I] (10**) with $[\text{Bu}_4\text{N}]\text{N}_3$.** Inside a glovebox, a vial was charged with Xantphos (29 mg; 0.05 mmol), Pd_2dba_5 (35 mg; 0.05 mmol of Pd), PPh_3O (14 mg; 0.05 mmol; internal standard), and benzene (5 mL). After stirring this reaction mixture for 1 min, PhI (100 μL) was added. $^{31}\text{P}\{^1\text{H}\}$ NMR analysis indicated full conversion of [(Xantphos)Pd(dba)] (**11**) to [(Xantphos)Pd(Ph)I] (**10**; s, 13.2 ppm) after 30 min. $[\text{Bu}_4\text{N}]\text{N}_3$ (16 mg; 0.06 mmol) was then added and the solution was again

analyzed by $^{31}\text{P}\{^1\text{H}\}$ NMR after 10 min to observe full conversion to $[(\text{Xantphos})\text{Pd}(\text{Ph})\text{N}_3]$ (**14**; s, 11.0 ppm).

Reaction of $[(\text{Xantphos})\text{Pd}(\text{Ph})\text{I}]$ (10**) with NaN_3 .** Inside a glovebox, a vial was charged with Xantphos (29 mg; 0.05 mmol), Pd_2dba_5 (35 mg; 0.05 mmol of Pd), PPh_3O (14 mg; 0.05 mmol; internal standard) and benzene (5 mL). After stirring for 1 min, PhI (100 μL) was added. $^{31}\text{P}\{^1\text{H}\}$ NMR analysis after 30 minutes indicated full conversion to $[(\text{Xantphos})\text{Pd}(\text{Ph})\text{I}]$ (**10**; s, 13.2 ppm). Argon-saturated water (5 mL) and sodium azide (32 mg; 0.5 mmol) were added. After 5 min of vigorous agitation, a 0.2 mL aliquot of the organic layer was diluted with C_6H_6 (1 mL) and analyzed by $^{31}\text{P}\{^1\text{H}\}$ NMR (IGD) to show ca. 60% conversion to $[(\text{Xantphos})\text{Pd}(\text{Ph})\text{N}_3]$ (**14**; s, 11.0 ppm). No change in the composition of the organic layer was observed ($^{31}\text{P}\{^1\text{H}\}$ NMR) after stirring the biphasic system for an additional hour.

Reaction of $[(\text{Xantphos})\text{Pd}(\text{Ph})\text{N}_3]$ (14**) with CO.** Inside a glovebox, a 5-mm NMR tube was charged with **14** (7 mg; 0.01 mmol) and toluene (0.6 mL) and sealed with a rubber septum. After the mixture was placed under CO by purging via a syringe needle for ca. 0.5 min, full conversion of **14** to $[(\text{Xantphos})\text{Pd}(\text{CO})_2]$ (**12**; s, 10.5 ppm) was observed within 10 min ($^{31}\text{P}\{^1\text{H}\}$ NMR). Layering the resultant solution with hexanes under CO produced X-ray quality crystals of $[(\text{Xantphos})\text{Pd}(\text{CO})_2]\cdot n\text{-C}_6\text{H}_{14}$ (**12**·hexane; see Figure 1.8).

Reaction of $[(\text{Xantphos})\text{Pd}(\text{Ph})\text{N}_3]$ (14**) with CO in the presence of PhI .** Inside a glovebox, a 5-mm NMR tube was charged with **14** (7 mg; 0.01 mmol), PhI (20 μL) and benzene- d_6 (0.6 mL) and sealed with a rubber septum. After reaction mixture was

placed under CO atmosphere by purging via a syringe needle for ca. 0.5 min, full conversion of **14** to [(Xantphos)Pd(COPh)I] (**13**; $^{31}\text{P}\{^1\text{H}\}$ NMR: s, 3.2 ppm) was observed within 10 min by $^{31}\text{P}\{^1\text{H}\}$ NMR. The formation of PhCON₃ (**2a**) was confirmed by FT-IR (neat, cm⁻¹): 2133 (N₃); 1694 (C=O). For independently prepared and isolated **2a**, FT-IR (neat, cm⁻¹): 2130 (N₃); 1691 (C=O). No characteristic band from NCO was observed (2247 cm⁻¹ for an authentic sample of PhNCO).

[Bu₄N]N₃. A 50% aqueous solution of tetra-*n*-butylammonium sulfate (5.8 g; 5.0 mmol of [NBu₄]₂SO₄) was concentrated on rotary evaporator. After a total of 2.1 g of water had been evaporated, NaN₃ (1.95 g; 30 mmol) was added and the resultant mixture was agitated for 20 h. Acetonitrile (30 mL) and anhydrous sodium sulfate (10 g) were added, the mixture was stirred for 30 min, and filtered. The solid on the filter was washed with acetonitrile (2 × 10 mL). The combined filtrate and the washings were evaporated on a rotary evaporator. Drying the residue under vacuum (ca. 1 mmHg) overnight produced a white solid (2.88 g). The thus obtained crude [Bu₄N]N₃ was brought to a glovebox and dissolved in dry benzene (20 mL). The resultant solution was filtered through a pad of Celite. The reaction flask was rinsed with dry benzene (2 × 10 mL) and the washings were filtered through the same pad. The combined filtrate and the washings were evaporated and dried under vacuum at ca. 1 mmHg for 20 h. Trituration of the residue with dry ether (40 mL) produced a white crystalline solid that was separated and dried under vacuum (ca. 1 mmHg) for 20 h. The yield of [Bu₄N]N₃ was 2.79 g (98%). This salt is hygroscopic and was therefore stored and used in a glovebox. ¹H NMR (500 MHz, CDCl₃), δ: 1.00 (t, *J* = 7.4 Hz, 3H), 1.45 (tq, *J* = 7.4 and 7.4 Hz, 2H), 1.68 (m, 2H), 3.35 (m, 2H). IR (neat, cm⁻¹): 1991 (N₃⁻). X-ray quality

Simplified forms of Eq 1.1:

For $k_1, k_{-1} \gg k_2$, as indicated by the computational data, Eq 1.1 can be simplified to (i) its general form (Eq 1.2); (ii) a second order rate equation with the assumption that [CO] remains constant (Eq 1.3); and (iii) a first order equation for $[\mathbf{B}] \gg [\mathbf{A}]$ and $[\mathbf{B}] = \text{constant}$ (Eq 1.4).

$$\frac{d[\mathbf{A}]}{d[t]} = -k_1 \frac{[\mathbf{A}][\mathbf{B}]}{[\text{CO}]} \quad (\text{Eq 1.2})$$

$$\frac{d[\mathbf{A}]}{d[t]} = -k_{II} [\mathbf{A}][\mathbf{B}] \quad (\text{Eq 1.3})$$

$$\frac{d[\mathbf{A}]}{d[t]} = -k_{III} [\mathbf{A}] \quad (\text{Eq 1.4})$$

The free Gibbs energy of activation (ΔG^\ddagger) was estimated using the following procedure: Inside a glovebox, a mixture of Xantphos (46 mg; 0.08 mmol) and Pd₂dba₅ (55 mg; 0.08 mmol of Pd) was dissolved in C₆H₆ (10.0 mL), sealed and brought out of a glovebox. Placing the resultant reaction mixture under CO produced a solution of [(Xantphos)Pd(CO)₂] (**12**; **A**) with [A] = 0.008 M. Inside a glovebox, 4-FC₆H₄I (**1j**; **B**; 89 mg; 0.4 mmol) and 4,4'-difluoro-1,1'-biphenyl (38 mg; 0.2 mmol; internal standard; ¹⁹F NMR, δ = -115.3 ppm) were dissolved in C₆H₆ (10.0 mL). The thus prepared solution was sealed, brought out of a glovebox, and placed under CO. ([B] = 0.04 M). Inside a glovebox, benzene-*d*₆ (0.4 mL) was placed in a 5-mm glass NMR tube. The tube was sealed, brought out of a glovebox, degassed by freeze-pump-thaw, and back-filled with CO. The solution of **A** (0.008 M; 0.5 mL) and then the solution of **B** (0.04 M; 100 μL) were syringed in the NMR tube containing benzene-*d*₆ under CO, and the reaction rate was measured by ¹⁹F{¹H} NMR. For integration, the sum of the signals

from **B** (-114.1 ppm) and the product **D** (-108.5 ppm) was normalized (100%). The starting concentrations of the reagents were $[A]_0 = [B]_0 = 0.004$ M.

The linear plot of $1/[B]$ vs. time (Figure 1.16) confirms second order of the reaction (Eq 1.3) and the proposed kinetic scheme (Scheme 1.21). The large integration error of ca. 30% stemmed from the necessity to use the low concentrations of **A** and **B** and, as a consequence, poor signal to noise ratios in the ^{19}F NMR spectra. From the data obtained, k_{II} was roughly estimated at 0.3 ± 0.2 L mol $^{-1}$ s $^{-1}$ at 23 °C (Figure 1.16). For $[B]_0 = 1\text{M}$, the kinetics were simplified to formal first-order (Eq 1.4) with $k_{III} = k_{II}[B]_0 = 1.2 \pm 0.8 \times 10^{-3}$ s $^{-1}$ and $\Delta G^\ddagger = 21.5 \pm 0.5$ kcal/mol (23 °C) was calculated using the Eyring equation.

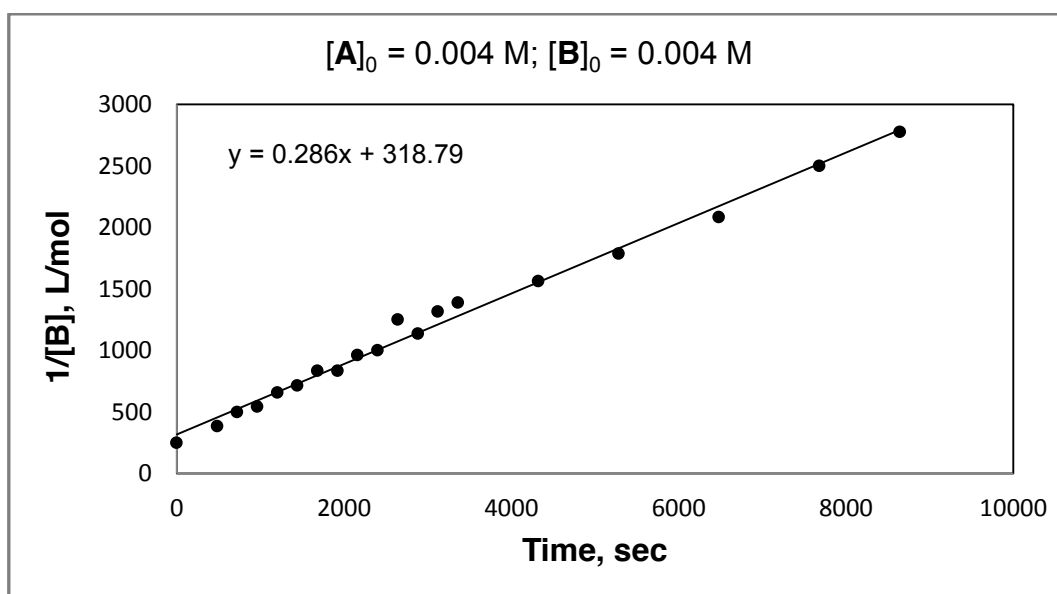
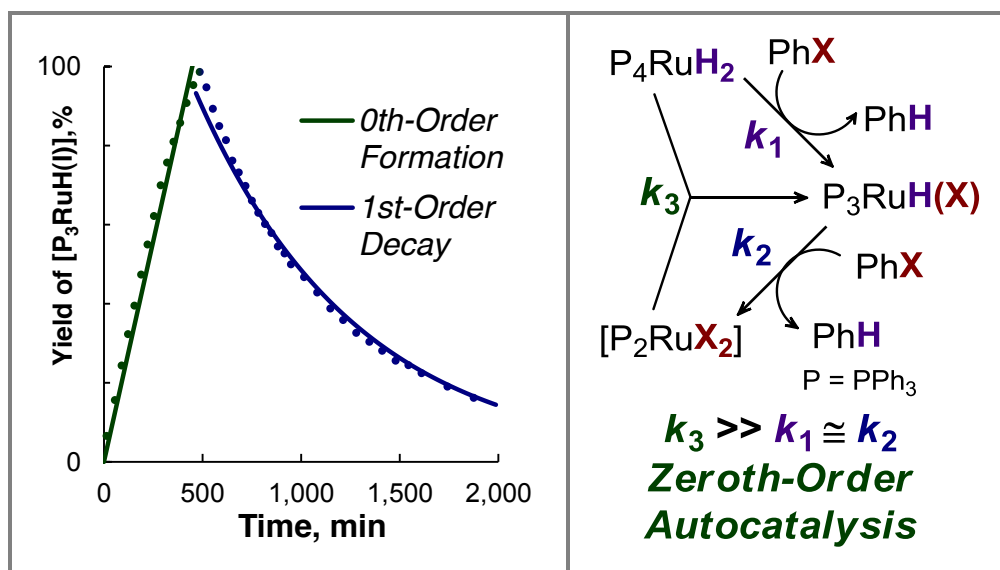


Figure 1.16. Kinetic of the oxidative addition of 4F-C₆H₄I (**1j**; **B**) to [(Xantphos)Pd(CO)₂] (**12**; **A**) in benzene at 23 °C.

Chapter 2

Mechanistic Study of Aryl Halide Activation with Ruthenium (II) Hydrido Complexes



Introduction

Efficient activation of inert bonds is a major goal of organometallic chemistry and catalysis with metal complexes.¹ As detailed in the General Introduction, the carbon-halogen bond of unactivated haloarenes is particularly targeted because of the special importance of its functionalization in organic synthesis.² While being most attractive from the economical point of view, aryl chlorides are especially challenging substrates because of the enhanced stability and low reactivity of the Ar-Cl bond.³ Complexes of Pd(0) are much less reactive toward chloroarenes than Ni(0). Since the pioneering work of Osborn^{4a} and Milstein,^{4b,c} it has been widely recognized³ that bulky, electron-rich phosphine ligands⁵ are critical for clean oxidative addition of the Ar-Cl bond to zerovalent Pd, the metal that is most efficiently and widely used in cross-coupling reactions.²

Chloroarene activation reactions with metals other than Pd and Ni are rare. Thoroughly designed Rh⁶ and Ir⁷ systems have been shown to cleave the C-Cl bond of

¹ Murai, S., Ed. *Activation of Unreactive Bonds and Organic Synthesis*; Springer: Berlin, 1999.

² (a) Crabtree, R. H. *The Organometallic Chemistry of the Transition Metals*, 3rd ed.; Wiley-Interscience: New York, 2001. (b) de Meijere, A.; Diederich, F., Eds. *Metal-Catalyzed Cross-Coupling Reactions*, 2nd Ed.; Wiley-VCH: Weinheim, 2004. (c) Hartwig, J. F. *Organotransition Metal Chemistry: From Bonding to Catalysis*; University Science Books: Sausalito, 2009.

³ For comprehensive reviews, see: (a) Grushin, V. V.; Alper, H. *Chem. Rev.* 1994, 94, 1047. (b) Grushin, V. V.; Alper, H. *Top. Organomet. Chem.* 1999, 3, 193. (c) Littke, A. F.; Fu, G. C. *Angew. Chem., Int. Ed.* 2002, 41, 4176. (d) Bedford, R. B.; Cazin, C. S. J.; Holder, D. *Coord. Chem. Rev.* 2004, 248, 2283.

⁴ (a) Huser, M.; Youinou, M. T.; Osborn, J. A. *Angew. Chem., Int. Ed. Engl.* 1989, 28, 1386. (b) Ben-David, Y.; Portnoy, M.; Milstein, D. *J. Am. Chem. Soc.* 1989, 111, 8742. (c) Ben-David, Y.; Portnoy, M.; Milstein, D. *J. Chem. Soc., Chem. Commun.* 1989, 1816.

⁵ It has been recently shown that Pd(0) bearing NiXantphos, an anionic Xantphos-type ligand with Ph substituents on the P atoms, can oxidatively add aryl chlorides at room temperature. The Pd center in this system is apparently extra electron-enriched by the overall negative charge of the coordinated diphosphine. See: Zhang, J.; Bellomo, A.; Trongsrirawat, N.; Jia, T.; Carroll, P. J.; Dreher, S. D.; Tudge, M. T.; Yin, H.; Robinson, J. R.; Schelter, E. J.; Walsh, P. J. *J. Am. Chem. Soc.* 2014, 136, 6276.

⁶ For selected examples, see: (a) Grushin, V. V.; Alper, H. *Organometallics* 1991, 10, 1620. (b) Willems, S. T. H.; Budzelaar, P. H. M.; Moonen, N. N. P.; de Gelder, R.; Smits, J. M. M.; Gal, A. W. *Chem. Eur. J.* 2002, 8, 1310. (c) Grushin, V. V.; Marshall, W. J. *J. Am. Chem. Soc.* 2004, 126, 3068. (d) Macgregor, S. A.; Roe, D. C.; Marshall, W. J.; Bloch, K. M.; Bakhmurov, V. I.; Grushin, V. V. *J. Am. Chem. Soc.* 2005, 127, 15304. (e) Gatard, S.; Celenligil-Cetin, R.; Guo, C.; Foxman, B. M.; Ozerov, O. V. *J. Am. Chem. Soc.* 2006, 128, 2808. (f) Douglas, T. M.; Chaplin, A. B.; Weller, A. S. *Organometallics* 2008, 27, 2918. (g) Ito, J.-I.; Miyakawa, T.; Nishiyama, H. *Organometallics* 2008, 27, 3312. (h) Gatard, S.; Guo, C.; Foxman, B. M.; Ozerov, O. V. *Organometallics* 2007, 26, 6066. (i) Puri, M.; Gatard, S.; Smith, D. A.; Ozerov, O. V. *Organometallics* 2011, 30, 2472.

unactivated aryl chlorides under mild conditions. There have been considerably fewer examples of Ar-Cl activation with Ru. By far the cheapest platinum group metal, ruthenium is particularly attractive for Ar-X activation. Some Ru(0) species have been reported to cleave the less inert C-X (X = I, Br) bond of iodo- and bromobenzene and -toluene at 125 °C.⁸ Highly reactive Ru derivatives of bulky, electron-rich Cy₃P have been shown to activate the Ph-I bond at ambient temperature,^{9a,b} but the Ar-Cl bond only at 80 °C.^{9c} A number of reports¹⁰ of Ru-catalyzed arylation reactions with chloroarenes, however, indicate that the Ar-Cl bond is usually activated at the ruthenium center only at 120-150 °C.

A few years ago, it was found in our group that unactivated aryl halides, chlorobenzene included, are efficiently activated with [(Ph₃P)₃Ru(H₂)(H)₂] (**1**) in the presence of styrene.¹¹ It was demonstrated that adding 1 equiv of styrene to a 1:1 mixture of [(Ph₃P)₃Ru(H₂)(H)₂] (**1**) and PhX (X = I, Br, Cl) in toluene triggered an instantaneous reaction that selectively produced benzene and [(Ph₃P)₃RuH(X)] (**2**), as shown in Scheme 2.1.

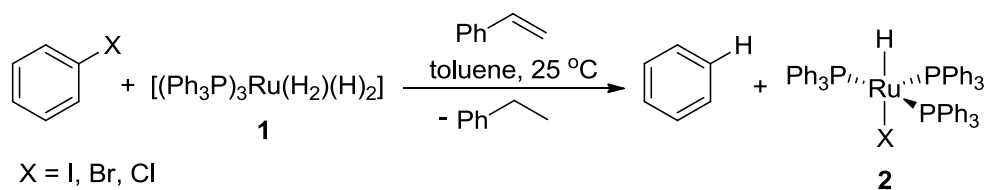
⁷ For facile Ph-Cl activation with Ir, see: Douvris, C.; Reed, C. A. *Organometallics* **2008**, *27*, 807.

⁸ (a) Deeming, A. J.; Speel, D. M. *Organometallics* **1997**, *16*, 289. (b) Grounds, H.; Anderson, J. C.; Hayter, B.; Blake, A. J. *Organometallics* **2009**, *28*, 5289.

⁹ (a) Chaudret, B.; Chug, G.; Eisenstein, O.; Jackson, S. A.; Lahoz, F. J.; Lopez, J. A. *J. Am. Chem. Soc.* **1991**, *113*, 2314. (b) Christ, M. L.; Sabo-Etienne, S.; Chaudret, B. *Organometallics* **1994**, *13*, 3800. (c) Cucullu, M. E.; Nolan, S. P.; Belderrain, T. R.; Grubbs, R. H. *Organometallics* **1999**, *18*, 1299.

¹⁰ For selected examples, see: (a) Gonell, S.; Peris, E. *ACS Catal.* **2014**, *4*, 2811. (b) Salam, N.; Kundu, S. K.; Roy, A. S.; Mondal, P.; Ghosh, K.; Bhaumik, A.; Islam, S. M. *Dalton Trans.* **2014**, *43*, 7057. (c) Arockiam, P. B.; Fischmeister, C.; Bruneau, C.; Dixneuf, P. H. *Green Chem.* **2013**, *15*, 67. (d) Dastbaravardeh, N.; Schnürch, M.; Mihovilovic, M. D. *Eur. J. Org. Chem.* **2013**, 2878. (e) Zhang, J.; Yang, Q.; Zhu, Z.; Yuan, M. L.; Fu, H. Y.; Zheng, X. L.; Chen, H.; Li, R. X. *Eur. J. Org. Chem.* **2012**, 6702. (f) Dastbaravardeh, N.; Schnürch, M.; Mihovilovic, M. D. *Org. Lett.* **2012**, 3792. (g) Ackermann, L.; Lygin, A. V. *Org. Lett.* **2011**, *13*, 3332. (h) Doherty, S.; Knight, J. G.; Addyman, C. R.; Smyth, C. H.; Ward, N. A. B.; Harrington, R. W. *Organometallics* **2011**, *30*, 6010. (i) Li, W.; Arockiam, P. B.; Fischmeister, C.; Bruneau, C.; Dixneuf, P. H. *Green Chem.* **2011**, *13*, 2315. (j) Yu, B.; Yan, X.; Wang, S.; Tang, N.; Xi, C. *Organometallics* **2010**, *29*, 3222. (k) Ackermann, L.; Vicente, R.; Potukuchi, H. K.; Pirovano, V. *Org. Lett.* **2010**, *12*, 5032. (l) Luo, N.; Yu, Z. *Chem. Eur. J.* **2010**, *16*, 787. (m) Ackermann, L.; Novák, P.; Vicente, R.; Pirovano, V. *Synthesis* **2010**, 2245. (n) Arockiam, P. B.; Fischmeister, C.; Bruneau, C.; Dixneuf, P. H. *Angew. Chem. Int. Ed.* **2010**, *49*, 6629. (o) Pozgan, F.; Dixneuf, P. H. *Adv. Synth. Catal.* **2009**, *351*, 1737. (p) Ackermann, L.; Born, R.; Vicente, R. *ChemSusChem* **2009**, *2*, 546. (q) Arockiam, P.; Poirier, V.; Fischmeister, C.; Bruneau, C.; Dixneuf, P. H. *Green Chem.* **2009**, *11*, 1871. (r) Özdemir, İ.; Demir, S.; Gürbüz, N.; Çetinkaya, B.; Toupet, L.; Bruneau, C.; Dixneuf, P. H. *Eur. J. Inorg. Chem.* **2009**, 1942.

¹¹ Muñoz, B. K., 2011, unpublished results.



Scheme 2.1. Reaction of $[(\text{Ph}_3\text{P})_3\text{Ru}(\text{H}_2)(\text{H})_2]$ (**1**) with haloarenes and styrene.

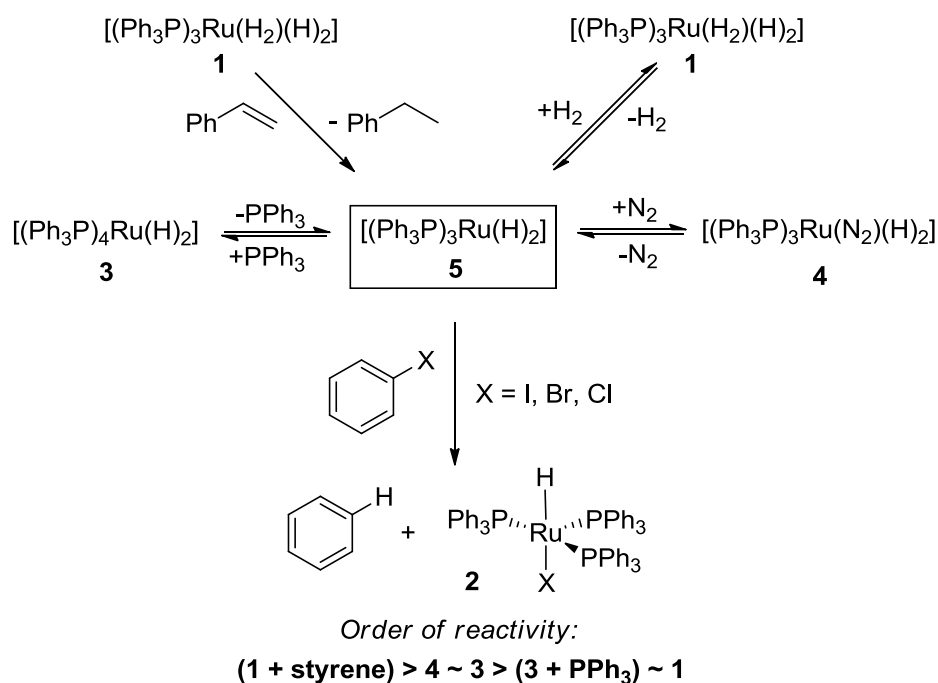
The facile Ph-X (X = Cl, Br) bond cleavage with ruthenium (Scheme 2.1) is unprecedented. Although these transformations bear resemblance to the formation of $[(\text{Cy}_3\text{P})_2\text{RuH}(\text{I})(\text{H}_2)]$ from PhI and $[(\text{Cy}_3\text{P})_2\text{RuH}_6]$,^{9a,b} **1** is devoid of highly basic, bulky phosphine ligands that are critical for efficient Ar-X activation, especially for X = Cl.³ The hydrodechlorination of chlorobenzene with Ru-R₃P (R = Cy or *i*-Pr) catalysts requires 80 °C to occur.^{9c}

Preliminary mechanistic studies¹¹ of the Ar-X activation with **1**-styrene showed that performing the reactions (Scheme 2.1) in THF-*d*₈ resulted in no significant incorporation of deuterium into the benzene product (<4% by GC-MS). This result, along with a lack of formation of bibenzyl in the reactions conducted in toluene suggested that free radicals are unlikely involved in the Ph-X activation process.

It was also found that in the absence of styrene, **1** reacted sluggishly even with PhI, the most reactive phenyl halide. Both $[(\text{Ph}_3\text{P})_4\text{Ru}(\text{H})_2]$ (**3**) and $[(\text{Ph}_3\text{P})_3\text{Ru}(\text{H})_2(\text{N}_2)]$ (**4**) are more reactive toward PhI than **1** (in the absence of styrene).¹¹ Deliberately added PPh₃ slowed down the reaction of **3** with PhI. These data suggest that the Ph-X bond is activated by the same reactive species generated from **1**, **3**, or **4**. The observed qualitative order of reactivity (**1** + styrene) > **4** ≈ **3** > (**3** + PPh₃) ≈ **1** indicates that this reactive species is likely $[(\text{Ph}_3\text{P})_3\text{Ru}(\text{H})_2]$ (**5**) that is produced upon removal of L from $[(\text{Ph}_3\text{P})_3\text{Ru}(\text{L})(\text{H})_2]$, where L = H₂ (**1**), PPh₃ (**3**), or N₂ (**4**) (Scheme 2.2). Indeed, the

long-established¹² higher lability of N₂ in **4** than of H₂ in **1** parallels the observed enhanced reactivity of **4** toward PhI as compared to **1**.

The literature data on [(Ph₃P)₃Ru(H)₂] (**5**) are not without controversy. Apparently, **5** is an elusive species that has been convincingly proposed as a highly reactive intermediate but never unambiguously characterized in the solid state or in solution.¹³ The formation of **5** could not be observed in low-temperature NMR studies of the reaction between **1** and styrene.¹¹



Scheme 2.2. Ph-X activation with “[*(Ph*₃P)₃Ru(H)₂]” (**5**) generated from **1**, **3** or **4**.

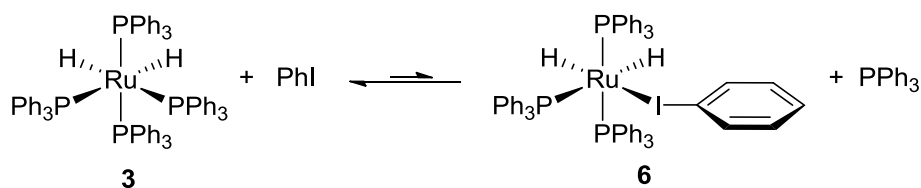
More recently it was found that the addition of PhI in large excess (ca. 75 equiv) to **3** results in partial dissociation of PPh₃ and the formation of a new species, *mer*-[(Ph₃P)₃Ru(H)₂(PhI)] (**6**).¹⁴ Under similar conditions, but with PhBr or PhCl in

¹² Knoth, W. H. *J. Am. Chem. Soc.* **1972**, *94*, 104.

¹³ Samouei, H.; Miloserdov, F. M.; Escudero-Adán, E. C.; Grushin, V. V. *Organometallics* **2014**, *33*, 7279 and references cited therein.

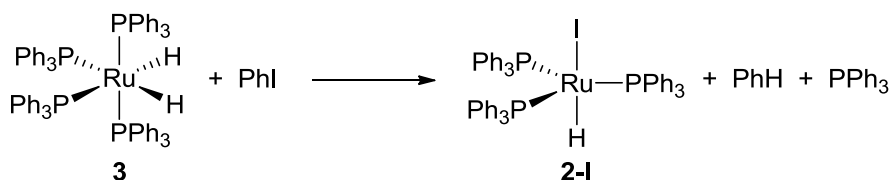
¹⁴ Samouei, H., 2013, unpublished results.

place of PhI, no formation of $[(\text{Ph}_3\text{P})_3\text{Ru}(\text{H})_2(\text{PhX})]$ ($\text{X} = \text{Br}$ or Cl) took place. These observations along with the fact that **6** is produced not only in THF but also in aromatic solvents indicate the PhI molecule in **6** is bound to the Ru center via the iodine atom rather than through the π -system of the aromatic ring (Scheme 2.3).¹⁵ This assignment is consistent with the chemical shifts of the hydrido resonances from **6** (-8.56 and -16.14 ppm at -40 °C).



Scheme 2.3. Equilibrium between $[(\text{Ph}_3\text{P})_4\text{Ru}(\text{H})_2]$ (**3**) and $[(\text{Ph}_3\text{P})_3\text{Ru}(\text{H})_2(\text{PhI})]$ (**6**).

A particularly striking observation was made in a preliminary kinetic study of the reaction of **3** with PhI in excess (Scheme 2.4).¹⁴ It was found that during the reaction the starting complex **3** decays and the product **2-I** appears *linearly* until nearly full conversion of **3** (90-95%). In other words, the rates of disappearance of **3** and of the formation of **2-I** were concentration independent, i.e. *zeroth* order. Such arresting kinetic behavior has not been reported for inert bond activation with a transition metal complex and cannot be rationalized by conventional kinetic schemes.¹⁶



Scheme 2.4. Reaction of $[(\text{Ph}_3\text{P})_4\text{Ru}(\text{H}_2)]$ (**3**) with iodobenzene.

¹⁵ For a review of metal complexes with halocarbon ligands, see: Kulawiec, R. J.; Crabtree, R. H. *Coord. Chem. Rev.* 1990, 99, 89.

¹⁶ Espenson, J. H. *Chemical Kinetics and Reaction Mechanisms*, 2nd Ed.; McGraw-Hill: New York, 1995.

Objectives

The findings described in the Introduction above are intriguing in at least two respects. First, the novel Ph-X (X = Cl, Br, I) activation reactions with Ru(II) complexes devoid of bulky, electron-rich phosphine ligands (Schemes 2.1, 2.2, and 2.4) are unprecedentedly facile, readily occurring at room temperature. Second, the preliminary mechanistic investigations performed in our group^{11,14} point unambiguously to an uncommon mechanism that governs these transformations. Considering the exceptional importance of aromatic carbon-halogen bond activation in chemistry, our objective was to carry out a detailed study of the reactions of $[(\text{Ph}_3\text{P})_4\text{Ru}(\text{H})_2]$ (**3**) with iodo-, bromo-, and chlorobenzene in order to establish their mechanism. To this end, we employed the most powerful modern approach to elucidation of reaction mechanisms, which involves both experimental and computational studies.¹⁷

¹⁷ The DFT computational studies were performed by Dr. D. McKay and Prof. S. A. Macgregor (Heriot-Watt University, U.K.).

Results

Kinetic Studies of the Reaction of **3 with PhI.** In order to elucidate the mechanism of the Ph-X activation with the ruthenium complexes, it was critical to understand the origin of the unexpected kinetic pattern previously observed in our laboratories (see above). First, we repeated the “zero-order” kinetic experiments to find them highly reproducible. All kinetic runs were performed with **3** containing 0.5 molecule of lattice PPh₃ per Ru, hereafter denoted as “**3**” for simplicity. As has been recently shown in an X-ray and solution study,¹³ the standard method to synthesize [(Ph₃P)₄Ru(H)₂] furnishes the product in the form of [(Ph₃P)₄Ru(H)₂]·0.5PPh₃·1.25C₆H₆. For kinetic studies, **3** was additionally washed with hexanes and then with ether in the glovebox and dried under vacuum. After that, the complex was found to have the composition [(Ph₃P)₄Ru(H)₂]·0.5PPh₃·0.5hexane (NMR). The presence of extra phosphine in the Ru complex used in the current work was taken into account in the treatment of the kinetic data. The reaction of **3** with PhI (300 equiv) in benzene-*d*₆ at 25 °C to give **2-I** with ca. 95% selectivity (Scheme 2.4) was monitored to 95% conversion by ¹H NMR in the presence of an external standard. Integration of the hydrido resonances from the starting complex (**3**) and from the product (**2-I**) confirmed the linear decay of **3** and the appearance of **2-I**, i.e. zeroth order kinetics. We then undertook a more detailed study of this reaction.

Using the method of initial rates, we determined the reaction order in each of the species originally present in the system. As shown in Figures 2.1-2.3, the reaction was found to be first order in both **3** and PhI and negative first order in PPh₃.¹⁸ The rate law (Eq. 2.1) derived from these experiments was consistent with a mechanism involving

¹⁸ (a) The reaction conditions were selected such that the equilibrium between **3** and **6** (Scheme 2.3) would be shifted toward **3**. (b) In some of these experiments employing PPh₃ in a 10-20-fold excess, side formation of minute quantities of Ph₄P⁺I⁻ was observed at high conversions of **3**.

pre-equilibrium between **3** and **6** (Scheme 2.3). However, Eq 2.1 could not account for the observed zeroth order. We therefore proposed that this discrepancy might be due to autocatalysis,¹⁹ and studied the reaction of **3** with PhI after full conversion to **2-I** in more detail.

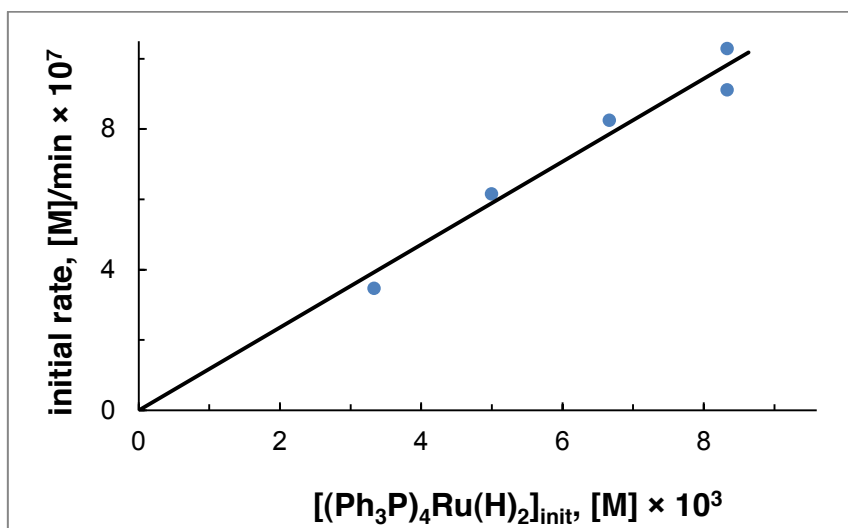


Figure 2.1. Dependence of the initial rate on the initial concentration of **3** in the reaction with PhI (1.49 M) in the presence of excess of PPh₃ (0.0833 M) at 23 °C.

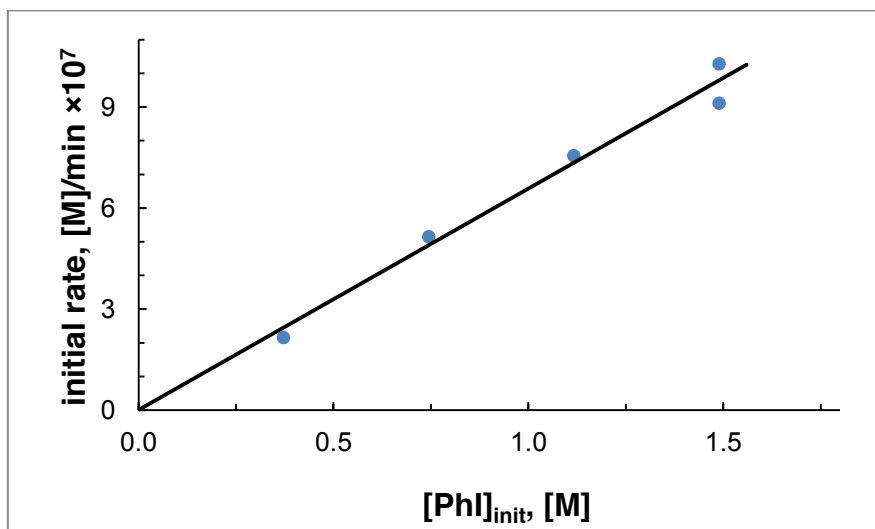


Figure 2.2. Dependence of the initial rate on the initial concentration of PhI in the reaction with **3** (0.00833 M) in the presence of excess of PPh₃ (0.0833M) at 23 °C.

¹⁹ (a) Singh, K. J.; Hoepker, A. C.; Collum, D. B. *J. Am. Chem. Soc.* 2008, *130*, 18008. (b) Hoepker, A. C.; Gupta, L.; Ma, Y.; Faggini, M. F.; Collum, D. B. *J. Am. Chem. Soc.* 2011, *133*, 7135.

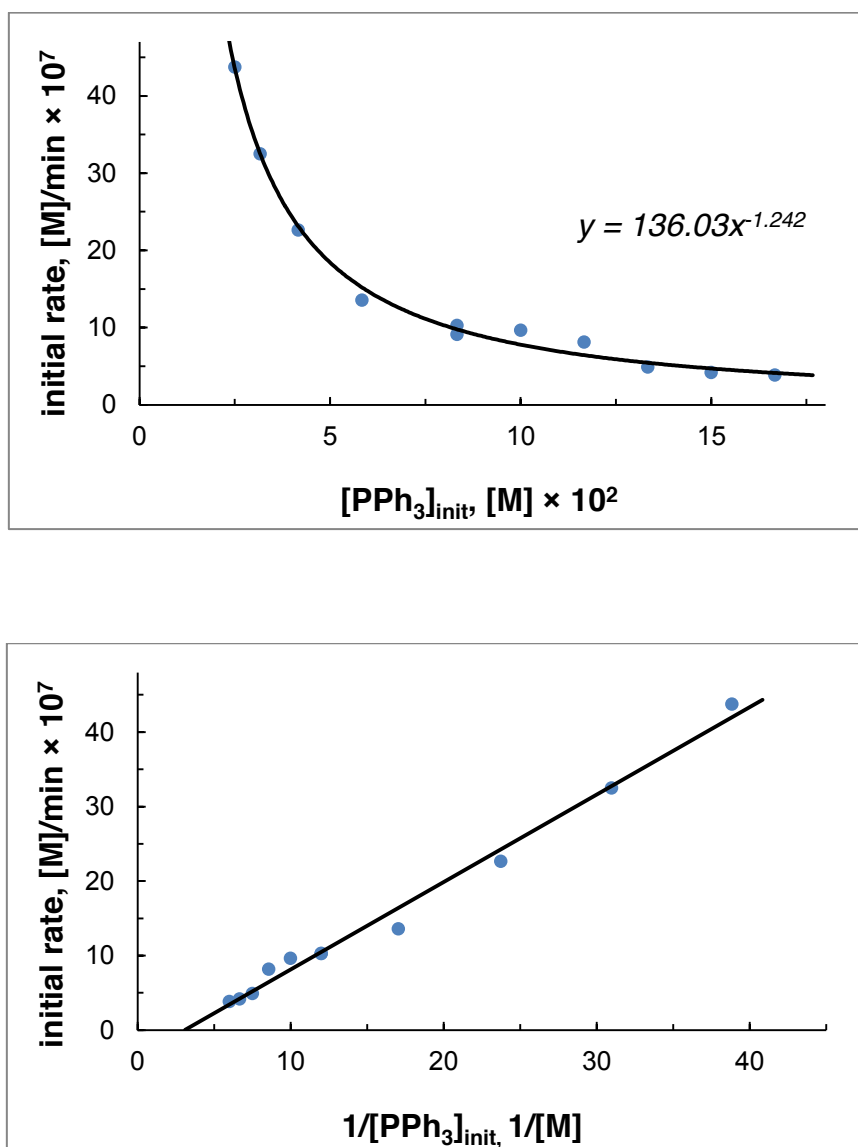


Figure 2.3. Dependence of the initial rate on the initial concentration of PPh₃ (top) and on 1/[PPh₃]_{init} (bottom) in the reaction of [(Ph₃P)₄Ru(H)₂] (0.00833 M) with PhI (1.49M) at 23 °C.

$$d[\mathbf{2-I}]/dt = k_1[\mathbf{3}][\text{PhI}][\text{PPh}_3]^{-1} \quad (\text{Eq 2.1})$$

Monitoring the reaction of **3** with PhI by ¹H and ³¹P{¹H} NMR revealed a startling kinetic profile shown in Figure 2.4 showing that after the nearly quantitative formation of **2-I**, it decayed exponentially.

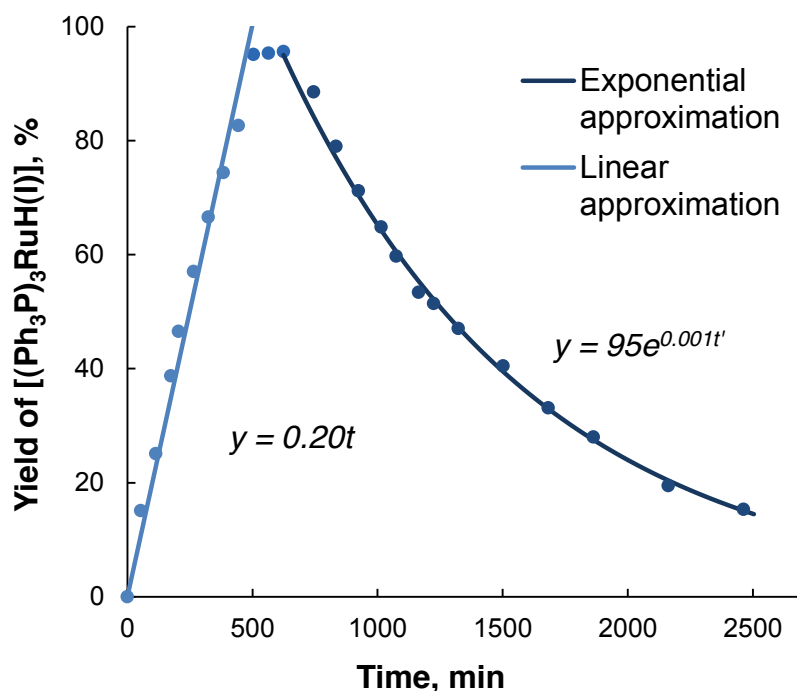


Figure 2.4. Kinetic profile from a preliminary study of the reaction of **3** (0.0051 M) with PhI (1.49 M) at 25 °C.

The following observations were made in a series of additional studies of the reaction leading to the disappearance of **2-I**.

(1) As **2-I** decayed, its deep purple color vanished and the reaction mixture turned brown. In parallel, the broad $^{31}\text{P}\{^1\text{H}\}$ NMR signal at 57.1 ppm from **2-I** was replaced with another broad resonance at 69.9 ppm, and the peak from free PPh_3 at -5.5 ppm grew in intensity.

(2) No new resonances appeared in the hydrido region of the ^1H NMR spectrum throughout the onward reaction of **2-I**.

(3) Quantitative $^{31}\text{P}\{^1\text{H}\}$ NMR analysis indicated that 2 equiv of free PPh_3 per Ru were produced at full conversion of **2-I**.

(4) In a scale-up experiment with **3** at a higher concentration in benzene at 40 °C, a black-brown precipitate was produced after full conversion of first **3** and then **2-I** was reached in 17 h. This solid appeared to be virtually insoluble in benzene, toluene, THF,

dichloromethane, and DMF. It was found, however, that this *dark* material dissolved in DMSO to give a *yellow* solution that displayed only one signal in the $^{31}\text{P}\{^1\text{H}\}$ NMR spectrum, a singlet at -5.5 ppm apparently from free PPh_3 . Elemental analysis data (C, H) obtained for this material were consistent with the composition $[(\text{Ph}_3\text{P})_2\text{RuI}_2]$. Such a species might well react with DMSO to give stable $[(\text{DMSO})_4\text{RuI}_2]^{20}$ with simultaneous liberation of PPh_3 . If calculated for the formula $[(\text{Ph}_3\text{P})_2\text{RuI}_2]$, the yield of this solid in the reaction of **3** with PhI at full conversion was quantitative. It was also noticed that this material readily precipitated from concentrated reaction mixtures but not from dilute solutions used in the kinetic experiments.

The above observations suggested that the ultimate product of the reaction of **3** with PhI was $[(\text{Ph}_3\text{P})_2\text{RuI}_2]_n$, likely²¹ a dimer, $[(\text{Ph}_3\text{P})_4\text{Ru}_2\text{I}_2(\mu\text{-I})_2]$ (**7**). We therefore attempted an independent synthesis of **7**. The reaction of $[(\text{Ph}_3\text{P})_3\text{RuCl}_2]$ with NaI in benzene-water gave **7**, as was established by single-crystal diffraction (Figure 2.5).

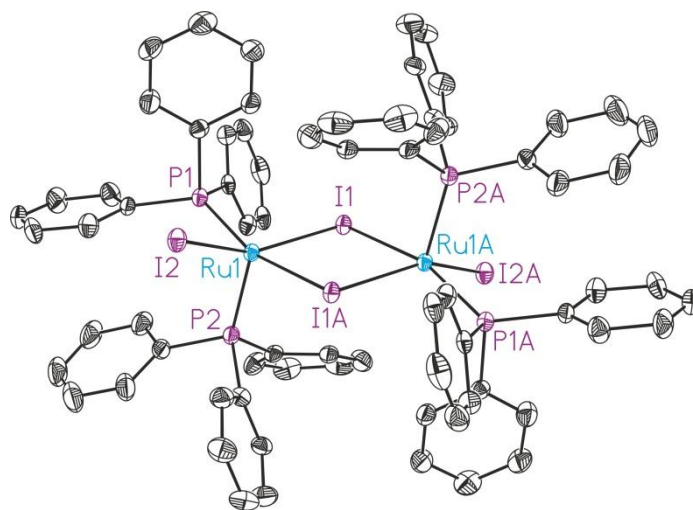
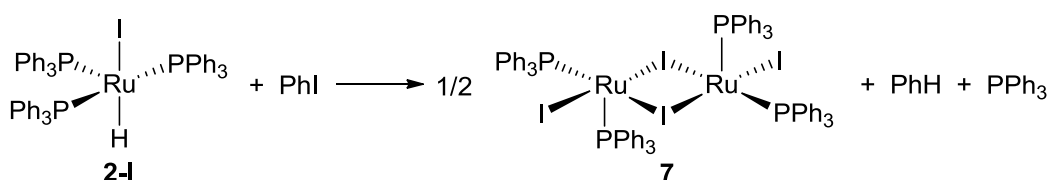


Figure 2.5. ORTEP drawing of $[(\text{Ph}_3\text{P})_4\text{Ru}_2\text{I}_2(\mu\text{-I})_2]$ (**7**) with all H atoms omitted for clarity and thermal ellipsoids drawn to the 50% probability level.

²⁰ Sarma, U. C.; Poddar, R. K. *Polyhedron* 1988, 7, 2627.

²¹ Hoffman, P. R.; Caulton, K. G. *J. Am. Chem. Soc.* 1975, 97, 4221.

The above data suggested that **2-I** produced in the first step reacts with PhI still present in a large excess to give **7** along with PhH and one equiv of PPh₃ released from the Ru center (Scheme 2.5). The reaction of independently prepared pure **2-I** leading to **7** obeyed the kinetic law presented in Eq 2.2, as established by the method of initial rates. Like the first step, i.e. the formation of **2-I** from **3** (Scheme 2.4 and Eq 2.1), the reaction of **2-I** with PhI was found to be positive first order in each **2-I** and PhI and negative first order in PPh₃ (Figures 2.6-2.8).



Scheme 2.5. Reaction of $[(\text{Ph}_3\text{P})_3\text{Ru}(\text{H})\text{I}]$ (**2-I**) with iodobenzene.

$$-d[\mathbf{2-I}]/dt = k_2[\mathbf{2-I}][\text{PhI}][\text{PPh}_3]^{-1} \quad (\text{Eq 2.2})$$

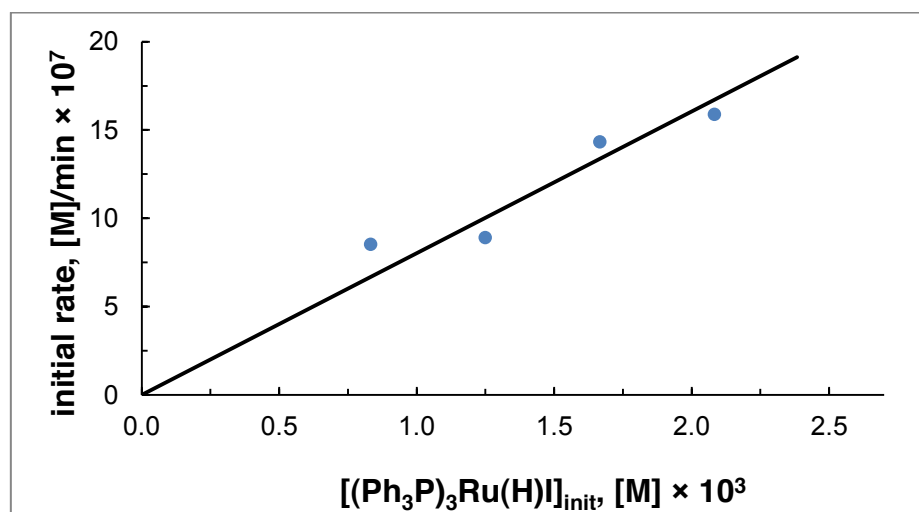


Figure 2.6. Dependence of the initial rate on the initial concentration of **2-I** in the reaction with PhI (1.49 M) in the presence of PPh₃ (0.00625 M) at 23 °C.

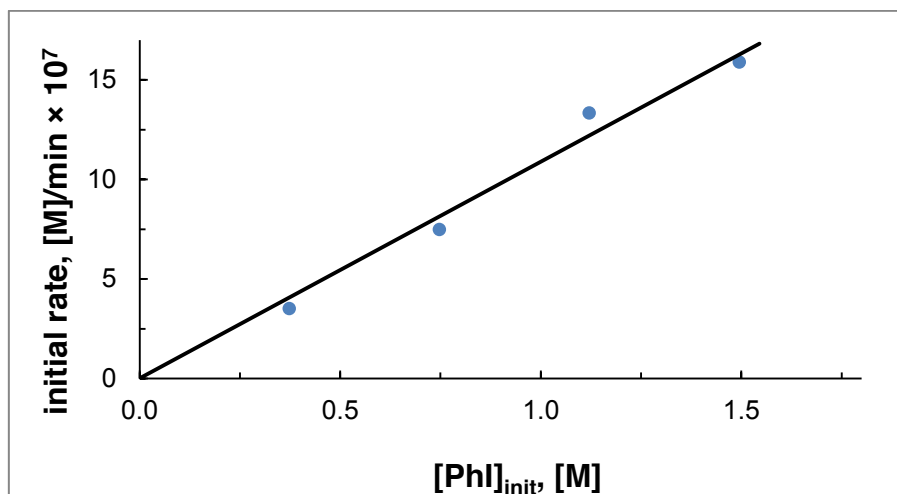


Figure 2.7. Dependence of the initial rate on the initial concentration of PhI in the reaction with **2-I** (0.00208 M) in the presence of PPh₃ (0.00625 M) at 23 °C.

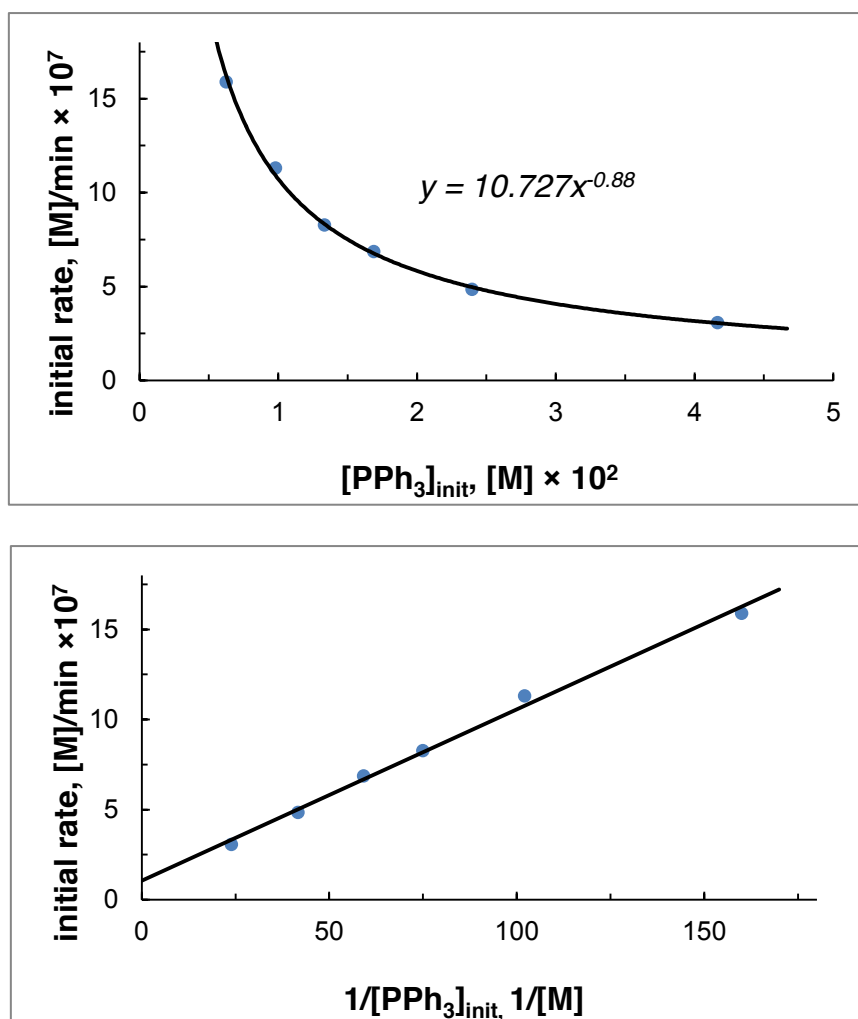


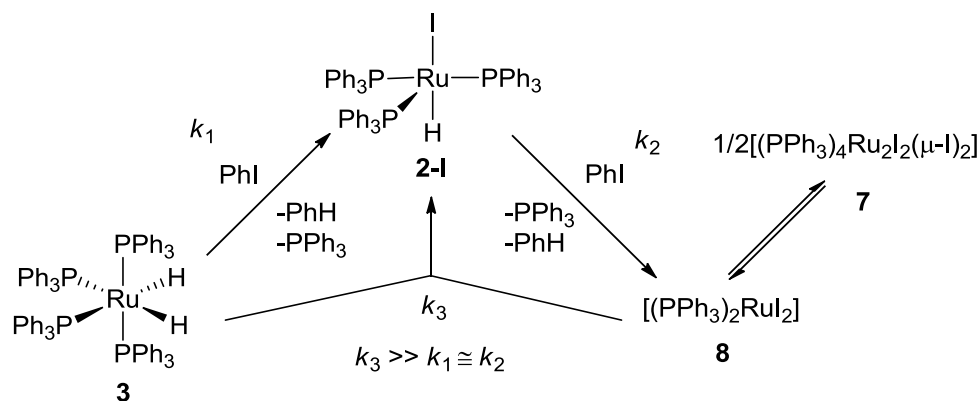
Figure 2.8. Dependence of the initial rate on the initial concentration of PPh₃ (top) and on 1/[PPh₃]_{init} (bottom) in the reaction of **2-I** (0.00208 M) with PhI (1.49 M) at 23 °C.

Schemes 2.4 and 2.5 are consistent with the experimentally determined stoichiometry of the reaction sequence involving the stepwise formation of first **2-I** and then **7** from **3** and PhI. However, none of the conventional kinetic schemes for two consecutive reactions¹⁶ could fit the peculiar kinetic profile of the current transformation (Figure 2.4). The observed zeroth order appearance of **2-I** and the apparent lack of its transformation to **7** until it is formed nearly quantitatively seemed inexplicable, considering the established rate laws (Eqs 2.1 and 2.2) and the observed similarity in rates for both steps (Figure 2.4).

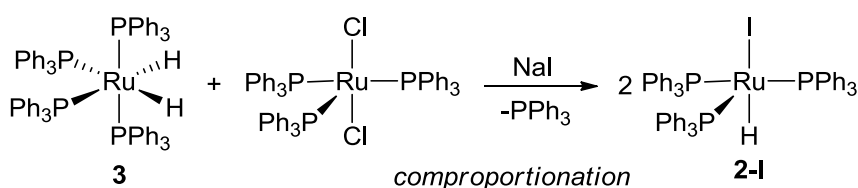
In an attempt to solve the mystery, we proposed that once formed in the first step, **2-I** reacts with PhI. The negative first order in PPh_3 (Eq 2.2) pointed to phosphine dissociation from **2-I** prior to Ph-I activation. Consequently, the Ru product of the C-I cleavage is likely a mononuclear four-coordinate species, $[(\text{Ph}_3\text{P})_2\text{RuI}_2]$ (**8**) that may dimerize to produce **7** (see above). We hypothesized, however, that **8** comproportionates with the as yet unreacted starting dihydride **3** to revive **2-I** in a reaction that is considerably faster than both that between PhI and **3** and the dimerization leading to **7**. This mechanistic proposal shown in Scheme 2.6 was confirmed by generating **8** in situ from $[(\text{Ph}_3\text{P})_3\text{RuCl}_2]$ and NaI in the presence of **3** in THF and observing the formation of **2-I** within the time of mixing (Scheme 2.7).²² Under identical conditions but in the absence of iodide, only a sluggish reaction of $[(\text{Ph}_3\text{P})_3\text{RuCl}_2]$ with **3** was observed, leading to **2-Cl** in ca. 30% yield after 1 day (60% after 0.3 h at 55 °C in a separate experiment). Although k_3 (Scheme 2.6) could not be accurately determined by experimental means, the instantaneous formation of **2-I** (Scheme 2.7) indicates that this comproportionation reaction is much faster than both Ph-I activation processes and

²² (a) Unlike well-known $[(\text{Ph}_3\text{P})_3\text{RuCl}_2]$, its iodo counterpart $[(\text{Ph}_3\text{P})_3\text{RuI}_2]$ has never been adequately characterized^{22b} and is expected²¹ to be unstable, easily losing PPh_3 and dimerizing to **7**. In a separate experiment, it was shown that pregenerated **7** reacts with **3** only slowly, evidently because this reaction requires the formation of **8** via cleavage of the Ru-I bridge. (b) Champness, N. R.; Levason, W.; Preece, S. R.; Webster, M.; Frampton, C. S. *Inorg. Chim. Acta* 1996, 244, 65.

therefore the condition for the proposed autocatalysis $k_3 \gg k_2$ (Scheme 2.6) is met. If, in addition, $k_1 \approx k_2$ and changes in the concentrations of PhI and PPh₃ are negligibly small during the process, the general equation for the first step in Scheme 2.6 (Eq 2.3) is transformed to Eq 2.4 accounting for the zeroth order behavior observed (Figure 2.4; see Experimental Section for the derivation of Eqs 2.3 and 2.4).²³ This rare kinetic case is methodologically similar to the autocatalysis in the lithium diisopropylamide-mediated ortho-lithiation reactions studied by Collum.¹⁹



Scheme 2.6. Mechanistic scheme for autocatalysis in the reaction of **3** with PhI.



Scheme 2.7. Comproportionation reaction of $[(\text{Ph}_3\text{P})_4\text{Ru}(\text{H})_2]$ (**3**) with $[(\text{Ph}_3\text{P})_3\text{RuCl}_2]$ in the presence of NaI.

$$d[\mathbf{2-I}]/dt = k_1[\mathbf{3}][\text{PhI}][\text{PPh}_3]^{-1} + k_2[\mathbf{2-I}][\text{PhI}][\text{PPh}_3]^{-1} \quad (\text{Eq 2.3})$$

$$d[\mathbf{2-I}]/dt = k'([\mathbf{3}] + [\mathbf{2-I}]) = \text{const.} \quad (\text{Eq 2.4})$$

²³ For the equilibrium between **3** and **6** shifted toward **3**.

To probe the proposed mechanism of the autocatalysis, we obtained the full kinetic profile for the reaction of **3** with PhI (Figure 2.9). Monitoring the reaction by both $^1\text{H}\{^{31}\text{P}\}$ and $^{31}\text{P}\{^1\text{H}\}$ NMR allowed us to follow changes in the concentrations of not only **3** and **2-I** but also the iodobenzene complex **6** and PPh_3 released in the reaction. The model shown in Scheme 2.6 produced an excellent fit to the kinetic data presented in Figure 2.9. Although the starting complex **3** equilibrates with **6** ($K_{eq} = 1.7 \pm 0.3 \times 10^{-3}$), this equilibrium (Scheme 2.3) establishes within the time of mixing and is therefore much faster than the rate-determining steps of both Ph-I activation reactions. The coincidental similarity of $k_1 = 1.24 \times 10^{-5} \text{ min}^{-1}$ (1st step, Eq 2.1) and $k_2 = 6.8 \times 10^{-6} \text{ min}^{-1}$ at 25 °C (2nd step, Eq. 2.2) fulfills the above-described condition for the zeroth order behavior observed for the decay of **3** and the formation of **2-I**.²⁴

Kinetics of PhBr Activation with 3. The full kinetic profile of the reaction of **3** with PhBr in benzene at 50 °C (Figure 2.10) is similar to that of the PhI activation reaction (Figure 2.9). The structure of the product **2-Br** was additionally confirmed by single-crystal X-ray diffraction (Figure 2.11). As mentioned above, the PhBr analogue of **6**, $[(\text{Ph}_3\text{P})_3\text{Ru}(\text{H})_2(\text{PhBr})]$, could not be observed. Instead, small quantities (ca. 10%) of $[(\text{Ph}_3\text{P})_3\text{Ru}(\text{H})_2(\text{H}_2)]$ (**1**) were detected in the reaction solution, evidently due to the reaction of **3** with adventitious water (Scheme 2.8).¹³ The presence of **1** was also observed in the reaction with PhI, albeit in much smaller quantities, ca. 3%, likely due to the milder reaction conditions. The presence of 3% of **1** was neglected in the kinetic scheme of the reaction with PhI. In the case of PhBr, however the presence of larger quantities of **1** prompted us to include it in the kinetic analysis as a species that is in fast equilibrium with **3**.

²⁴ The value of $k_1 = 1.24 \times 10^{-5} \text{ min}^{-1}$ is applied when the equilibrium between **3** and **6** is largely shifted toward **3**. When the quantity of **6** is significant, the observable k_1 value (k_1') depends on the position of the equilibrium (see Experimental Section for details). For the conditions of the kinetic experiment (Figure 2.9), k_1' is estimated at $7.8 \pm 0.6 \times 10^{-6} \text{ min}^{-1}$, even closer to the k_2 ($6.8 \times 10^{-6} \text{ min}^{-1}$) than k_1 .

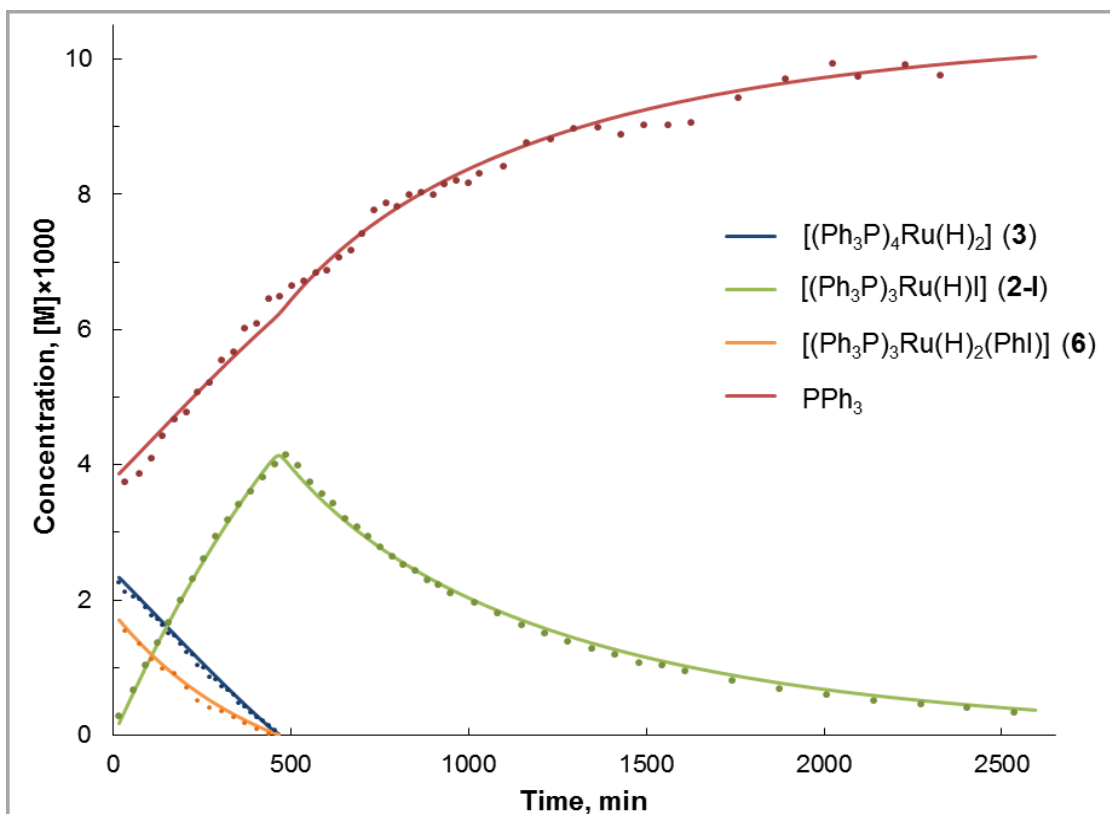
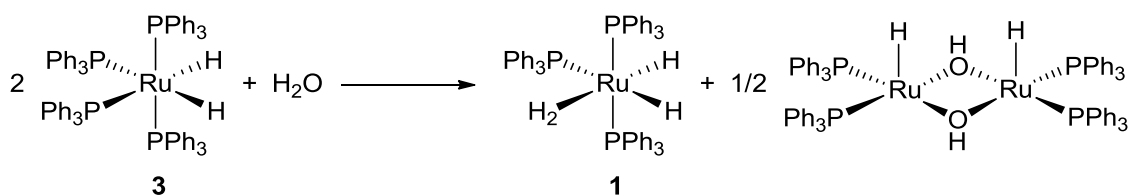


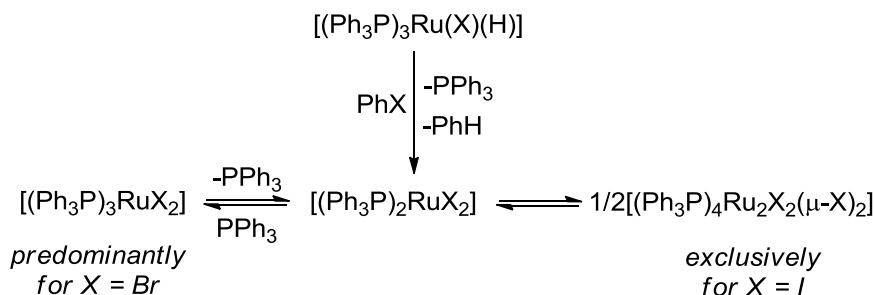
Figure 2.9. Plot of concentrations versus time for the reaction of $[(\text{Ph}_3\text{P})_4\text{Ru}(\text{H})_2]$ (0.0042 M initial concentration) with PhI (1.49 M) at $25\text{ }^\circ\text{C}$ monitored by $^1\text{H}\{^31\text{P}\}$ and $^{31}\text{P}\{^1\text{H}\}$ NMR spectroscopy. Data points are from the experimental measurements. The curves are from the kinetic model.



Scheme 2.8. Reaction of $[(\text{Ph}_3\text{P})_4\text{Ru}(\text{H})_2]$ (**3**) with water.¹³

A better exponential fit for the second stage of the reaction with PhBr deals with the difference in the composition of the final $[(\text{Ph}_3\text{P})_n\text{RuX}_2]$ ($n = 2$ or 3) product for $\text{X} = \text{Br}$ and for $\text{X} = \text{I}$. As described above, a total of 2 equiv of PPh_3 is released in the reaction with PhI , one in each of the two steps (Schemes 2.4 and 2.5). Likewise, 1 equiv of PPh_3

is produced in the first step of the reaction of PhBr with **3**. In contrast, however, the second step of the reaction involving PhBr gives rise to only small quantities of free phosphine. As illustrated in Scheme 2.9, this is due to $[(\text{Ph}_3\text{P})_2\text{RuBr}_2]$ (**9**) being more prone to add PPh_3 rather than dimerize, whereas $[(\text{Ph}_3\text{P})_2\text{RuI}_2]$ (**8**) is stabilized only by dimerization.²² Phosphine coordination to **9** gives stable $[(\text{Ph}_3\text{P})_3\text{RuBr}_2]$ (**10**) that, in contrast with elusive $[(\text{Ph}_3\text{P})_3\text{RuI}_2]$,²² has been widely known for nearly 50 years²⁵ and structurally characterized.²⁶ Nonetheless, **10** has been shown²¹ to produce small quantities of $[(\text{Ph}_3\text{P})_4\text{Ru}_2\text{Br}_2(\mu\text{-Br})_2]$ (**11**) and PPh_3 in solution. When monitoring the kinetic runs by $^{31}\text{P}\{^1\text{H}\}$ NMR we observed signals from both **10** (br s, 43.7 ppm)²¹ and **11** (br s, 59.3 ppm)²¹ in a ca. 5:1 molar ratio. As a result, only ca. 0.3 equiv of free PPh_3 is released in the second step of the reaction of **3** with PhBr. This translates into less autoinhibition and, as a consequence, weaker deviation from the exponential decay observed for the second step in the case of PhBr.



Scheme 2.9. Final Ru dihalide products in the reactions of **3** with PhI and with PhBr.

The autocatalysis in the reaction of **3** with PhBr was confirmed by observing the quick formation of **2-Br** upon addition of **3** to a solution of **10** produced in the reaction of **3** with PhBr at 50 °C (Scheme 2.10). The zeroth order pattern observed for the first step of the reaction (Figure 2.10) is due to the close proximity of $k_1 = 4.3 \times 10^{-6} \text{ min}^{-1}$ and $k_2 = 3.2 \times 10^{-6} \text{ min}^{-1}$.

²⁵ Stephenson, T. A.; Wilkinson, G. *J. Inorg. Nuclear Chem.* 1966, *28*, 945.

²⁶ MacFarlane, K. S.; Joshi, A. M.; Rettig, S. J.; James, B. R. *Inorg. Chem.* 1996, *35*, 7304.

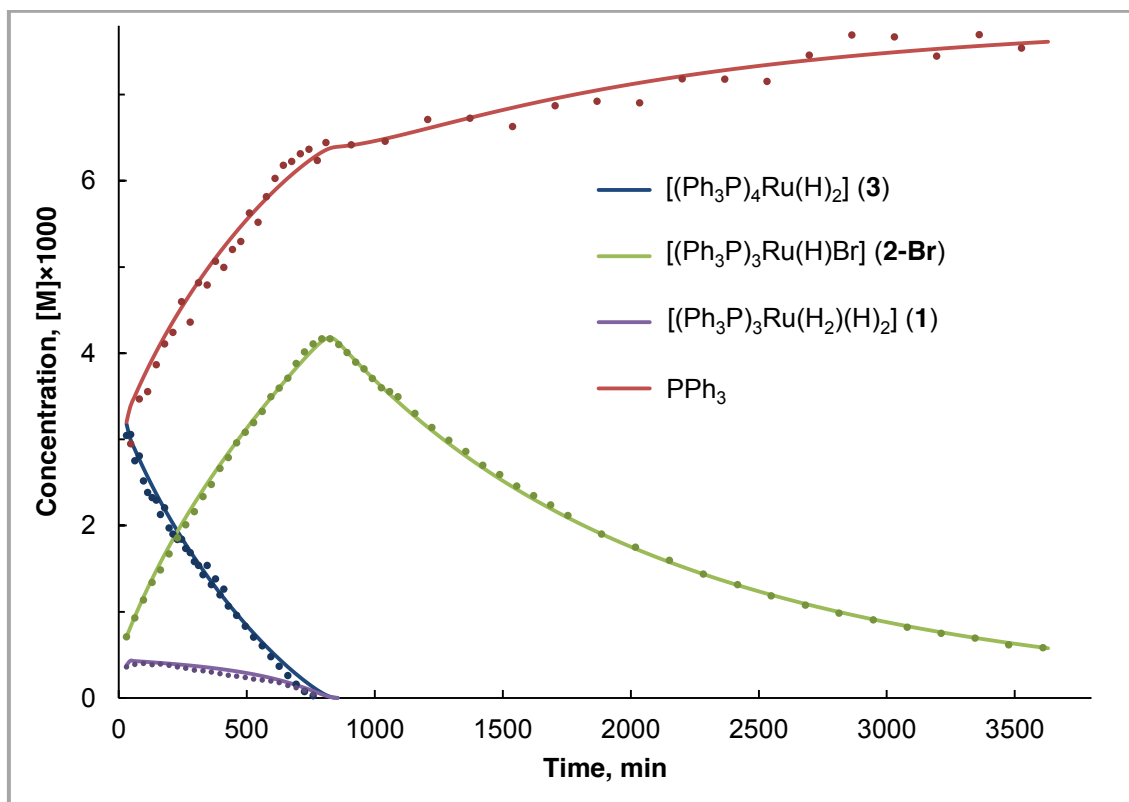


Figure 2.10. Plot of concentrations versus time for the reaction of **3** (0.0042 M) with PhBr (1.59 M) at 50 °C monitored by $^1\text{H}\{^31\text{P}\}$ and $^31\text{P}\{^1\text{H}\}$ NMR spectroscopy. Data points are from the experimental measurements. The curves are from the kinetic model.

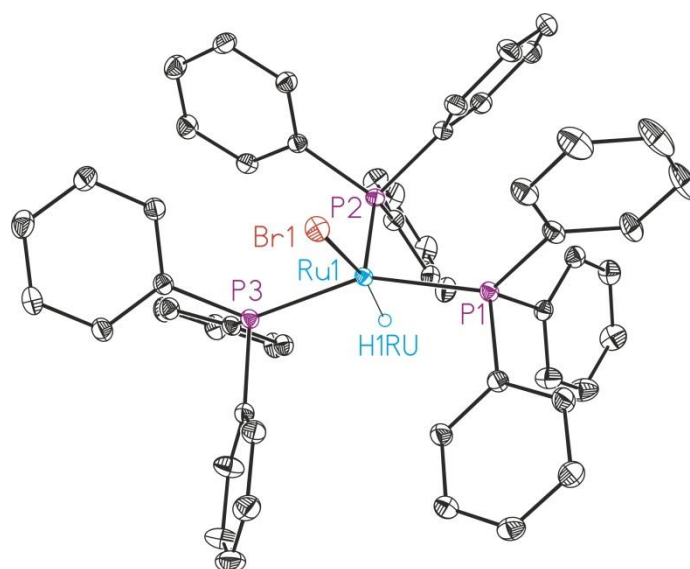
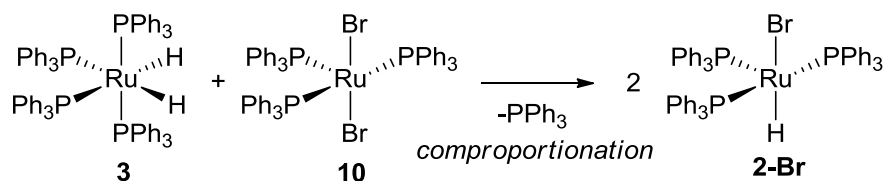


Figure 2.11. ORTEP drawings of $[(\text{Ph}_3\text{P})_3\text{RuH}(\text{Br})]$ (**2-Br**), with all H atoms, except Ru-H, omitted and thermal ellipsoids drawn to the 50% probability level.



Scheme 2.10. Comproportionation reaction of $[(\text{Ph}_3\text{P})_4\text{Ru}(\text{H})_2]$ (**3**) with $[(\text{Ph}_3\text{P})_3\text{RuBr}_2]$.

Kinetics of PhCl Activation with 3. The reaction of **3** with neat PhCl and its kinetic studies were performed at 55 °C. Visual signs of this reaction were similar to those of the PhI and PhBr activation reactions described above. At the beginning, the reaction solution turns purple, the color of **2-Cl**, and then eventually brown, which might be suggestive of the formation of $[(\text{Ph}_3\text{P})_3\text{RuCl}_2]$. Indeed, **2-Cl** is first accumulated to 70% yield, after which it decays. However, the decomposition of **2-Cl** was nonselective, leading to a complex mixture of products ($^{31}\text{P}\{^1\text{H}\}$ NMR). We propose that this is due to **2-Cl** being more prone to hydrolysis with adventitious water than **2-Br** and **2-I**. The kinetics of the reaction of **3** with PhCl (Figure 2.12) is different from those observed for the activation of PhI and PhBr with **3** and shown in Figures 2.9 and 2.10, respectively. A nearly exponential decay of **3** with concomitant nonlinear growth of **2-Cl** is observed, showing no unambiguous signs of autocatalysis. Nonetheless, the latter might contribute to the overall process, because $[(\text{Ph}_3\text{P})_3\text{RuCl}_2]$ does react with **3** to give **2-Cl** (see above). However, this comproportionation is less efficient than that involved in the reactions of PhI and PhBr. In addition, the overall lower selectivity of the Ph-Cl activation precluded accurate treatment of the kinetic data yielding an adequate model.²⁷

²⁷ A crude estimation provided a k_2 value ca. $1 \times 10^{-7} \text{ min}^{-1}$, assuming pseudo-first order conditions ($[\text{PPh}_3] = 0.0045 \text{ M}$ and $[\text{PhCl}] = 8.22 \text{ M}$) and $\tau_{1/2} = 3500 \text{ min}$.

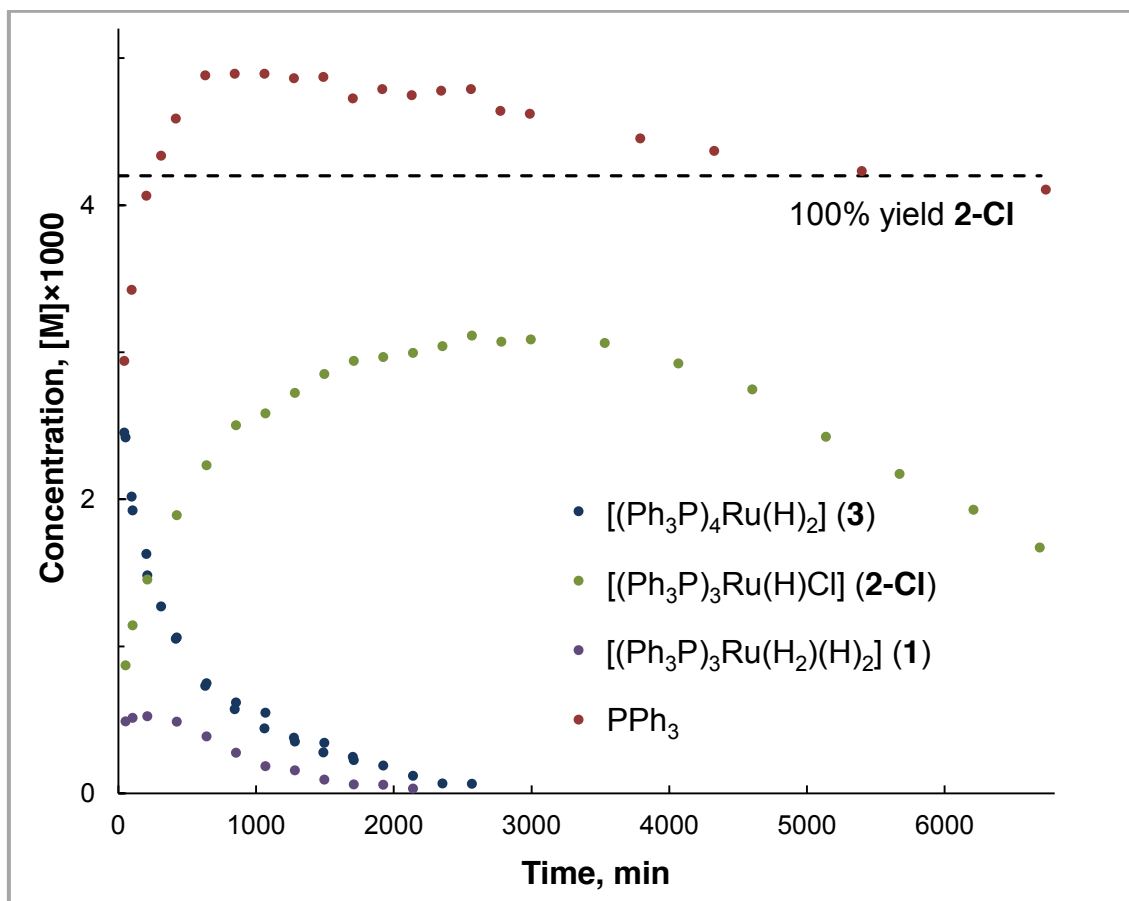


Figure 2.12. Plot of concentrations versus time for the reaction of $[(\text{Ph}_3\text{P})_4\text{Ru}(\text{H})_2]$ (0.0042 M initial concentration) with PhCl (8.22M) at 55 °C monitored by $^1\text{H}\{^31\text{P}\}$ and $^31\text{P}\{^1\text{H}\}$ NMR spectroscopy. Data points are from the experimental measurements.

General Kinetic Scheme. From the perspective of kinetics, the reaction of $[(\text{Ph}_3\text{P})_4\text{Ru}(\text{H})_2]$ (**3**) with PhI or PhBr (Figures 2.9 and 2.10) may be considered as a sequence of the following steps.

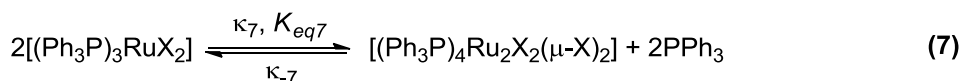
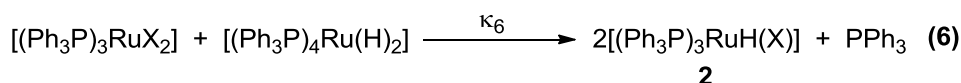
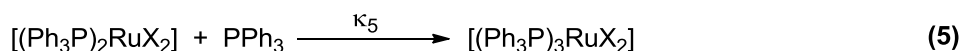
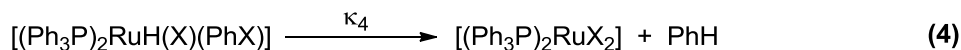
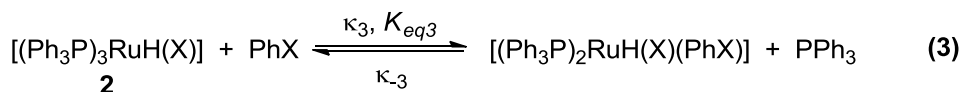
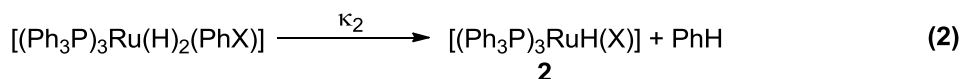
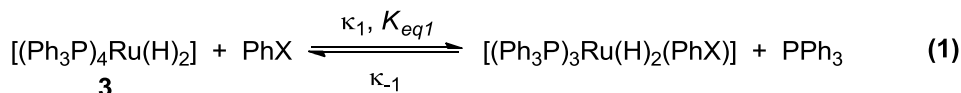
1) The initial transformation of **3** to **2** in roughly up to 20% conversion is predominantly achieved through the direct reaction of **3** with the corresponding aryl halide (reactions (1) and (2) in Scheme 2.11). The experimental determination of the reaction orders for the PhI activation along with the computational studies below suggest that pre-equilibrium (1) is much faster than the subsequent C-X bond cleavage (2). As a result, the kinetic equation for the formation of **2** can be simplified first to

more general Eq 2.5 and further to Eq 2.6 if the pre-equilibrium between **3** and **6** is largely shifted to **3**. Derivations of Eqs 2.5 and 2.6 are presented in the Experimental Section below. Extra PPh₃ inhibits the Ph-X activation. By stoichiometry, one equiv of PPh₃ is released per each equiv of **2** produced in both cases (X = Br, I). However, in the reaction of PhBr, PPh₃ is released gradually, whereas with iodobenzene in a large excess (350 equiv), a considerable amount of free phosphine is produced prior to Ph-I activation due to pre-equilibrium (1).

$$\frac{d[\mathbf{2}]}{dt} = \kappa_2 K_{eq1} \frac{[\mathbf{3} + \mathbf{6}][\text{PhX}]}{[\text{PPh}_3] \left(1 + K_{eq1} \frac{[\text{PhX}]}{[\text{PPh}_3]}\right)} \quad (\text{Eq 2.5, see Scheme 2.11})$$

$$d[\mathbf{2}]/dt = k_1[\mathbf{3}][\text{PhX}][\text{PPh}_3]^{-1} \quad (\text{Eq 2.6, see Scheme 2.11})$$

where $k_1 = \kappa_2 K_{eq1}$

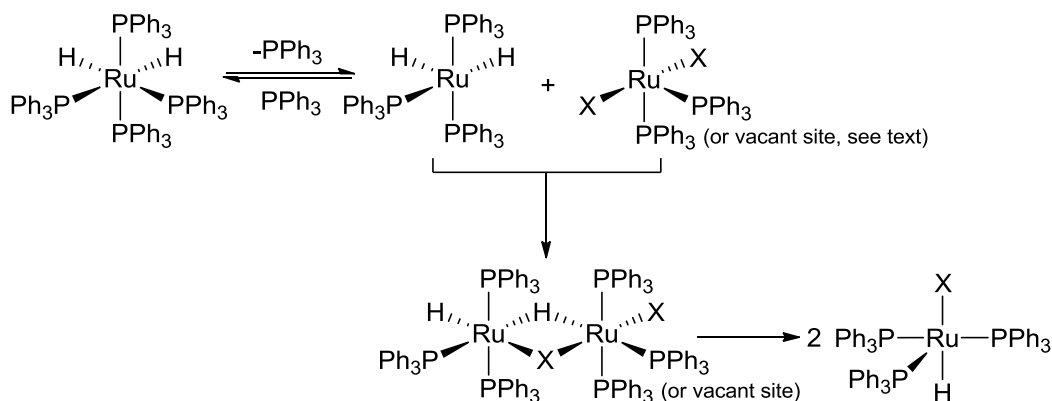


Scheme 2.11. General kinetic scheme for the reaction between **3** and PhX.

2) At ca. 20% to ca. 80% conversion of **3**, the formation of **2** occurs simultaneously by both direct and autocatalytic pathways (Eq 2.7). The rate equation for this step is derived as a sum of the rates of these two processes. As mentioned above, the autocatalysis involves two steps, (i) the rate limiting Ph-X activation with **2** (reactions (3) and (4) in Scheme 2.11) and (ii) the fast comproportionation of the resulting ruthenium dihalide product with the starting dihydride **3** (reactions (5) and (6) in Scheme 2.11). Phosphine pre-dissociation from **2** has been experimentally confirmed for both reactions, with PhI and with PhBr. In particular, the reaction with PhI has been found to be negative first order with respect to PPh₃. The experimental data for the decay of **2-Br** could be simulated only by inclusion in the kinetic model of autoinhibition with the PPh₃ released. The [(Ph₃P)₂RuX₂] product can comproportionate with the as yet unreacted **3** to yield two equivalents of **2**, thereby triggering the autocatalysis. Although the mechanism of this comproportionation remains unknown, facile¹³ phosphine dissociation from **3**, an 18-e coordinatively-saturated complex, is most likely involved. The dihalide partner could be [(Ph₃P)₂RuX₂] or [(Ph₃P)₃RuX₂] as both are coordinatively-unsaturated species (Scheme 2.12). For X = I and Br, the comproportionation, controlled by the rate constant k_3 , occurs much faster than both Ph-X activations, i.e., $k_3 \gg k_1, k_2$, which fulfills the critical condition for the autocatalysis. Although the dichloro complex also comproportionates with **3** (yet more slowly), the autocatalysis in the reaction with PhCl is not as recognizable because of the lower selectivity of the overall process. The available qualitative data suggest that the reactivity of the dihalo complexes toward **3** decreases in the order I > Br > Cl. The similarity of the rate constants for the direct and autocatalytic pathways (Eq 2.7) results in the observed zeroth order behavior. Both the autocatalytic and direct pathways are inhibited by extra phosphine.

$$d[\mathbf{2}]/dt = k_1[\mathbf{3}][\text{PhX}][\text{PPh}_3]^{-1} + k_2[\mathbf{2}][\text{PhX}][\text{PPh}_3]^{-1} \quad (\text{Eq 2.7, see Scheme 2.11})$$

where $k_1 = \kappa_2 K_{eq1}$; $k_2 = \kappa_4 K_{eq3}$



Scheme 2.12. Proposed mechanism for comproportionation of **3** and $[(\text{Ph}_3\text{P})_n\text{Ru}(\text{X})_2]$

($n = 3$ or 2).

3) The last 20% of **3** reacts predominantly via the autocatalytic pathway. It is worth to note that $[(\text{Ph}_3\text{P})_3\text{Ru}(\text{H}_2)(\text{H})_2]$ (**1**) that is side-produced by hydrolysis with trace adventitious water, is largely consumed at this later stage. On the basis of this observation we propose that the autocatalysis should be the main mechanism for the reaction of pure **1** with PhX. The rate-determining step of the autocatalysis is Ph-X bond activation (for the rate law, see Eq 2.8). However, as the reaction occurs, the concentration of **3** decreases, thereby slowing down the comproportionation whose rate first becomes comparable to, and eventually lower than, that of the Ph-X activation.

$$d[\mathbf{2}]/dt = k_2[\mathbf{2}][\text{PhX}][\text{PPh}_3]^{-1} \quad (\text{Eq 2.8, see Scheme 2.11})$$

where $k_2 = \kappa_4 K_{eq3}$

4) After the autocatalysis becomes slower than the PhX activation with **2**, the latter stops to accumulate and starts to decay obeying the rate law expressed by Eq 2.9. As discussed above, the product of this transformation depends on the nature of X (Scheme 2.9). For X = I, the dimer $[(\text{Ph}_3\text{P})_4\text{Ru}_2\text{I}_2(\mu\text{-I})_2]$ (**7**) is formed along with another equiv of PPh_3 , which inhibits the reaction. For X = Br, the mononuclear complex $[(\text{Ph}_3\text{P})_3\text{RuBr}_2]$ (**10**) is predominantly formed together with small quantities of the corresponding dinuclear complex $[(\text{Ph}_3\text{P})_4\text{Ru}_2\text{Br}_2(\mu\text{-Br})_2]$ (**11**). As a result, only a small quantity of free PPh_3 is produced in the reaction of **2-Br** with PhBr, which accounts for the experimentally observed much weaker reaction inhibition.

$$-d[\mathbf{2}]/dt = k_2[\mathbf{2}][\text{PhX}][\text{PPh}_3]^{-1} \quad (\text{Eq 2.9, see Scheme 2.11})$$

$$\text{where } k_2 = \kappa_4 K_{eq3}$$

The kinetic study described above provided us with critical mechanistic information on the Ph-X activation (X = I, Br) with complexes **2** and **3**. In particular, it became clear that these transformations involve phosphine dissociation before the rate limiting step, which we expected to be the carbon-halogen bond cleavage at the Ru center. The observed similarity of k_1 and k_2 values in the reactions of both PhBr and PhI was especially intriguing. In an attempt to uncover the origin of this similarity and gain deeper insight into intimate details of the Ph-X activation processes, a computational study was performed.

Computational Studies.¹⁷ Density functional theory (DFT) calculations were initially focused on the reaction of **3** with PhI, for which the experimental studies provide quantitative data, including (i) the pre-equilibrium formation of **6** with $K_{\text{eq}} = 1.7 \pm 0.3 \times 10^{-3}$ at 298 K, corresponding to $\Delta G = +3.8 \pm 0.1$ kcal/mol, and (ii) rate constants for both the formation of **2-I** from **3** and PhI ($k_1 = 1.24 \times 10^{-5} \text{ min}^{-1}$) and the onward reaction of **2-I** with PhI ($k_2 = 6.8 \times 10^{-6} \text{ min}^{-1}$), corresponding to $\Delta G^\ddagger = 26.6$ and 26.9 kcal/mol, respectively. A BP86-D3(benzene) protocol has been used, i.e. based on BP86 optimizations in the gas-phase, with free energies corrected for dispersion and solvation effects via subsequent single point energy calculations. This approach has been shown to perform well in previous studies of Ph-I activation.²⁸ The computed reactivity of PhI will also be compared with PhBr and PhCl.

The reaction of **3** with PhI proceeds via initial PPh₃/PhI substitution to give an adduct **6**, in which the iodobenzene substrate is bound through iodine. This I-bound form of **6** has a free energy of +10.1 kcal/mol and is 10.3 kcal/mol more accessible than the next most stable alternative, which is a σ -complex bound through a C_{meta}-H bond; the most stable π -bound isomer is **Int2** at +23.8 kcal/mol (see below). That the I-bound form **6** is most accessible is consistent with experimental observations that imply such a structure to be favored.¹⁴ Two C-I bond activation processes could be characterized directly from **6** (Figure 2.13). The first is a concerted oxidative addition via **TS(6-Int1)** at +31.3 kcal/mol and features elongation of the C-I bond with concomitant Ru-Ph and Ru-I bond formation. As this occurs a reductive coupling of the two hydride ligands is also seen and the species formed, **Int1** ($G = +1.4$ kcal/mol), exhibits an elongated η^2 -H₂

²⁸ Miloserdov, F. M.; McMullin, C. L.; Belmonte, M. M.; Benet-Buchholz, J.; Bakhmutov, V. I.; Macgregor, S. A.; Grushin, V. V. *Organometallics* 2014, **33**, 736.

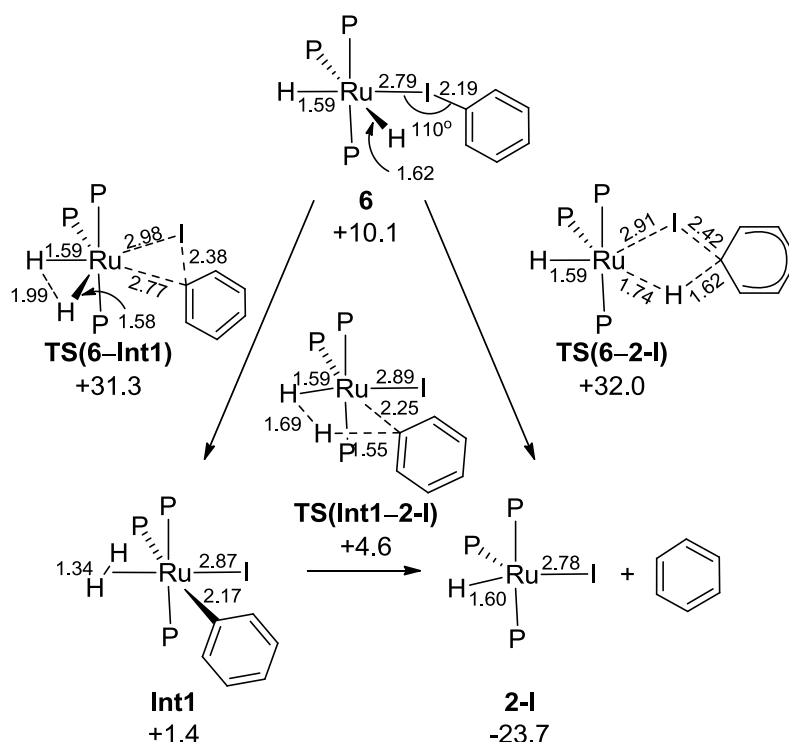


Figure 2.13. Reaction pathway (BP86-D3(benzene), kcal/mol) for Ph-I activation at iodobenzene adduct **6** (P = PPh₃). All free energies are quoted relative to **3** + free PhI set to 0.0 kcal/mol; selected distances in Å and angles in degrees.

ligand (H...H = 1.34 Å) *trans* to iodide.²⁹ **Int1** can then readily undergo reductive elimination to form benzene and **2-I** as products ($G = -23.7$ kcal/mol).

The second C-I activation pathway derived directly from **6** draws on the previous work of Whittlesey, Macgregor, and coworkers on the hydrodefluorination (HDF) of fluoroaromatics at Ru-NHC complexes,³⁰ which showed how nucleophilic attack by a hydride ligand can induce C-X bond cleavage. A similar process was characterized here, where H-transfer onto the arene ring caused a concerted displacement of iodide directly onto the Ru via **TS(6-2-I)** at +32.0 kcal/mol. However, both pathways in Figure 2.13

²⁹ For η^2 -H₂ complexes such as **Int1** we tested for alternative dihydride, formally Ru(IV) isomers but these could not be located as either a singlet or a high spin triplet form.

³⁰ (a) Panetier, J. A.; Macgregor, S. A.; Whittlesey, M. K. *Angew. Chem., Int. Ed.* 2011, *50*, 2783. (b) Macgregor, S. A.; McKay, D.; Panetier, J. A.; Whittlesey, M. K. *Dalton Trans.* 2013, *42*, 7386. (c) McKay, D.; Riddlestone, I. M.; Macgregor, S. A.; Mahon, M. F.; Whittlesey, M. K. *ACS Catal.* 2015, *5*, 776.

entail barriers above 31 kcal/mol and so are significantly higher than the value of 26.6 kcal/mol derived from experiment. Alternative routes were therefore considered.

The previous work of Whittlesey and Macgregor³⁰ also highlighted the importance of mechanisms involving π -bound intermediates and so this possibility was assessed here (Figure 2.14). Such a species, **Int2** ($G = +23.8$ kcal/mol), can be accessed via dissociation of PhI from **6** (to give **5** and free PhI at +24.0 kcal/mol) and then re-association through **TS(5–Int2)** at +27.8 kcal/mol. **Int2** features an asymmetrically bound arene (Ru-C_{ipso} = 2.25 Å, Ru-C_{ortho} = 2.47 Å), as well as a significantly elongated C-I distance of 2.34 Å (*cf.* a computed value of 2.14 Å in free iodobenzene). C-I bond cleavage in **Int2** is therefore readily accessible and occurs via **TS(Int2–Int3)** ($G = +25.6$ kcal/mol) in a process corresponding to the nucleophilic displacement of iodide from the arene ring by the Ru center.³¹ This leads to **Int3** ($G = +15.5$ kcal/mol), a cationic Ru-Ph species which also features an η^2 -H₂ ligand (H-H = 0.93 Å) as a result of reductive coupling of the two hydride ligands. The displaced iodide in **Int3** is loosely associated with the H₂ ligand (H...I = 2.70 Å), however, moving this anion to the vacant site *trans* to Ph ligand gives a much more stable species, **Int4** ($G = +0.4$ kcal/mol) which is an isomer of **Int1** with the η^2 -H₂ ligand now *trans* to PPh₃. As found for **Int1** facile hydrogenolysis of the Ru-Ph bond can occur and here proceeds via **TS(Int4–2-I)** at +10.4 kcal/mol.³² The overall rate-limiting transition state in Figure 2.14 is **TS(5–Int2)** and equates to an overall barrier of 27.8 kcal/mol. This is both significantly more accessible than the pathways in Figure 2.13 and better reflects the experimental value of 26.6 kcal/mol.

³¹ As **TS(Int2–Int3)** involves iodide dissociation we also optimised this species in benzene solvent, but found neither the geometry nor the relative energy ($G = +26.3$ kcal/mol) to be significantly affected.

³² An alternative onward pathway involving deprotonation of the η^2 -H₂ ligand in **Int3** by iodide was also assessed but the transition state for this step lies 4.4 kcal/mol above **TS(Int4–I-2)**.

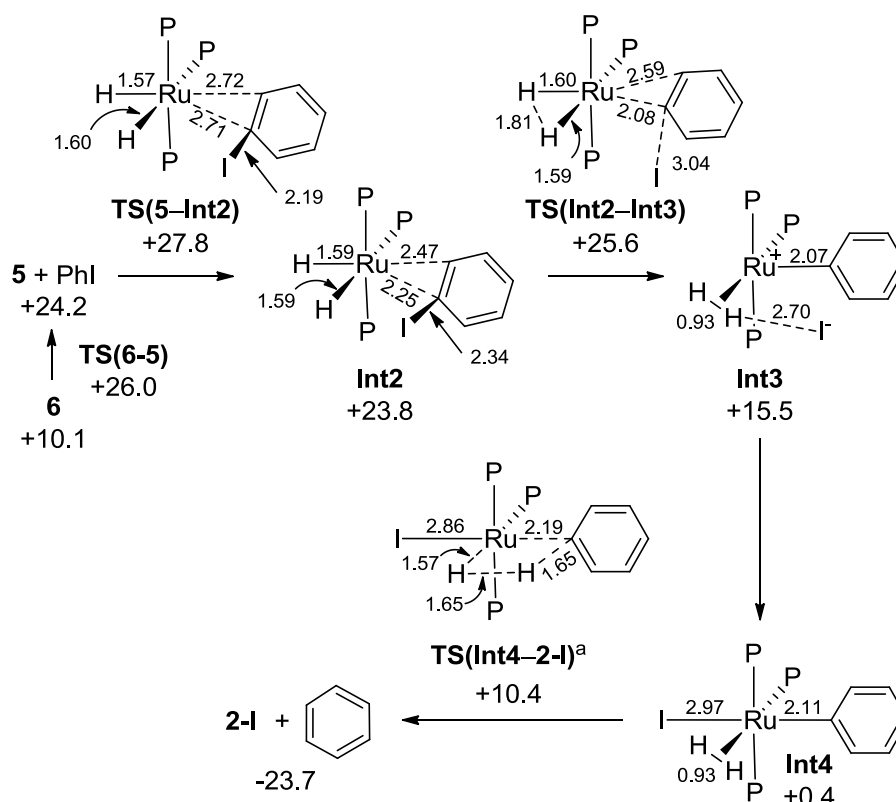


Figure 2.14. Reaction pathway (BP86-D3(benzene), kcal/mol) for Ph-I activation via **Int2** ($P = PPh_3$). Free energies are quoted relative to **3** + free PhI set to 0.0 kcal/mol; selected distances in Å. ^aReductive elimination involves an intermediate C,H-bound C_6H_6 σ -complex at +0.2 kcal/mol.

Once formed, **2-I** can also effect Ph-I activation and this process, as with the equivalent reaction at **3**, shows an inverse dependence on $[PPh_3]$, consistent with initial PPh_3/PhI exchange. The calculations suggest this results in the formation of **Int5** ($G = +21.8$ kcal/mol) as an I-bound iodobenzene adduct (Figure 2.15) which can then isomerize to **Int6** ($G = +26.1$ kcal/mol) in which the major interaction is with the *ipso* carbon ($Ru-C_{ipso} = 2.12$ Å) with significant lengthening of the C-I bond (2.29 Å). **Int6** provides access to a facile 3-centered oxidative addition via **TS(Int6-Int7)** at

+27.4 kcal/mol.³³ The initial product of C-I bond activation is **Int7** ($G = +18.2$ kcal/mol) which has an unusual structure, featuring a rather short $C_{ipso} \cdots H$ non-bonded distance of 2.01 Å. This could be interpreted as an ‘elongated benzene σ -complex’, with a square-pyramid geometry at Ru, an axial PPh_3 ligand and ‘ C_6H_6 ’ occupying a basal position trans to iodide ($trans\text{-I-Ru-C}_{ipso} = 141^\circ$; $trans\text{-I-Ru-H}_{ipso} = 151^\circ$). Although **Int7** is a well-defined stationary point the transition state for the subsequent Ph-H reductive elimination lies 0.5 kcal/mol lower in free energy, indicating the facile formation of $[(Ph_3P)_2RuI_2]$, **8-I**, plus free benzene at -27.8 kcal/mol.

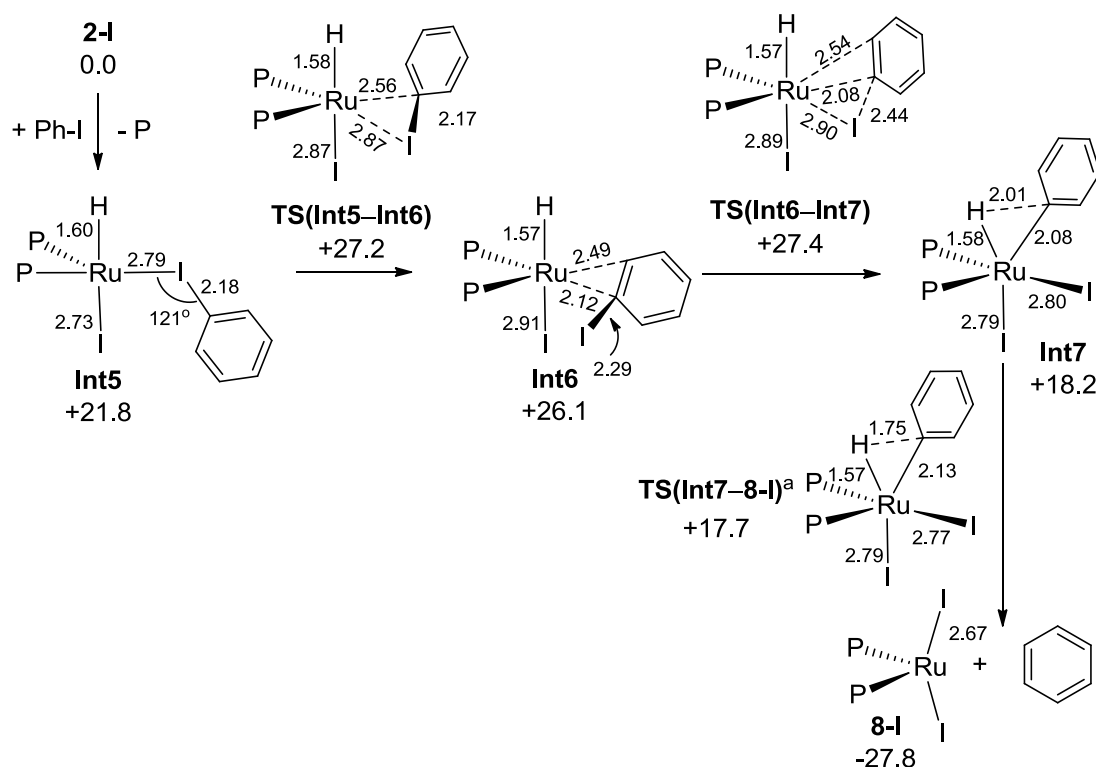


Figure 2.15. Reaction pathway (BP86-D3(benzene), kcal/mol) for Ph-I activation with **2-I** ($P = PPh_3$). Free energies are quoted relative to **2-I** + free PhI set to 0.0 kcal/mol; selected distances in Å and angles in degrees. ^aReductive elimination involves an intermediate C,H-bound C_6H_6 σ -complex at +5.4 kcal/mol.

³³ Alternative pathways based on direct hydride attack (in either Int5 or Int6) or via nucleophilic displacement by Ru (in Int6) could not be characterized, with optimizations failing or converging on TS(Int6-Int7) instead.

The two favored pathways computed for C-I activation at **3** and **2-I** have calculated overall barriers of 27.8 kcal/mol and 27.4 kcal/mol respectively, and so are in good agreement with the values determined experimentally while reiterating the similar barriers for C-I activation at both these species. For **2-I** the C-I bond cleavage transition state, **TS(Int6–Int7)**, is the highest point on the profile and this lies marginally above the preceding isomerisation transition state at +27.2 kcal/mol that links I-bound **Int5** and π -bound **Int6**. For **3** the highest transition state corresponds to the association of PhI to form the π -bound precursor **Int2** via **TS(5–Int2)** and the C-I bond activation transition state is somewhat lower in energy, at +25.6 kcal/mol. The nature of the C-I bond cleavage event also differs in the two systems: nucleophilic displacement of iodide by Ru in **TS(Int2–Int3)** or a more conventional concerted oxidative addition in **TS(Int6–Int7)**. This difference may stem from the greater steric encumbrance of the $\{(\text{Ph}_3\text{P})_3\text{Ru}(\text{H})_2\}$ moiety in **TS(Int2–Int3)** that does not readily provide access to two additional coordination sites, with the result that iodide is initially expelled from the inner coordination sphere. In contrast, in **TS(Int6–Int7)** the smaller $\{(\text{Ph}_3\text{P})_2\text{RuH}(\text{I})\}$ moiety permits a concerted oxidative addition with formation of the new Ru-Ph and Ru-I bonds. The computed geometries for the key intermediates and transition states involved in the Ph-I activation with **3** and **2-I** are shown in Figure 2.16.

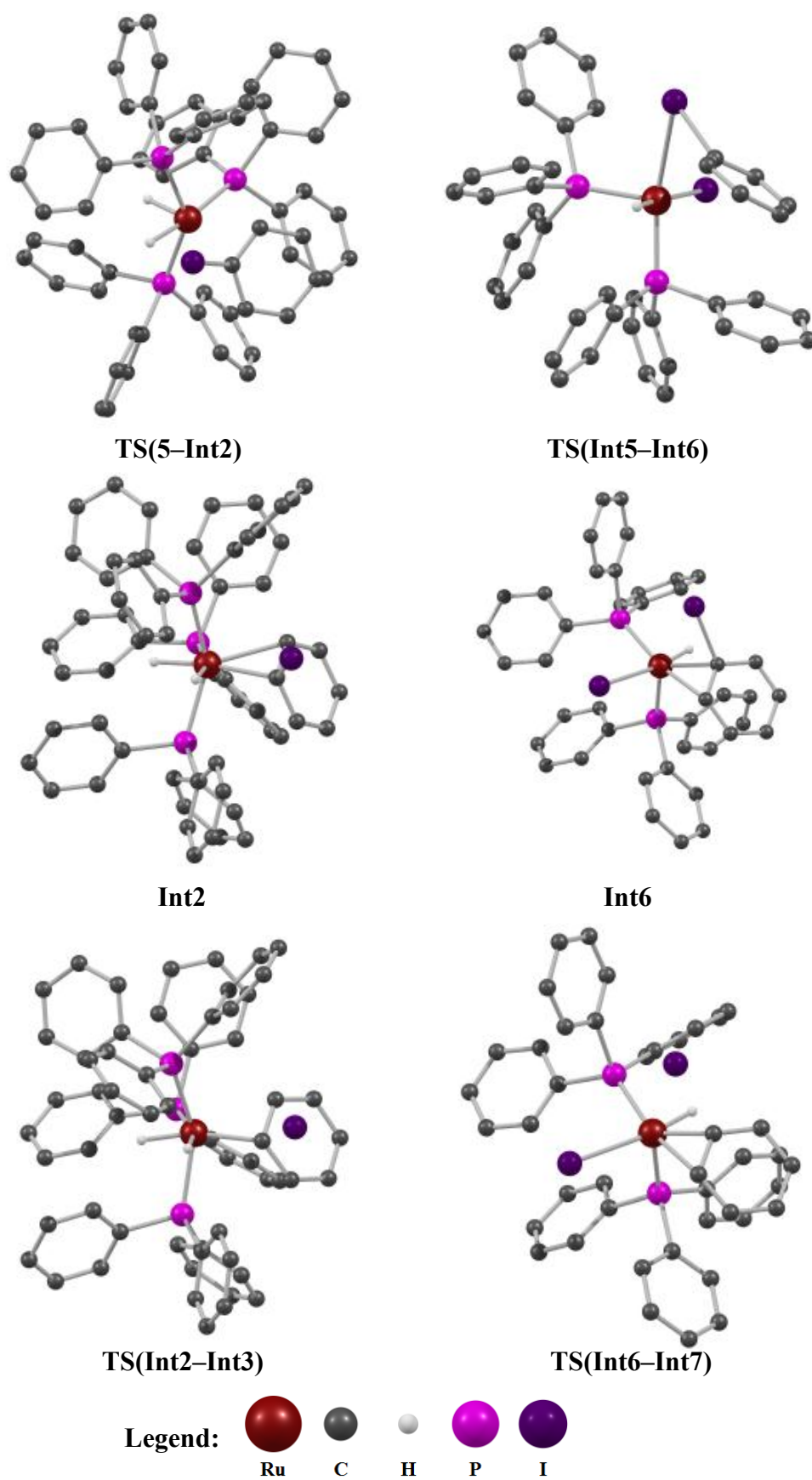


Figure 2.16. Computed geometries for selected key intermediates and transition states involved in the Ph-I activation with **3** and **2-I**.

Further calculations showed analogous pathways to be operative for Ph-Br activation at **3** and **2-Br**, with computed barriers of 30.4 kcal/mol and 31.3 kcal/mol respectively. These are again in good agreement with the rate constants determined experimentally, which correspond to free energies of activation of 29.5 kcal/mol and 29.7 kcal/mol, respectively. The same mechanisms are also in play for Ph-Cl activation, with computed barriers of 34.0 kcal/mol at **3** and 33.8 kcal/mol at **2-Cl**. For the reactions of PhBr and PhCl at **3** the rate-determining transition state corresponds to the C-X cleavage step, rather than the formation of the π -bound precursors.³⁴ This reflects increased barriers associated with cleaving the stronger C-Br and C-Cl bonds, but also a trend towards a weaker Ru-X interaction (and hence more facile rearrangement): the Br and Cl-bound analogues of **6** lie 13.7 kcal/mol and 16.5 kcal/mol above **3** and the free haloarene, respectively, compared to 10.1 kcal/mol for **6** itself.

Extensive testing was also performed on the computed data via single point energy calculations using a range of functionals applied to the BP86-optimised geometries. As already noted, the BP86-D3 approach produces excellent agreement with the experimental data in terms of both the absolute barriers involved and in reproducing the similar barriers for PhI activation at both **3** and **2-I**. Inclusion of the dispersion correction is crucial in obtaining this good agreement, as in its absence the computed barriers are ca. 10 kcal/mol too low. This reflects the contribution of the PPh₃/PhI ligand substitution step to the overall PhI activation barrier and the sensitivity of this process to dispersion effects, in particular when the participating ligands have significantly

³⁴ Location of TS(6-5) (for X = Br and Cl) and of TS(5-Int2) (for X = Cl) proved problematic, however linear transits clearly showed these structures were more accessible than the relevant C-X bond cleavage transition state TS(Int2-Int3). In addition for X = Cl, Ph-Cl cleavage via TS(Int2-Int3) leads to deprotonation of the H₂ adduct Int3 by Cl⁻. Facile product formation then occurs via protonolysis of the Ru-Ph bond by HCl.

different steric bulk.^{28,35,36} Other pure and hybrid functionals displayed similar behavior without reaching the good agreement seen with the BP86-D3 approach. In contrast, functionals incorporating dispersion effects were less successful, either overestimating (M06-2X, ω B97xD) or underestimating the barriers (M06L), or giving rather different barriers for PhI activation at **3** and **2-I** (e.g. M06: $\Delta G^\ddagger = +28.3$ kcal/mol and $+23.8$ kcal/mol respectively).

The experimental study also quantified the free energy change for PPh₃/PhI exchange at **3** to give **6** ($\Delta G = +3.8 \pm 0.1$ kcal/mol) and thus provided a further benchmark for the calculations. In this case the value computed with BP86-D3 is rather too high ($+10.1$ kcal/mol) whereas M06 shows improved performance ($\Delta G = +4.1$ kcal/mol).

A further issue that can be assessed computationally is the behavior of the [(Ph₃P)₂RuX₂] species (**8-X**) initially formed upon Ph-X activation at **2-X**. In particular, the ease of comproportionation with the [(Ph₃P)₄Ru(H)₂] precursor (**3**) is crucial as this reforms **2-X** and so drives the autocatalysis seen in the reactions of PhI and PhBr. The computed thermodynamics for comproportionation and PPh₃ addition (as well as dimerization, see below) are shown in Figure 2.17, with results computed at the BP86-D3 and (in parenthesis) M06 levels. Both approaches show the same pattern for each process, i.e. the ease of comproportionation follows the trend X = I > Br > Cl, while the opposite trend is computed for PPh₃ addition. However, the *balance* of these two processes depends on the functional: with BP86-D3 PPh₃ addition is favored over comproportionation for all X, whereas the opposite is true with M06. In this regard the

³⁵ (a) Algarra, A. G.; Cross, W. B.; Davies, D. L.; Khamker, Q.; Macgregor, S. A.; McMullin, C. L.; Singh, K. *J. Org. Chem.* 2014, **79**, 1954. (b) McMullin, C. L.; Jover, J.; Harvey, J. N.; Fey, N. *Dalton Trans.* 2010, **39**, 10833.

³⁶ For other examples highlighting the importance of dispersion corrections in phosphine dissociation energies see: (a) Ahlquist, M. S. G.; Norrby, P. O. *Angew. Chem., Int. Ed.* 2011, **50**, 11794. (b) Minenkov, Y.; Occhipinti, G.; Jensen, V. R. *J. Phys. Chem. A* 2009, **113**, 11833. (c) Ryde, U.; Mata, R. A.; Grimme, S. *Dalton Trans.* 2011, **40**, 11176. (d) Sieffert, N.; Buehl, M. *Inorg. Chem.* 2009, **48**, 4622. (e) Zhao, Y.; Truhlar, D. G. *Org. Lett.* 2007, **9**, 1967.

latter approach more closely captures experiment, as comproportionation occurs readily for X = I and Br and may also occur to some extent with **2-Cl**, albeit in this case obscured by other decomposition processes.

Experimentally, once all of **3** has been consumed the fate of **8-X** again depends on X: dimer formation (X = I) or PPh₃ addition (dominant for X = Br and exclusive for X = Cl). Here M06 provides improved performance, favoring dimerization for X = I, PPh₃ addition for X = Cl, and suggesting these processes will be in competition for X = Br. Overall it appears that the thermodynamics of these ligand exchange processes in the current system are better modelled with the M06 functional; however this approach cannot compete with BP86-D3 in terms of modeling the available kinetic data. Our study indicates that no single functional is able to represent all aspects of this system; it also emphasizes the great value of having quantitative experimental data available as a probe of the accuracy of the DFT methodology.

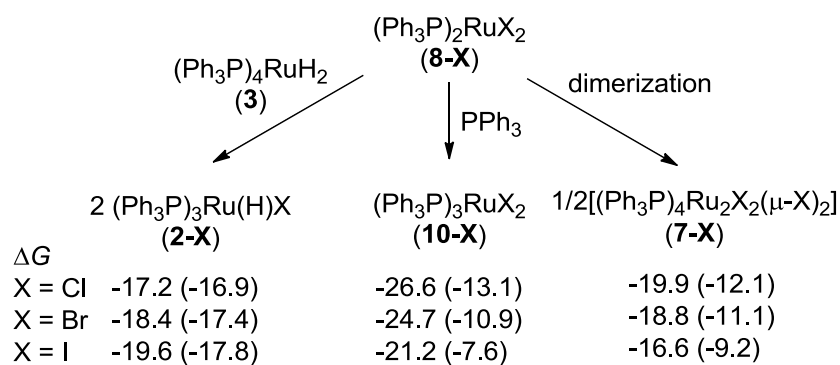
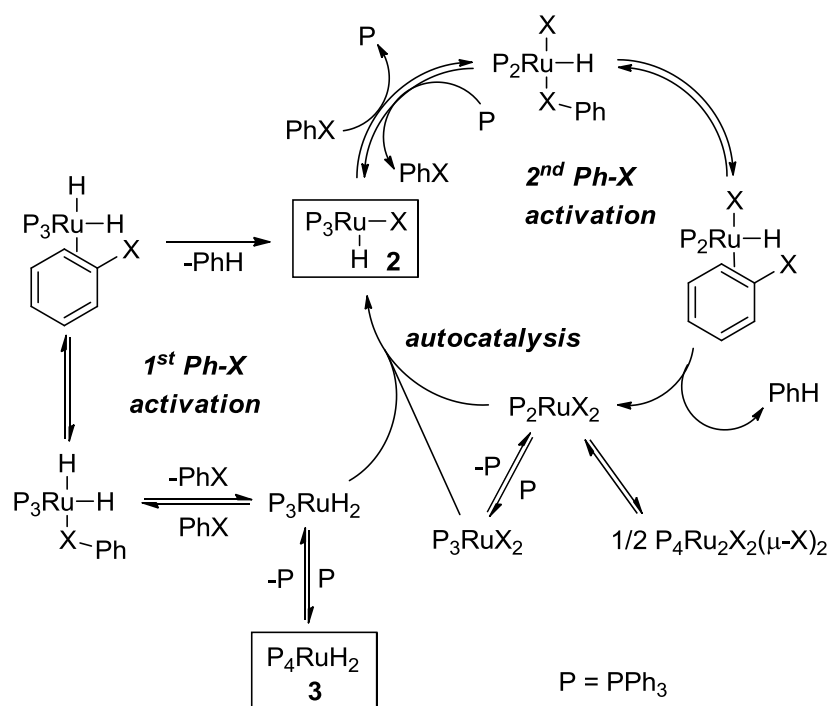


Figure 2.17. Computed free energy changes (kcal/mol) for the comproportionation of **8-X** with **3** to give **2-X**, and the competing processes; PPh₃ addition to **10-X** and dimerization to **7-X**. Results are for BP86-D3 and (in parenthesis) M06//BP86, both corrected for benzene solvent.

Discussion of the Mechanism. The reaction mechanism is summarized in Scheme 2.13. The observed zeroth order kinetics is due to $k_1 \approx k_2$, i.e. roughly the same reactivity of **3** and **2** toward PhX (X = I, Br) for the same X. As can be seen from Table 2.1, the experimentally determined and BP86-D3-derived activation barriers for the reactions of PhX with **3** (k_1) are remarkably close to those with the corresponding **2-X** (k_2). The computed ΔG^\ddagger values deviate from the experimentally determined ones only by 0.5-1.6 kcal/mol, showing an excellent agreement of the BP86-D3 and kinetic data (Table 2.1). Let us consider factors determining the ability of **3** and **2** to cleave the Ph-X bond.



Scheme 2.13. Mechanism of the reaction of **3** with PhX including two C-X activations and autocatalysis.

Table 2.1. Experimentally determined and computed ΔG^\ddagger values (kcal/mol) for the reactions of **3** (1st activation) and **2-X** (2nd activation) with PhX.

	1 st Ph-X Activation		2 nd Ph-X Activation	
	Experiment	DFT	Experiment	DFT
I	+26.6	+27.8 ^a	+26.9	+27.4
Br	+29.5	+30.4	+29.7	+31.3
Cl	-	+34.0	+32.4 ^b	+33.7

^a Highest lying transition state corresponds to PhI addition to form a π -bound precursor (Int2); in all other cases Ph-X cleavage is rate-limiting. ^b See footnote 27.

To bind to the PhX substrate, the Ru center must be Lewis acidic. Coordinatively saturated 18-e **3** must and does lose one phosphine¹³ prior to the Ru-XPh bond formation. In contrast, **2** is a 5-coordinate 16-e species with a vacant coordination site on Ru that, in principle, could accept an electron pair donor. However, the Lewis acidity of **2** may be reduced due to the π -donation from the halide, which increases in the order I < Br < Cl.^{37,38} Therefore, as shown experimentally (see above), phosphine dissociation not only from **3** but also from **2** is required prior to PhX binding to the Ru and subsequent C-X bond activation.

After the halogen of PhX coordinates to the metal center of the reactive species $[(\text{Ph}_3\text{P})_3\text{Ru}(\text{H})_2]$ (1st activation, Scheme 2.13) or $[(\text{Ph}_3\text{P})_2\text{Ru}(\text{X})\text{H}]$ (2nd activation, Scheme 2.13), the halogen-bound adduct rearranges to the π -bound η^2 -PhX complex before the C-X bond can be completely broken at the metal. This energetically uphill isomerization is accompanied by substantial Ph-X bond elongation and hence contributes noticeably to the overall activation process. Steric factors are heavily

³⁷ (a) Caulton, K. G. *New J. Chem.* 1994, 18, 25. (b) Poulton, J. T.; Sigalas, M. P.; Folting, K.; Streib, W. E.; Eisenstein, O.; Caulton, K. G. *Inorg. Chem.* 1994, 33, 1476.

³⁸ The π -donation might be counterbalanced, to some extent, by steric effects, i.e., the size of the halogen atom (I > Br > Cl) on Ru in **2**.

involved in this step. In the case of PhI reacting with **3** the η^2 -PhI intermediate (**Int2**) is particularly crowded and the formation of this species is computed to be the rate-limiting step of the entire process.

Both steric factors and electron donation from Ru to the π -bound halobenzene ligand play a critical role in the Ph-X cleavage event. In the rate-determining transition states of the 1st reaction, the Ru atom bears three PPh₃ ligands, two hydrides, and PhX. Their congeners in the 2nd, onward reaction are not as electron rich yet less sterically crowded with only two phosphines, one hydride, one halogen, and PhX in the first coordination sphere. These differences apparently cancel each other out, which results in similar reactivity of **2** and **3** toward PhX. The C-X bond is cleaved by **3** via what might be formally viewed as an S_N-type reaction and by **2** in a three-center concerted manner. Although the two transition states display different geometries (Figure 2.17 and Table 2.2), both activations are oxidative addition reactions with a flow of electrons from Ru(II) to the π -bound PhX molecule in comparable ligand environments. Oxidative addition to Ru(II) implies the formation of Ru(IV). However, the higher formal oxidation state is mitigated by the simultaneous reductive coupling of two hydrides in **Int3** (1st C-X activation) and the short Ph...H non-bonding contact in **Int7** (2nd C-X activation). Consequently, both reactions are governed by comparable factors, which apparently results in similar barriers for the first and for the second activation steps for the same haloarene substrate (Scheme 2.13).³⁹ The similar reactivity of **2** and **3** toward PhX for the same X is a notable coincidence that translates in a remarkably interesting kinetic case.

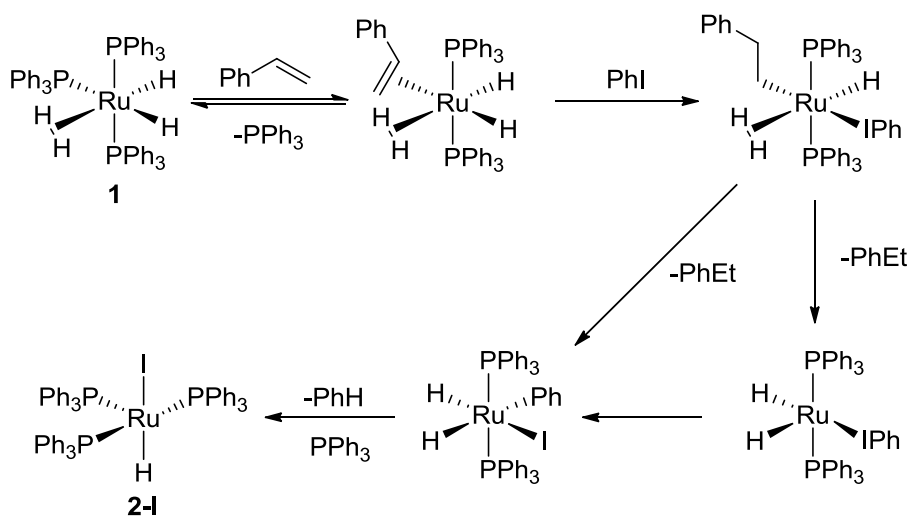
³⁹ The similarity of the Ru-C distances in TS(Int2-Int3) and TS(Int6-Int7) might be a sign of similarity of the C-X bond activation with **3** and **2**.

Table 2.2. Selected geometry parameters of *TS(Int2–Int3)* and *TS(Int6–Int7)*.

	X = I		X = Br		X = Cl	
	TS (Int2-Int3)	TS (Int6-Int7)	TS (Int2-Int3)	TS (Int6-Int7)	TS (Int2-Int3)	TS (Int6-Int7)
C–X (Å)	3.04	2.44	3.02	2.23	2.87	2.10
Ru–C (Å)	2.08	2.08	2.05	2.06	2.05	2.05
Ru–C–X (°)	122	80	119	78	115	77

Activation of PhI with 1 in the presence of styrene. As described above, the [(Ph₃P)₃Ru(H)₂](H)₂] (**1**)-styrene system is vastly more reactive toward PhX (Scheme 2.1) than **3** and **4**. It was originally proposed¹¹ that the exceptional activity of **1**-styrene dealt with the efficient generation of [(Ph₃P)₃Ru(H)₂] (**5**) in high concentrations via styrene hydrogenation (Scheme 2.2). If that was the case, the reaction of **1** (0.005 M), styrene (0.8 equiv), and PhI (350 equiv) in C₆D₆ at 25 °C would quickly produce ethylbenzene and **6** that would then decay to **2-I** at 50% conversion after ca. 1 h (as predicted by the established kinetic model). However, the reaction under such conditions (i) was much faster, $\tau_{1/2} < 0.25$ h; (ii) produced ethylbenzene and **2-I** simultaneously; and (iii) exhibited the presence of only small quantities of **6** (<15%) throughout the run. These observations were obviously inconsistent with the original proposal of styrene hydrogenation with **1**, followed by Ph-I coordination to the resultant **5** to give rise to **6** and subsequent Ph-I activation. Clearly, a different sequence of transformations governs the PhI activation with **1**-styrene. For instance, the reaction sequence shown in Scheme 2.14 is conceivable. First, one PPh₃ in 18-e **1** is displaced with styrene via a dissociative mechanism, followed by migratory insertion giving rise to [(Ph₃P)₂Ru(H)₂](H)(CH₂CH₂Ph)]. Reversible coordination of PhI to the Ru center and

Ph-Et coupling produce a species that is predisposed to facile Ph-I activation via oxidative addition. Finally, Ph-H reductive elimination and PPh₃ addition conclude the transformation. The formation of small amounts of free PPh₃ and **3** observed by NMR during the reaction lends support to this proposed mechanistic scheme. A separate study is needed, however, in order to firmly establish the mechanism of the formation of **2** from **1**-styrene and PhX.



*Scheme 2.14. Proposed mechanism of activation of PhI by **1** in the presence of styrene.*

Conclusions

The objectives of this research project have been fully met. The preliminary results obtained in our group^{11,14} had shown the need for a detailed mechanistic study of the activation of PhI with $[(\text{Ph}_3\text{P})_4\text{Ru}(\text{H})_2]$ (**3**). The performed kinetic investigation of this reaction has revealed an unusual kinetic pattern including an almost quantitative *linear* formation of $[(\text{Ph}_3\text{P})_3\text{RuH}(\text{I})]$ (**2-I**) up to >95% conversion, followed by its exponential decay. The latter leads to $[(\text{Ph}_3\text{P})_4\text{Ru}_2\text{I}_2(\mu\text{-I})_2]$ (**7**) as a final product, which has been isolated and fully characterized, including by single-crystal X-ray diffraction. The determination of reaction orders for the PhI activation with both **3** (**3**, +1; PhI, +1; PPh₃, -1) and **2-I** (**2-I**, +1; PhI, +1; PPh₃, -1) suggested that an autocatalytic process is involved, occurring at rates similar to those of the direct activation of PhI with **3**. This autocatalysis has indeed been established by observing fast comproportionation of **3** and $[(\text{Ph}_3\text{P})_2\text{RuI}_2]$ (generated in situ) to give **2-I**. Similar autocatalysis has been found for the reaction of **3** with PhBr and studied in as much detail. Full kinetic analysis has been performed for both transformations involving the original and onward Ph-X activation reactions. The excellent fit of the experimental data with the autocatalysis model has produced values for the rate constants k_1 (initial activation with **3**) and k_2 (activation with **2** formed in the first step) and K_{eq} for the equilibrium between **3** and the key iodine-bound intermediate *mer*- $[(\text{Ph}_3\text{P})_3\text{Ru}(\text{H})_2(\text{PhI})]$ (**6**).¹⁴ A similar kinetic study has been performed for Ph-Cl activation with **3**. However, the data obtained could not be quantitatively analyzed because of the lower selectivity of the process.

The computational study by McKay and Macgregor accords with the experimental data showing that both the initial and onward reactions involve phosphine pre-dissociation from Ru as the first step. Halobenzene coordination to Ru through the

halogen atom and subsequent rearrangement to a π -bound η^2 -PhX complex leads to the efficient Ph-X bond breaking, followed by Ph-H reductive elimination. The calculations suggest that the rate-determining step in all of the reactions of PhX (X = I, Br, Cl) but one is the cleavage of the C-X bond. The only exception, likely for steric reasons, is the reaction of **3** with PhI, where the highest barrier was calculated for the formation of the π -bound η^2 -PhX adduct. The computed ΔG^\ddagger values are in excellent agreement with those derived from the experimentally determined rate constants k_1 and k_2 using the Eyring equation.

It is hoped that the mechanistic information obtained from the current study can be useful not only for further academic research in the area of inert C-X bond activation, but also for catalytic applications, such as hydrogenolysis of polychlorinated aromatic compounds.

Experimental Section

General consideration. All manipulations were performed under argon in a glovebox or using Schlenk techniques, unless noted otherwise. $\text{RuCl}_3 \cdot x\text{H}_2\text{O}$, PPh_3 , and NaBH_4 were used as received. Anhydrous, oxygen-free hexane, benzene, benzene- d_6 , toluene- d_8 , THF, and THF- d_8 were obtained by distillation from Na/OCPh_2 under argon and stored over freshly activated 4 Å molecular sieves in an argon-filled glovebox. $[(\text{Ph}_3\text{P})_3\text{RuCl}_2]$ was prepared by the literature procedure.⁴⁰ NMR spectra were recorded on Bruker Avance Ultrashield 400 and 500 MHz spectrometers. Single-crystal X-ray diffraction studies were performed on Bruker FR591 and Apex DUO Kappa 4-axis diffractometers equipped with APEX II 4K CCD area detectors.

As has been demonstrated,¹³ complexes **1**, **2** and **3** easily form solvates, and **3** can also contain lattice PPh_3 . The composition of these materials may vary significantly depending on minor changes in crystallization conditions. It is therefore recommended that each batch of the complexes obtained be carefully analyzed by ^1H and ^{31}P NMR to determine the amount of cocrystallized solvents and/or PPh_3 .

All experiments with air-sensitive Ru complexes were conducted in an argon rather than nitrogen atmosphere. Under N_2 , solutions of both **1** and **3** gave rise to $[(\text{Ph}_3\text{P})_3\text{Ru}(\text{N}_2)(\text{H})_2]$ (**4**) in various quantities, as can be easily detected by ^1H and $^{31}\text{P}\{^1\text{H}\}$ NMR.¹³ Even under argon containing adventitious N_2 , solutions of **1** and **3** produced small yet NMR-detectable quantities of **4** after a few hours. Contamination of the argon atmosphere with N_2 in a circulation glovebox can represent a serious problem when working with **1** and **3**.

⁴⁰ Hallman, P. S.; Stephenson, T. A.; Wilkinson, G. *Inorg. Synth.* 1970, 12, 237.

[(Ph₃P)₃Ru(H₂)(H)₂] (1). A slightly modified literature procedure¹² was used. A 1-L round-bottom flask equipped with a rubber septum, a gas inlet, and a PTFE-coated magnetic stir-bar was charged under argon with [(Ph₃P)₃RuCl₂].PPh₃^{13,40} (3.69 g, 3.02 mmol) and a deaerated 4:3 v/v mixture of ethanol and benzene (460 mL). To this mixture, at stirring, NaBH₄ (420 mg, 11.1 mmol) was added in small portions over a period of 10 minutes. The originally brown reaction mixture turned lighter in color and a white precipitate appeared within 20 min of agitation. After stirring for an additional 2 h, the pinkish slurry was filtered under argon and the off white product was thoroughly washed on the filter with deaerated EtOH (1 × 40 mL), deaerated water (2 × 30 mL), deaerated EtOH (2 × 40 mL), and deaerated hexane (2 × 40 mL). Drying the washed solid first with a flow of argon and then under vacuum (~1 mbar) for 10 minutes gave crude **1** (2.30 g) containing cocrystallized benzene (1 molecule) and residual water (¹H NMR). For further purification, the crude product (1.03 g) was dissolved under argon in warm (ca. 50 °C) THF (50 mL) and allowed to cool to room temperature. After 6 h at -32 °C, the precipitated fiber-like white needles of were separated by filtration, washed with THF (3 × 3 mL), and dried first with a flow of argon and then under vacuum (~1 mbar) for 10 minutes. The yield of the thus recrystallized slightly off white, air-sensitive **1** (1.3 THF solvate) was 0.61 g (46%). ¹H NMR (C₆D₆), δ: 7.41 (br s, 18H), 6.96, (t, *J* = 7.3 Hz, 9H), 6.88 (t, *J* = 7.5 Hz, 18H), -7.07 (br s, 4H). ³¹P {¹H} NMR (C₆D₆), δ: 57.6 (s).

[(Ph₃P)₃Ru(H)I] (2-I). In a glovebox, a solution of styrene (72 μL; 0.63 mmol) in THF (5 mL) was slowly added (5 min) via syringe to a stirring solution of [(Ph₃P)₃Ru(H₂)(H)₂] (**1**; 446 mg; 0.50 mmol) and PhI (70 μL; 0.63 mmol) in THF (50 mL). After 10 min, the deep purple reaction mixture was placed into a freezer at

-30 °C for 1 day to complete precipitation of **2-I**. The mixture was then reduced in volume to ca. 25 mL by evaporation with a flow of argon, the deep purple crystals of **2-I** were separated, washed with Et₂O (3 × 5 mL), and dried under vacuum. A 100-mg portion of the thus obtained crude **2-I** (430 mg) was dissolved in benzene at room temperature (30 mL) and filtered. Evaporation of the filtrate and drying under vacuum gave pure **2-I**·3C₆H₆ in 69% yield (100 mg). ¹H{³¹P} NMR (THF-*d*₈), δ: 7.30 (18H, 3C₆H₆), 7.24 (d, *J* = 7.5 Hz 18H), 7.15 (t, *J* = 7.5 Hz, 9H), 6.95 (t, *J* = 7.5 Hz, 18H), -15.13 (s).

[(Ph₃P)₄Ru(H)₂] (3). A slightly modified literature procedure⁴¹ was used. A 1-L three-neck round-bottom flask equipped with a rubber septum, a gas inlet, and a PTFE-coated magnetic stir-bar was charged with PPh₃ (18.0 g, 67 mmol), C₆H₆ (180 mL), and MeOH (300 mL). After agitation under argon for 10 min, [(Ph₃P)₃RuCl₂] (3.00 g, 3.1 mmol) was added and the reaction mixture was stirred for an additional 10 min. As stirring continued, NaBH₄ (4.50 g, 119 mmol) was added in 5 portions over a period of 20 min. During the addition the originally brown reaction mixture turned yellow. After stirring for an additional hour, the mixture was diluted with deaerated MeOH (300 mL), the yellow solid was filtered under argon, washed with deaerated MeOH (3 × 50 mL), deaerated and deionized water (4 × 50 mL), deaerated MeOH (3 × 50 mL), anhydrous, oxygen-free hexane (3 × 60 mL) and Et₂O (3 × 60 mL), and dried under vacuum. The product containing cocrystallized phosphine and hexane (see above) is air-sensitive in solution and in the solid state. The yield of **3** was 3.63 g (88%; calculated for [(Ph₃P)₄Ru(H)₂]·0.5PPh₃·0.5C₆H₁₄). ¹H NMR (C₆D₆), δ: 7.44-6.73 (m), -10.13 (m). ³¹P{¹H} NMR (C₆D₆), δ: 49.1 (t, *J* = 13.8 Hz, 2P), 40.9 (t, *J* = 13.8 Hz, 2P), -5.5 (s, 0.5P).

⁴¹ Young, R.; Wilkinson, G. *Inorg. Synth.* **1990**, 28, 337.

[(Ph₃P)₄Ru₂I₂(μ-I)₂] (7). In a glovebox, a 20-mL vial was charged with [(Ph₃P)₄Ru(H)₂]₂·0.5PPh₃·0.5hexane (**3**, 126 mg, 0.095 mmol), PhI (1 mL), and benzene (5 mL). The mixture was agitated first at 40 °C for 17 h, and then at 60 °C for 5 h. At that point, full conversion of **3** and intermediate **2-I** was observed by ¹H{³¹P} NMR. The resultant dark brown solid was separated inside the glovebox, washed with benzene (3 × 2 mL), and dried under vacuum. The yield of **7** was 84 mg (100%). This solid appeared to be virtually insoluble in benzene, toluene, THF, dichloromethane, and DMF. It was found, however, that **7** dissolves in DMSO to give a *yellow* solution that displayed only one signal in the ³¹P{¹H} NMR spectrum, a singlet at -5.5 ppm, evidently from free PPh₃. Quantitative analysis in the presence of an internal standard (Ph₃PO) indicated that ca. 2 equiv. of PPh₃ had been released from each Ru atom. Anal. Calcd. for C₇₂H₆₀I₄P₄Ru₂: C, 49.2; H, 3.4. Found: C, 49.5; H, 3.5. To obtain X-ray quality crystals of **7**, a solution of [(Ph₃P)₃RuCl₂] (50 mg) in deaerated C₆H₆ (10 mL) was treated, under argon, with a solution of NaI (2.0 g) in deaerated deionized water (5 mL). After 40 h, the organic phase was separated and layered with pentane to give X-ray quality crystals of **7**.

Kinetic studies.

Determination of reaction orders for PhI activation with [(Ph₃P)₄Ru(H)₂] (3**).**

In an argon-filled glovebox, iodobenzene was added to a solution of [(Ph₃P)₄Ru(H)₂] (**3**) and PPh₃ in C₆D₆ in a 5-mm NMR tube. The reaction mixture was shaken, sealed with a rubber septum, and monitored to 5-15% conversion by ¹H{³¹P} NMR at 23 °C. See Table 2.3 for specifics. The data was analyzed in the assumption of the sum of concentrations of [(Ph₃P)₄Ru(H)₂] and [(Ph₃P)₃Ru(H)I] in the presence of excess PPh₃ being constant and equal to the initial concentration of [(Ph₃P)₄Ru(H)₂]. For entries

8-11, additional correction of the initial concentrations of PPh₃ and the Ru complexes was made, taking into account the equilibrium between **3** and [(Ph₃P)₃Ru(H)₂(PhI)] (**6**). In all other runs, this correction was unnecessary because the amount of **6** present was estimated at <4% of the initial concentration of **3**. The plots obtained are presented in Figures 2.1, 2.2, and 2.3.

Table 2.3. Determination of reaction orders for the reaction of [(Ph₃P)₄Ru(H)₂] with PhI by the method of initial rates.

Entry	[(Ph ₃ P) ₄ Ru(H) ₂] ₀ , M × 10 ³	[PhI] ₀ , M	[PPh ₃] ₀ , M × 10 ²	Initial rate, M/min × 10 ⁷	Amount of 6 , (%)
1	8.33	1.49	8.33	9.11	3
2	6.67	1.49	8.33	8.24	3
3	5.00	1.49	8.33	6.15	3
4	3.33	1.49	8.33	3.46	3
5	8.33	1.12	8.33	7.55	2
6	8.33	0.75	8.33	5.15	2
7	8.33	0.37	8.33	2.15	1
8	8.33	1.49	2.50	43.8	10
9	8.33	1.49	3.17	32.5	8
10	8.33	1.49	4.17	22.6	6
11	8.33	1.49	5.83	13.6	4
12	8.33	1.49	8.33	10.3	3
13	8.33	1.49	10.0	9.65	3
14	8.33	1.49	11.7	8.15	2
15	8.33	1.49	13.3	4.90	2
16	8.33	1.49	15.0	4.18	2
17	8.33	1.49	16.7	3.85	2

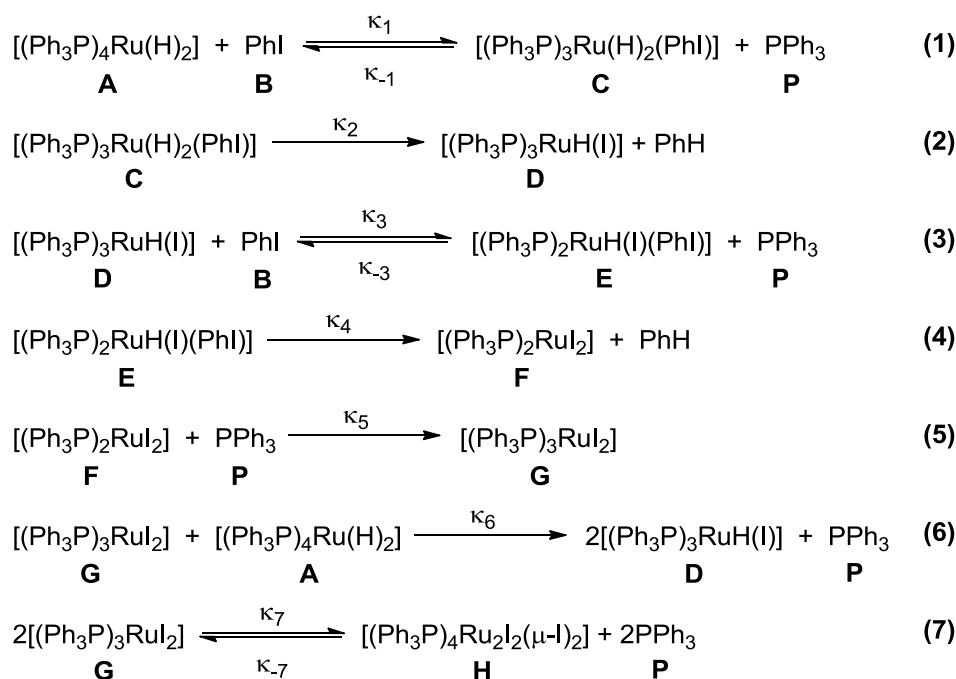
Determination of reaction orders for activation of PhI with [(Ph₃P)₃Ru(H)I]

(2-I). In an argon-filled glovebox, PhI was added to a solution of [(Ph₃P)₃Ru(H)I]·3C₆H₆ (**2-I**), PPh₃, and cyclohexane (internal standard) in C₆D₆ in a 5-mm NMR tube. The reaction mixture was shaken, sealed with a rubber septum, and monitored to 10-20% conversion by ¹H{³¹P} NMR at 23 °C. See Table 2.4 for specifics. The plots are presented in Figures 2.6, 2.7, and 2.8.

Table 2.4. Determination of reaction orders for the reaction of [(Ph₃P)₃Ru(H)I] with PhI by the method of initial rates.

Entry	[(Ph ₃ P) ₃ Ru(H)I] ₀ , M × 10 ³	[PhI] ₀ , M	[PPh ₃] ₀ , M × 10 ²	Initial rate, M/min × 10 ⁷
1	2.08	1.49	0.63	15.9
2	2.08	1.49	1.33	8.27
3	2.08	1.49	2.40	4.85
4	2.08	1.49	4.17	3.07
5	2.08	1.49	0.98	11.3
6	2.08	1.49	1.69	6.86
7	2.08	1.12	0.63	13.3
8	2.08	0.75	0.63	7.49
9	2.08	0.37	0.63	3.51
10	1.67	1.49	0.63	14.3
11	1.25	1.49	0.63	8.90
12	0.83	1.49	0.63	8.52

Full kinetic profile of the reaction of $[(\text{Ph}_3\text{P})_4\text{Ru}(\text{H})_2]$ with PhI. In an argon-filled glovebox, $[(\text{Ph}_3\text{P})_4\text{Ru}(\text{H})_2] \cdot 0.5\text{PPh}_3 \cdot 0.5\text{hexane}$ (**3**; 13 mg; 0.01 mmol) was dissolved in C_6D_6 (2.0 mL). A 500- μL aliquot of the thus prepared solution, PhI (100 μL), and a flame-sealed capillary containing an external standard (dppf in CDCl_3) were placed in a 5-mm NMR tube. The tube was sealed with a rubber septum and the reaction was monitored by $^1\text{H}\{^31\text{P}\}$ and $^{31}\text{P}\{^1\text{H}\}$ IGD NMR at 25 °C. The data obtained were manually fitted to the model (Scheme 2.15) using the KINET⁴² and Tenua⁴³ programs (See Table 2.5 for details and Figure 2.9).



Scheme 2.15. Kinetic model for the reaction of **3** with PhI.

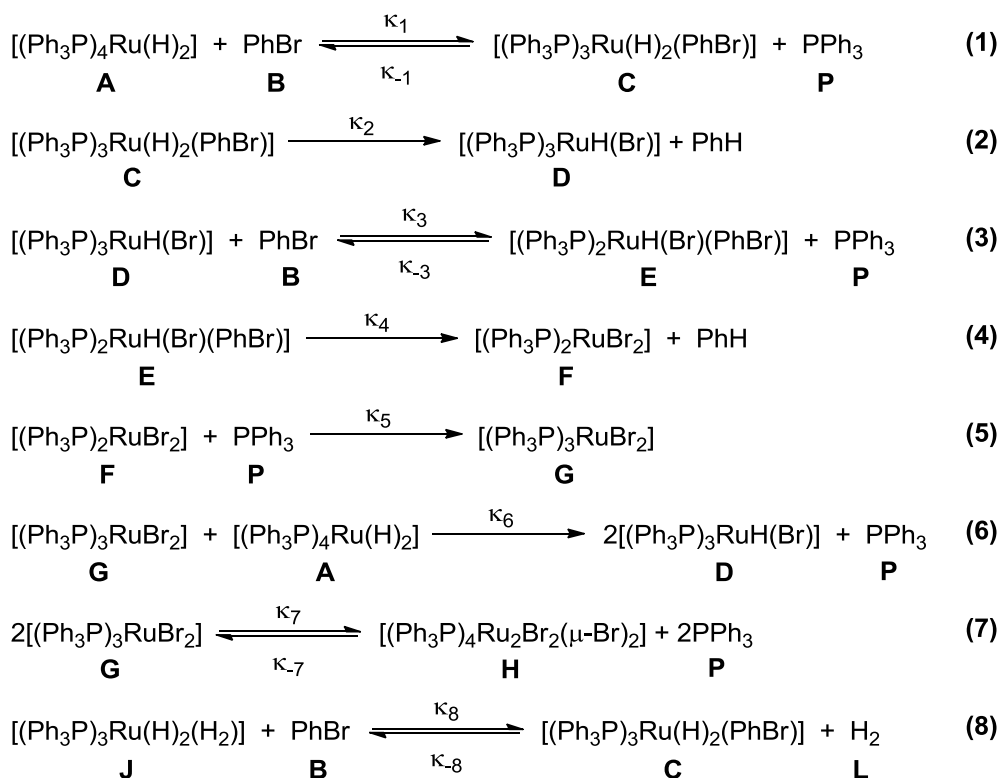
⁴² Abramnikov, A. V. *Kinet*, version 0.8; a program for the numerical modeling of complicated chemical reaction kinetics; Chemistry Department of Moscow State University, Division of Physical Chemistry; Moscow, Russia, 2012.

⁴³ Wachsstock, D. *Tenua*, version 2.0; the kinetics simulator for Java; 2005.

Table 2.5. Parameters used in the simulation of the kinetic model presented in Scheme 2.15.

Compound	Initial concentration, M	Rate constant	Value	Significant <i>k</i> and ΔG values
A	4.2×10^{-3}	κ_1	1.9×10^2	$K_{eq}(1) = \kappa_1/\kappa_{-1} = 1.9 \times 10^{-3}$ $\Delta G = 3.7$ kcal/mol
B	1.49	κ_{-1}	1×10^5	
C	1×10^{-5}	κ_2	6.5×10^{-3}	$k_1 = \kappa_2 \times \kappa_1/\kappa_{-1} = 1.24 \times 10^{-5} \text{ min}^{-1}$ $\Delta G^\ddagger = 26.6$ kcal/mol
D	1×10^{-3}	κ_3	1×10^2	
E	0	κ_{-3}	1×10^7	$k_2 = \kappa_4 \times \kappa_3/\kappa_{-3} = 6.8 \times 10^{-6} \text{ min}^{-1}$ $\Delta G^\ddagger = 26.9$ kcal/mol
F	0	κ_4	6.8×10^{-1}	
G	0	κ_5	1×10^3	
H	0	κ_6	5×10^{-4}	
		κ_7	1×10^5	
		κ_{-7}	1	

Full kinetic profile of the reaction of $[(\text{Ph}_3\text{P})_4\text{Ru}(\text{H})_2]$ with PhBr. In an argon-filled glovebox, $[(\text{Ph}_3\text{P})_4\text{Ru}(\text{H})_2] \cdot 0.5\text{PPh}_3 \cdot 0.5\text{hexane}$ (**3**; 13 mg; 0.01 mmol) was dissolved in C_6D_6 (2.0 mL). A 0.5-mL aliquot of the thus prepared solution, PhBr (100 μL), and a flame-sealed capillary containing an external standard (dppf in CDCl_3) were placed in a 5-mm NMR tube. The tube was sealed with a rubber septum and the reaction was monitored by $^1\text{H}\{^{31}\text{P}\}$ and $^{31}\text{P}\{^1\text{H}\}$ IGD NMR at 50 °C. The data obtained were manually fitted to the model (Scheme 2.16) using the KINET⁴² and Tenua⁴³ programs (See Table 2.6 for details and Figure 2.10).

**Scheme 2.16.** Kinetic model for the reaction of **3** with PhBr.**Table 2.6.** Parameters used in the simulation of the kinetic model presented in Scheme 2.16.

Compound	Initial concentration, M	Rate constant	Value	Significant values
A	3.18×10^{-3}	κ_1	1×10^2	$k_1 = \kappa_2 \times \kappa_1 / \kappa_{-1} = 4.3 \times 10^{-6} \text{ min}^{-1}$ $\Delta G^\ddagger = 29.5 \text{ kcal/mol}$
B	1.59	κ_{-1}	1×10^7	
C	0	κ_2	4.3×10^{-1}	
D	7.1×10^{-4}	κ_3	1×10^2	$k_2 = \kappa_4 \times \kappa_3 / \kappa_{-3} = 3.2 \times 10^{-6} \text{ min}^{-1}$ $\Delta G^\ddagger = 29.7 \text{ kcal/mol}$
E	0	κ_{-3}	1×10^7	
F	0	κ_4	3.2×10^{-1}	
G	0	κ_5	1×10^3	$Keq(7) = \kappa_7 / \kappa_{-7} = 5.9 \times 10^3$ $\Delta G = 3.3 \text{ kcal/mol}$
H	0	κ_6	2×10^3	
J	3.8×10^{-3}	κ_7	1×10^3	
L	1×10^{-4}	κ_{-7}	1.7×10^5	
		κ_8	1×10^2	
		κ_{-8}	1×10^8	

Full kinetic profile of the reaction of $[(\text{Ph}_3\text{P})_4\text{Ru}(\text{H})_2]$ with PhCl. In an argon-filled glovebox, $[(\text{Ph}_3\text{P})_4\text{Ru}(\text{H})_2] \cdot 0.5\text{PPh}_3 \cdot 0.5\text{hexane}$ (**3**; 13 mg; 0.01 mmol) was dissolved in a mixture of PhCl (2.0 mL) and C_6D_6 (0.4 mL). A 600- μL aliquot of this solution and a flame-sealed capillary containing an external standard (dppf in CDCl_3) were placed in 5-mm glass NMR tube that was sealed with a rubber septum. The sample was placed in a pre-heated (55 $^\circ\text{C}$) NMR probe and reaction progress was monitored by $^1\text{H}\{^{31}\text{P}\}$ and $^{31}\text{P}\{^1\text{H}\}$ IGD NMR (Figure 2.13). The lower selectivity of the transformation, apparently due to side-hydrolysis, did not allow us to perform kinetic simulation.

Kinetic study of the reaction of $[(\text{Ph}_3\text{P})_3\text{Ru}(\text{H})_2(\text{H}_2)]$ (1**) with PhI in the presence of styrene.** Under argon, a 0.20 M solution of styrene in C_6D_6 (10 μL ; 0.002 mmol; 0.8 equiv) was added to a solution of $[(\text{Ph}_3\text{P})_3\text{Ru}(\text{H})_2(\text{H}_2)]$ (**1**) in C_6D_6 (0.005 M; 500 μL ; 0.0025 mmol) and PhI (100 μL ; 350 equiv) in a 5-mm NMR tube. The tube was shaken and immediately placed in the probe of an NMR spectrometer for monitoring the reaction by $^1\text{H}\{^{31}\text{P}\}$ and the formation of **6** and PPh_3 by $^{31}\text{P}\{^1\text{H}\}$ NMR. The data are summarized in Table 2.7.

Table 2.7. Kinetic data for the reaction of $[(\text{Ph}_3\text{P})_3\text{Ru}(\text{H})_2(\text{H}_2)]$ (**1**) with PhI and styrene, as monitored by $^1\text{H}\{^{31}\text{P}\}$ NMR.

Time, min.	1 , %	2-1 , %	3 , %	PhCHCH ₂ , %	PhEt, %
7	76	21	3	75	25
15	42	54	4	38	62
26	22	75	4	19	81
33	18	78	4	17	83
42	15	82	3	12	88

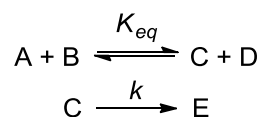
Comproportionation reactions.

Reaction of [(Ph₃P)₄Ru(H)₂] (3) with [(Ph₃P)₃RuCl₂]. In an argon-filled glovebox, a solution of [(Ph₃P)₄Ru(H)₂]·0.5PPh₃·0.5hexane in THF-*d*₈ (0.005 M; 0.5 mL) and a solution of [(Ph₃P)₃RuCl₂] in THF-*d*₈ (0.005 M; 0.5 mL) were mixed in a 5-mm NMR tube. No signs of reaction were observed for 1 h at room temperature. After 34 h, the reaction mixture turned more reddish in color and the presence of **2-Cl** (ca. 30% yield) was detected by ¹H{³¹P} NMR (s, -18.01 ppm). In a similar experiment at 55 °C, **2-Cl** was produced in ca. 60% yield within 20 min.

Reaction of [(Ph₃P)₄Ru(H)₂] (3) with [(Ph₃P)₃RuCl₂] and NaI. In an argon-filled glovebox, a solution of [(Ph₃P)₄Ru(H)₂]·0.5PPh₃·0.5hexane in THF-*d*₈ (0.005 M; 0.5 mL) and a solution of [(Ph₃P)₃RuCl₂] in THF-*d*₈ (0.005 M; 0.5 mL) were added to NaI (40 mg; 0.27 mmol). Vigorous agitation of the reaction mixture at room temperature for 15 minutes produced a purple solution containing **2-I** (ca. 70% yield; ¹H{³¹P} NMR: s, -15.15 ppm).

Reaction of [(Ph₃P)₄Ru(H)₂] (3) with [(Ph₃P)₃RuBr₂]/[(Ph₃P)₄Ru₂Br₂(μ-Br)₂]. The reaction of [(Ph₃P)₄Ru(H)₂] (3) with PhBr (see above) was driven to full conversion of first **3** and then **2-Br**, as monitored by ¹H{³¹P} NMR. To the thus produced equilibrated mixture of [(Ph₃P)₃RuBr₂]/[(Ph₃P)₄Ru₂Br₂(μ-Br)₂], was added 500 μL of a 0.005 M solution of **3** in C₆D₆ (1 equiv). The reaction mixture was shaken and analyzed by ¹H{³¹P} NMR. After 2 h at room temperature, [(Ph₃P)₃Ru(H)Br] was produced in ca. 5% yield. After 15 min at 50 °C (oil bath), ¹H{³¹P} NMR analysis indicated the formation of [(Ph₃P)₃Ru(H)Br] in 90 % yield (s, -16.50 ppm).

General equation for 2nd order / 2nd order pre-equilibrium with subsequent first order reaction.



Considering B is present in excess ($[B] \gg [A] + [C]$),

$$[A] + [C] = [A+C]$$

$$K_{eq} = [C][D]/[A][B]$$

$$[C] = [A+C] - [C][D]/K_{eq}[B]$$

$$[C] + K_{eq}[B][C]/[D] = K_{eq}[A+C][B]/[D]$$

$$[C] = K_{eq} \frac{[A + C][B]}{[D] \left(1 + K_{eq} \frac{[B]}{[D]}\right)}$$

$$\frac{d[E]}{dt} = -\frac{d[A]}{dt} - \frac{d[C]}{dt} = k[C]$$

$$\frac{d[E]}{dt} = kK_{eq} \frac{[A + C][B]}{[D] \left(1 + K_{eq} \frac{[B]}{[D]}\right)} \quad (\text{Eq 2.10})$$

If the equilibrium is shifted to the right ($K_{eq}[B]/[D] \gg 1$), Eq 2.10 can be simplified to:

$$\frac{d[E]}{dt} = k[C] \quad (\text{Eq 2.11})$$

If the equilibrium is shifted to the left ($K_{eq}[B]/[D] \ll 1$), Eq 2.10 can be simplified to:

$$\frac{d[E]}{dt} = kK_{eq} \frac{[A][B]}{[D]} \quad (\text{Eq 2.12})$$

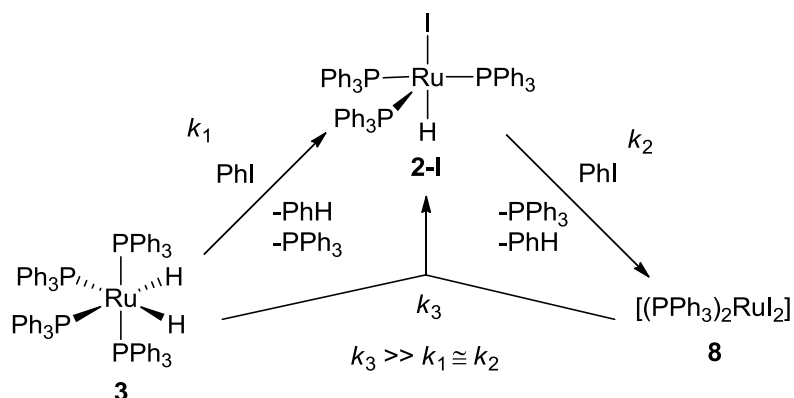
The values of $k \times K_{eq}$ are k_1 and k_2 in the main text.

The value of k_1' for the kinetic experiment with PhI was derived from equation Eq 2.10:

$$k_1' = kK_{eq} \frac{1}{\left(1 + K_{eq} \frac{[B]}{[D]}\right)} \quad (\text{Eq 2.13})$$

Considering $[B] = [\text{PhI}] = 1.49 \text{ M}$, $[D] = [\text{PPh}_3] = 0.005 \pm 0.001 \text{ M}$, $k = k_2 = 6.5 \times 10^{-3}$, and $K_{eq}(I) = 1.9 \times 10^{-3}$ (Figure 2.9, Table 2.5) gives $k_1' = 7.8 \pm 0.6 \times 10^{-6} \text{ min}^{-1}$.

Derivation of equation 2.3.



Scheme 2.17. Mechanism of the autocatalysis in the formation of **2-I** from **3** and *PhI*.

For the autocatalysis scheme above (Scheme 2.17),

$$d[\mathbf{2-I}]/dt = k_1[\mathbf{3}][\text{PhI}][\text{PPh}_3]^{-1} - k_2[\mathbf{2-I}][\text{PhI}][\text{PPh}_3]^{-1} + 2k_3[\mathbf{3}][\mathbf{8}]$$

and

$$d[\mathbf{8}]/dt = k_2[\mathbf{2-I}][\text{PhI}][\text{PPh}_3]^{-1} - k_3[\mathbf{3}][\mathbf{8}]$$

Steady state approximation ($d[\mathbf{8}]/dt = 0$) gives:

$$d[\mathbf{2-I}]/dt = k_1[\mathbf{3}][\text{PhI}][\text{PPh}_3]^{-1} - k_2[\mathbf{2-I}][\text{PhI}][\text{PPh}_3]^{-1} + 2k_2[\mathbf{2-I}][\text{PhI}][\text{PPh}_3]^{-1}$$

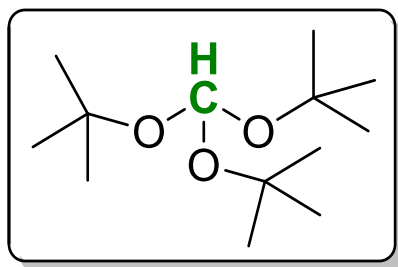
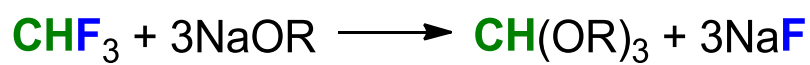
or

$$d[\mathbf{2-I}]/dt = k_1[\mathbf{3}][\text{PhI}][\text{PPh}_3]^{-1} + k_2[\mathbf{2-I}][\text{PhI}][\text{PPh}_3]^{-1}$$

This is Eq 2.3 on page 146.

Chapter 3

Alcoholysis of Fluoroform



80-120 °C

**R = Me, Et, *i*-Pr,
t-Bu, Allyl**

55-90% yield

Introduction

Fluoroform (CHF_3 , trifluoromethane, HFC-23, R-23), a gas (b.p. $-82\text{ }^\circ\text{C}$) and the lightest member of the haloform family, was first reported by Meslans¹ and Chabrié² over 120 years ago. In the 1930's, Henne³ and Ruff et al.⁴ developed efficient synthetic procedures furnishing CHF_3 in sufficient quantities for isolation in pure form and thorough studies. Numerous experiments carried out back then, particularly by Henne,³ established that fluoroform is an exceptionally chemically and biologically inert compound. In addition to being nontoxic and highly unreactive, CHF_3 is ozone-friendly and, consequently, is not on the Montreal Protocol list of chemicals depleting the ozone layer. It is not surprising therefore, that for many decades CHF_3 was considered to be a rather unremarkable, nonhazardous compound. As a result, large quantities of gaseous HFC-23 side-produced by the fluorochemicals and fluoropolymers industries could be disposed of by venting into the atmosphere without much environmental concern. This state of affairs, however, has recently changed dramatically.

In recent years, CHF_3 has become a center of attention as a potent greenhouse gas with the second highest global warming potential of 11,700 (100 years) and a long, 264-year atmospheric lifetime.⁵ The release of HFC-23 into the atmosphere should be stopped as otherwise it would likely lead to an ecological disaster.⁶ Therefore, the large quantities of the side-generated fluoroform should be destroyed or utilized. As fluoroform currently lacks industrial applications on a scale comparable with that of its

¹ Meslans, M. *C. R. Acad. Sc. (Paris)* 1890, 110, 717.

² Chabrié, M. C. *Bull. Soc. Chim. Fr.* 31892, 7, 18.

³ Henne, A. L. *J. Am. Chem. Soc.*, 1937, 59, 1200.

⁴ Ruff, O.; Bretschneider, O.; Luchsinger, W.; Miltschitzky, G. *Ber. Dtsch. Chem. Ges.* 1936, 69B, 299.

⁵ (a) Han, W.; Li, Y.; Tang, H.; Liu, H. *J. Fluorine Chem.* 2012, 140, 7. (b) Oram, D. E.; Sturges, W. T.; Penkett, S. A.; McCulloch, A.; Fraser, P. J. *Geophys. Res. Lett.* 1998, 25, 35. (c) McCulloch, A.; Lindley, A. A. *Atmos. Environ.* 2007, 41, 1560. (d) Miller, B. R.; Rigby, M.; Kuijpers, L. J. M.; Krummel, P. B.; Steele, L. P.; Leist, M.; Fraser, P. J.; McCulloch, A.; Harth, C.; Salameh, P.; Mühle, J.; Weiss, R. F.; Prinn, R. G.; Wang, R. H. J.; O'Doherty, S.; Grealley, B. R.; Simmonds, P. G. *Atmos. Chem. Phys.* 2010, 10, 7875.

⁶ Bomgardner, M. M. *Chem. Eng. News* 2013, 91, 6.

production, the destruction of HFC-23 is the only viable solution to the problem.^{5a} The available methods to eliminate large quantities of fluoroform, a flame retardant, are thermal oxidation, catalytic hydrolysis, and plasma destruction. All of these processes are costly and none of them are free from considerable drawbacks.

Utilizing HFC-23 waste streams as a chemical feedstock would provide an ideal solution to the problem. However, the exceptional inertness of fluoroform makes its use as a reagent a considerable challenge. This task is further complicated by the requirements of industrially viable conditions and sufficiently low-cost chemicals and materials for converting CHF₃ to useful products on a scale commensurate with that of its side-production, ca. 20000-25000 metric tons annually. Since 1990's, considerable progress has been made toward the development of new chemical transformations of fluoroform. Strong bases have been demonstrated to deprotonate CHF₃, a weak acid (pK_a = 27 in H₂O),⁷ to generate CF₃⁻ carbanion equivalents, e.g., for trifluoromethylation of carbonyl compounds and some other electrophiles.⁸ These reactions have been reviewed.⁹ Over the last few years, a novel approach to H-CF₃ activation has emerged, employing transition metals.¹⁰ Although none of these

⁷ Symons, E. A.; Clermont, M. J. *J. Am. Chem. Soc.* 1981, *103*, 3127.

⁸ (a) Shono, T.; Ishifune, M.; Okada, T.; Kashimura, S. *J. Org. Chem.* 1991, *56*, 2. (b) Barhdadi, R.; Troupel, M.; Périchon, M. *Chem. Commun.* 1998, 1251. (c) Russell, J.; Roques, N. *Tetrahedron* 1998, *54*, 13771. (d) Folléas, B.; Marek, I.; Normant, J.-F.; Saint-Jalmes, L. *Tetrahedron Lett.* 1998, *39*, 2973. (e) Folléas, B.; Marek, I.; Normant, J.-F.; Saint-Jalmes, L. *Tetrahedron* 2000, *56*, 275. (f) Large, S.; Roques, N.; Langlois, B. R. *J. Org. Chem.* 2000, *65*, 8848. (g) Billard, T.; Bruns, S.; Langlois, B. R. *Org. Lett.* 2000, *2*, 2101. (h) Blond, G.; Billard, T.; Langlois, B. R. *Tetrahedron Lett.* 2001, *42*, 2473. (i) Prakash, G. K. S.; Jog, P. V.; Batamack, P. T. D.; Olah, G. A. *Science* 2012, *338*, 1324. (j) Iida, T.; Hashimoto, R.; Aikawa, K.; Ito, S.; Mikami, K. *Angew. Chem., Int. Ed.* 2012, *51*, 9535. (k) Kawai, H.; Yuan, Z.; Tokunaga, E.; Shibata, N. *Org. Biomol. Chem.* 2013, *11*, 1446. (l) Thomason, C. S.; Dolbier, W. R., Jr. *J. Org. Chem.* 2013, *78*, 8904. (m) Zhang, Y.; Fujiu, M.; Serizawa, H.; Mikami, K.; *J. Fluorine Chem.* 2013, *156*, 367.

⁹ (a) Langlois, B. R.; Billard, T. *Synthesis* 2003, 185. (b) Langlois, B. R.; Billard, T. *ACS Symp. Ser.* 2005, *911*, 57. (c) Jog, P. V.; Prakash, G. K. S. *J. Postdoc. Res.* 2013, *1*, 1.

¹⁰ (a) Tomashenko, O. A.; Grushin, V. V. *Chem. Rev.* 2011, *111*, 4475. (b) Popov, I.; Lindeman, S.; Daugulis, O. *J. Am. Chem. Soc.* 2011, *133*, 9286. (c) Choi, J.; Wang, D. Y.; Kundu, S.; Choliy, Y.; Emge, T. J.; Krogh-Jespersen, K.; Goldman, A. S. *Science* 2011, *332*, 1545. (d) Zanardi, A.; Novikov, M. A.; Martin, E.; Benet-Buchholz, J.; Grushin, V. V. *J. Am. Chem. Soc.* 2011, *133*, 20901. (e) Novák, P.; Lishchynskiy, A.; Grushin, V. V. *Angew. Chem., Int. Ed.* 2012, *51*, 7767. (f) Novák, P.; Lishchynskiy, A.; Grushin, V. V. *J. Am. Chem. Soc.* 2012, *134*, 16167. (g) Kononov, A. I.; Benet-Buchholz, J.; Martin, E.; Grushin, V. V. *Angew. Chem., Int. Ed.* 2013, *52*, 11637. (h) Lishchynskiy, A.; Novikov, M. A.;

reactions⁸⁻¹⁰ have been commercialized for various reasons, some seem to hold promise.^{8l,10c-g,i-m} A number of high-temperature transformations of fluoroform have also been developed, including the gas-phase flow pyrolysis to CF₂=CF₂ (TFE) and hydrogenolysis to mixtures of hydrofluorocarbons (HFC's),¹¹ the catalytic iodination to CF₃I,¹² and the co-pyrolysis with TFE yielding hexafluoropropylene¹³ and with methane to produce various fluorinated products.¹⁴

Martin, E.; Escudero-Adán, E. C.; Novák, P.; Grushin, V. V. *J. Org. Chem.* 2013, *78*, 11126. (h) Takemoto, S.; Grushin, V. V. *J. Am. Chem. Soc.* 2013, *135*, 16837. (i) Grushin, V. V. *Chim. Oggi – Chem. Today* 2014, *32*, 81. (j) Mazloomi, Z.; Bansode, A.; Benavente, P.; Lishchynskiy, A.; Urakawa, A.; Grushin, V. V. *Org. Process Res. Dev.* 2014, *18*, 1020. (k) Lishchynskiy, A.; Berthon, G.; Grushin, V. V. *Chem. Commun.* 2014, *50*, 10237. (l) Kononov, A. I.; Lishchynskiy, A.; Grushin, V. V. *J. Am. Chem. Soc.* 2014, *136*, 13410. (m) Lishchynskiy, A.; Mazloomi, Z.; Grushin, V. V. *Synlett* 2015, *26*, 45.

¹¹ Romelaer, R.; Kruger, V.; Baker, J. M.; Dolbier, W. R., Jr., *J. Am. Chem. Soc.* 2001, *123*, 6767.

¹² (a) Nagasaki, N.; Morikuni, Y.; Kawada, K.; Arai, S. *Catal. Today* 2004, *88*, 121. (b) Yang, G.-C.; Lei, S.; Pan, R.-M.; Quan, H.-D. *J. Fluorine Chem.* 2009, *130*, 231.

¹³ Moon, D. J.; Chung, M. J.; Kim, H.; Kwon, Y. S.; Ahn, B. S. *Ind. Eng. Chem. Res.* 2002, *41*, 2895.

¹⁴ (a) Kennedy, E. M.; Kundu, S. K.; Mackie, J. C.; Holdsworth, C. I.; Molloy, T. S.; Gaikwad, V. V.; Dlugogorski, B. Z. *Ind. Eng. Chem. Res.* 2012, *51*, 11279. (b) Han, W.; Kennedy, E. M.; Kundu, S. K.; Mackie, J. C.; Adesina, A. A.; Dlugogorski, B. Z. *J. Fluorine Chem.* 2010, *131*, 751. (c) Han, W.; Yu, H.; Kennedy, E. M.; Mackie, J. C.; Dlugogorski, B. Z. *Env. Sci. Tech.* 2008, *42*, 5795. (d) Yu, H.; Kennedy, E. M.; Mackie, J. C.; Dlugogorski, B. Z. *Env. Sci. Tech.* 2006, *40*, 5778.

Objectives

As follows from the above, finding new reactions of fluoroform and the development of new methods for its destruction and degradation are in demand. Considering this, the objective of the current work was to study reactions of fluoroform with simple bases such as NaOH and KOH as well as with alkali metal alkoxides in the corresponding alcohols. Surprisingly little has been reported on such reactions, although mineralization of CHF₃ with solid alkali metal hydroxides and alkali and alkaline earth metal carbonates at 200-400 °C has recently been investigated in considerable detail.¹⁵

¹⁵ Vakulka, A.; Tavčar, G.; Skapin, T. *J. Fluorine Chem.* 2012, 142, 52.

Results

In their original publications on the synthesis of fluoroform, both Meslans¹ and Chabrié² mentioned that CHF₃ reacted with alcoholic KOH to give a mixture of potassium fluoride and potassium formate (Figure 3.1). Meslans conducted the hydrolysis in a sealed tube at 160 °C,¹ whereas in Chabrié's report, the reaction conditions were not specified.² In 1956, Hine et al. published a detailed kinetic study of alkaline hydrolysis of six haloforms in 2:1 dioxane-water to determine the following order of reactivity CHBrClF >> CHBrCl₂ > CHBr₂Cl ≈ CHCl₂I > CHBr₃ > CHCl₃ >> CHF₃, also reporting that “the reaction of fluoroform was too slow to measure”.¹⁶ Hine's observations are consistent with the fact that fluoroform is ca. 10⁶ times less reactive than chloroform toward H/D exchange with aqueous alkali.⁷ Very recently, Thomason and Dolbier⁸¹ demonstrated that CHF₃ reacts with KOH in aqueous dioxane or acetonitrile in the presence of phenols or thiophenols to give ArOCF₂H and ArSCF₂H, respectively. It was concluded that “*The mechanism of the reaction almost certainly involves the intermediacy of difluorocarbene, which would be formed by deprotonation of CHF₃ by hydroxide followed by loss of fluoride ion*”.⁸¹

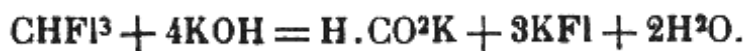
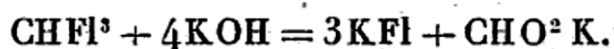
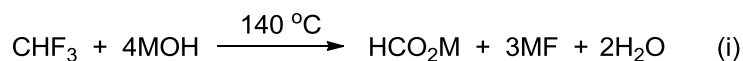


Figure 3.1. The chemical equations for the reaction of CHF₃ with KOH, exactly as they appear in the original articles by Meslans¹ (1890; top) and Chabrié² (1892; bottom).

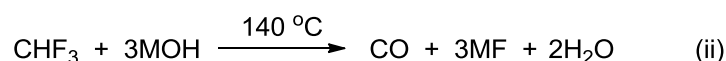
Note the old symbol “F” used for fluorine.

¹⁶ Hine, J.; Dowell, A. M., Jr.; Singley, J. E., Jr. *J. Am. Chem. Soc.* 1956, 78, 479.

We first confirmed that CHF_3 reacted with NaOH or KOH under solvent-free conditions to give the corresponding formate salt (Table 3.1, entries 1-3; Scheme 3.1, i). These reactions were carried out with freshly ground (in air) NaOH or KOH, in Fischer-Porter tubes at 140 °C under initial CHF_3 pressure of 50 psi (3.45 bar). The products were analyzed by ^1H and ^{19}F NMR, using sodium acetate and sodium trifluoroacetate as internal standards for the aqueous phase and 1,3-benzodioxole and benzotrifluoride for the organic extracts (see the Experimental Section for details). With ca. 85% KOH (eutectic, m.p. = ca. 100 °C),¹⁷ the reaction occurred in the melt, whereas NaOH remained solid throughout the experiment and, therefore, agitation was especially important for faster CHF_3 hydrolysis with sodium hydroxide (Table 3.1, entries 1 and 3). After 65-75% conversion was reached at stirring, the reaction virtually stopped. It is unlikely that considerably higher conversions could be achieved under such conditions because as the reaction occurs, water is produced, diminishing the basicity and reactivity of the alkali in the system. The yield of the formate anion (55-65%) was roughly 10% lower than that of fluoride because of the competing reaction leading to CO (Scheme 3.1, ii), in accord with the literature data.¹⁵ The formation of CO was confirmed by GC analysis of the gas phase after the reaction.



M = Na, K

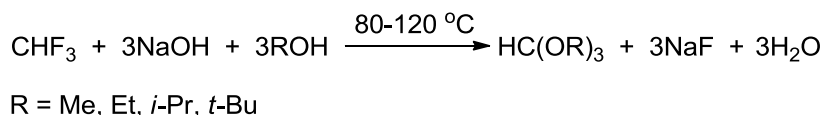


M = Na, K

Scheme 3.1. Reactions of fluoroform with alkali metal hydroxides.

¹⁷ Vogel, W. M.; Routsis, K. J.; Kehrer, V. J.; Landsman, D. A.; Tschinkel, J. G. *J. Chem. Eng. Data.* 1967, 12, 465.

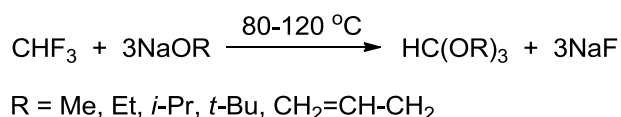
We then studied reactions of fluoroform with NaOH in various alcohols, ROH (Table 3.1, entries 4-7). These reactions occurred in the temperature range of 80-120 °C to give NaF, HCO₂Na, and the corresponding orthoformate HC(OR)₃ as a result of a competition between the two processes shown in Schemes 3.1 and 3.2. We are unaware of publications reporting the formation of orthoformates from fluoroform, although the reaction of chloroform with alkali metal alkoxides is widely used to prepare the corresponding orthoformate esters.¹⁸ The conversion of the base did not exceed 45-60%, with the yield of the orthoformate decreasing in the order R = Et (20%) > Me (15%) > *i*-Pr (10%) > *t*-Bu (<0.5%). The formation of small quantities of the corresponding CHF₂(OR) (ca. 0.5%) was observed in all of these reactions.



Scheme 3.2. Reactions of fluoroform with alkali metal hydroxides in alcohols.

Orthoformates are valuable reagents that find numerous applications in organic synthesis.¹⁸ To favor the formation of orthoformates from fluoroform, NaOH was replaced with alkali metal alkoxides under anhydrous conditions (Table 3.1, entries 8-14; Scheme 3.3). With MeONa in MeOH (entry 8), the reaction gave HC(OMe)₃ in 55% yield, along with 75% of NaF. Although the yield of methyl orthoformate increased to 70% at ca. 90% conversion in diglyme (entry 9), C2 products (MeO)₂C=C(OMe)₂ (ca. 2%) and (MeO)₃C-CH(OMe)₂ (ca. 10%) were detected by GC-MS in the reaction mixture. This is apparently because the slower formation of HC(OMe)₃ at the lower overall concentration of MeOX (X = Na, H) favored dimerization of the carbene intermediates.

¹⁸ DeWolfe, R. H. *Carboxylic Ortho Acid Derivatives; Preparation and Synthetic Applications* (Organic Chemistry, a Series of Monographs, Vol. 14); Academic Press: New York, 1970.



Scheme 3.3. Reactions of fluoroform with alkali metal alkoxides.

The reactions of EtONa and *i*-PrONa in the corresponding alcohols furnished the corresponding orthoformate esters in 55% and 90% yield, respectively (entries 10 and 11). Likewise, allyl orthoformate was produced in 60% yield under similar conditions (entry 14). Of special interest, however, is the reaction of fluoroform with *t*-BuOM (M = Na, K) in *t*-BuOH (entries 12 and 13). These reactions afforded, in 75-80% yield, tri-*tert*-butyl orthoformate HC(OBu-*t*)₃, a simple yet exceedingly rare and exotic compound. This bulkiest orthoformate ester has appeared only once in the chemical literature. In 1969, Hine et al.¹⁹ reported the synthesis and isolation of HC(OBu-*t*)₃ in only 3% yield from the reaction of CHFCl₂ with *t*-BuOK in *t*-BuOH. In their article, Hine, Dalsin, and Schreck also noted that “*in the preparation of orthoformates from haloforms and alkali metal alkoxides, dichlorofluoromethane is the haloform of choice*” and that “*fluoroform is relatively unreactive*” under such conditions.¹⁹ As can be seen from our results (entries 12 and 13), fluoroform can be successfully used to produce HC(OBu-*t*)₃ in >75% yield. In a scale-up of the reaction of CHF₃ with *t*-BuONa (0.1 mol) in *tert*-butanol, NMR-spectroscopically pure HC(OBu-*t*)₃ was isolated in 62% yield as a white, low-melting (m.p. 25-26 °C)¹⁹ crystalline solid. The structure of HC(OBu-*t*)₃ was confirmed by a single crystal diffraction study (Figure 3.2). Also interesting is the fact that in all our reactions of ROM/ROH with CHF₃, the corresponding difluoromethyl ethers CHF₂OR were formed in only small amounts (0.5-1.5%), whereas similar transformations of haloforms bearing two fluorine atoms

¹⁹ Hine, J.; Dalsin, P. D.; Schreck, J. O. *J. Org. Chem.* 1969, *34*, 3609.

have been reported to conventionally produce large quantities of such difluoromethyl ethers.²⁰

We also probed the reactivity of CHF_3 toward $\text{Mg}(\text{OEt})_2$ and $\text{Al}(\text{OPr-}i)_3$ with CHF_3 in EtOH and *i*-PrOH, respectively. At temperatures up to 120 °C, no reaction was observed with these much less basic alkoxides. On the other hand, the pyrrolide anion generated from pyrrole and NaH reacted with fluoroform at 120 °C to give NaF (30%), three isomers of $\text{HC}(\text{C}_4\text{H}_4\text{N})_3$ in a 5:3:2 ratio, and ca. 1% of $(\text{C}_4\text{H}_4\text{N})\text{CHF}_2$ (one isomer), as detected by GC-MS.

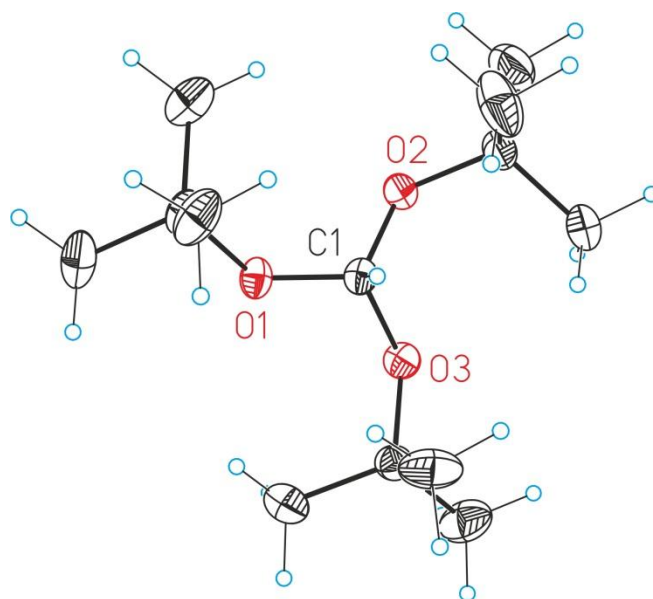
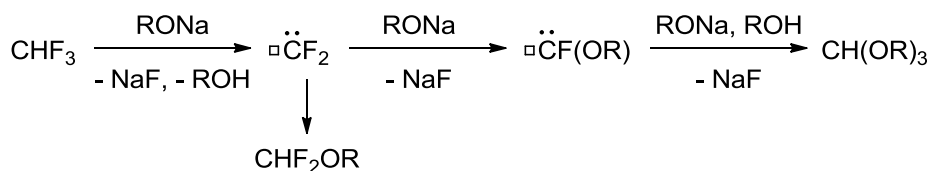


Figure 3.2. ORTEP drawing of $\text{HC}(\text{OBu-}t)_3$ with thermal ellipsoids drawn at the 50% probability level.

²⁰ (a) Hine, J.; Tanabe, K. *J. Am. Chem. Soc.* 1957, *79*, 2654. (b) Hine, J.; Porter, J. J. *J. Am. Chem. Soc.* 1957, *79*, 5493. (c) Hine, J.; Tanabe, K. *J. Am. Chem. Soc.*, 1958, *80*, 3002.

The reactions described above likely involve the intermediacy of difluorocarbene CF_2 .¹⁹⁻²¹ A plausible mechanism for the formation of HC(OR)_3 as the main product and of the small quantities of CHF_2OR is presented in Scheme 3.4. It is conceivable that the CF(OR) carbene proposed by Hine²⁰ is converted to C(OR)_2 that, as has been shown by Moss et al. for $\text{R} = \text{Me}$,²² readily reacts with ROH to give HC(OR)_3 . The difluoromethyl ethers CHF_2OR produced in only 0.2-1.5% yield in the reactions, are most likely end products rather than intermediates in the formation of the orthoformates.^{20b}



Scheme 3.4. Proposed mechanism for the formation of orthoformate esters from CHF_3 .

²¹ Le Noble, W. J. *J. Am. Chem. Soc.*, 1965, *87*, 2434.

²² Moss, R. A.; Wlostowski, M.; Shen, S.; Krogh-Jespersen, K.; Matro, A. *J. Am. Chem. Soc.* 1988, *110*, 4443.

Table 3.1. Reactions of fluororoform with alkali metal hydroxides and alkoxides.^a

Entry	Base (g)	Solvent (mL)	T, °C	Conversion of base, %	Yield of HCO ₂ M, %	HC(OR) ₃ (yield, %)
1	NaOH (0.82)	-	140	75	65	
2	KOH (1.32)	-	140	65	55	
3 ^b	NaOH (0.82)	-	140	30	20	
4	NaOH (0.82)	MeOH (1.5)	120	60	35	CH(OMe) ₃ (15)
5	NaOH (0.82)	EtOH (1.5)	120	45	15	CH(OEt) ₃ (20)
6	NaOH (0.82)	<i>i</i> -PrOH (1.5)	120	50	40	CH(OPr- <i>i</i>) ₃ (10)
7	NaOH (0.82)	<i>t</i> -BuOH (5.0)	80	55	50	CH(OBu- <i>t</i>) ₃ (<0.5)
8	MeONa (1.08)	MeOH (1.5)	120	75		CH(OMe) ₃ (55)
9	MeONa (1.08)	diglyme (1.5)	120	90		CH(OMe) ₃ (70)
10	EtONa (1.36)	EtOH (1.5)	120	55		CH(OEt) ₃ (55)
11	<i>i</i> -PrONa (1.64) ^c	<i>i</i> -PrOH (5.0)	120	90		CH(OPr- <i>i</i>) ₃ (90)
12	<i>t</i> -BuONa (1.92)	<i>t</i> -BuOH (5.0)	80	80		CH(OBu- <i>t</i>) ₃ (80)
13	<i>t</i> -BuOK (2.24)	<i>t</i> -BuOH (5.0)	80	85		CH(OBu- <i>t</i>) ₃ (75)
14	CH ₂ =CHCH ₂ ONa (1.60) ^c	CH ₂ =CHCH ₂ OH (5.0)	120	60		CH(OCH ₂ CH=CH ₂) ₃ (60)

^a Reaction conditions: base (20 mmol), CHF₃ (initial pressure 50 psi), 90-mL Fisher-Porter tube, 24 h. NMR yields (±5%) calculated using equations in Schemes 3.1-3.3 on the total amount of base used for the reaction (see the Experimental Section for details). ^b Without agitation. ^c Generated *in situ* by adding 0.8 g of NaH (60% suspension in mineral oil) to the specified amount of the corresponding alcohol.

Conclusions

The objectives of this project have been successfully met. In this work, we have confirmed that, in full accord with the original early 1890's reports by Meslans¹ and Chabrié,² fluoroform reacts with NaOH or KOH at 140 °C to give mixtures of the corresponding metal fluoride and formate. Solutions of NaOH in various alcohols ROH (R = Me, Et, *i*-Pr and *t*-Bu) also hydrolyze CHF₃ to NaF and HCOONa. Importantly, however, the corresponding orthoformate (up to 20%) is also produced in these reactions. Against previously reported observations,^{19,20} fluoroform can be sufficiently reactive toward MOR (M = Na, K) in ROH (R = Me, Et, *i*-Pr, *t*-Bu, and Allyl) to give the corresponding orthoformate esters in 55–90% yield, provided the reactions are carried out at 80–120 °C. Of particular interest is the formation of HC(OBu-*t*)₃ (70–80% yield), a simple yet extremely rare and poorly accessible organic compound that has been previously synthesized only once and in only 3% yield. A scale-up of the reaction of CHF₃ with *t*-BuONa (0.1 mol) in *t*-BuOH produced HC(OBu-*t*)₃ that has been isolated pure in 62% yield and structurally characterized. It is hoped that the overall simple, low-cost transformations developed in the current work may contribute to a solution for the HFC-23 ecological problem.

Experimental Section

General consideration. Chemicals were purchased from Aldrich (EtONa, *t*-BuONa, (EtO)₂Mg, (*i*-PrO)₃Al, pyrrole, allyl alcohol, CF₃CO₂Na, 1,3-benzodioxole, PhCF₃), Alfa Aesar (MeONa, *t*-BuOK, *t*-BuOH, CH₃CO₂Na), Acros (NaH, 60% suspension in mineral oil), Apollo Scientific (CHF₃), Panreac (NaOH, 98%), and Carlo Erba (KOH, 85%). Methanol, ethanol, isopropanol, *tert*-butanol, toluene, and pentane were used as received, unless otherwise noted. Anhydrous MeOH, EtOH, *i*-PrOH, *t*-BuOH, allyl alcohol, and pyrrole were distilled from CaH₂ under argon and stored over freshly activated 4 Å molecular sieves in an argon glovebox. Sodium trifluoroacetate was dried at 130 °C under vacuum (0.05 mmHg) and stored in the glovebox. ¹H and ¹⁹F NMR spectra were recorded on a Bruker Avance 400 Ultrashield NMR spectrometer. 1,3-Benzodioxole, benzotrifluoride, sodium acetate, and sodium trifluoroacetate were used as internal standards for quantitative ¹H and ¹⁹F (D1 = 5 s) NMR analysis. Agilent Technologies 7890A-5975C and 7890B instruments were used for GC-MS and GC-TCD analyses, respectively.

Alkaline hydrolysis of CHF₃ (Table 3.1, entries 1-3). A 90-mL Fisher-Porter tube containing a Teflon-coated magnetic stir bar was charged, in air, with freshly ground alkali (20 mmol; calculated on the MOH assay in the reagent used), evacuated, and pressurized with CHF₃ to 50 psi. After 24 h of heating at 140 °C (oil bath; see Table 3.1 for specifics), the tube was allowed to cool to room temperature and the gas phase was analyzed for CO by GC-TCD. To the contents of the tube, were added water (100 mL), sodium acetate, and sodium trifluoroacetate as internal standards (Table 3.2). A ca. 0.6-mL aliquot of the resultant aqueous solution was admixed with D₂O (0.1 mL) and quantitatively analyzed by ¹H (for HCO₂⁻) and ¹⁹F (for F⁻) NMR (see Tables 3.1

and 3.2). The amount of the base consumed in the reaction was calculated using the stoichiometry displayed in Scheme 3.1, as a sum of the amounts of the F^- and HCO_2^- produced.

Reactions of CHF_3 with NaOH in alcohols (Table 3.1, entries 4-7). A 90-mL Fisher-Porter tube containing a Teflon-coated magnetic stir bar was charged in air with freshly ground NaOH (98% purity; 0.82 g; 20 mmol) and an alcohol (see Table 3.1 for specifics), quickly evacuated, and pressurized with CHF_3 to 50 psi. After 24 h of agitation at 80 °C or 120 °C (oil bath; see Table 3.1), the tube was allowed to cool to room temperature, unsealed, and its contents were treated with toluene (40 mL) containing 1,3-benzodioxole (200 μ L; 237 mg) and benzotrifluoride (50 μ L; 58 mg) as internal standards. Upon agitation, a solid inorganic phase and a liquid organic phase were produced. A ca. 0.6-mL aliquot of the organic phase was filtered through Celite and the filtrate was admixed with C_6D_6 (0.1 mL) and analyzed, within an hour, first by 1H and ^{19}F NMR (see Tables 3.1 and 3.2) and then by GC-MS. (A longer delay in carrying out the analysis may produce incorrect data because of partial slow hydrolysis of the orthoformate product with residual moisture in the toluene solvent and in the atmosphere). The solid inorganic phase was separated by filtration, washed with toluene (3 \times 15 mL), and dissolved in water (200 mL). Sodium acetate and sodium trifluoroacetate were added as internal standards. A ca. 0.6-mL aliquot of this aqueous solution was admixed with D_2O (0.1 mL) and quantitatively analyzed by 1H and ^{19}F NMR (see Tables 3.1 and 3.2). The amount of the base consumed in the reaction was calculated using the stoichiometry displayed in Schemes 3.1 and 3.2, as a sum of the amounts of the F^- and HCO_2^- produced.

Reactions of CHF₃ with MOR in alcohols (Table 3.1, entries 8, 10, 12, and 13).

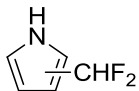
A 90-mL Fisher-Porter tube containing a Teflon-coated magnetic stir bar was charged, in a glovebox, with a metal alkoxide (20 mmol) and the corresponding anhydrous alcohol (see Table 3.1 for specifics), brought out, quickly evacuated, and pressurized with CHF₃ to 50 psi. After 24 h of agitation at 80 °C or 120 °C (oil bath; see Table 3.1), the tube was allowed to cool to room temperature, unsealed, and its contents were treated with toluene (40 mL) containing 1,3-benzodioxole (200 μL; 237 mg) and benzotrifluoride (50 μL; 58 mg) as internal standards. A ca. 0.6-mL aliquot of the resultant suspension was filtered through Celite and the filtrate was admixed with C₆D₆ (0.1 mL) and analyzed, within an hour, first by ¹H and ¹⁹F NMR (see Tables 3.1 and 3.2) and then by GC-MS. (A longer delay in carrying out the analysis may produce incorrect data because of partial slow hydrolysis of the orthoformate product with residual moisture in the toluene solvent and in the atmosphere). To the rest of the reaction mixture, were added water (200 mL) and sodium trifluoroacetate as an internal standard. A ca. 0.6-mL aliquot of this aqueous solution was admixed with D₂O (0.1 mL) and quantitatively analyzed by ¹H and ¹⁹F NMR (see Tables 3.1 and 3.2).

Reactions of CHF₃ with NaOR generated in situ from NaH in ROH (Table 3.1, entries 11 and 14). A 90-mL Fisher-Porter tube containing a Teflon-coated magnetic stir bar was charged, in a glovebox, with NaH (60% suspension in mineral oil; 0.80 g; 20 mmol) and anhydrous *i*-PrOH or allyl alcohol (see Table 3.1 for specifics) and brought out. After stirring for 30 min at 120 °C (oil bath), the tube was cooled to room temperature, quickly evacuated, and pressurized with CHF₃ to 50 psi. After 24 of agitation at 120 °C (oil bath; see Table 3.1), the tube was allowed to cool to room temperature, unsealed, and its contents were treated with toluene (40 mL) containing

1,3-benzodioxole (200 μL ; 237 mg) and benzotrifluoride (50 μL ; 58 mg) as internal standards. A ca. 0.6-mL aliquot of the resultant suspension was filtered through Celite and the filtrate was admixed with C_6D_6 (0.1 mL) and analyzed, within an hour, first by ^1H and ^{19}F NMR (see Tables 3.1 and 3.2) and then by GC-MS. (A longer delay in carrying out the analysis may produce incorrect data because of partial slow hydrolysis of the orthoformate product with residual moisture in the toluene solvent and in the atmosphere). To the rest of the reaction mixture, were added water (200 mL) and sodium trifluoroacetate as an internal standard. A ca. 0.6-mL aliquot of this aqueous solution was admixed with D_2O (0.1 mL) and quantitatively analyzed by ^1H and ^{19}F NMR (see Tables 3.1 and 3.2).

Preparation of $\text{HC}(\text{OBu-}t)_3$. A 450-mL Fisher-Porter bottle containing a Teflon-coated magnetic stir bar was charged, in a glovebox, with $t\text{-BuONa}$ (9.60 g; 100 mmol) and $t\text{-BuOH}$ (25 mL), brought out, quickly evacuated, and pressurized with CHF_3 to 50 psi. After 21 h of agitation at 80 $^\circ\text{C}$ (oil bath), the bottle was allowed to cool to room temperature and opened to air. Pentane (60 mL) was added and the mixture was transferred to a 250-mL flask. The bottle was rinsed with pentane (3×30 mL) and the combined reaction mixture and the washings were evaporated on a rotary evaporator to remove the pentane and $t\text{-BuOH}$. Vacuum transfer of the residue at ca. 0.06 mmHg with gentle heating, followed by drying on a rotary evaporator (ca. 50 mbar at 40 $^\circ\text{C}$ for 1 h) gave 4.81 g (62%) of $\text{HC}(\text{OBu-}t)_3$ as a colorless liquid that crystallized on cooling to +8 $^\circ\text{C}$. The compound was spectroscopically pure. ^1H NMR (dry CDCl_3), δ : 1.27 (s, 27H), 5.67 (s, 1H). ^{19}F NMR (dry CDCl_3), δ : 29.5, 73.7, 104.4.

Table 3.2. NMR data for compounds obtained and for internal standards (in reaction mixtures).

Compound	¹ H NMR, δ	¹⁹ F NMR, δ
1,3-benzodioxole	5.45 (s, 2H), 6.70-6.79 (m, 4H)	-
CH(OMe) ₃	3.25 (s, 9H), 4.91 (s, 1H)	-
CH(OEt) ₃	1.24 (t, <i>J</i> = 7 Hz, 9H), 3.63 (q, <i>J</i> = 7 Hz, 6H), 5.18 (s, 1H)	-
CH(OPr- <i>i</i>) ₃	1.27 (d, <i>J</i> = 6 Hz, 18H), 4.07 (sept, <i>J</i> = 6 Hz, 3H), 5.39 (s, 1H)	-
CH(OBu- <i>t</i>) ₃	1.37 (s, 27H), 5.78 (s, 1H)	-
CH(Oallyl) ₃	4.12 (m, 6H), 5.15 (m), ^a 5.25-5.50 (m), ^a 5.92 (m, 3H)	-
CH ₃ CO ₂ Na	1.90	-
HCO ₂ Na	8.44	-
PhCF ₃	-	-63.7
CHF ₂ OMe	5.74 (t, <i>J</i> _{FH} = 75 Hz)	-87.5 (d, <i>J</i> _{FH} = 75 Hz)
CHF ₂ OEt	5.82 (t, <i>J</i> _{FH} = 75 Hz)	-84.7 (d, <i>J</i> _{FH} = 75 Hz)
CHF ₂ OPr- <i>i</i>	5.89 (t, <i>J</i> _{FH} = 76 Hz)	-81.7 (d, <i>J</i> _{FH} = 76 Hz)
CHF ₂ OBu- <i>t</i>	6.05 (t, <i>J</i> _{FH} = 77 Hz)	-77.3 (d, <i>J</i> _{FH} = 77 Hz)
CHF ₂ Oallyl	- ^b	-84.9 (d, <i>J</i> _{FH} = 75 Hz)
	- ^b	-89.1 (d, <i>J</i> _{FH} = 62 Hz)
CF ₃ CO ₂ Na	-	-75.5
F ⁻	-	-120.1

^a Signals overlapped with those from the residual allyl alcohol. ^b Although the ¹H NMR signals could not be observed because of their low intensity and overlap with other resonances, the presence of these products was confirmed by ¹⁹F NMR and GC-MS.

UNIVERSITAT ROVIRA I VIRGILI
NEW TRANSFORMATIONS BASED ON ACTIVATION OF INERT CARBON-HALOGEN BONDS WITH AND WITHOUT TRANSITION
Miloserdov Fedor Mikhailovich
Dipòsit Legal: T 825-2015

UNIVERSITAT ROVIRA I VIRGILI
NEW TRANSFORMATIONS BASED ON ACTIVATION OF INERT CARBON-HALOGEN BONDS WITH AND WITHOUT TRANSITION
Miloserdov Fedor Mikhailovich
Dipòsit Legal: T 825-2015



UNIVERSITAT ROVIRA I VIRGILI

Tarragona 2015